Guanidine-Based DNA Binders and Strategies Toward their Platinum Complexes as Anticancer Dual Agents

A thesis presented to the University of Dublin
for the degree of Doctor of Philosophy

by

Patrick O'Sullivan, B. Sc.

Under the supervision of Prof. Isabel Rozas

School of Chemistry
Trinity College Dublin

March 2016

Declaration

This work comprises a doctoral thesis submitted for the consideration of Trinity College Dublin.

I declare that this thesis has not been submitted as an exercise for a degree at this or any other university and it is entirely my own work, with due acknowledgement and reference given to the work of others, where appropriate.

I agree to deposit this thesis in the University's open access institutional repository or allow the library to do so on my behalf, subject to Irish Copyright Legislation and Trinity College Library conditions of use and acknowledgement.

…….
Patrick O'Sullivan

March 2016
Trinity College Dublin

Acknowledgements

First and foremost, I would like to thank Prof. Isabel Rozas for your help over the last four and a half years. You have guided me on the journey from student to scientist and for that I will forever be grateful. You have been a boss, a teacher and a friend and I thank you from the bottom of my heart.

To all the members of the Rozas group- past and present- you have been an inspiration throughout. I would like to specifically thank Caitríona for being my biophys guru and great friend, Brendan for his expertise in docking, especially for the detailed study in Section 3.1.2, and his valuable insights into chemistry and life in general, Elena Diez for her inspirational work hard-play hard attitude, and Julian for rekindling my love of chemistry and being the resident Pd expert. I also thank the current Rozas group members, Dr Cristina Trujillo for the nicest and most patient computational chemistry expert in the world, Viola for being my biochemistry saviour, my councillor and a true friend, and Aaron for his work on Pt complexation as my summer student and his inquisitiveness and boundless enthusiasm as a fellow PhD student. I would also like to thank my 4th year project students Maeve and Ayat for their work on the aminoguanidine section and my summer student Rory for helping out with some Pt complexes. Thanks also to Ale and Pilar for their work in the very beginning!

A special mention goes to the most efficient, dedicated, and craziest chemist I know. Michela, you have been with me pretty much from the beginning to the end of my PhD and I have become a better chemist by following your example. More than that, you have been a cherished friend and companion throughout. I could not in a million years have picked a better person to share the last four years with.

To the many people in the School of Chemistry who helped me, from the staff in the office to the technicians to fellow postgrads, postdocs and lecturers, I thank you all. To Dr John O'Brien for your encyclopaedic NMR knowledge, friendship and willingness to always run "just one more sample" for me, Dr Manuel Ruether for help on NMR, UV/vis, CD and HPLC, Dr Brendan Twamley the king of crystallography and Dr Martin Feeney and Dr Gary Hessman for running the mass spectrometry facility. There are too many fellow students to name individually but Helen, Andy and Elena de Calatrava deserve a special mention. Thanks guys for your humour, companionship and chemistry tips. We have lifelong friendships to look forward to!

I would like to thank Prof. Aidan McDonald and Prof. Bob Baker for their advice on Pt chemistry and inorganic chemistry in general. Through your insightful questioning and suggestion I learned a great deal. Thanks to Fergus in the Gunnlaugsson group for help with the biophysical measurements and Aoife in the Senge group for her expertise in measuring $^1O_2$ generation. To Prof. Celine Marmion in the RCSI and your students James, Ziga and Reece, I would like to thank you for your help with Pt complexation and ideas for malonate-based ligand synthesis. To Celine I also thank you for initially conceiving these parts of the project with Isabel. Thanks are also due to Maite Garcia and Prof. Daniela Zisterer in the School of Biochemistry for help with the cytotoxicity section of the project.

To each and every member of the Trinity Trampoline Club, especially fellow postgrads Danny, Aideen and Naoise, I cannot explain in words how much you all mean to me. Without you, I would not have lasted more than three months in Dublin. I wish everybody every possible success in everything you do.

A special mention is due to my secondary school chemistry teacher, Liz O'Riordan for igniting the first flame in my love of chemistry in Coláiste an Chraoibhín. I cannot thank you enough for all you have done.

To all my friends and family, thank you for being so supportive in the last few years. Your encouragement has meant everything to me. I would like to especially thank all my previous housemates for putting up with me, and in particular my Corkonian companions Anne-Marie and Mary. Both of you were constant sources of assistance, reassurance and necessary distraction and it has been my pleasure to live with you guys.

Finally, to my parents, Michael and Patsy, and my brother James, your incessant love and support have made me everything I am. Thank you for believing in me, for lifting me up when I was down, and for bringing me down to earth when I needed it! No matter how far from home I am, you are always in my heart. I dedicate this work to you.

Ní neart go cur le chéile

Abstract

One in three people will be diagnosed with cancer in their lifetime. One of the main targets of chemotherapy is DNA. Platinum-based anti-cancer agents form covalent bonds with bases in the major groove of DNA in cancer cells, causing death of these cells. The platinum-based coordination compound cisplatin (Platinol®) and its derivatives carboplatin (Paraplatin®) and oxaliplatin (Eloxatin®) are used in 50% of chemotherapies and are especially efficacious against testicular cancer, where platinum-based drugs have increased the five-year survival rate from 10% in the 1960s to 98% today. One of the most recent chemotherapies to gain approval for cancer treatment is trabectedin (Yondelis®), a natural product that works as a DNA minor groove binder (MGB) and specifically treats liposarcomas by binding covalently to the minor groove of DNA.

Over the past 10 years, Rozas' group has developed dicationic guanidinium-like DNA MGBs that strongly bind to AT-rich DNA sequences and have demonstrated varying cytotoxic activity in cancer cells. In this work, we sought to improve the cytotoxicity of these MGBs by enhancing their lipophilicity, constraining their structures in a planar conformation, or by coordinating them to Pt to create covalent DNA binders. Additionally, aryl guanidine- and aminoguanidine-based platinum complexes were synthesised to explore their cytotoxic effect. Firstly, a family of diaryl *bis*-(2-amino-1,4,5,6-tetrahydropyridinium) MGBs was prepared. Secondly, a method to synthesise *N*-amino-*N'*-arylguanidinium salts was developed. Thirdly, we created new *bis*-(2-aminoimidazolinium)-containing malonic ester derived MGBs using either a flexible diaryl scaffold or a conformationally restricted and planar 3,6-substituted fluorene motif. Furthermore, using a variety of Pt precursor complexes and neutral *N*'-arylguanidine ligands, we discovered a wide range of cyclometalated and non-cyclometalated structural motifs containing Pt-arylguanidine and *N*-amino-*N*'-arylguanidine complexes. We then applied this knowledge to the synthesis of Pt-MGB complexes bound *via* a guanidine.

The above compounds were tested using biophysical measurements to evaluate DNA binding and using biochemical measurements to assess cytotoxicity on the HL-60 leukemia cell line.

Abbreviations

ALL	Acute Lymphocytic Leukemia
AML	Acute Myeloid Leukaemia
ATP	Adenosine Triphosphate
BCL-2	B-cell Lymphoma gene 2
Boc	*tert*-Butoxycarbonyl
br s	broad singlet
CD	Circular Dichroism
CML	Chronic Myleoid Leukaemia
DACH	1,2-diaminocylohexane
DACP	1,2-diaminocyclopentane
DFT	Density Functional Theory
DMF	Dimethylformamide
DMSO	Dimethyl sulfoxide
DNA	Deoxyribonucleic Acid
ER	Endoplasmic Reticulum
FDA	Food and Drug Administration
HAPT1	High-Affinity Pentamidine Transporter
HB	Hydrogen bond
IC_{50}	Half Maximal Inhibitory Concentration
IR	Infrared
kDNA	kinetoplast DNA
LUMO	Lowest Unoccupied Molecular Orbital

NER	Nucleotide Excision Repair
PCD	Programmed Cell Death
PDT	Photodynamic Therapy
PSA	Polar Surface Area
PTA	1,3,5-triaza-7-phophoadamantane
RNS	Reactive Nitrogen Species
ROS	Reactive Oxygen Species
rt	Room Temperature
SOMO	Singly Occupied Molecular Orbital
T_M	Melting Temperature
TFAA	Trifluoroacetic Anhydride
TPA	Trans Planar Amine
UV	Ultraviolet

Table of Contents

1.0 Introduction

1.1 Cancer Overview

Cancer is a leading cause of death worldwide.[1,2] The term "cancer" is used to identify uncontrolled cell growth (tumour formation) at a primary site in the body as well as the invasion of these tumour cells into secondary sites (metastasis). Cancer is an umbrella term that encompasses over 100 different diseases, varying by the cell type of the primary tumour, its shape and where it has spread to as well as the expression of proteins in the tumour.[3]

Cancer is a huge burden on society, with one in three people worldwide directly affected; the longer a person lives, the greater the risk of developing cancer.[1,2] In Ireland 29,775 people were diagnosed with cancer in 2009 and the average 5-year survival rate in 2009 was 60%.[4] Symptoms of cancer include swelling, pain or pressure around the tumour, blood in the urine or faeces, severe coughing, anemia and/or haemorrhaging.[5] Although current therapies are constantly improving patient prognosis, new drugs are needed to further improve patient outcomes.

Cancers exert their malignancy by growing so large that they obstruct necessary bodily functions in their primary and secondary sites, such as liver, brain and lung function, and also by starving the rest of the body of essential nutrients. These tumours can be caused in a variety of ways depending on the location of the pre-cancerous tissue, *i.e.* it is known that smoking causes lung cancers and UV radiation causes skin cancers since these cancer-causing factors (carcinogens) have better access to the respective areas. Thus, the methods of treatment are inherently different too. Cancers of the skin are much more accessible for surgery than lung cancers. Moreover, depending on the epigenetics of the cell types (for example, what proteins are expressed) these cancers grow and spread distinctly and they also respond differently to treatment.[3]

Oncology (*cf.* Greek *onkos*= swelling) is the study of cancer. Oncologists use many terms to describe different cancers. Carcinoma *in situ* is where cells form a tumour, *i.e.*, loss of tissue identity, rapid and unregulated growth but confined to the specific area or organ. Invasive carcinoma (*cf.* Greek *karkinos*- a tumour "has the veins stretched on all sides as the animal the crab has its feet, whence it derives its name")[6] is where the tumour grows beyond the original tissue layer or location, and may metastasise, *i.e.* spread to surrounding tissues or lymph nodes. A sarcoma is a tumour of the supportive, connective or soft tissue; whereas an adenoma is defined as a tumour localised in a gland and an adenocarcinoma is where the

adenoma has spread outside the gland of origin. Leukemia is a cancer that begins in bone marrow and gives rise to abnormal blood cells. Lymphoblastic/lymphocytic leukemia is cancer of marrow that goes on to form lymphocytes, typically B cells. In contrast, myeloid leukemia is cancer of marrow cells that give rise to red blood cells, other white blood cells and platelets.[6]

Biochemically, many cancer cells have certain *hallmarks* that differentiate them from surrounding tissue. These include increased proliferative signalling, evasion of growth suppressors, avoidance of immune destruction, replicative immortality, tumour-promoting inflammation, tissue invasion and metastasis, angiogenesis, genomic instability, resistance to cell death and mitochondrial imbalance. Each of these hallmarks can theoretically be targeted by pharmaceuticals (Figure 1.1.1).[7]

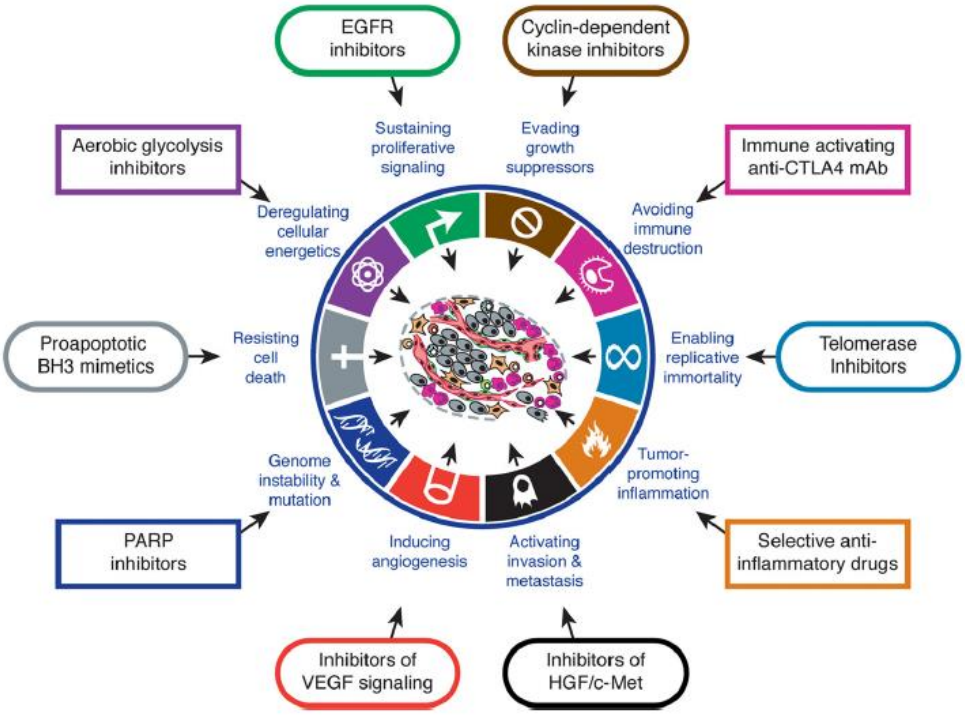

Figure 1.1.1. The Hallmarks of Cancer and Chemotherapetic Targets.[7]

However, the problem is that each hallmark can arise from a number of causes and the specific combination of these mutations is unique, not only to the cancer subtype, but to the patient. Indeed the recently discovered variance of genotypes within every tumour has

revealed that cancer chemotherapy needs to hit many of these hallmarks to give the patient a chance of recovery.[8]

Paradoxically, in a landmark study in *Nature* in 2007, 73 out of 210 cancer patients did not have a single mutation in their cancer tumours compared to normal tissue.[9] Undoubtedly, a large component of cancer pathology is not only related to somatic mutations but to the expression or suppression of wild-type gene products in a cancer-causing environment (e.g. tissue). Thus, abnormal crosstalk between cells, and not necessarily within a single cell, is also thought to cause cancer and its hallmarks. With this in mind, several cancer researchers are calling for a paradigm shift from thinking about cancer as a somatic disease to cancer as a developmental disease, with the fundamental idea that a cancer is cancer tissue (*i.e.* tumour mass) and not a single cell.[10,11] In the future, it is hoped that advances at both the somatic and tissue level, will provide better anticancer therapies for the patients.[12]

It is important to stress that primary tumours (i.e. solid tumours that have not yet spread beyond the local region) are termed *benign*. In general, if a tumour is confined to only one area, the damage it causes is not life-threatening and the pain and symptoms are localised to the tissue type. If a tumour is able to spread and metastasise, then is called a *malignant* tumour. When a tumour spreads from a primary site to the lungs, liver or brain, it can disrupt the function of these organs and lead to death, in fact, about 90% of cancer deaths are due to these malignant tumours.[6] Indeed, metastasis has been described as the "one true *hallmark*" of cancer.[13]

Most methods of cancer classification involve describing how far a solid tumour has spread. Typically, stage I is a tumour where abhorrent cells are present only in the primary tumour area; stage II is where the tumour has spread locally (i.e. within the affected organ); stage III cancers contain regional metastases; and stage IV tumours have distant metastases, where the secondary tumours are found far from the primary tumour site. In general, late-stage cancers have a worse prognosis and are more difficult to treat than early stage tumours.[6] Recently a *Periodic Table for Cancers* has been published based on the resistance of a cancer to apoptosis and its aggressiveness. The authors were able to show a number of associations between prognosis, origin and patterns of specific mutations in relation to apoptotic susceptibility and likelihood of metastasis.[14] These patterns may be useful in guiding future cancer treatments because drugs that are effective for a certain cancer tend to display efficacy towards cancers grouped close by on this table.

1.2 Overview of cancer treatments

Due to the previously mentioned differences in cancer cells between primary tissue type, among patients and even within the primary tumour, a plethora of anti-cancer treatments are used. Various combinations of surgery, radiation and chemotherapy are utilised based on tumour location, stage and presence of growth factors. However, owing to the intrinsic (pre-treatment) and acquired (during treatment) resistance ability of cancer cells to chemotherapies, the patient may have to go through a number of rounds of different treatments to find a satisfactory result. In addition, chemotherapy treatments are associated with side effects such as fatigue, nausea, immunosuppression, chemo brain (chemotherapy-related cognitive impairment),[15] and pain. These side effects are often dose-limiting and can cause the oncologist to curtail or change treatment.

There are two broad classes of cancer treatment: curative (with a view to completely eradicate the disease), and palliative (to lessen the pain and improve quality of life for patients who are dying). Current chemotherapeutic options do not do enough to eradicate malignant cancer while maintaining a tolerable side effect profile. Novel generations of active pharmaceuticals are necessary in the fight against this deadly disease. The survival data from Figure 1.2.1 show that we are making progress, although the progress may be exaggerated by the improvements in early detection procedures.[16]

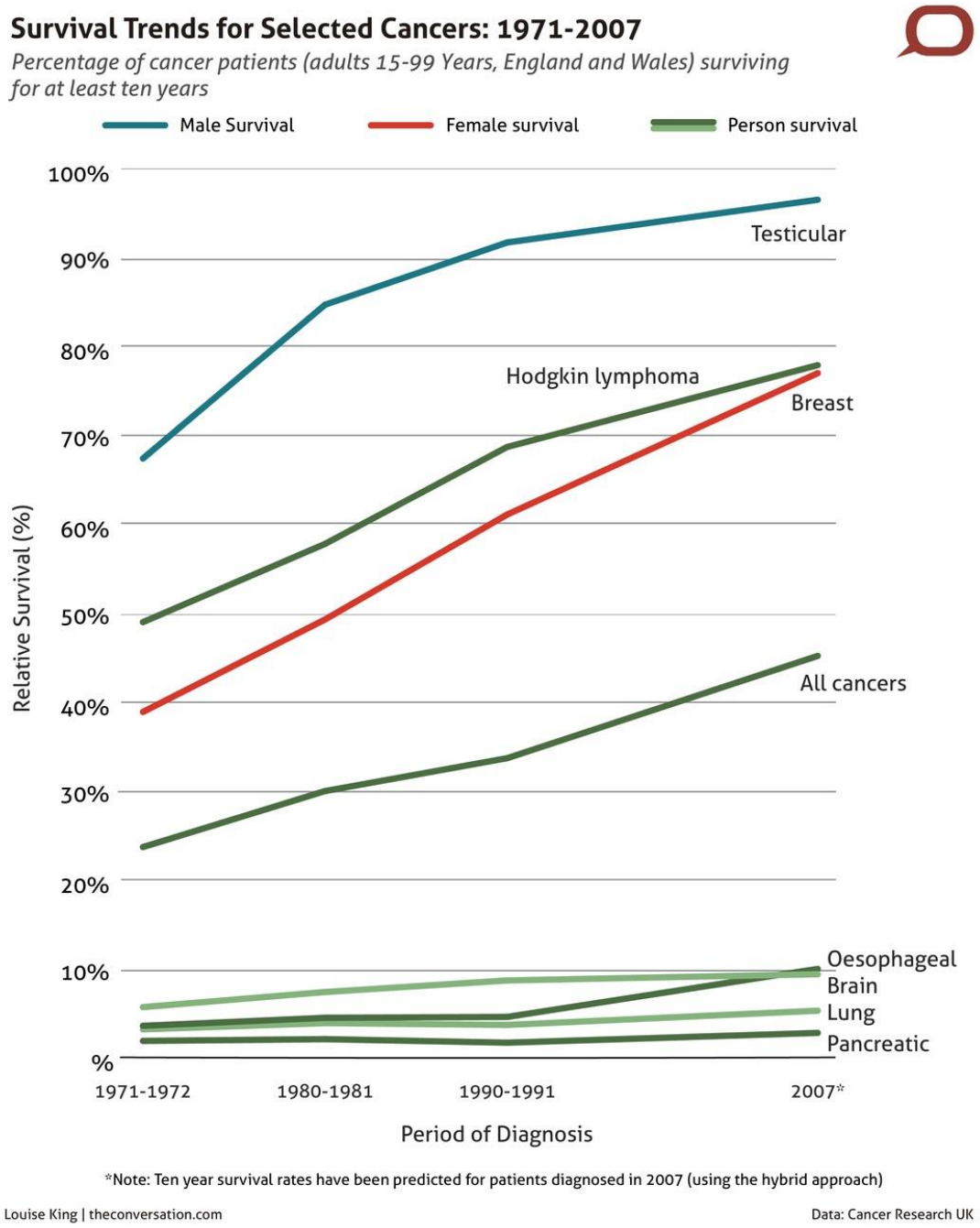

Figure 1.2.1. The relative ten-year survival rates of cancer patients as a function of time.[16]

1.3 Chemotherapy: Drugs in the clinic that kill cancer cells

In contrast to surgical resection and radiotherapy, that both affect cancer at a tumour level, the goal of cancer chemotherapy is to bring about cell death selectively in a cancer cell. Immunological approaches target both the individual cells and the tumour mass and are an

area of active research. The recently FDA-approved immunomodulatory mono-clonal antibody ipilimumab prevents T-cell inhibition in the tumour microenvironment.[17]

Other targeted theraopies include androgen and oestrogen receptor blockers flutamide and tamoxifen, developed in the 1960s.[18] More recent targets for chemotherapy include kinases, important in initiating and maintaining cell growth. There are currently over 25 kinase inhibitors on the market that have efficacy against cancer, with the first kinase inhibitor, Gleevec®/imatinib, gaining FDA approval in 2001.[19] However, redundancy in kinase signalling and mutations in the kinase active site mean that many cancers evolve resistance to kinase inhibitors in 12 months.[20] Epigenetic regulation of DNA by histones is important for cancer cells to grow and divide. Inhibitors of histone deacetylases (HDACi's) approved in the clinic include vorinostat (SAHA) for cutaneous T cell lymphoma and panobinostat for multiple myeloma.[21] Microtubule assembly/disassembly occurs during mitosis and can be targeted with drugs such as the vinca alkaloids (*e.g.* vinblastin, approved by the FDA in 1961), or paclitaxel (FDA-approved in 1992, Figure 1.3.2.1).

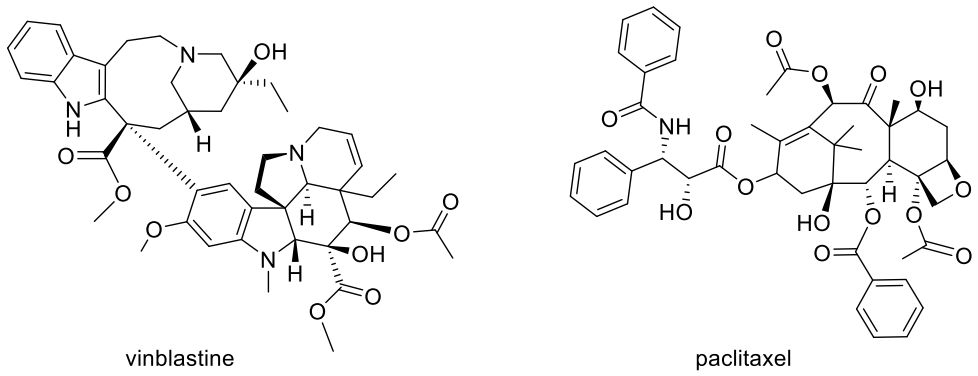

Figure 1.3.2.1. FDA-approved microtubule inhibitors.

The most commonly targeted macromolecule in cancer chemotherapy is DNA (Section 1.4). DNA-interacting agents approved by the FDA and EMA include DNA alkylators (nitrogen mustards, platinum-based drugs),[18] DNA intercalators (dactinomycin, doxorubicin),[22] DNA topoisomerase inhibitors (camptothecin),[23] DNA minor groove binders (trabectedin),[24] and DNA anti-metabolites (5-fluorouracil).[18]

1.3.1 Chemotherapy invokes Cell death

Cell death is important in a range of circumstances, for example when the host cell is infected with a virus or bacteria, when the cell is producing abhorrent proteins and when the cell has genomic damage; then for the good of the whole organism, ideally the cell will die. There are many mechanisms by which cell death can occur, such as apoptosis, autophagy, necroptosis, oncosis and pyroptosis. Apoptosis, a form of programmed cell death, is a highly regulated process by which the cell undergoes "nuclear fragmentation (karyorrhexis), plasma membrane blebbing and engulfment by resident phagocytes (*in vivo*)."[25] The many biochemical pathways that can lead to this morphology are not fully understood but most involve caspases (Cysteine-dependant ASPartate-directed proteASE).[26] The most commonly known form of apoptosis is when the cell ultimately activates effector caspases (Caspase-3) that recognise and cleave structural proteins, as well as activate endonucleases that cut DNA. These caspases are activated by cytochrome c release from the mitochondria, through pores created by Bax and Bak. In normal cell function, Bax and related proteins are inhibited by Bcl-2 and others. These apoptotic pathways result in cell shrinkage and phagocytosis. [25]

All non-apoptotic cell death was previously referred to as necrosis and was thought of as a chaotic, "accidental" form of cell death. Necrosis is defined as "gain in cell volume (oncosis), swelling of organelles, plasma membrane rupture and subsequent loss of intracellular contents."[25] We now know that cell death mechanisms leading to necrosis are highly regulated and also follow a number of biochemical signalling cascades. The most important events are PARP-1 activation, causing ATP depletion, which triggers DNA cleavage, mitochondrial membrane polarisation and Ca^{2+} release. Calpains (non-caspase Ca-dependant proteases) are activated by near-μM levels of Ca^{2+} in the cell and cleave structural proteins, leading to membrane rupture. The term "necroptosis" is now used more frequently to describe necrosis that occurs through RIP-1 activation of PARP-

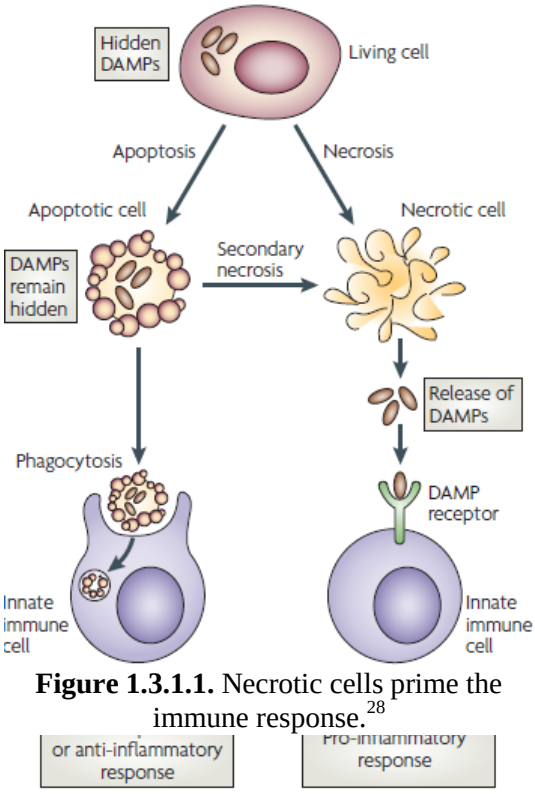

Figure 1.3.1.1. Necrotic cells prime the immune response.[28]

1, demonstrating another form of programmed cell death. Many of these programmed cell death (PCD) pathways are redundant, i.e. if an FADD knock-out mouse (cannot form a DISC with FasL in extrinsic apoptosis) is given a death signal, it will die *via* a necroptotic pathway.[27]

Necrotic cells were previously thought to cause damage to cells surrounding the dead cell, by increasing levels of ROS (reactive oxygen species) and other toxic cell components. However, necrotic cells allow the contents of the damaged cell to present themselves to the immune system. In this manner, macrophages and other members of the innate immune system come into contact with antigens, such as mutated proteins and DNA as well as DAMPs (Danger-Associated Molecular Patterns), which would otherwise remain mostly hidden in an apoptotic cell (Figure 1.3.1.1). Subsequent recruitment of the inflammatory response allows targeting of other similarly damaged cells for destruction.[28] Examples of DAMPs include extracellular HMGB1 (a DNA-binding protein normally found only in the nucleus) and extracellular ATP (the "find-me" signal) that not only increases the immune response, but also allows the immune system to find the damaged cell by chemotaxis, and cause immunogenic cell death (ICD).[29]

Mitochondria have an influential role in cancer by sequestering cytochrome c and other cell death mediators, important in apoptosis.[30] In fact, Seyfried *et al*. have postulated that defective mitochondria are a cause rather than an effect of cancer tumours.[31] Also, many anticancer drugs, including vitamin E derivatives, arsenates and tamoxifen among others, have a direct effect on mitochondria and are termed *mitocans* (mitochondrial targeting agents for the treatment of cancer).[32] Furthermore, Letai *et al.* have recently published a method to predict the efficacy of chemotherapies by measuring the balance of pro-apoptotic and anti-apoptotic proteins in the mitochondria of a patient's tumour cells *ex vivo*.[33]

DNA damage can cause a cell death cascade *via* release of p53 (causing apoptosis), PARP-1 (causing necroptosis) or HMGB1 (causing ICD, *vide supra*). For this reason, many chemotherapeutic agents target DNA in some form.

1.4 DNA targeting

1.4.1 Overview of DNA

DNA (deoxyribonucleic acid) is an information storage polymer, present mainly in the nucleus of the cell. This process is extraordinarily accurate, with 1 error for every 10^8 DNA bases.[34] The stability of DNA in a non-humid environment is such that 300,000 year old mitochondrial DNA has recently been sequenced.[34]

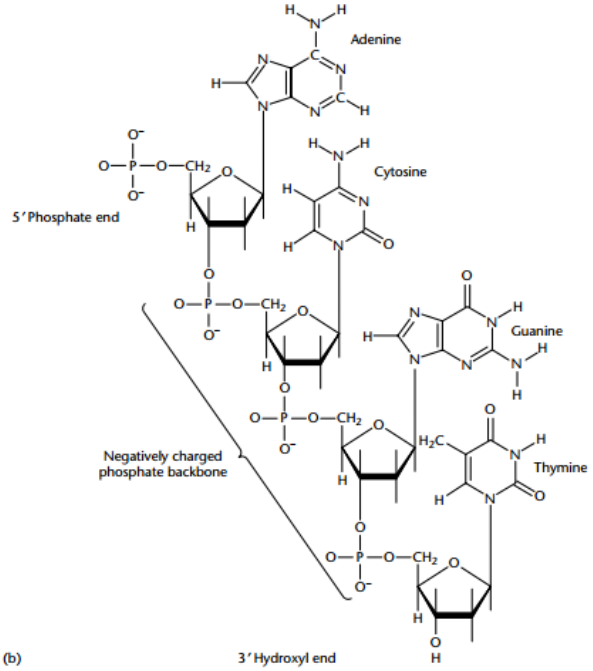

Figure 1.4.1.1. DNA oligomer showing ACGT oligomer.[35]

The monomeric building blocks of DNA (Figure 1.4.1.1) are nucleotides, containing a nucleoside and a phosphate group. These nucleosides are composed of 2'-deoxyribose and a nucleobase. The four DNA bases are two purines [adenine (A) and guanine (G)], and two pyrimidines [cytosine (C) and thymine (T)]. These monomers are connected in a primary sequence where the 3'-OH of the deoxyribose of one nucleoside is connected via an O-P(O)$_2$-O link to the 5'-OH of the next nucleoside. Each purine can forms HBs (hydrogen bonds) with a corresponding pyrimidine; thus, A-T interactions typically contain two HBs and G-C interactions have three HBs (Figure 1.4.1.2). In this way, DNA exists as a double-stranded helix.

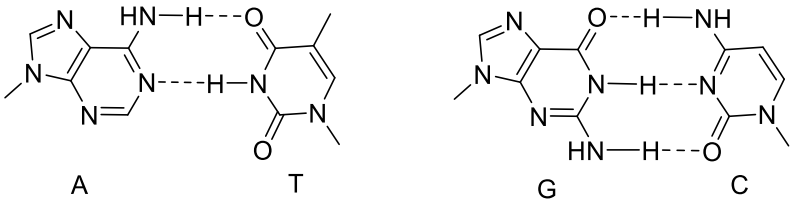

Figure 1.4.1.2. Watson-Crick interactions between DNA base pairs.[36]

This double helix is strengthened by π-π stacking interactions, especially between guanines stacked on each other. Also electrostatic interactions help to keep the hydrophobic bases on the interior and keep negatively charged phosphates in contact with bulk solvent and cations. Guided by the chirality of the deoxyribose unit, these structures are generally a right-handed helix. As shown in Figure 1.4.1.3, DNA can possess a helix whereby both grooves are the same size (termed "A-DNA") or where each groove is different (B-DNA). Poly-CG strands in very high salt concentrations (>4M NaCl) can adopt a left-handed helix with very wide grooves (Z-DNA).[36]

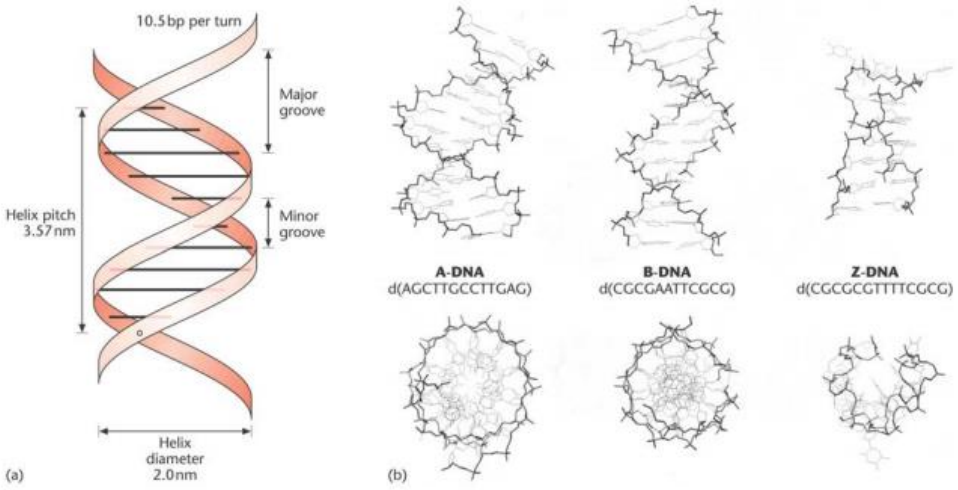

Figure 1.4.1.3. Schematic of B-DNA as proposed by Watson and Crick (*left*) and views along the axis and down the axis of A-, B- and Z-DNA from crystal structures (*right*).[35]

In long G repeats in DNA, most notably in telomers, the dsDNA can adopt a ssDNA stacked structure known as the G-quadruplex (Figure 1.4.1.4), important in protein recognition. Metal ions are required for stabilisation of these structures, which can be identified using Circular Dichroism (CD) or X-ray crystallography techniques. G-quadruplexes can also be found outside of telomeres, especially when stabilised by DAPI, which is a small molecule *bis*-amidine that acts as a minor groove binder (MGB).[37] The planar compound MM45 (Figure

1.4.1.4) was recently shown to inhibit growth of AR+ (androgen receptor positive) cancer cell lines by binding to the G-quadruplex of the AR promotor region, blocking transcription.[38] There are currently two quadruplex-based compounds in clinical trials: quarfloxin (CX-3543, Figure 1.4.1.4), designed to inhibit the G-quadruplex that initiates c-Myc transcription by disrupting a quadruplex-protein interaction;[39] and AS1411, a 26-base G-rich aptamer (short ssDNA sequence), which targets nucleolin, the same protein involved in the anti-cancer effect of quarfloxin.[40]

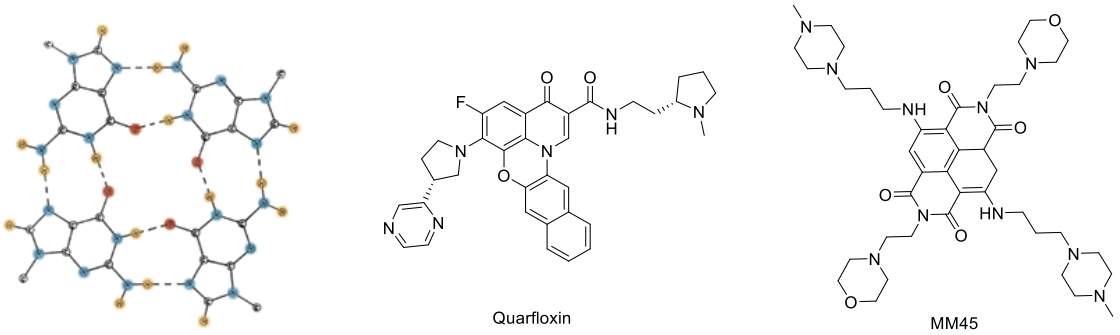

Figure 1.4.1.4. Structure of the G4 tetrad of a G-quadruplex,[39] and G-quadruplex binders Quarfloxin and MM45.

In the cell, DNA is confined mostly to the nucleus and is tied in a tertiary structure with positively-charged proteins called histones.[34] These histones contain a number of epigenetic markers that, depending on cell type and stress, force the histone to open and expose DNA at certain points or to close and hide DNA. When a cell is dividing, DNA needs to open completely to replicate its entire strand. However, when the DNA is being transcribed into RNA, it only needs to open an exon (DNA gene that eventually encodes a protein).

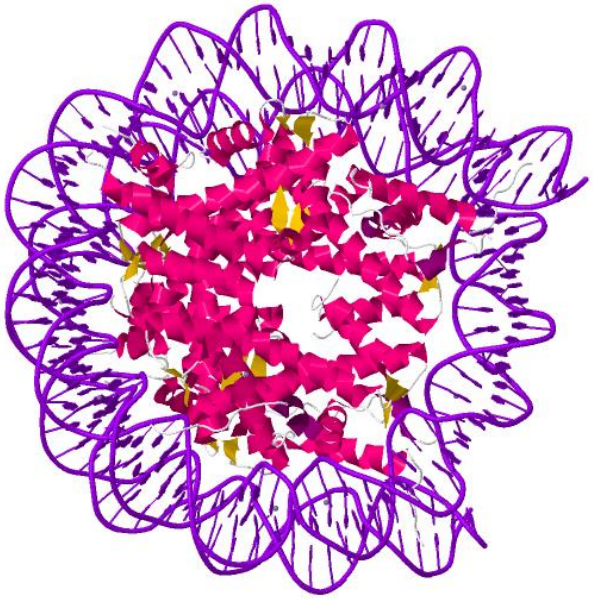

Figure 1.4.1.5. Crystal structure (1.9 Å) of two DNA strands (purple) wrapped around histone proteins (magenta).[41]

Besides nuclear DNA (nDNA), there exists a large quantity of mitochondrial DNA (mtDNA) in the cell. There are many differences between mtDNA and nDNA such as cellular location, morphology, copy number, repair and protein synthesis. Mitochondrial DNA (mtDNA) is located in discrete structures called nucleoids, in the cytoplasm of mitochondria. As opposed to nDNA chromosomes, each copy of mtDNA is a circular plasmid, encoding only 33 genes vital for correct mitochondrial functioning. The other 1000+ genes for proteins used in the mitochondria are all located in the nucleus. Different species contain different distributions of mitochondrial genes between mtDNA and nDNA.[34] Furthermore, the systems used for mitochondrial protein synthesis have not been fully established, but are inhibited by the antibiotic chloramphenicol, providing more evidence to the theory that mitochondria were originally bacteria engulfed by proto-eukaryotes and co-evolved in symbiosis.[34]

1.4.2 Main classes of DNA-targeting agents

Depending on their mode of binding, DNA-targeting chemotherapies can inhibit or strengthen protein-DNA interactions by binding directly to the protein (HDACi), to the protein-DNA ternary complex (intercalators) or to the DNA itself (MGBs and alkylators, Figure 1.4.2.1).

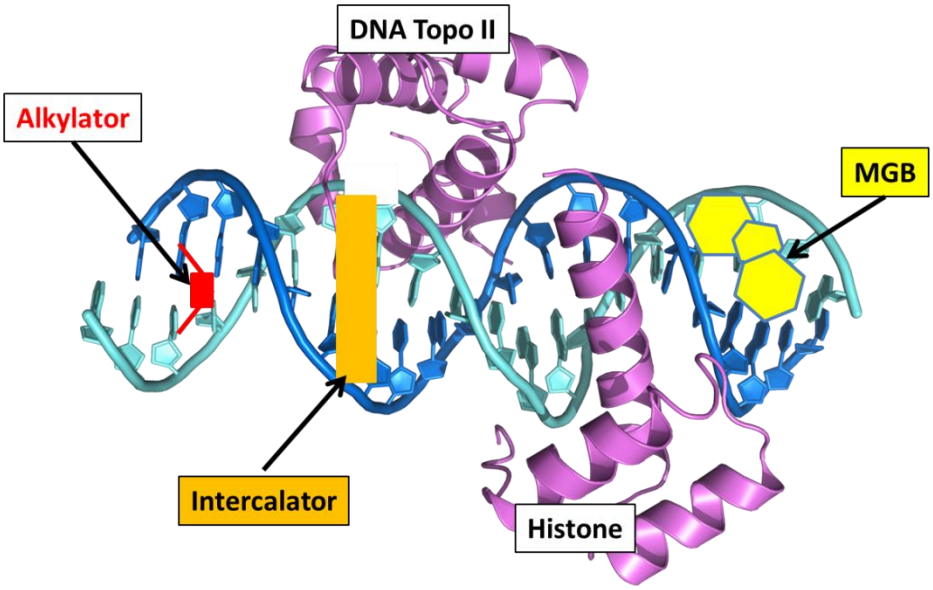

Figure 1.4.2.1. Key DNA-drug interactions.

One key DNA-interaction protein is the enzyme DNA topoisomerase I (topo I), required to relax supercoiled DNA, by introducing a single-stranded breakage.[23] The DNA rotates to relieve torsional stress and the breakage is repaired by topo I. The natural product camptothecin (natural product from *Camptotheca acuminate*, Figure 1.4.2.1) forms a ternary complex between DNA and topo I, blocking repair of the break.[23] Camptothecin suffered from poor water solubility, and after extensive derivatization, two analogues were approved by the FDA in 1996 for the treatment of solid tumours. Topotecan (Hycamtin®) is used to treat SCLC, ovarian and cervical cancers while irinotecan (Camptosar®) is approved for colon cancer. All three α-hydroxyester oxygen atoms (Figure 1.4.2.2) are required for topo I binding and the compound binds to DNA by intercalation across the DNA bases where the single strand break occurred.[23]

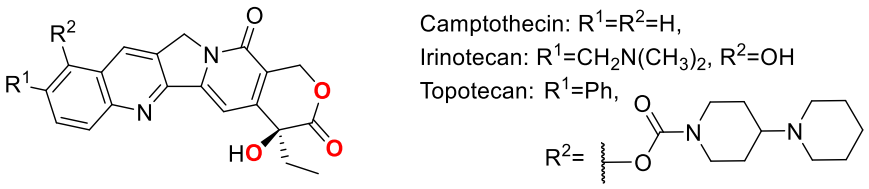

Figure 1.4.2.2. DNA topo I inhibitors irinotecan and topotecan and their parent molecule camptothecin.

Approved by the FDA in 1983, the clinically important drug etoposide (Figure 1.4.2.3) binds to DNA topoisomerase II (topo II) and DNA, forming a stable ternary complex, which prevents topo II from repairing specific DNA strand breaks. [42] The sugar and phenolic E-ring bind to topo II and the tetracyclic core intercalates into the distorted DNA bases. From crystal structure evidence, two molecules of etoposide are required to stabilise these distortions.[42]

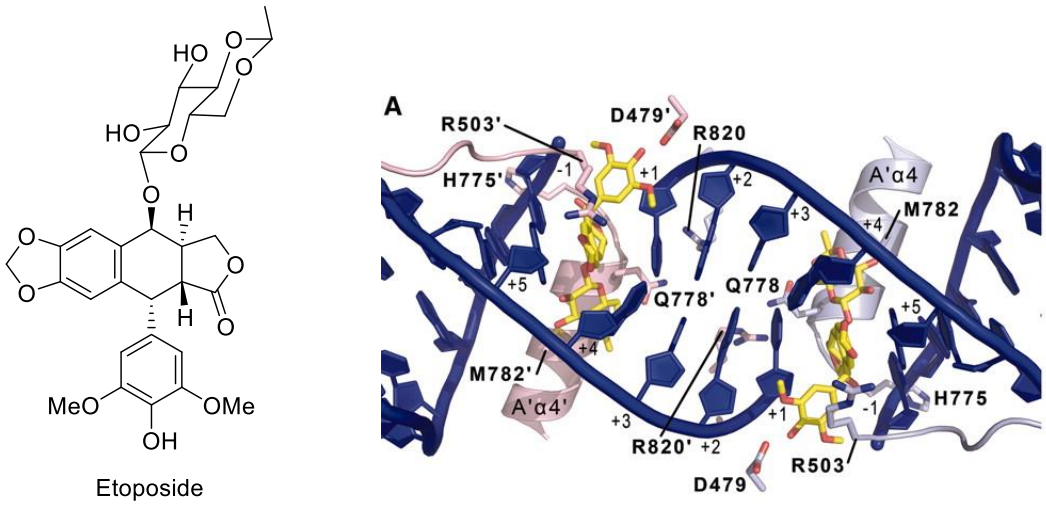

Figure 1.4.2.3. Etoposide and its interactions with DNA.[42]

Conversely, the Cu and Fe binder bleomycin (FDA approval in 1973), causes DNA double strand breaks that disrupt the structure of DNA, triggering apoptosis.[43] Although the transport of bleomycin to the nucleus is complicated, the active species is a Fe^{III} peroxide complex that forms a 4'-radical intermediate on deoxyribose, which results in sugar decomposition and dsDNA cleavage. The complex structure of bleomycin (Figure 1.4.2.4) contains, among other moieties, a pentadentate metal binding domain comprising a primary and a secondary amines, amide N atom, pyrimidine N-1 and imidazole N atom; a guanine recognition site containing only the HB donor acceptor pair of the 4-aminopyrimidine N-4 and N-3; a disaccharide that aids in DNA binding through an unknown mechanism; the DNA-binding bithiazole, that can interact either as a MGB or intercalator; and a positively charged tail that aids in electrostatic binding to DNA. The side-effect profile has little immunosuppression or myelosuppression, but the dose-limiting condition is pneumonitis (inflammation of the lungs) that occurs in up to 46% of patients, killing 3%.[43]

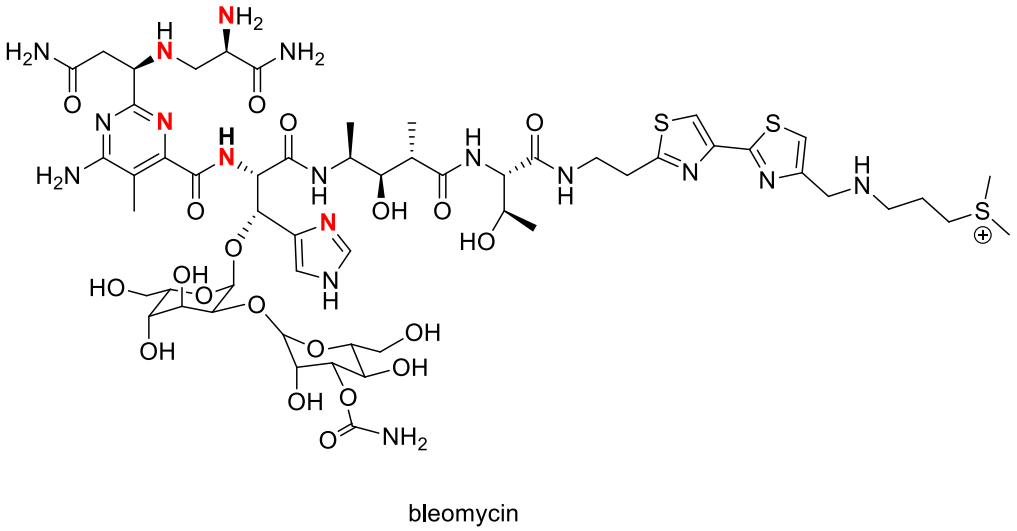

Figure 1.4.2.4. ROS generator bleomycin showing sites of Fe coordination in **red**.

Radical-promoted cell death cause by generation of reactive oxygen species is achieved in the clinic using a number of agents other than bleomycin. Photodynamic therapy (PDT) drugs like temoporfin, liberate ROS in the presence of light, damaging the DNA of exposed cells and causing necrosis by activation of caspases and PARP. [44] Only cells that receive light undergo cell death. Unfortunately, patients undertaking PDT are extremely light-sensitive and are required to stay away from sunlight and even bright rooms indoors. These drugs are limited by access to light- thus only melanomas or easily accessible tumours (by means of optic devices) are amenable to treatment.[44] TOOKAD®, the Pd complex of a bacteriophorbide, is currently undergoing clinical trials in prostate cancer.[45]

Intercalators

Chemotherapeutic agents that bind directly to DNA were some of the first anti-cancer drugs discovered. One important class of anti-cancer agents are intercalators. These anticancer compounds are large, hydrophobic, planar molecules that intercalate in between DNA bases through a combination of π-π stacking (between the intercalator LUMO and purine HOMO) and hydrophobic interactions and disrupt the shape of DNA. Cationic intercalators have a stronger DNA binding than neutral intercalators, due to both electrostatic effects and lowering of the intercalator LUMO.[22] Originally, it was assumed that their mode of action was by disturbing DNA in such a way that important recognition proteins cannot bind. In fact, this was not quite the case. It is now known that intercalators generally act by DNA topo

II inhibition. Intercalators create a ternary structure with DNA and topo II after a single strand break occurs, rendering the enzyme unable to complete the double strand breakage, and sterically blocking any other enzyme from repairing the break. For optimal activity, DNA intercalators need to bind strongly enough to DNA to stabilise the mentioned ternary complex, but the binding needs to be dynamic enough to allow the intercalator to detach from DNA and reattach to the DNA-protein binding region upon single strand breakage. For this reason, DNA binding constants, K_{DNA}, should be in the region of 10^3-10^4 M^{-1}.[18] DNA intercalators are routinely used as vehicles to attach other drugs or agents to DNA. Due to the range of derivatives, acridines with pendant amines or carboxylic acid residues are often used with this purpose (Figure 1.4.2.5). Interestingly, the anthracycline intercalators, e.g. doxorubicin (DXR), bind to haem-containing proteins, *e.g*. complex 1 of the mitochondrial OxPhos system (thought to be the cause of cardiotoxicity), and also specifically to mtDNA. Ethidium bromide also selectively depletes cells of mtDNA.[46]

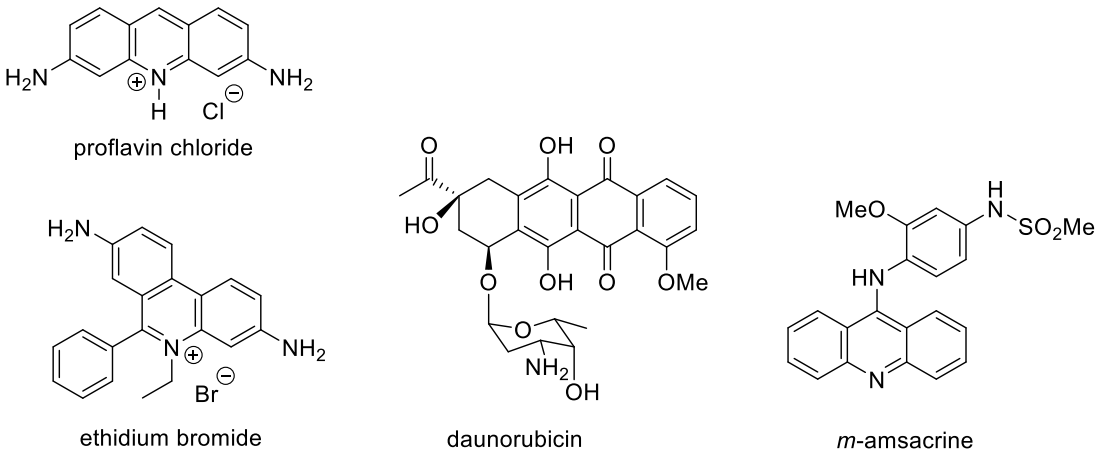

Figure 1.4.2.5. Selected DNA intercalators.

A tetracationic acridine *bis*-intercalator (Figure 1.4.2.6) binds specifically to 4-way Holliday junctions, vital in DNA replication events.

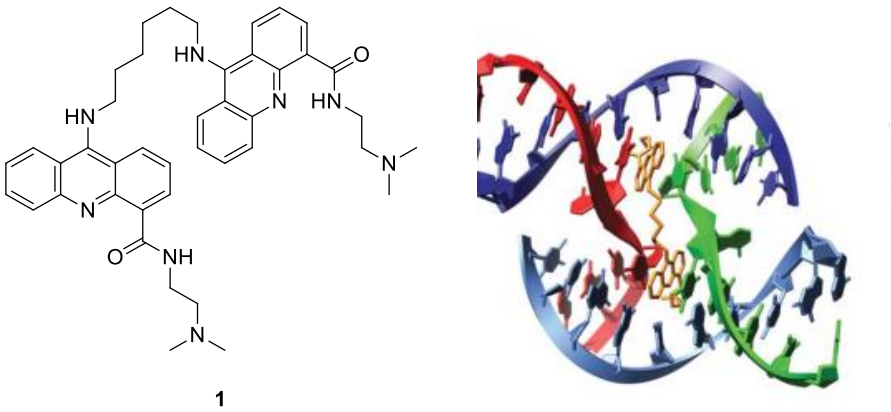

Figure 1.4.2.6. Diagram of *bis*-intercalator structure **1** alone and bound to 4-way Holliday junctions.

Alkylators

Alkylators are a very important class of compounds that form covalent bonds with DNA. Alkylators such as nitrogen mustards (*e.g.* melphalan, Figure 1.4.2.7) have been studied extensively as anti-cancer agents since World War II. Due to these covalent interactions (usually with N7 of guanine), DNA replication and transcription processes are altered and DNA repair proteins need to fix these errors.[18]

Nitrogen mustards are considered the first ever class of chemotherapeutic agents, and were discovered serendipitously in 1943; they are used in leukemias and generally form electrophilic aziridinium rings *in situ*. Most nitrogen mustards in the clinic have the ability to form two such electrophilic sites and predominantly form DNA interstrand crosslinks, but can also induce DNA-protein crosslinks.[18]

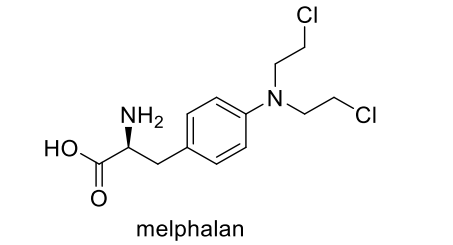

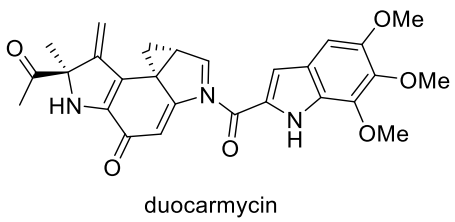

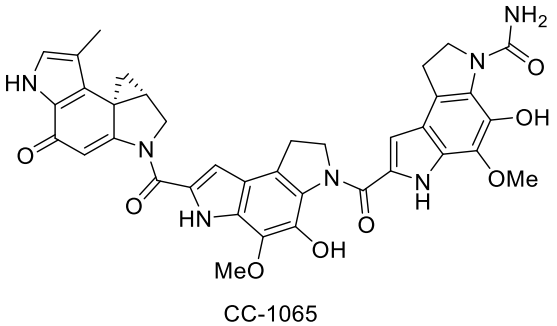

Figure 1.4.2.7. Alkylating agents including nitrogen mustard melphalan and minor groove-binding alkylators duocarmycin and CC-1065.

Another clinically relevant family, the duocarmycins, also bind covalently to DNA; however, with specificity for the adenine N-3 position in AT rich sequences. This can be partially explained by CC-1065 and duocarmycin's ability to bind to the DNA minor groove (Figure 1.4.2.7).[47]

Finally, a very important class of compounds that form a covalent bond to DNA through metals instead of alkyl groups are platinum-based "alkylating" agents. These will be discussed more in depth in Section 1.5.

Major groove binders: Zn finger domains

In the cell, protein affinity for specific exposed DNA regions, such as gene promotor regions, is necessary for correct functioning of the cell. Many DNA recognition regions of these proteins, including Zn finger domains, interact with major groove (Figure 1.4.2.1).[48] The major groove is large, and contains more base-specific groups than the minor groove, such as heteroatoms and methyl groups. The enormous size of protein subunits compared to small drug-like molecules means that proteins can take advantage of the large major groove by engaging in a range of non-covalent interactions. Protein binding to the major groove has an allosteric effect on the minor groove. Thus, when Zn finger proteins and polyamide MGBs were mixed in the presence of DNA they had a negative binding effect on each other- one compound binding, blocks the binding of the other. This negative cooperativity was shown by the authors to be an allosteric change in the minor groove when the Zn finger protein was bound.[48] The result indicates that small molecule binding in the minor groove may allosterically "displace" cell proteins from the major groove.

1.4.3 Minor groove binders

The DNA major groove is about twice as wide as the minor groove. Generally AT-rich regions have deeper minor grooves. In GC-rich regions, the exocyclic N atom on guanine points into the minor groove, blocking it. The minor groove has a *spine of hydration*, a tight, highly-organised network of hydrogen bound water molecules.[36] Hydrophobic interactions

that displace the spine of hydration cause a large entropic increase favouring the binding and for this reason, many proteins have DNA-recognition domains that strongly bind to the minor groove. In fact, transcription promoter regions, including TATA boxes, are rich in AT sequences and aid in initial binding of a transcription complex to the DNA exon.[36]

Many crescent-shaped, positively charged, planar small molecules are known to bind strongly to DNA minor grooves. These minor groove binders (MGBs, Figure 1.4.3.1) can disrupt the important protein-DNA interactions and have found application in the treatment of many diseases, including cancer, parasitic, bacterial and viral infections[36] Most of these drug-DNA interactions are non-covalent, but an exception is trabectedin which is known to both bind into the minor groove and alkylate DNA.[24]

The range of different MGB structures, in terms of planarity, length, hydrogen bonding and ability to covalently bind, indicates that these structures have different pathways to be taken up into the cell, have specificity for different DNA sequences and preferentially induce cell death in different organisms and cell types. The smaller *bis*-cationic moieties are thought to enter cells via OCT (organocation transporter) proteins whereas the larger polyamides may enter the cell through phagocytosis. [36]

Compounds that bind in the minor groove of DNA have a number of key characteristics. These compounds tend to be concave and possess two or more planar aromatic rings, are cationic in nature and have the ability form hydrogen bonds. The aromatic rings are lipophilic and displace water molecules from the spine of hydration along the DNA minor groove. [49] The compounds are cationic, allowing them to interact electrostatically with the overall negative charge of DNA and to the negative potential at the floor of the minor groove.[49] Crystal structures of DNA with metal cations localise in the minor groove of AT-rich regions.[50] Many MGBs form H bonds with the A and T bases in the bottom of the groove in the adenine N3 and thymine O2.[49]

A huge amount of research has taken place in this area. Most notably, *bis*-amidines such as pentamidine, furamidine and berenil have been used clinically to treat trypanosomal infections in humans and animals and the DAPI stain is a fluorescent MGB used to pinpoint the nucleus in cell staining (Figure 1.4.3.1).[51] The Hoechst dyes are another important class of molecules that use benzamidines and amines to retain solubility (Figure 1.4.3.1).[51]

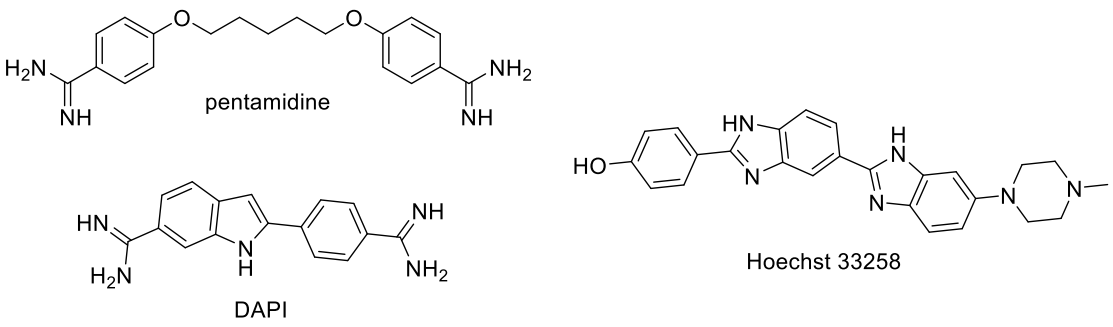

Figure 1.4.3.1. Small molecule MGBs.

More clinically-relevant compounds include the polyamide class of MGBs (Figure 1.4.3.1), for example distamycin A, which binds to the minor groove but is devoid of anticancer effects. The dual drug derivative, tallimustine, which incorporates a nitrogen mustard, was ineffective in humans, giving one four month partial remission out of 42 patients with malignant mesothelioma (cancer of the lining of the lung). [24] The dose limiting toxicities were neutropenia and thrombocytopenia (low neutrophil and platelet count respectively). [24] Unsurprisingly, the drug fared better in AML (Acute Myeloid Leukemia), a blood cancer, with 4 out of 26 patients responding to treatment. The most promising distamycin-based treatment in clinical trials is the guanidine-containing bromoacryloyl derivative brostallicin. Interestingly, brostallicin is activated by high glutathione levels, making the drug selective for drug-resistant tumour cells (Figure 1.4.3.2). The side effects were much less severe than tallimustine in a phase I study, and 6 patients demonstrated a response in advanced solid tumours.[24]

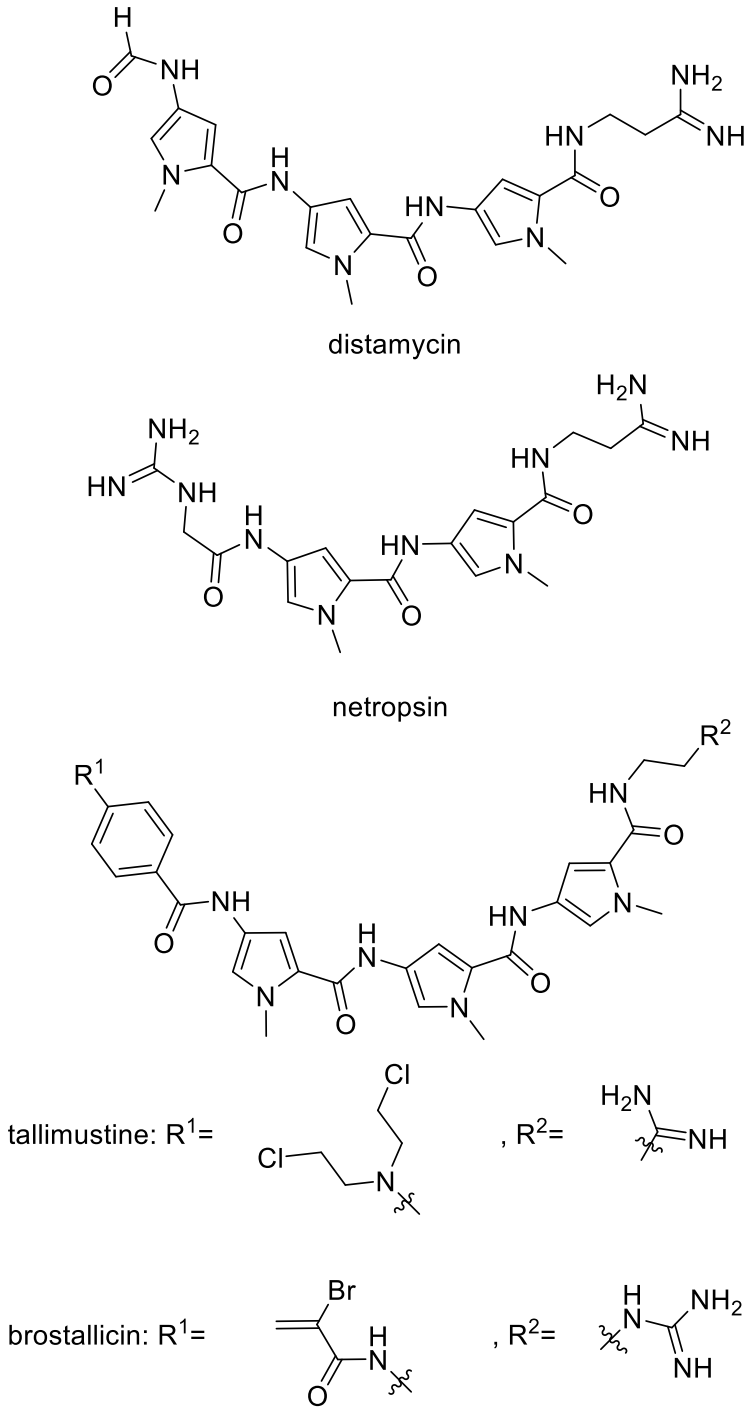

Figure 1.4.3.2. Distamycin-derived alkylating MGBs tallimustine and brostallicin.

Attaching electrophilic groups to MGBs has proven fruitful in the clinic. The most successful of these partnerships is undoubtedly trabectedin (Yondelis®), a natural product that prevents transcription of the MDR1 gene (multi-drug resistance pump 1), as well as binding to guanine N2 in the minor groove (Figure 1.4.3.3).[24] The electrophilic carbinolamine moiety is in

equilibrium with a reactive iminium cation *in vivo*, with the pentacyclic core binding to the DNA minor groove. The tetrahydroisoquinoline is unnecessary for activity. The drug is particularly successful in myxoid liposarcoma, a rare soft tissue tumour.[24] Trabectedin was approved by the FDA in October 2015 for soft tissue sarcoma.

Based on the natural products neotrypsin and distamycin, medicinal chemists were able to design polyamides that had sequence specificity for short DNA sequences. These MGBs have an antiviral effect, which is thought to be by disrupting the virus's attachment process to the host cell and not by binding to DNA at all. In fact, it is possible that many MGBs may have their anti-infective effects by non-DNA-binding mechanisms.

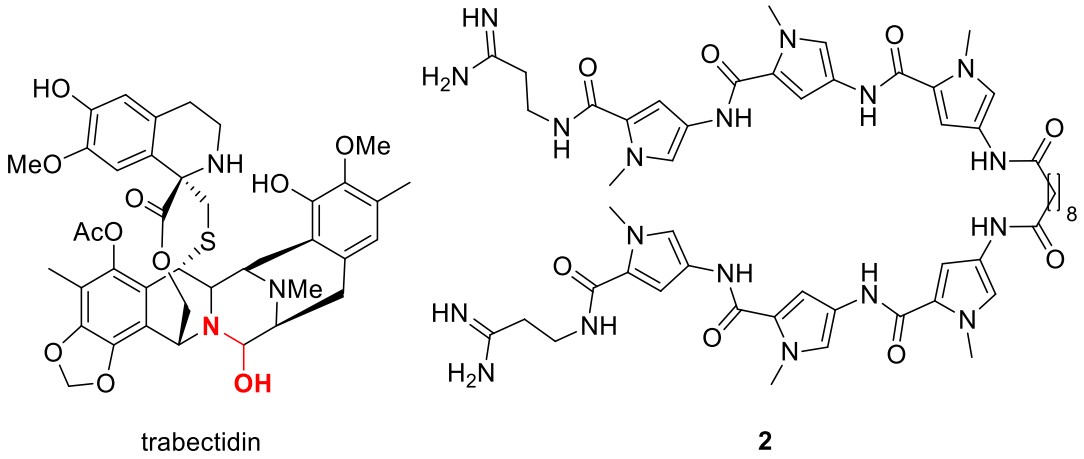

Figure 1.4.3.3. MGB trabectedin (Yondelis®) with electrophilic aminal in **red**. Also shown is a hairpin MGB **2**.

MGBs are not only useful in treating cancer. In fact, much of the recent interest in MGBs has been in the field of anti-parasitic infection. For example, pentamidine isethionate (Figure 3.1.1) was first approved in 1956 in France as an intravenous second-line treatment for human African trypanosomiasis (African sleeping sickness) and it is also used by inhalation to treat pneumonia caused by trypanosome infection, typically in HIV-infected patients. Pentamidine is transported into trypanosome cells *via* high-affinity pentamidine transporter 1 (HAPT1) and P2 aminopurine transporter (P2). Pentamidine-resistant cell lines have been cultured in laboratory conditions that do not express these transporters. However, while field reports of pentamidine resistance in patients are scarce, its main problems are its side effect profile, which includes nephrotoxicity, severe hypotension, hypoglycemia, acute pancreatitis and cardiac arrhythmia; as well as pentamidine's inability to cross the blood-brain barrier

(BBB).[52] Therefore, a number of second generation anti-typanosomal *bis*-amidines have been developed for clinical use, with two compounds developed by Wilson and Boykin reaching clinical trials: furamidine (DB75, Figure 1.4.3.4) and its *N*-methoxy prodrug DB289.[53] Preclinical candidates such as the substituted *bis*-amidine (DB829) and its *N*-methoxy prodrug (DB868) recently gave excellent results in murine and velvet monkey models of the disease, with excellent BBB permeability.[53]

Boykin and Wilson's *bis*-amidines were designed to target AT-rich minicircles in the mitochondrial kinetoplasts (kDNA) in *Trypanosoma brucei*, *T. cruzi*, *Leishmania* and related organisms. Fluorescence and electron microscopy demonstrated that kDNA is significantly altered shortly after diamidine treatment, and the kinetoplast organelle itself is destroyed after 24 h, followed by death of the parasite. However, DNA binding measurements do not always correlate with anti-trypanosome activity, suggesting that other mechanisms of action, including topoisomerase II inhibition, are to be considered.[54] In general, the activity of these *bis*-amidines correlates well to BBB permeability, suggesting that pharmacokinetics of entering the kinetoplast are as important as DNA binding.[55] Possible non-nucleic acid targets of pentamidine include the family of SOCS enzymes and heparin-like oligosaccharides.[56,57]

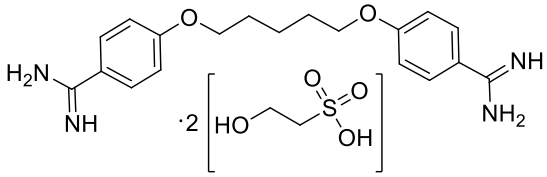

Pentamidine isethionate

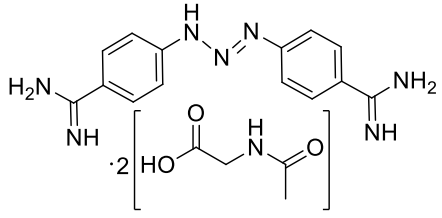

Berenil, diminazene diaceturate

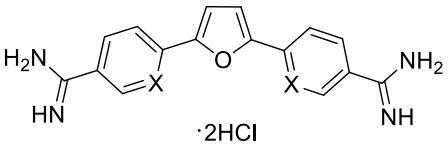

X= CH Furamidine, DB75
X= N DB829

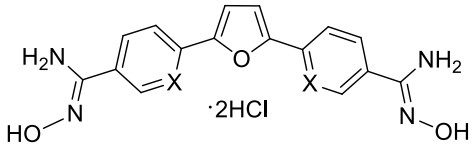

X= CH DB289
X= N DB868

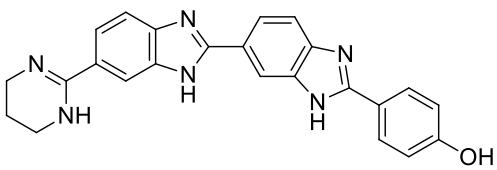

DB173 (IC_{50}= 177 nM against N. fowleri)
SI over J774 murine macrophages= 44.6

Figure 1.4.3.4. Known di-aryl *bis*-amidines with anti-parasitic activity.

Furthermore, the *bis*-benzimidazole DB173 (Figure 1.4.3.5), which was highly active (IC_{50} = 117 nM) in a high throughput screen against *Naegleria fowleri*, contains an amidine-like system in the form of a tetrahydropyrimidine (THP).[58] This free-living amoebae strain is the causative agent of primary amoebic meningoencephalitis (PAM), a fatal disease affecting hundreds of people, mostly in the developed world, of which only three people have been documented to survive.[58] Of a broad range of *bis*-benzimidazoles the THP group of DB173 was essential for strong cytotoxicity and very high selectivity index over mammalian cells.[58] In veterinary medicine, another known DNA MGB berenil® (Figure 3.1.1), is well tolerated in cattle in Africa and Asia as an anti-parasitic administered by injection.[53]

Besides the Rozas group (as discussed in Section 1.5.7), Wilson and Boykin as well as Dardonville have prepared and tested a range of molecules as AT-selective DNA MGBs and some interesting examples are shown in Figure 3.1.2. For instance, the linear derivative DB921 utilises an interstitial water molecule to obtain sufficient curvature to strongly bind into the minor groove.[59] To probe the activity of other linear *bis*-cationic molecules, 2,7-substituted fluorene **3**[60] and 3,6-substituted acridine **4**[61] were synthesised by Wilson and Boykin from their corresponding commercial diamines and tested for DNA binding. Fluorene **3** retained minor groove binding activity whereas acridine **4** was shown to intercalate into DNA. Extended furamidine-type *bis*-amidine DB1851 was shown to increase DNA binding compared to furamidine in AT-rich pockets. Furthermore, substantial lengthening of the cations and addition of a pyridine core as in DB2120 resulted in high selectivity for AAAAGTTTT regions, aided by H-bonding between the pyridine N atom and the guanine NH_2 group.[62] Hence, the effect on DNA binding of a rigid core should be further explored.

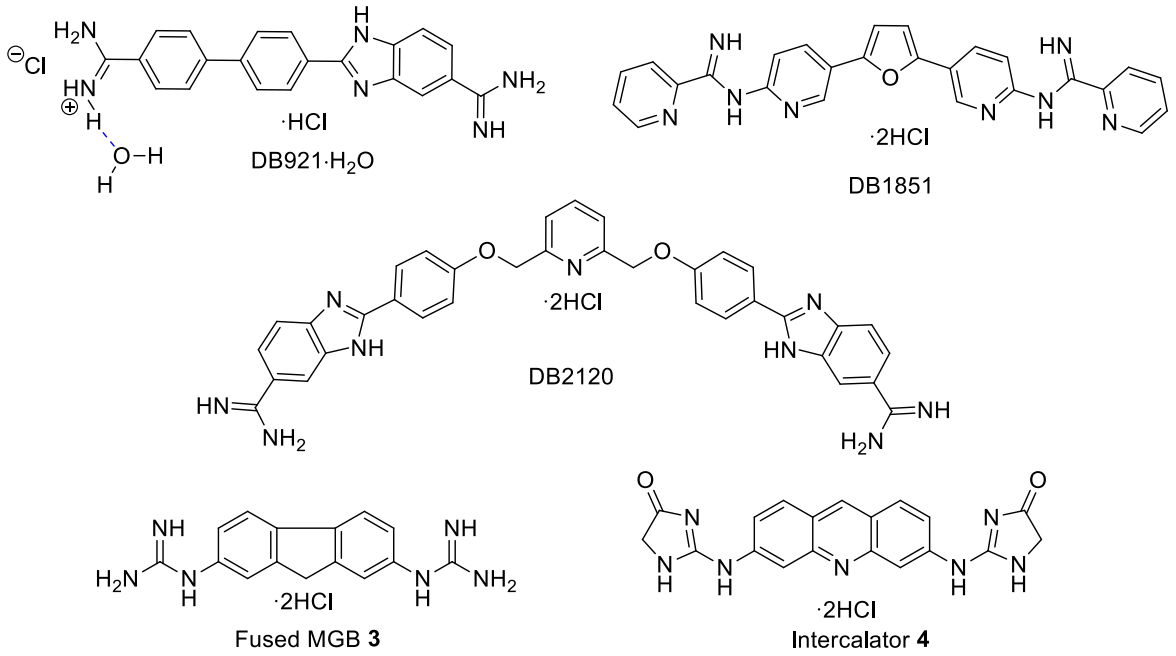

Figure 1.4.3.5. Some interesting DNA binding molecules: DB921,[59] DB1851,[62] DB2120,[62] fused MGB **3**,[60] and intercalator **4**.[61]

A library of arylguanidine-based MGBs has been designed in the Rozas lab. These compounds will be discussed in Section 1.5.7.

1.4.4 Characterisation of DNA- binding agents by biophysical methods

To determine whether a compound binds to DNA as well as the mode of binding, a number of biophysical techniques are available. DNA thermal denaturation,[63] SPR (Surface Plasmon Resonance)[64] and STD (Saturation Transfer Difference) NMR[65] can be utilised to quantitatively measure binding to a specific DNA oligomer or an *ex vivo* DNA extract from salmon testes or calf thymus. Furthermore, to determine whether a compound binds covalently or non-covalently, a competitive inhibition assay can be performed and the most usual is by displacement of a known (usually fluorescent) ligand from DNA, *e.g.* ethidium bromide. Knowing the binding constant of this ligand, it is possible to calculate a binding constant for the test compound.

A compound can potentially bind non-covalently to a host of regions: the major groove, the minor groove, intercalated between the DNA bases, electrostatically to the phosphates or

bound to G-quadruplexes. Compounds that bind covalently generally bind to the N7 of guanine as it is the most nucleophilic site (DNA-binding compounds tend to be electrophilic).[18] In solid phase of course, it is possible to obtain crystal structures of compounds bound to short DNA oligomers. The palindromic Dickerson and Drew dodecamer is widely used as a binding model since it crystallises easily and in the B-DNA form.[66,67]

However, the behaviour of DNA in solid phase is not necessarily the same as in solution. It is thus preferred to use many solution phase techniques. A standard method for calculating the strength of DNA binding is by its Thermal Denaturation. Double-stranded DNA (dsDNA) will become denatured (split into two strands of ssDNA) under a range of conditions, including increasing temperature, salt concentration, acidity or basicity.[63] This titration can be followed by an increase in UV absorption. DNA thermal denaturation experiments provides with a melting temperature (T_M) where half of the DNA is double stranded and half is a single stranded random coil. When a compound is added and binds to DNA, it stabilises the dsDNA, increasing its T_M. This increment in T_M, called ΔT_M, is a measure of a compound's affinity for DNA.[63] The value of ΔT_M is dependent on salt concentration, buffer composition, pH, rate of heating, ratio of DNA base pair to drug (expressed as phosphate to drug ratio or P/D) and composition of the DNA oligomer. ΔT_M values for a range of compounds (ligands for DNA) where the previously mentions variables are held constant give a good measure of the order of dsDNA affinity of these compounds, as long as the compounds have a similar binding site size. For example, if the reaction kinetics are first order in DNA and in the ligand, then the size of the binding site can be measured by comparing the ΔT_M vs. P/D ratio.[63] Since the T_M of a DNA oligomer changes markedly depending on base composition, a quick, albeit prohibitively expensive, method to determine sequence specificity of a compound is to perform the thermal denaturation using equimolar concentrations of many DNA oligomers. The experiment is performed with and without the compound of interest and the ΔT_M is measured by comparing the shift in sigmoidal curve for every DNA sequence. In practice, this is carried out accurately by a computer-generated first derivative of the data (Figure 1.4.4.1).[63]

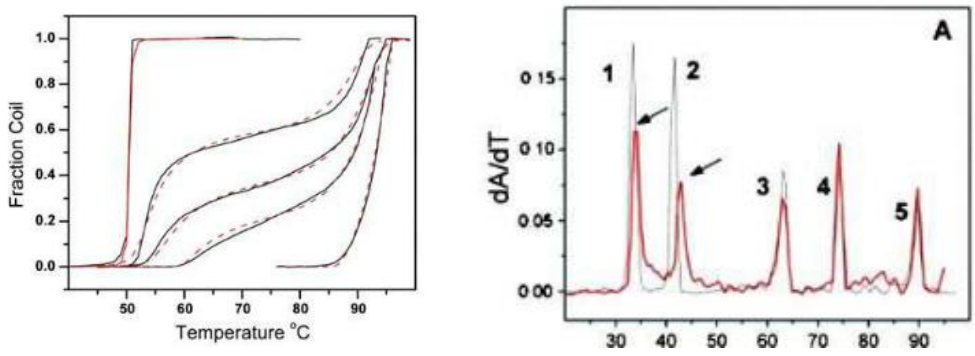

Figure 1.4.4.1. Left shows netropsin thermal denaturation curves at constant *poly dA:poly dT* DNA concentration (45 μM) shifting to the right with increasing drug concentration (0-12.6 μM). Right shows selectivity of netropsin (2 μM) against five DNA oligonucleotides ([bp]=40 μM per oligo).[63]

A crude measurement of binding can be achieved by measuring the binding of a ligand to AT-rich DNA oligomers *vs*. GC-rich oligomers. In general, compounds that bind to AT-rich regions are MGBs whereas compounds that bind to GC-rich regions are either major groove binders or intercalators. This can be explained by the stronger π-stacking interactions of guanine and the N3 of guanine blocking the minor groove. Where a compound binds similarly to AT-rich and GC-rich sequences, the compound can have base-independent mode of binding, such as phosphate clamp or simply electrostatic interactions with the phosphate group, an example of this type of compouds is the polyamine spermine.[67,36]

Routinely, CD (circular dichroism) and LD (linear dichroism) are used to determine DNA-binding modes of ligands. DNA bases, though planar, are in a chiral environment due to being close to the chiral deoxyribose sugars and also by being in a right-handed helix. As a result their chromophores are chiral and absorb left- and right-handed circularly polarised light differently. When an achiral ligand is bound in the groove it absorbs asymmetric electronic transition moments and gives rise to a large induced circular dichroism (ICD) peak. This signal can be used to measure the binding constant to DNA. Unfortunately, this is difficult to do as the mode of binding is concentration-dependent. There are many DNA-binding compounds that have a number of binding modes; for example, minor groove binders are known to stack on top of each other at high concentrations. This gives rise to very large exciton coupling of the two identical electronic transition moments and leads to a very large ICD signal.[68]

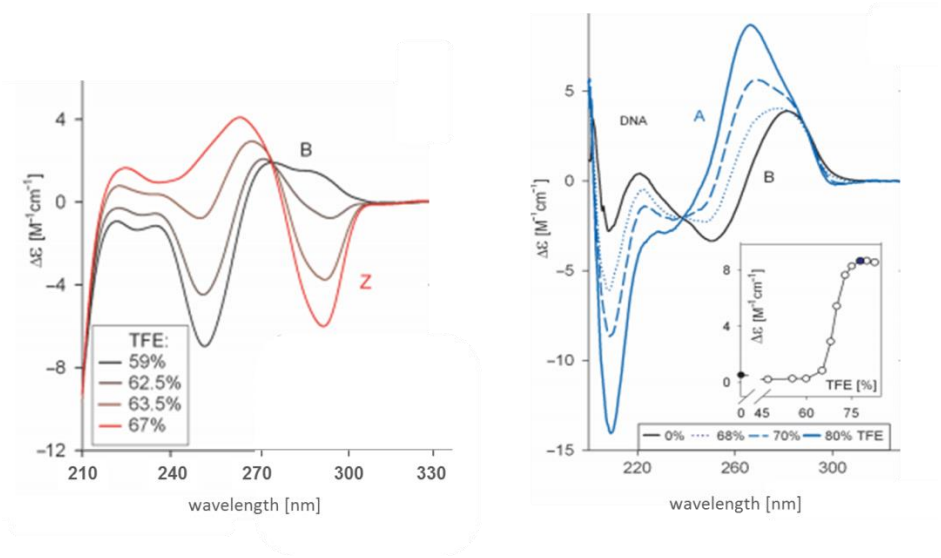

Figure 1.4.4.2. CD spectra of B-Z transition (*left*) and B-A transition (*right*) of two DNA oligomers upon trifluoroethanol addition. [69]

CD is a powerful tool for determining the secondary structure of DNA. Figure 1.4.4.2 shows different DNA oligomers undergoing B-Z and B-A transitions when exposed to increasing concentrations of trifluoroethanol (TFE).[69] Since Z-DNA is a left-handed helix, the shape of the graph changed from a negative trough at 255 nm and positive peak at 280 nm for B-DNA to a positive peak around 255 nm and negative trough around 280 nm. However, in the B-A transition, The shape of the graph is similar, but the magnitudes and λ_{max} shifted as the major and minor grooves of B-DNA averaged to the almost symmetrical groove width of A-DNA over the course of the titration. These conformational changes induced a measurable difference in how the macromolecule absorbed circularly polarised light.

LD makes use of plane-polarised light. The compound has to be positioned along an axis (generally by flow) and light is shone in the plane of the flow as well as in the plane perpendicular to that of the flow. Whether the magnitude of the difference is positive or negative, can indicate whether the DNA is bound to an intercalator (absorbs light perpendicular to the flow) or a minor groove binder (absorbs light in the plane of the flow).[68]

In summary, techniques to detect and assess DNA binding, such as thermal denaturation and CD in particular, can provide qualitative and quantitate data on the strength of binding and mode of interaction of ligands to DNA in solution.

The next few sections will describe the status of DNA-binding platinum-based drugs, especially cisplatin, in the clinic and in preclinical development. The modes of DNA binding

of these drugs will be presented and the field of Pt-drug conjugates will be surveyed. Other metal-based anti-cancer agents will be briefly summarised and the previous work in the Rozas group towards DNA-binding molecules and anticancer agents will be discussed.

1.5 Metal Complexes with Anticancer Activity

1.5.1 Cisplatin: A Platinum-Based Alkylating Agent

Since the accidental discovery by Rosenberg in 1969 of the anticancer properties of *cis*-diamminedichloroplatinum(II) (cisplatin),[70] Pt-based alkylating agents have been widely studied, tested and derivatised.[71] At present, three Pt-based anticancer drugs are in clinical use worldwide: the parent molecule cisplatin, FDA-approved in 1978, and its analogues carboplatin, approved 1992, and oxaliplatin, approved 2002 (Figure 1.5.1.1). Their biological action is initiated by losing one or both of their leaving groups (chloride or a carboxylate group) by the nucleophilic attack of water. The electrophilic aqua species is then subject to further attack from electron-rich DNA purine bases. Cisplatin preferentially attacks guanine N7 due to greater basicity of the guanine N and favourable H-bonding with guanine O6 compared to repulsive interactions with the N6 HB donor on adenine.[72]

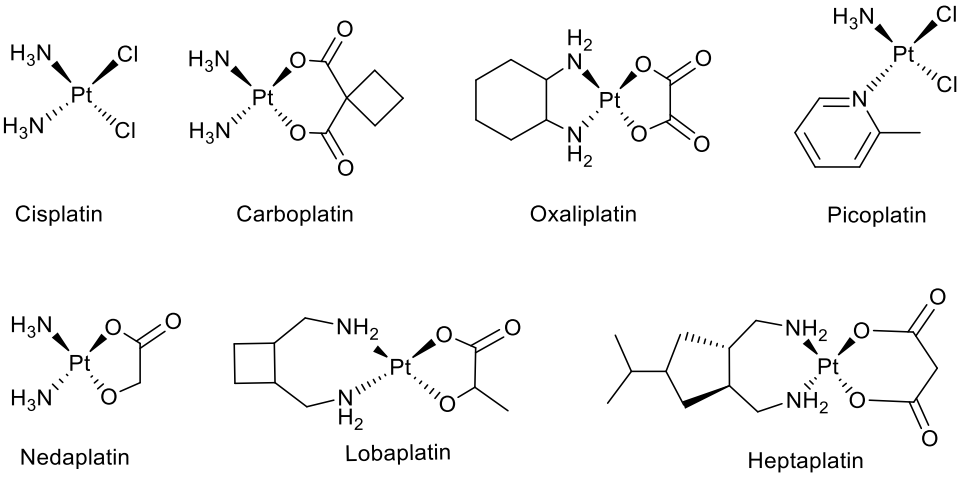

Figure 1.5.1.1. Traditional Platinum based anticancer drugs.

Owing to its *cis*-geometry, the species can react again with another purine base on the same strand, forming either 1,2- or 1,3- intrastrand crosslinks.[73] These crosslinks are heavily strained around the DNA-Pt-DNA angle. Binding of HMG (High Mobility Group) proteins to

this complex forces the angle around Pt to almost 90°, greatly easing the steric strain (Figure 1.5.1.2). These Pt-DNA-HMG adducts are highly stable and prevent access by nucleoside excision repair proteins and also block the transcription factor NF1.[71] If the concentration of Pt adducts is high enough, HMG proteins could cease binding to other sites, causing downstream effects leading to cell death. Another mechanism of anticancer action is that DNA mismatch repair enzymes can attempt futile repair of the DNA strand opposite to that of the Pt adduct. Constant formation of DNA nicks can eventually trigger apoptotic pathways. A reason as to why cisplatin is so effective against testicular cancer in particular is that testes produce a specific variant of the lysine-rich histone H1 protein. This isoform has higher affinity for cisplatin-modified DNA than for unmodified DNA, preventing transcription and replication of the cell.[71]

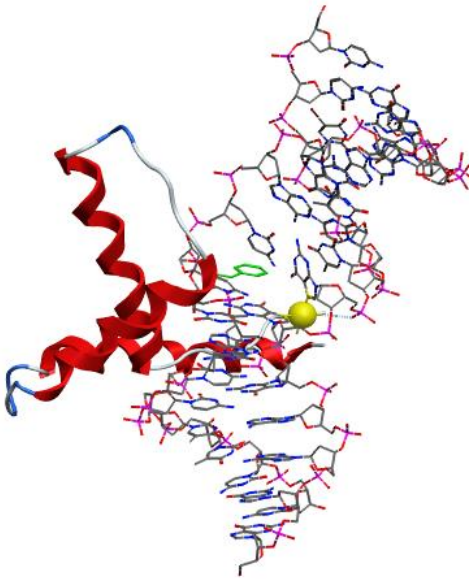

Figure 1.5.1.2. Crystal structure of cisplatin (yellow) covalently bound to DNA oligomer and non-covalently binding to HMGB1 domain (red ribbon) showing important intercalation of phenylalanine residue (green).

Recent literature has uncovered evidence that mitochondria are implicated in cisplatin action. One study illustrates selective binding of cisplatin to mtDNA over nDNA. This is attributed to comparatively less repair of these Pt-mtDNA adducts.[74,75] Moreover, cisplatin binds to, and is sequestered in mitochondrial voltage-dependant anion channels (VDACs).[74]

Cisplatin can be synthesised from iodoplatin (**10**), which is made from K_2PtCl_4 (**5**). Treatment with excess KI precipitates out KCl to give K_2PtI_4 (**6**, Scheme 1.5.1.1),[76] which has no

isomers as all ligands are identical. However, reacting **6** with 2 equivalents of aqueous $AgNO_3$ gives exclusively the *cis*-diaqua isomer (**9**).[76] It is widely accepted that the *trans effect* of ligands accounts for this.[77] Most reactions at Pt^{II} employ an addition-elimination mechanism *via* a 5-membered trigonal bipyramidal intermediate, **4**.[77] The geometry of the intermediate, as the leaving group dissociates, determines the *cis*- or *trans*- configuration of the remaining ligands. The 18 valence electron intermediate is stabilised by donation of electrons into empty π orbitals of strong π-accepting ligands, such as CO and alkenes. Strong σ-donors, *e.g.*, H^- and CH_3^- can make complexes more reactive by destabilising the bond *trans* to the ligand in the square planar complex.[77]

Scheme 1.5.1.1.

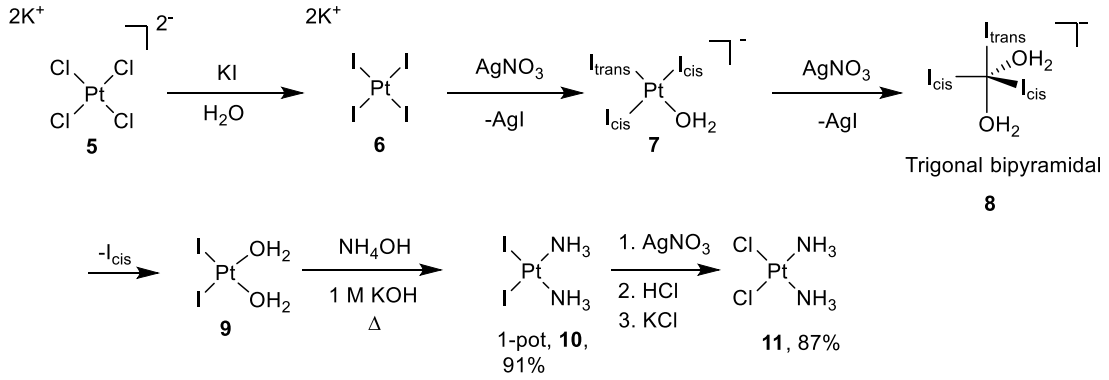

This knowledge can be used to direct the formation of *cis*-complexes. Addition of one equivalent of $AgNO_3$ to **6** in H_2O precipitates AgI to give an aqua complex **7** with two chemically inequivalent iodo ligands, *cis* and *trans* to the aqua ligand, *i.e.* an I *trans* to H_2O (I_{trans}) and I trans to another I (I_{cis}). Since I is a stronger σ-donor than H_2O, the I *trans* will be more destabilised and will form a trigonal bipyramidal intermediate **8** with both I_{cis} ligands on the equatorial plane. This will collapse to give the *cis*-diaqua complex **9**. Similarly, when a source of ammonia is added, the ligands *trans* to I, *i.e*. aqua, are lost to form iodoplatin, **10**. Addition of a further 2 equivalents of $AgNO_3$ in the absence of light precipitates out the iodo groups to give a *cis*-diaqua intermediate, as before. Excess $AgNO_3$ is quenched in 1M HCl and subsequently KCl is added, forming cisplatin, **11**.[76]

1.5.2 Traditional Platinum-based anticancer agents

Cisplatin (Platinol®) has shown miraculous efficacy in ovarian, head and neck, and especially testicular cancer, which 60 years ago suffered from a 10% five year survival rate. Due largely to a combination therapy of bleomycin, etoposide and cisplatin (BEP), 98% of men diagnosed with testicular cancer in the UK today will survive longer than five years.[16] However, cisplatin suffers from many serious side-effects including severe nausea, vomiting in almost all patients and cumulative ototoxicity (permanent loss-of-hearing) especially in children, but a remarkable lack of myelosuppression (reduction in number of blood cells derived from bone marrow- occurring in just 25-30% of patients) compared to antimetabolites, other alkylating agents and anthracyclines. Early clinical trials demonstrated that cisplatin causes substantial nephrotoxicity. Extensive pre-hydration protocols using 1-2 L of saline solution, then long infusion times (6-8 h) with the drug dissolved a total of 2 L saline or 5% dextrose solution, followed by monitoring of hydration and urinary output for 24 h post-infusion have largely circumvented the nephrotoxicity effects. However, geriatric patients in particular are still susceptible to kidney failure. Anaphalactic-like symptoms are also reported to occur within minutes of exposure to cisplatin in a small number of cases. Standard anti-inflammatory drugs such as adrenaline, corticosteroids and antihistamines are sufficient to control these symptoms.[71]

Carboplatin (Paraplatin®, Figure 1) was designed as a safer analogue. Medicinal chemists correctly hypothesised that the chloride leaving groups of cisplatin were too reactive to the nucleophilic attack of water, and subsequently to the nucleophilic attack of sulfur in proteins in the cytoplasm. A bidentate dicarboxylate ligand without metabolically active α-hydrogens was designed and tested as a replacement of the two chloride leaving groups but the *cis*-ammines (metal-bound NH_3 groups), thought to be of importance in hydrogen bonding to DNA bases, remained. Carboplatin was just as effective as cisplatin in ovarian cancer but not in testicular or head and neck cancers. Remarkably, no loss of hearing and little nausea and vomiting were reported as side effects. The most common of these were bone-marrow suppression and hair loss, the latter not described in cisplatin administration.[71]

Cisplatin and carboplatin suffer from cross-resistance, i.e. if a tumour stops responding to one it will not respond to the other drug either. A third drug candidate was then developed, this time by slightly varying the nitrogenous groups. Oxaliplatin (Eloxatin®, Figure 1) contains a 1-(*R*)-2-(*R*)-diaminocyclohexane ligand (DACH) instead of the ammines and also replaced

the bidentate ligand with an oxalate group. It shows no cross-resistance with cisplatin or carboplatin and is on the market as a chemotherapeutic agent for colorectal cancer, in combination with 5-fluorouracil and folinic acid (collectively named FOLFOX) or the topo I inhibitor irinotecan.[71] Oxaliplatin presents none of the dose-limiting side effects of cisplatin or carboplatin but reversible sensory neuropathy (patients complain of "tingling" sensations in their mouths at first and this gradually spreads to their extremities as the therapy continues) is well-documented. Discontinuation of the therapy coincides with cessation of these sensations. [78,79] Production-wise, carboplatin is synthesised analogously to cisplatin, using sodium cyclobutane-1,1-dicarboxylate instead of KCl.[80] Oxaliplatin is made by reacting *cis*-$PtI_2(OH_2)_2$ with (R,R)-1,2-diaminocyclohexane and treating the resulting complex with aqueous $AgNO_3$ and sodium oxalate.[80]

All of these complexes enter the cell *via* passive transport through Cu transporters Ctr1 and Ctr2 as well as active transport through human organocation transporters hOCT1-3. The efflux of cisplatin and related compounds is mostly through P-type active transporters ATP7A and ATP7B, among others.[81] Ctr1 expression in cancer cells generally indicates good outcomes in patients while high Ctr1 expression in the renal tubules is a likely cause of nephrotoxicity. In mice, the inner and outer hair cells of the cochlea and surrounding nerve cells express Ctr1, implicating the receptor in ototoxicity. Both Ctr1 mutation and ATP7B expression in tumours correlates well with a poor patient outcome in cisplatin treatment. The mechanism of cisplatin transport through Ctr1 is unknown but may not be directly analogous to Cu transport. Ctr1 is inhibited by Ag^I ions and not by divalent cations, implying that Cu^I is the substrate for Ctr1. Copper enters the cone-like Ctr1 (Figure 1.5.2.1) through Cu chaperone proteins, passing from the 8 Å extracellular entrance to the 22 Å wide exit on the cell interior through the membrane. Unbound to any other ligand, Cu dynamically changes its inner sphere coordination through four levels of three methionine residues each, followed by a histidine ring and finally a cysteine ring, where Cu attaches to the intracellular transport protein ATOX1. Cisplatin (≈7 Å in diameter) can fit through the exterior pore and may lose Cl ligands as it travels through the pore. Cisplatin bound to ATOX1 has been observed and ATOX1 is known to translocate to the nucleus upon Cu exposure, providing an interesting mechanism by which cisplatin can enter the nucleus.[82] However, cisplatin resistance is related to intracellular glutathione and metallothionein (thiol-containing proteins) concentration, implying that free cisplatin or its active mono- or di-aqua forms are present in the cytosol.[83]

Passive diffusion of cisplatin across complex cell membranes has not been proven. Furthermore, neither cisplatin nor oxaliplatin leak from liposomes.[82]

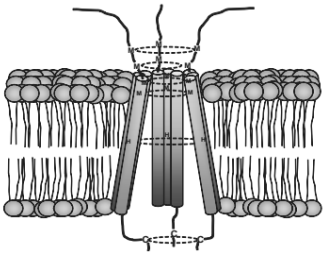

Figure 1.5.2.1. Schematic diagram of Ctr1.[82]

These three examples of "traditional" Pt-based chemotherapeutic agents have a number of common features. They are neutral complexes sharing a square-planar Pt(II) core attached to two leaving groups and two N ligands, both in a *cis* arrangement to each other. This motif has been utilised in many Pt-based drugs since Rosenburg's original discovery. Indeed, nedaplatin (approved in Japan),[84] lobaplatin (approved in China for CML- chronic myeloid lymphoma)[84] and heptaplatin (approved in South Korea),[84] share these features and have a broadly similar mechanism of action (Figure 1.5.1.1). Nedaplatin demonstrates efficacy across the same range of cancers as cisplatin, with similar efficacy and also the associated nephrotoxicity and thrombocytopenia, without the other associated toxicities. Lobaplatin shows activity in cisplatin-resistant cancers *in vitro* and *in vivo*, with a milder side effect profile than cisplatin, albeit lower efficacy in general. Heptaplatin, similar to nedaplatin has a lower side effect profile but lower activity in comparison to cisplatin across the same series of cancers. Broadly speaking, the severity of side effects of these types of platinum complexes is directly related to their anticancer effects.[84]

To enhance delivery to the tumour area and reduce side effects, the first generation liposomal formulations of cisplatin and oxaliplatin, known as Lipoplatin® and Aroplatin® respectively, entered clinical trials.[85] However, these complexes were not as active as their parent compounds in the clinic. ProLindac® a second generation delivery system comprising of oxaliplatin-like Pt^{II} bound to a functionalised HMPA (hydroxypropylmethacrylamide) polymer *via* a pH-sensitive linker, is currently in clinical trials.[86] Animal models of these drug delivery systems showed a much improved side effect profile and a similar or better anti-cancer effect compared to the parent compounds.[87]

1.5.3 Anti-cancer metal complexes in general

Although cisplatin was approved by the FDA in 1978, anti-tumour complexes of metals other than platinum have been slow to follow. Today a great amount of research is concentrated on compounds that are efficacious in cisplatin-resistant cell lines. The mode of action of many of these complexes is *via* generation of reactive oxygen species (ROS) and reactive nitrogen species (RNS).[88] Besides platinum, many metal complexes are cytotoxic to cancer cells *in vitro* and in animal models, including palladium[89] ,copper[90] and gold.[91] Anti-cancer metal complexes in clinical trials include ruthenium and samarium.[92,91]

The most diverse range of non-platinum based anti-cancer metal complexes in preclinical and clinical trials are ruthenium compounds.[92] The most interesting of these compounds is NAMI-A, in phase II trials.[92] This compound is selective for metastatic tumours, showing reduction of metastasis in preclinical models of up to 100%.

The only other ruthenium complex in clinical trials is KP1019, which is remarkably effective in preclinical models of colorectal cancer.[92] In contrast to NAMI-A, KP1019 does not predominantly affect metastatic tumours, is more active in its Ru^{II} oxidation state and binds to DNA in a similar manner to cisplatin. KP1019 causes apoptosis via the mitochondrial pathway and also generates ROS. The pharmacokinetics of KP1019 are similar to NAMI-A in humans and has shown disease stabilisation in 5 out of 6 evaluable colorectal cancer patients in phase I trials.[92]

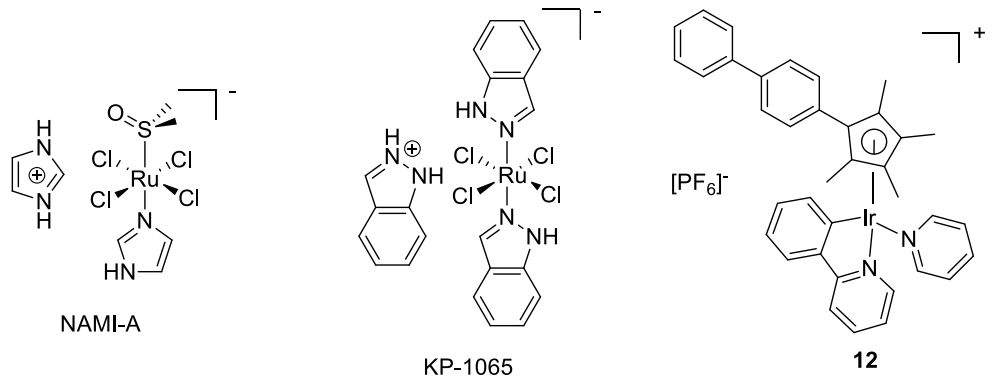

Figure 1.5.3.1. Selected anti-cancer metal complexes.

The precious metal iridium is a component of many catalysts, and in a recent paper, a cyclometalated Ir^{III} piano-stool complex (**12**) has been shown to catalytically generate ROS

and RNS (reactive nitrogen compounds) and displayed sub-nanomolar IC_{50} values across a broad range of cancer cell lines. [93]

The radioactive samarium compound lexidronam (Figure 1.5.3.2) is in Phase II clinical trials for bone metastases. Using a highly anionic phosphonate ligand, the compound localises in damaged bone. The compound is taken as an analgesic, with pain relief from the first week and lasting several months. Lexidronam contains the isotope ^{153}Sm, releasing β-particles that ultimately kill the tumours.[91]

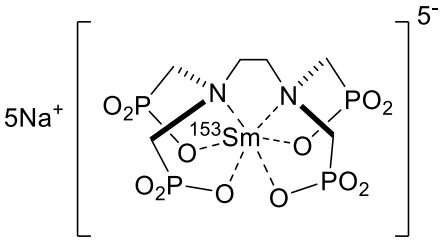

Samarium (^{153}Sm) lexidronam

Figure 1.5.3.2. Radioisotope used to treat pain from bone metastases.

All of these metal complexes show enormous promise for future therapy. However, the clinical success of cisplatin and its derivatives has prompted many research groups to explore improved anticancer drugs based on platinum. This new wave of research is dominated by non-traditional platinum complexes, as explored in the next section.

1.5.4 Non-traditional Platinum-Based Anti-cancer agents

The traditional mononuclear square-planar complexes of Pt^{II} bound to two N atoms and two leaving groups in a *cis*-configuration (Figure 1.5.1.1) suffers from many drawbacks, including similar toxicity, cross-resistance and poor water solubility. The shape, oxidation state and substitution pattern around Pt have been changed to give a wide range of compounds that retain cytotoxicity to cancer cells, while improving the therapeutic index.[83,94]

The structure-activity relationship of a small subset of anti-cancer metal complexes developed in the 1970s has taken a considerable amount of time to discredit. Firstly, the pseudo-dogma that *trans*-bound ligands were undesirable in an anticancer drug was

questioned in 1993, when Coluccia and co-workers published their research on the cytotoxicity of *trans*-platinum iminoether complexes (**13**, Figure 1.5.4.1), synthesised from attack of alkyl alcohols on coordinated nitriles. These complexes were much more active in a range of cancer cells and *in vivo* mouse models than their *cis* analogues.[95,96] Since then, the field of anti-cancer *trans*-platinum complexes has flourished. Work carried out by Navarro-Ranninger showed that platinum complexes of simple bulky aliphatic amines bound *trans* to each other (**14**) were more cytotoxic than their *cis*-counterparts and cisplatin in diverse cell lines.[97]

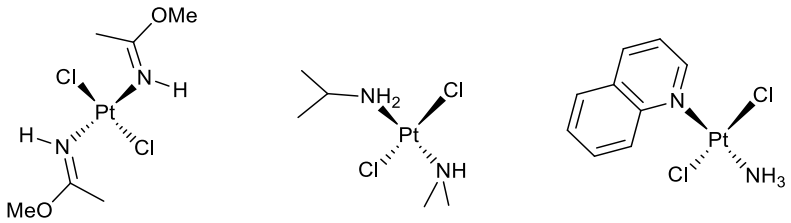

13 **14** **15**

Figure 1.5.4.1. Examples of *trans*-Pt complexes from the groups of Coluccia (**13**) Navarro-Ranniger (**14**) and Farrell (**15**).

Farrell's group have investigated aromatic heterocyclic compounds bound to Pt in a *trans*-fashion that are more cytotoxic than cisplatin and demonstrate activity in cisplatin-resistant cell lines.[98] These *trans*-planar amine (TPA) complexes, for example quinoline derivative **15**, are postulated to bind to DNA on one side of platinum and on the other side bind either to the opposite DNA strand or to a nucleosomal protein. The shape of DNA is thus changed in a different way to cisplatin and thus, the DNA is not recognised by translational proteins, probably triggering apoptosis. Furthermore, the distortion is different to the characteristic bending of cisplatin so the cell presumably cannot fix these lesions in the same manner. This explains the activity of these complexes in cisplatin resistant cells. Moreover, transplatin-type compounds can covalently link DNA and proteins, causing very large adduct formation.[98]

Not only do platinum drugs not need two leaving groups, but these compounds can be cytotoxic with one or even no leaving groups. Lippard's laboratory have developed drugs that utilise only one labile metal site to bind to DNA.[99] Figure 1.5.4.2 shows pyriplatin, a cisplatin-derived drug that binds to DNA in one position and can block RNA pol II action. The group rationalised, from a crystal structure of the compound bound to DNA and RNA

pol II, that increasing steric bulk of the heterocycle would be beneficial. The best next-generation compound, phenanthriplatin (Figure 1.5.4.2), is indeed cytotoxic at a lower dose than pyriplatin and also has been shown to block RNA pol II.[100,99]

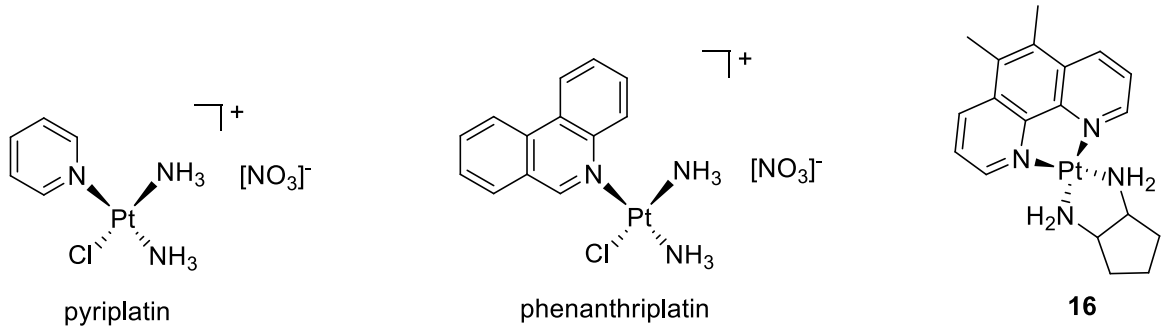

Figure 1.5.4.2. Lippard's pyriplatin and phenanthriplatin, and Aldrich-Wright's intercalator.

Aldrich-Wright's group has developed a class of DNA intercalating agents combining the 1,2-diaminocyclohexane (DACH) motif of oxaliplatin with bipyridine-based intercalators to create a platinum complex with no labile groups.[89] They found that increasing methylation on the intercalator was beneficial and that changing the DACH for a 1,2-diaminocylopentane (DACP) to give compound **16** also helped the cytotoxicity. The absolute stereochemistry of the cyclic diamine was important for the activity,[101] however, the group give no explanation of why their compound is more cytotoxic than the bipyridine ligand alone. Perhaps cell transport mechanisms are implicated or Pt-binding increases π-π stacking interactions.

Of particular interest to our work are the platinum complexes of aliphatic guanidines synthesised and tested in cancer cells (**17**-**20**, Figure 1.5.4.3).[102] These compounds are very soluble in water and in cell media. The compounds were synthesised from addition of gaseous ammonia to solutions of the cyanamide complexes. These derivatives have similar efficacies as cisplatin in the cell lines tested and, in general, the *cis*-dichloride complexes (**17**) are more cytotoxic. Some compounds contained the *cis*-diamine moiety (*i.e.* no anionic leaving group, **18**) and are less cytotoxic than the dichloro species but active nonetheless.[102] This may be attributed to loss of ammonia upon protein or DNA binding.

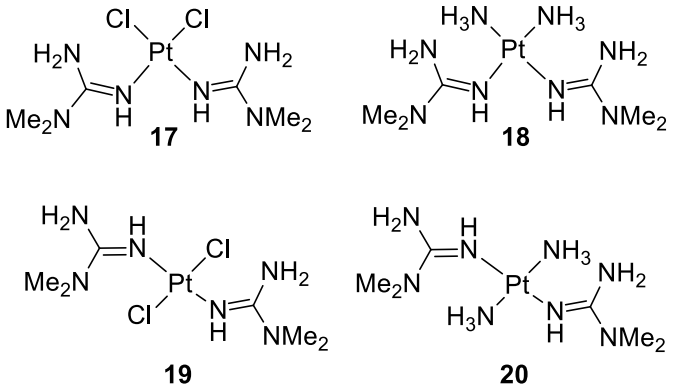

Figure 1.5.4.3. Cytotoxic alkyl guanidine Pt complexes.[102]

A family of *trans*-diiodo compounds was also developed by the group of Quiroga.[103] They found that the diiodo compounds interact stronger with DNA than their corresponding dichloro analogues. The compound with the strongest anticancer activity (**21**, Figure 1.5.4.4) has similar IC_{50} values for certain cell lines compared to cisplatin, but causes cell death by a different mechanism.[103]

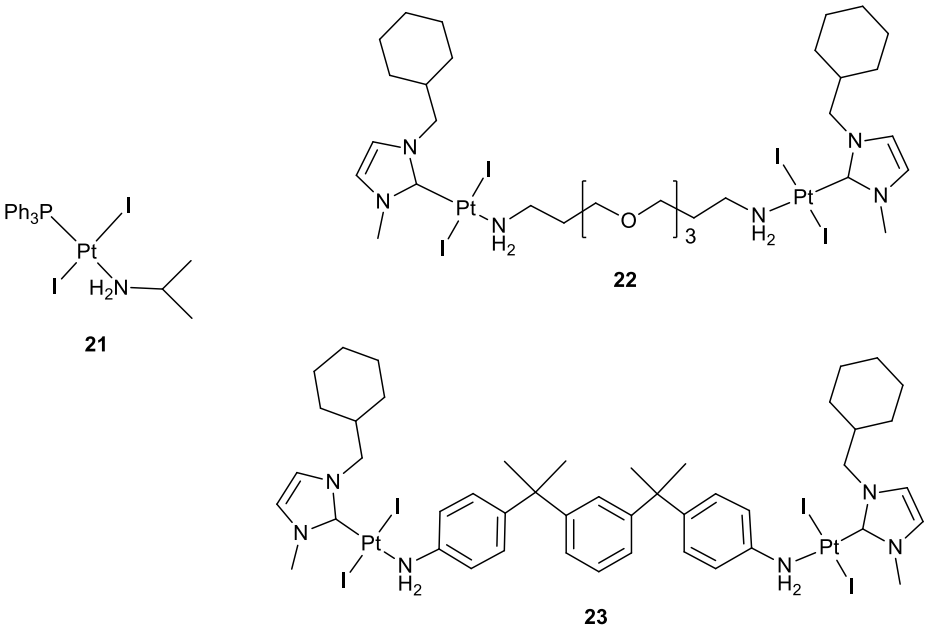

Figure 1.5.4.4. Mono- and bi-nuclear *trans*-diiodo Pt complexes with anti-cancer activity.[103,104]

Similarly, a family of NHC-substituted dinuclear *trans*-iodoplatinum compounds have shown efficacy in a range of cancer cell lines and have cytotoxicity against cisplatin-resistant cells (Figure 1.5.4.4).[104] The cytotoxicity depends largely on the linker between Pt atoms. Alkyl

diamines of various lengths gave poor cytotoxicity whereas a HB accepting ether **22** and rigid aryl linker **23** gave the best cytotoxicity.[104]

A variety of dinuclear Pt compounds in particular has appeared in the recent literature. The symmetrical dinuclear tetrazole complex **24** (Figure 1.5.4.5) has a bridging μ-hyroxide and bridging tetrazole *via* two different N atoms. This compound has an IC_{50} value of 1.2 μM in L1210 and 1.4 μM in L1210R cisplatin-resistant murine leukemia cells and the cytotoxicity trend of the family correlates well with cellular uptake of Pt. Interestingly, when exposed to 9-ethylguanine (9EtG), each Pt lost the μ-hyroxide linkage to gain one molecule of 9EtG each and changed coordination to the tetrazole from a 2,3-*bis*-metalated system to a 1,3-*bis*-metalated product (**25**).[105]

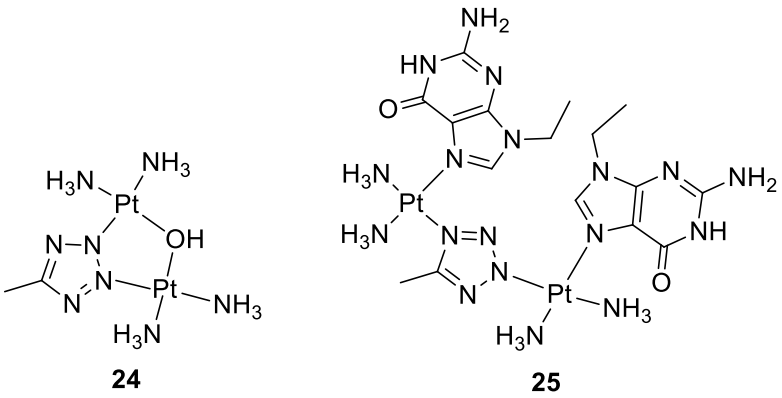

Figure 1.5.4.5. Binuclear PtII complex **24** and 9EtG isomerisation product **25**.

Farrell's group have previously been involved in *trans*-platinum compounds and recently published on a range of polynuclear platinum(II) complexes with cytotoxic effects. These compounds contain no obvious leaving groups and instead bind to DNA *via* a novel non-covalent "phosphate clamp" mechanism. The positively charged compounds avail of polyarginine transporters to enter the cell and are attracted to DNA via an ionic interaction with DNA phosphate groups. Their lead compound, Triplatin-NC, is more active than cisplatin against a host of cancer cell lines.[67,106]

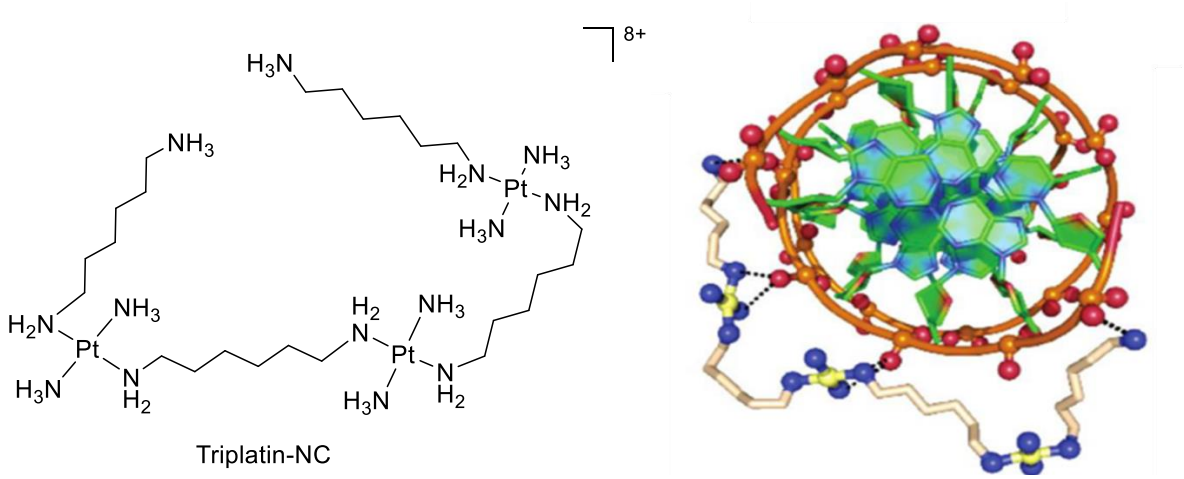

Figure 1.5.4.6. TriplatinNC and crystal structure of one type of phosphate clamping interaction with DNA phosphates.

The oxidation state of Pt has proven to be vital for cytotoxic activity. Platinum complexes are active only in the 2+ oxidation state. However, octahedral d^6 low-spin Pt^{IV} prodrugs have been the objective of a great deal of research. Some of Rosenberg's early compounds with anticancer activity were Pt^{IV} prodrugs that included two extra leaving groups in their octahedral geometry.[71] Their ease of access *via* oxidation of a square planar Pt^{II} starting material to the *trans* diol with H_2O_2 facilitates their study. The orally available satraplatin (Figure 1.5.4.7) has gone through phase III clinical trials but did not meet its efficacy targets. Satraplatin is thought to undergo reduction to a 4-coordinate Pt^{II} compound upon absorption into the body: however, satraplatin produces a mixture of Pt^{II} species with different coordination modes and geometries in the presence of biologically relevant reductants and the relative cytotoxic effect of each species is not known.[107]

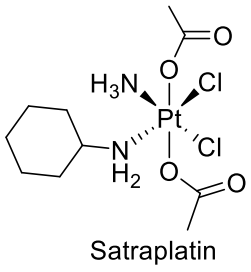

Figure 1.5.4.7. Satraplatin, a cytotoxic Pt^{IV} complex.

1.5.5 Platinum-based dual drug conjugates

To achieve a broad spectrum of activity across cancers and decrease the toxicity of platinum-based agents, a plethora of dual acting cancer-targeting conjugates of platinum derivatives have been synthesised to aid in selective accumulation of the cytotoxic agent in cancer cells (Figure 1.5.5.1). Ordinarily, the Pt-binding moiety contains one or two leaving groups to ensure DNA-binding will take place. Attached either to the leaving group or the chelated *N*-ligand is a linker that is easily synthetically accessible. The conjugated active compound should not lose activity upon attachment to the Pt-binding scaffold. The choice of linker to either enable synergistic interactions with DNA (in the case of dual DNA-binders) or prevent the Pt-binding moiety from interfering with the receptor-binding or photophysical activity is crucial to the overall activity of the molecule. In general, Pt-drug conjugates are designed to increase cancer cell selectivity by increasing uptake, or to overcome cisplatin resistance by altering the DNA-binding mode.

Some of these conjugates contain drugs which are active at certain receptors overexpressed in cancer cells, as for example oestrogen linked to a Pt-complex (**26**). Another example contains a carboplatin-like moiety tethered to a thiol-binding maleimide functionality (**27**), designed as a prodrug to enter the cell on thiol-containing transport proteins. Other interesting examples include a Pt-based phosphonate devised to target bone tumours (**28**) and a pH-activated prodrug that was proposed to ring open in the acidic tumour microenvironment (**29**).

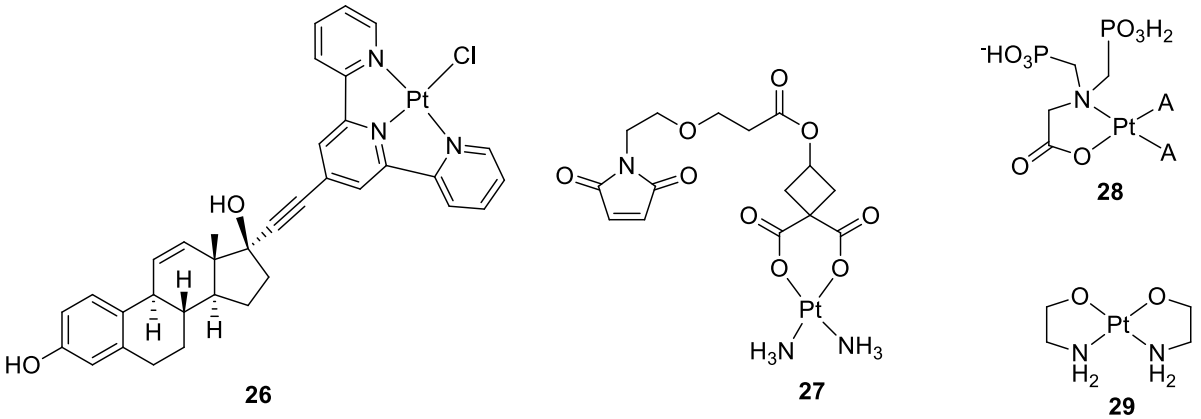

Figure 1.5.5.1. Examples of tumour-targeting Pt conjugates.

Figure 1.5.5.2 shows two Pt^{II} *mono*-saccharide derivatives designed to take advantage of these highly water soluble glucose-like molecules that avail of glucose transporters

overexpressed on cancer cells.[108] One Pt-glucose conjugates (**31**) was progressed through pre-clinical toxicity and efficacy assays on mice showing that it was better tolerated and more efficacious than oxaliplatin.[109]

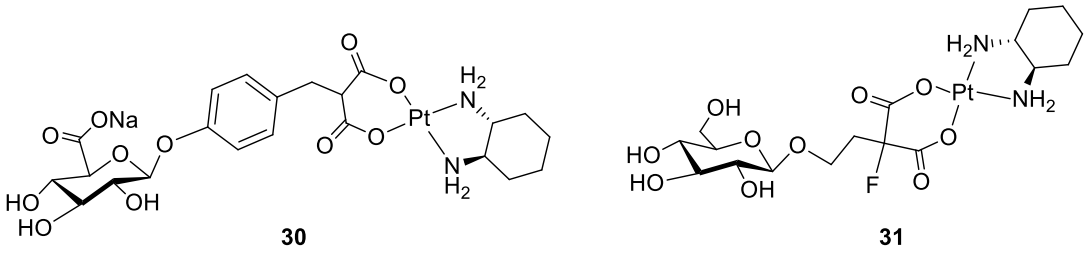

Figure 1.5.5.2. Utilising a tumour cell's high uptake of glucose in Pt^{II} conjugates.

Marmion's group have developed two conjugates of a HDAC inhibitor and a Pt^{II} complex (Figure 1.5.5.3).[110–112] Their approach was to functionalise the inhibitor with a malonate group (shown by *in silico* docking to not affect enzyme affinity) that would bind Pt and release it *in vivo*. The authors expected that the HDAC inhibition would open DNA to attack with a cisplatin-type compound, with a synergistic benefit in cancer cell death. However, these compounds showed similar IC_{50} values to malonatoplatin and were not as effective as the parent compounds belinostat and SAHA in a HDAC inhibition assay.

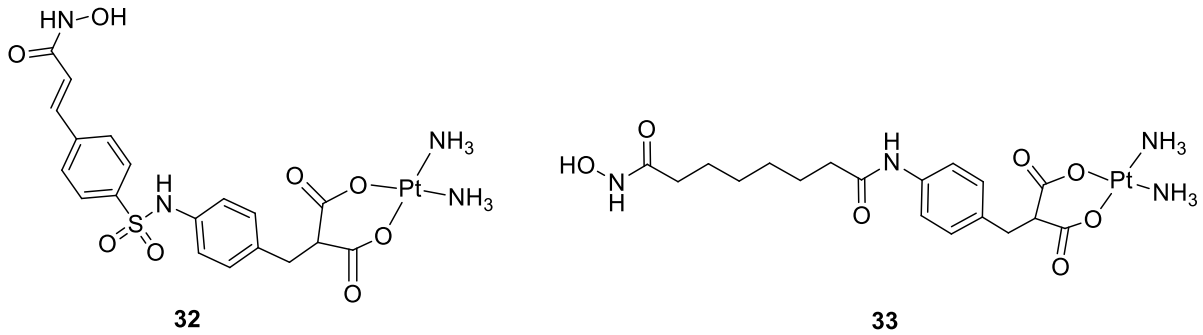

Figure 1.5.5.3. Selection of Marmion's HDACi-Pt conjugates.[110–112]

Finally, attaching Pt to a fluorophore has proven useful in determining cellular localisation of the complex *in vitro* without the need for differential centrifugation of cell fractions (Figure 1.5.5.4).[113] However, this type of complex may possess different localisation than cisplatin if

the fluorophore binds to any other cellular machinery. The facile synthesis of BODIPY (boron-dipyrromethene)-Pt conjugate **34** enabled researchers to visualise the localisation of this complex in the nucleus by live fluorescence imaging.[113] The compound was slightly less toxic than cisplatin in a cell model.

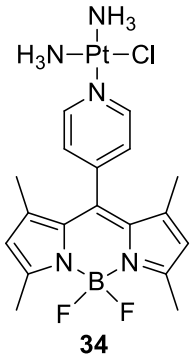

34

Figure 1.5.5.4. Fluorescent BODIPY-Pt conjugate

1.5.6 Increasing Pt-drug DNA binding

Recently, there has been a lot of activity designing dual drugs that have a platinum complex with a DNA-binding moiety.[114] These complexes have a different mode of action to cisplatin and may overcome cisplatin resistance in cell lines. A *bis*-thiourea-bound Pt complex containing a spacer linked to acridines has been shown to intercalate into DNA and be cytotoxic to cancer cells *in vitro*.[114] The authors used NOE NMR spectroscopy on a DNA octamer to understand the binding and, then, created an energy-minimised molecular modelling structure using AMBER to model the complex (Figure 1.5.6.1).

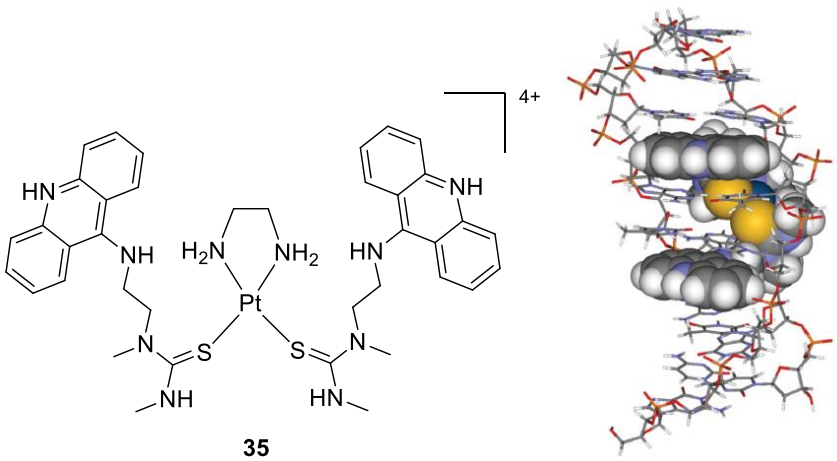

35

Figure 1.5.6.1. The chemical structure of $[Pt(ACRAMTU)_2(en)]^{4+}$ bound to a $d(GCTATACG)_2$ DNA octamer.

Naphthalimides, which are another class of intercalating agents, complexed to Pt^{II} show an increased binding to DNA, better cytotoxicity against MCF-7 breast cancer lines and overcome resistance in cisplatin-resistant cells.[115]

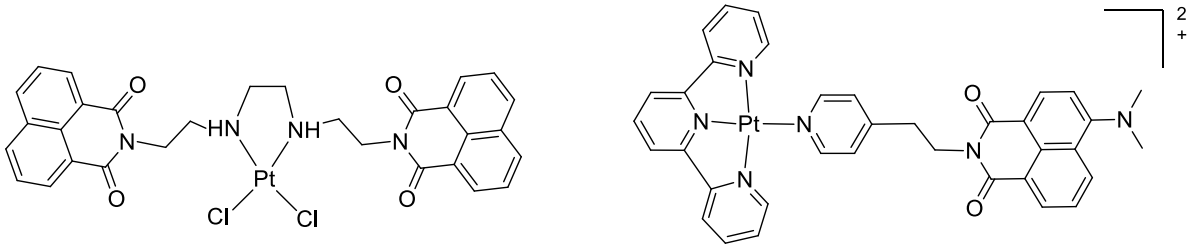

Figure 1.5.6.2. Pt-naphthalimide adducts that have increased DNA binding and cytotoxicity over cisplatin in a MCF-7 breast cancer line.

A library of platinum conjugates of DNA minor groove binding polyamides (Figure 1.5.6.3) was synthesised by both solid-phase and solution-phase synthesis in Aldrich-Wright's laboratory. [116] Unfortunately, these long compounds, including compound **38**, were not sufficiently water soluble for testing, even after dilutions in DMSO and DMF. Although the authors give no explanation as to why these compounds are so insoluble, it is possible that intramolecular HB formation creates a secondary structure (hairpin) whereby the hydrophilic groups are shielded from the solvent.

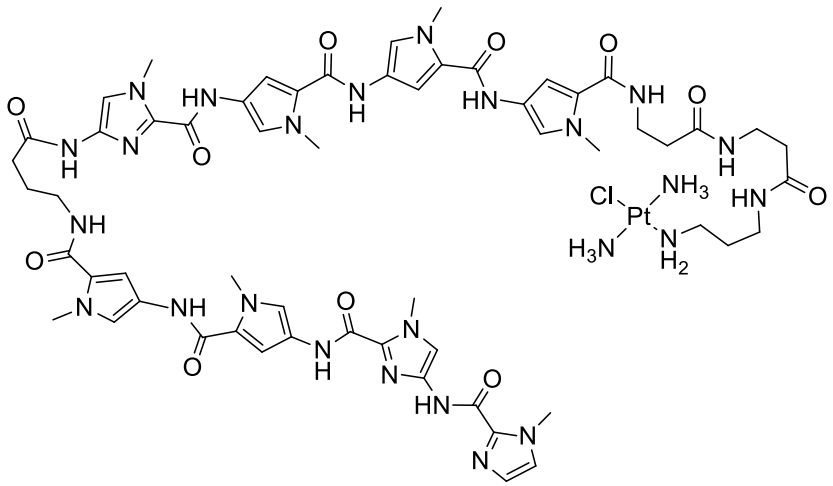

38

Figure 1.5.6.3. Pt bound to DNA hairpin MGB.[116]

Similar to the intercalating complexes above, shorter, more water soluble Pt complexes of minor groove-binding compounds may also demonstrate activity in cisplatin-resistant cell lines. These compounds would overcome the problems and difficult synthesis and purification of Aldrich-Wright's DNA-hairpin complexes and they form the basis of the present work.

1.5.7 *Bis*-guanidinium-based DNA Minor groove binders: Possible Pt ligands

In the Rozas laboratory, a library of water soluble organic compounds has been developed that both bind to the DNA minor groove and are cytotoxic to cancer cells *in vitro*. All these compounds have a similar scaffold: two aryl rings connected by a short linker, *para*-substituted with guanidinium-like cations. Structures and DNA binding affinity are presented in Table 1.5.7.1. The trend relating cations with DNA binding strength is clear: *mono*-cationic series **1** (guanidine/amine),[117] **6** (isourea/alcohol),[118] and **8** (acridine/guanidine),[117] as well as dicationic **7** (*bis*-hydroxyguanidine),[119] are poor DNA binders; series **2** (*bis*-guanidine),[120] **3** (guanidine/aminoimidazoline),[121] and **4** (*bis*-aminoimidazoline)[120] are clearly strong DNA binders and, finally, series **5** (*bis*-isourea)[118] and **9** (guanidine/alkyl amine)[122] are moderate DNA binders. The importance of the linker remains to be fully elucidated; thus, compounds with the NH linker generally show very good binding to DNA, followed by those with CO. However, in some series, compounds with O or CH_2 linkers have the best DNA affinity. In the families of compounds which DNA affinity has been measured in both unspecific salmon testes (stDNA) and specific poly(dA·dT) DNA, the results do not necessarily correlate (see series **2** especially). The strongest DNA binders correspond to compound **4** (*bis*-amino-2-imidazolinium) with the NH linker being the strongest poly(dA·dT) DNA binder measured to date.

Every compound measured gave higher thermal denaturation values for poly(dA·dT) over stDNA, signifying that these molecules are AT-selective. In general terms, AT-selective compounds are minor groove binders because the minor groove is rich in A-T pairs.[24] To confirm this in series **2** and **9**, CD and LD experiments were performed. The presence of a positive induced peak above 300 nm in both techniques confirmed that the complexes are minor groove binders.[123]

Table 1.5.7.1. Thermal denaturation assay results for selected *bis*-aryl compounds.

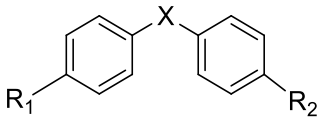

Series	R^1	R^2	X	ΔT_M stDNA	ΔT_M poly(dA·dT)$_2$
1	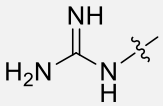	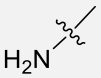	CH_2 CO NH	3 0 2	N/A N/A N/A
2	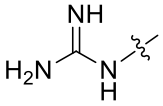	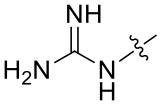	CH_2 CO NH O	8 4 8 N/A	15 27.6 29.6 22.1
3	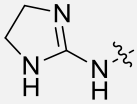	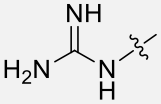	CH_2 CO NH	6 8 12	6 15 17.5
4	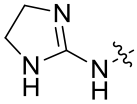	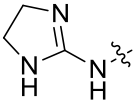	CH_2 NH	N/A N/A	18.8 38.5
5	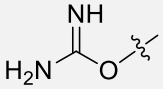	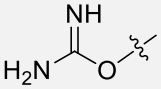	CH_2 O NH(CO) S	4 6 2 5	N/A N/A N/A N/A
6	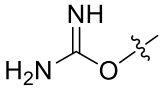		CH_2 O S	2 4 2	N/A N/A N/A
7	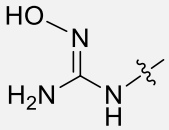	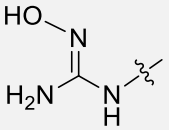	CH_2 O NH(CO) CO	0 1 1 0	N/A N/A N/A N/A
8	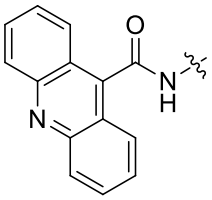	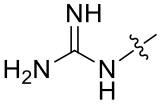	NH CH_2 CH_2CH_2	2 2 2	N/A N/A N/A
9	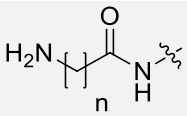	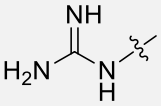	NH (n=4) O (n=4) NH (n=11)	6 6 5	6 N/A 6.5

In silico structure optimisation of the structures in series **2** showed that the lowest energy conformations of the NH and CO linked molecules exhibit a high degree of co-planarity of the aromatic rings compare to those of the molecules linked by CH_2 or O. To investigate whether fixing the scaffold in a planar conformation would further increase binding, compounds **39** and **40** (Figure 1.5.7.1) were synthesised and characterised by biophysical techniques. These planar diaryl scaffolds were chosen as their respective diamine analogues were commercially available, although they did not exhibit the *para/para* substitution found in previous compounds. These two derivatives were different in their preferred DNA-binding sequence, which can also be explained by their *in silico* lowest energy conformations. In the dioxolane derivative, the orientation of the imidazoline rings with respect to the planar scaffold is more stable when the imidazoline rings are arranged parallel to each other (**40a**), whereas in the fluorene scaffold where both the imidazoline rings are on the side far from the CH_2 (**39a**) or close to the CH_2 (**39b**) are of similar energy. The conformations along the axis of the planar scaffold (**39a** and **40a**) are primed for intercalating into DNA whereas the curved conformation (**39b** and **40b**) is more likely to undergo minor groove binding.[124]

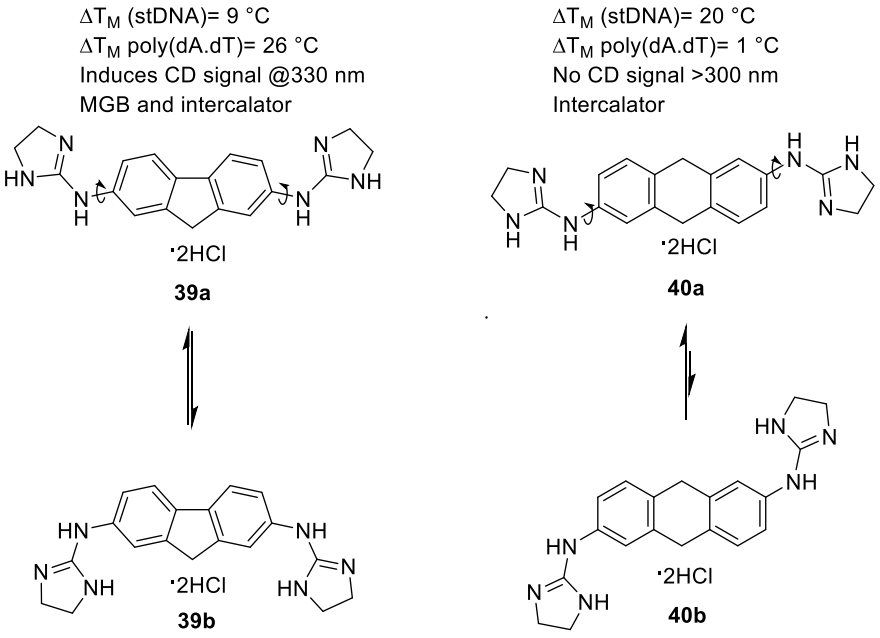

Figure 1.5.7.1. Planar *bis*-aminoimidazolines have novel DNA-binding properties that depend on low energy conformations.

Most of these compounds were screened in HL-60 leukemia lines and, it was observed that, even though in general there is a good correlation between, cytotoxicity and DNA binding, in

some particular cases compounds with poor DNA binding showed good cytotoxicity (Series **4**, Table 1.5.7.1). It was thought that these particular compounds could produce their anti-cancer effect by kinase inhibition since there are a number of reported kinase inhibitors with similar *bis*-aryl scaffolds. With that in mind, families of *meta/para*-substituted *bis*-guanidines (**42**) were synthesised, culminating in the discovery of a compound (**43**) with cytotoxicity comparable to that of the clinically prescribed anticancer agent sorafenib in HL-60, RKO and Kelly cell lines. These particular set of molecules target the MAPK pathway, most likely by inhibiting the cytosolic kinase B-RAF.[125] SAR studies are active in our group to further increase cytotoxicity (Figure 1.5.7.2).

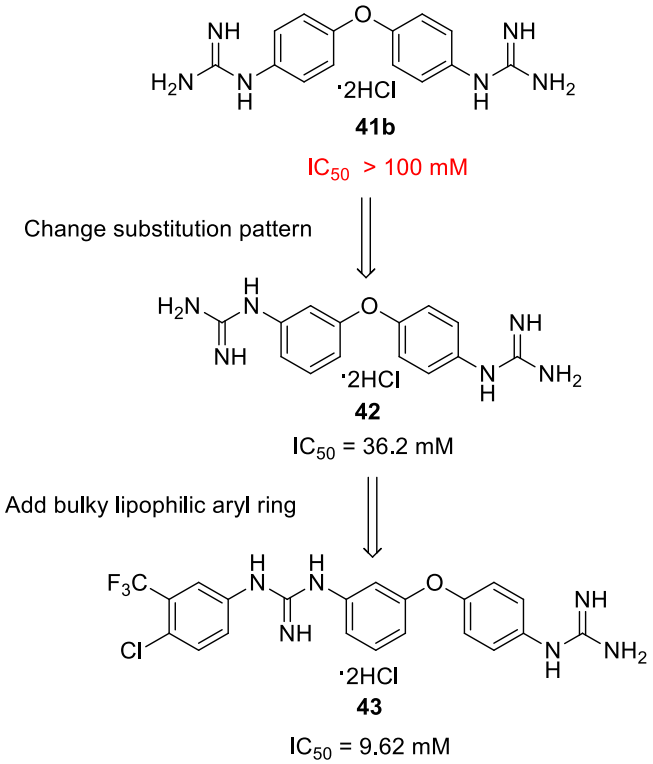

Figure 1.5.7.2. Modifying the bis-guanidine scaffold to improve cytotoxicity towards HL-60 cells.

To utilise these findings in developing a Pt-based drug conjugate with good activity *in vitro* and *in vivo*, we aim to create a cisplatin derivative conjugated to a molecule with a different DNA-binding mode. We can achieve this by using *para/para*-substituted diaryl *bis*-guanidines and *bis*-2-aminoimidazolines as a scaffold, attaching a Pt system to allow for DNA binding in the minor groove. The minor groove binder moiety of the drug conjugate need not demonstrate high cytotoxicity on its own since the molecule will be expected to be highly cytotoxic when conjugated to Pt as well as when Pt is released. This type of Pt-minor

groove binder conjugate is expected to help bringing the Pt moiety into the cell, through OCT transporters, for example, avoiding cisplatin's reliance on Cu transport.

2.0 Objectives

Considering the good DNA binding properties and cytotoxicity of some of our previous guanidine-based DNA minor groove binders (MGBs) and the known cytotoxic effect of platinum complexes (e.g. cisplatin), we hypothesised that Pt complexes of these MGBs will result in better anticancer agents by bringing the Pt moiety inside the cell and near DNA and by acting upon DNA in a dual manner. Therefore, the purpose of this thesis is to create Pt-containing DNA-binding molecules with anti-cancer activity based on the structure of MGBs previously developed in the Rozas group. Based on their chemical characteristics, the compounds prepared and studied in this work can be classified in three groups: (a) organic dicationic molecules, (b) platinum complexes with at least one bond to a guanidine N atom, and (c) platinum (II) complexes bound to the O atoms of a malonate group. All of these compounds possess the common characteristic of an aryl guanidine-like moiety and based on their similarities with previous MGBs and molecular modelling studies all are expected to interact with DNA. Additionally, we aim to assess the DNA binding and cytotoxicity of all the compounds prepared by means of different biophysical and cell cytotoxicity experiments.

2.1 Synthetic aims

2.1.1 New DNA-binding compounds based on the diaryl *bis*-iminoimidazolidine scaffold

One risk we might run by attaching Pt to our MGB compounds is a decrease in the affinity for DNA and possibly an alteration in its binding mode. To deal with this potential problem and to develop a complete set of structure-activity relationships the first goal of this work will be to explore modifications in the diaryl *bis*-guanidine-like scaffold in three ways:

(i) by changing the linker between the aryl rings (Figure 2.1.1.1, Families I-IV);
(ii) by altering the structure of the cation well by increasing lipophilicity (Figure 2.1.1.1, Family I) or well by increasing the amount of HB donors (Figure 2.1.1, Family II); and
(iii) by fixing the planarity (Figure 2.1.1.1, Family III).

Some of these families will incorporate moieties with the potential to chelate platinum (i.e. aminoguanidines in Family II and the malonic group in Families III and IV).

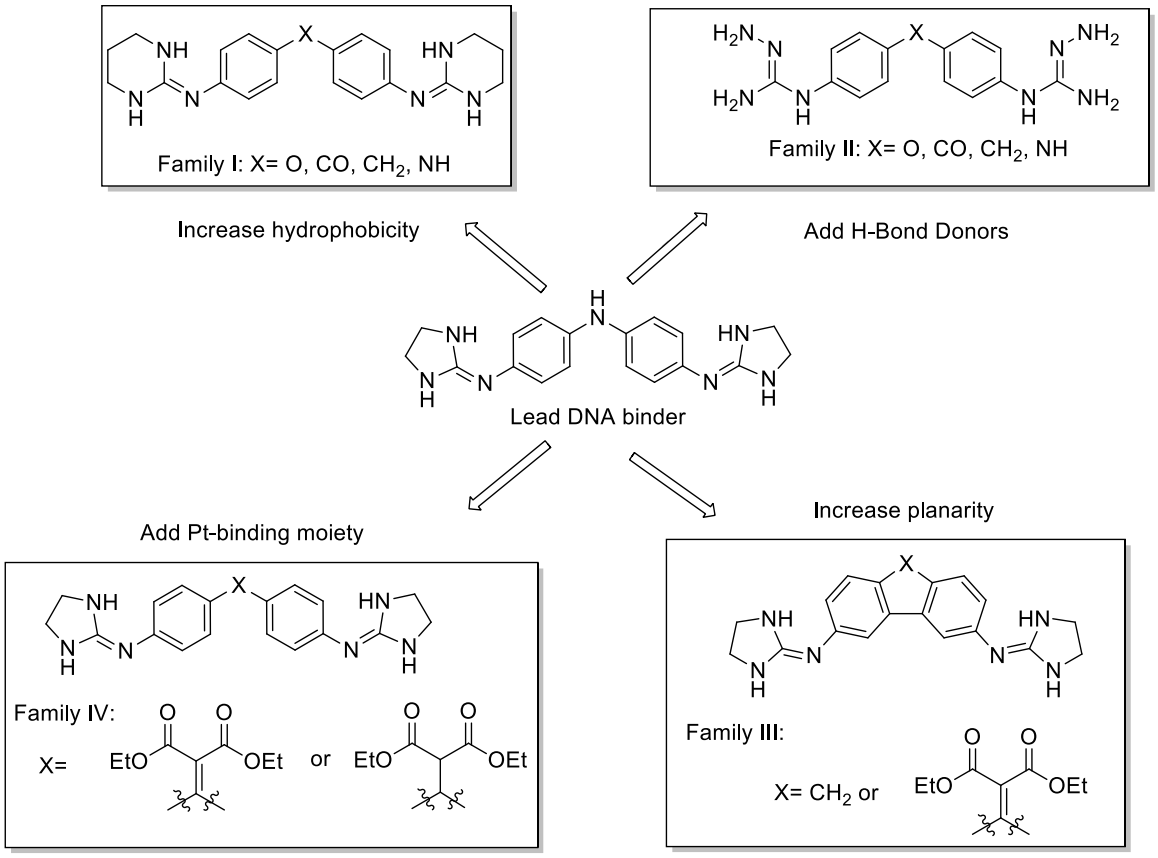

Figure 2.1.1.1. Rationale of the design followed for the new MGBs proposed

2.1.2 Platinum complexes of monoaryl guanidines

Although aliphatic guanidine-metal complexes are well known, aryl guanidines as ligands are less studied. In particular, there is a gap in the literature concerning monoaryl guanidine complexes of platinum. Accordingly, the second synthetic goal of this work will be to investigate the binding modes, water solubility, stability and reactivity of monoaryl guanidine-platinum complexes (Figure 2.1.2.1).

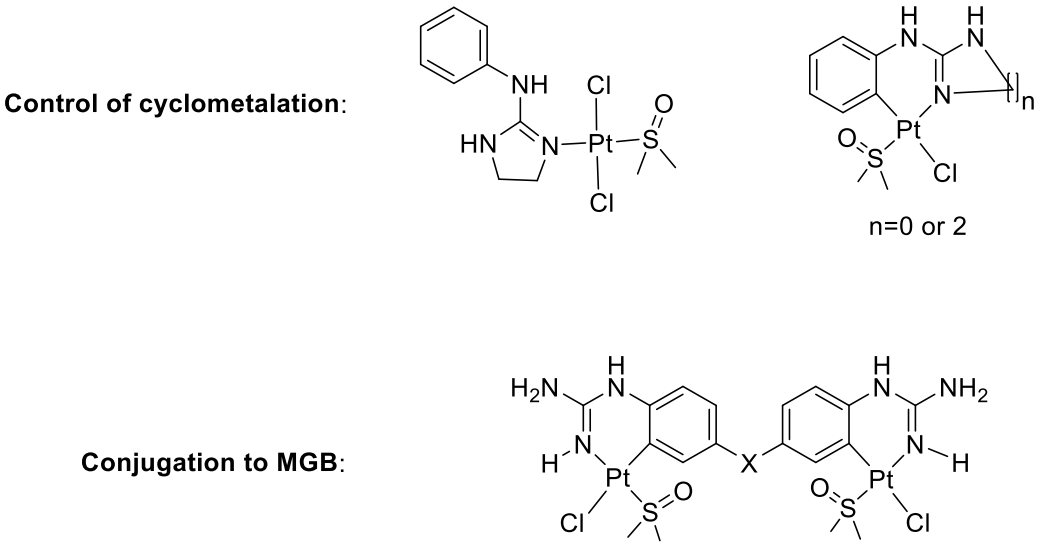

Figure 2.1.2.1. Selected families of monoaryl guanidine-platinum complexes to be synthesised in this work.

2.1.3 Platinum complexes of diaryl malonate derivatives

The coordination chemistry of platinum(II) with malonate groups has been studied extensively. As a result, many research labs have attached bio- and photo-active molecules to Pt *via* a malonate linker. We hypothesised that we could install a malonate moiety to our MGB scaffold without a detrimental loss in activity, and that this MGB-malonate ligand could bind platinum. In designing the platinum "head", we will incorporate the *cis*-diammine component of cisplatin and carboplatin and also the 1,2-diaminocyclohexane portion of oxaliplatin to give families that are biologically relevant (Figure 2.1.3.1).

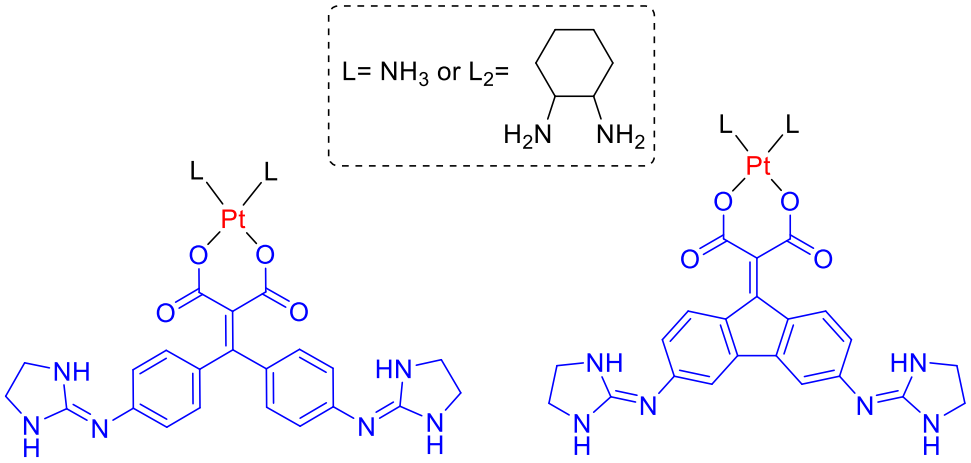

Figure 2.1.3.1. Families of malonate-derived platinum complexes proposed based on organic Families III and IV, and clinical agents carboplatin and oxaliplatin.

2.2 Biophysical aims

The compounds will be assessed for DNA binding by thermal denaturation and circular dichroism (CD). Thermal denaturation experiments will be carried out to measure the binding of the compound to DNA. Two types of DNA will be used- natural DNA isolated from salmon testes (stDNA) and synthetic poly(dA-dT)$_2$. By comparing results obtained for each DNA, the selectivity of the compounds for AT-rich sequences will be evaluated. This data will give us an indication of how the compounds bind to DNA, since selectivity for AT-rich regions is typical for MGBs.

To confirm whether the compounds are groove binding or intercalating, CD experiments will be performed. From observing the change in the CD spectrum as compound is titrated into a solution of DNA, and particularly by looking for an induced CD (ICD) signal from the compound, we will definitively state whether a compound bound mostly to the minor groove or intercalated in between the DNA bases. Similar to the thermal denaturation experiments, we will measure the CD spectra of our compounds with both stDNA and poly(dA-dT)$_2$ DNA. From comparing these results, we will check if removing GC base pairs could switch the preferred mode of DNA binding from intercalating to minor groove binding.

These tests will be carried out on all fully water soluble compounds.

2.3 Cell Cytotoxicity aims

The anti-cancer activity of these compounds will be tested on the treatment-sensitive HL-60 leukemia cell line. Since this cell line is derived from blood cells, HL-60 cells do not adhere to each other or the plate. As such, the cells are well supplied with nutrients and, in our case, cytotoxic drugs. Clinically, HL-60 cells are a poor model of the solid tumour microenvironment but are an excellent general screening assay. The IC_{50} will be measured up to 100 μM and compounds with a higher IC_{50} were deemed inactive. Activity will be measured using the AlamarBlue® viability assay and compared to carboplatin, the MGB furamidine and the multi-kinase inhibitor sorafenib. Furthermore, we will evaluate whether covalently connecting platinum to our MGB-based ligands kills cancer cells synergistically by comparing the results of the dual binders to a control where HL-60 cells were treated with the ligand alone and cisplatin.

In executing these objectives, we will achieve a greater understanding of the SAR of the DNA-binding diaryl *bis*-guanidine-like skeleton, we will create and study novel Pt-guanidine complexes and attempt to combine these properties into a single moiety, with the aim of creating efficient cisplatin derivatives of DNA-binders.

3.0 Results and Discussion

3.1 Organic DNA Binders

3.1.1 *Bis*-2-Amino-1,4,5,6-tetrahydropyrimidine diaryl derivatives (Family I)

3.1.1.1 Design of Family I

Collating previous results from Rozas laboratory, a clear trend of increased DNA-binding with increased lipophilicity in the cationic moiety was observed, from the weaker DNA binders of the *bis*-guanidinium family (compounds **41**) to the medium strength binders of the asymmetric guanidinium/amino-2-imidazolinium derivatives (**44**), to the strongest *bis*-2-aminoimidazolinium (**45**) MGBs (Figure 3.1.1.1.1). We hypothesised that by further increasing the lipophilicity with the addition of an extra methylene group to the 2-aminoimidazoline cation (as in 2-amino-1,4,5,6-tetrahydropyrimidines, **46**), we could increase the interactions of the resulting compounds with the hydrophobic floor of the DNA minor groove, thus enhancing binding affinity.[126]

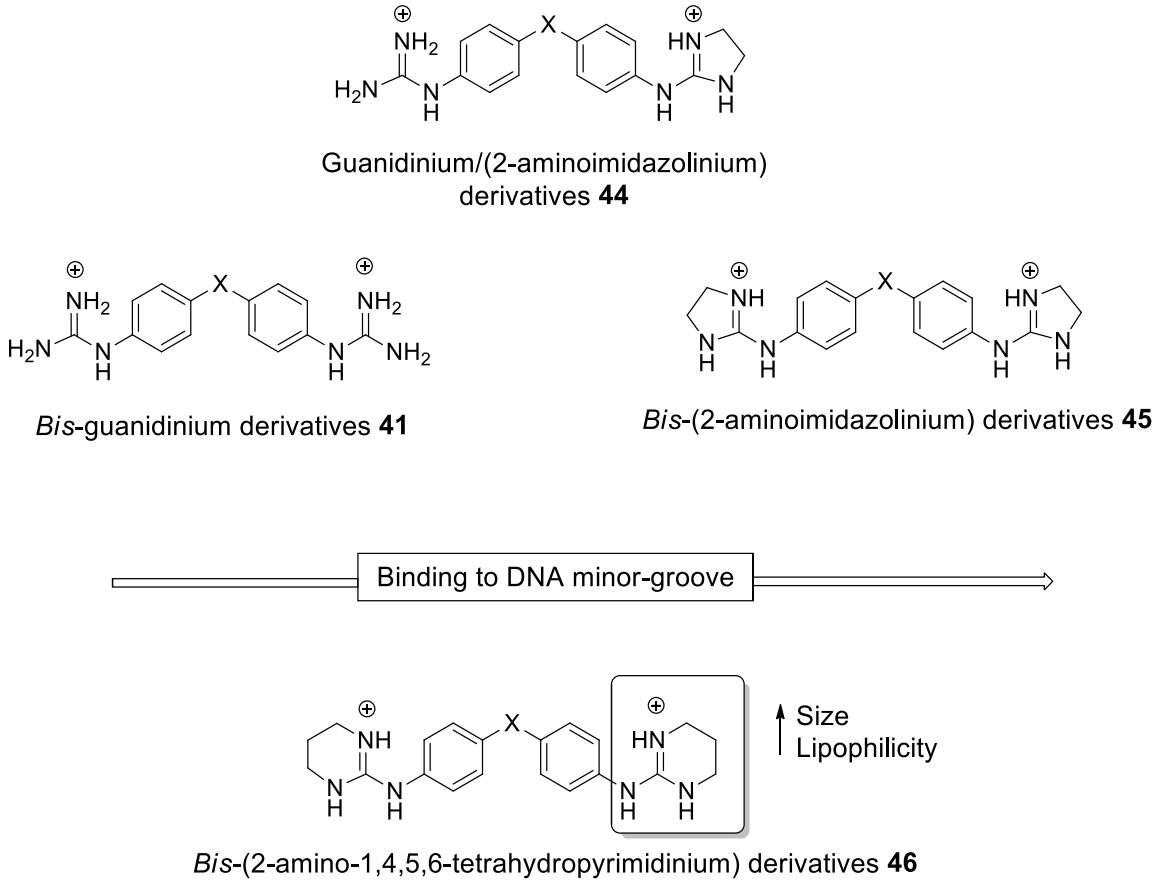

Figure 3.1.1.1.1. Rationale for the design of Family I.

Using the theoretical values for log P and Polar Surface Area (PSA) calculated with the Marvin package,[127] we found an increase in computed logP (ClogP) across the series of cations with the six-membered ring of 2-amino-1,4,5,6-tetrahydropyridinium giving an increase of 0.12 log units over 2-aminoimidazolinium and 0.65 log units on average over guanidinium (Table 3.1.1.1.1). The PSA values obtained were the same for both 2-aminoimidazolinium and 2-amino-1,4,5,6-tetrahydropyridinium cations. These properties indicate that Family I will bind well to the hydrophobic floor of the DNA minor groove.

Table 3.1.1.1.1. Theoretical logP and PSA values calculated with the Marvin package[127] for the three series of *bis*-guanidinium-like derivatives studied (compounds **41**, **45** and **46**).

Cation[a] (Compd)	Linker (X)	logP	PSA/Å^2
Gua (**41a**)		1.38	140.87
Imi (**45a**)	CO	2.04	89.91
Thp (**46a**)		2.16	89.91
Gua (**41b**)		1.42	133.03
Imi (**45b**)	O	2.08	82.07
Thp (**46b**)		2.20	82.07
Gua (**41c**)		2.01	123.80
Imi (**45c**)	CH_2	2.67	72.84
Thp (**46c**)		2.79	72.84
Gua (**41d**)		1.36	135.83
Imi (**45d**)	NH	2.02	84.87
Thp (**46d**)		2.14	84.87

[a]Gua = guanidinium, Imi = 2-aminoimidazolinium, Thp = 2-amino-1,4,5,6-tetrahydropyrimidinium.

Furthermore, using AutoDockVina[128] we performed *in silico* nonrigid-rigid docking between our ligands and DNA oligomer d(CTTAATTCGAATTAAG)$_2$ using as a template the crystal structure of the complex formed between this oligomer and compound **45d** (PDB code: 3FSI).[129] Thus, we observed that all four members of the 2-amino-1,4,5,6-tetrahydropyrimidinium family (compounds **46a-d**) could bind to the DNA oligomer in the same conformation.

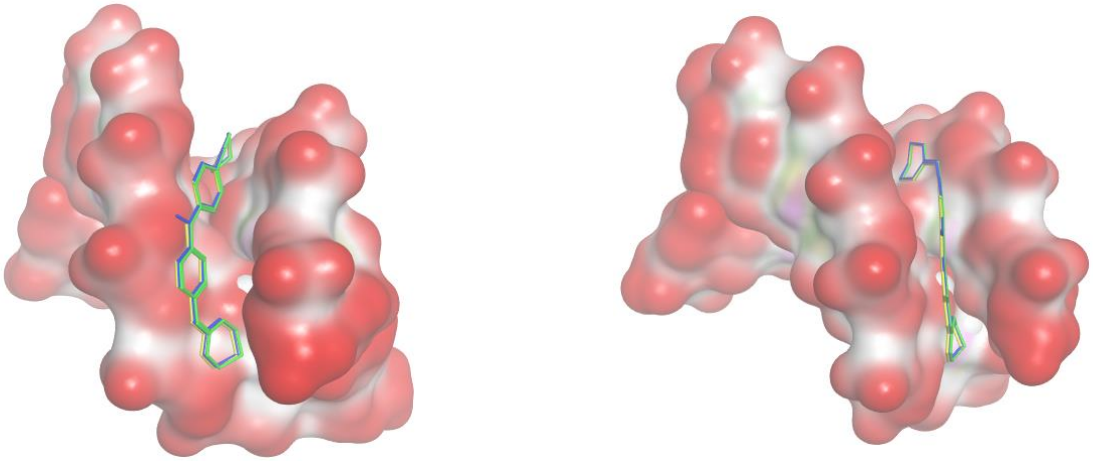

Figure 3.1.1.1.2 Rotated views of compounds **46a-d** (stick models) docked into the rigid d(CTTAATTCGAATTAAG)$_2$ nucleotide (in red) using AutoDock Vina.

Although the docking experiments were initially performed allowing all the bonds on the ligands to rotate, the best docking scores were obtained by fixing the dihedral angles between rings to be the same as for compound **45d** in the 3FSI crystal structure. All the members of Family I showed the lowest energy binding in the same area of the minor groove (Figure 3.1.1.1.2); however this was not the exact same binding area as found for **45d** in the 3FSI crystal structure even though docking scores for all five compounds were similar (Figure 3.1.1.1.3, *Left*). A major difference between the binding of **45d** compared to that of compounds **46a-d** was that the HB formed between the imidazolinium N-H of **45d** and a C=O in thymine, as visualised by the 3FSI crystal structure (Figure 3.1.1.1.3, *Right*), is absent in the binding of compounds of Family I.

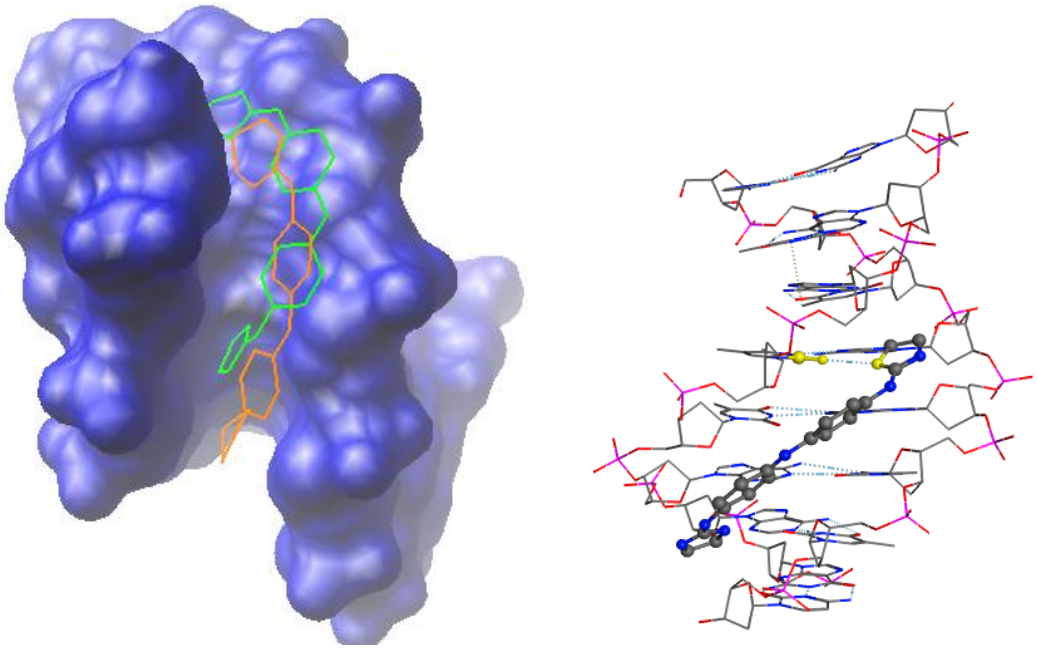

Figure 3.1.1.1.3. *Left:* Overlay of the binding pockets of **45d** (green) and **46d** (brown) in the DNA dodecamer (as in crystal structure 3FSI) using AutoDock Vina. *Right:* 3FSI crystal structure of **45d** in the Dickerson-Drew dodecamer showing a HB between a imidazoline NH and a thymine C=O (indicated in yellow).

Despite this discrepancy, the *in silico* results for the proposed structures **46a-d**, overall were positive, namely better ClogP, the same PSA, and similar docking scores as our lead DNA binder, compound **45d**. Thus, we proceeded with the preparation of the compounds of Family I expecting good binding to DNA.

3.1.1.2 Synthesis of Diaryl bis-tetrahydropyrimidine-2-amines (Family I)

The methodology to prepare compounds in Family I was adapted from a Buchwald-Hartwig based synthetic route previously developed in our group.[130] The steps involved initial generation of the diaryl dibromides from diaryl amines *via* Sandmeyer reactions; then, Pd-catalysed coupling with 2-aminopyrimidine and subsequent Pd-catalysed hydrogenation in acidic conditions to generate the corresponding diaryl *bis*-tetrahydropyrimidine-2-amine hydrochloride salts in moderate yield. In some cases, deviation from this method was necessary as it will be explained. The general scheme is presented in Figure 3.1.1.2.1.

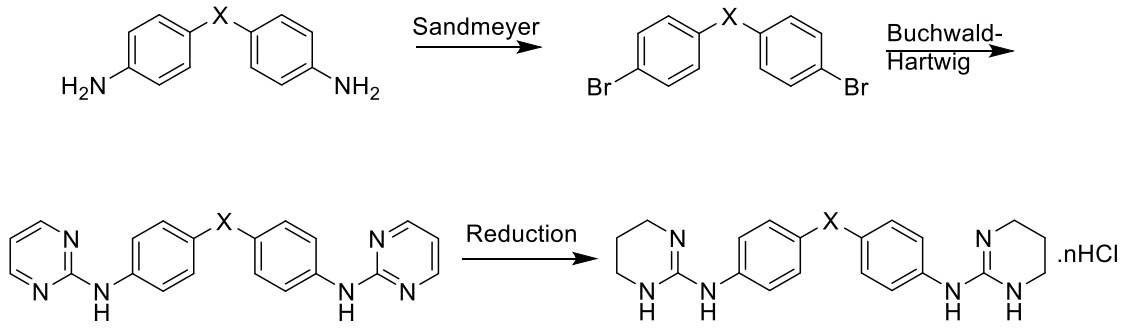

Figure 3.1.1.2.1. General scheme of synthesis for *bis*-2-amino-1,4,5,6-tetrahydropyrimidines

3.1.1.3 Synthesis of dibromo compounds

The synthesis of dibromoaryl compounds from dianilines can be achieved via a diazonium salt using modified Sandmeyer reaction conditions. Thus, we modified some literature procedures for the synthesis of *mono*-bromides, employing two eq. of $NaNO_2$ and three eq. of CuBr in aqueous HBr.[131,132] The preparation of the dianilines required heating the solvent at reflux for extended periods to ensure complete dissolution. The reactions of dianilines **47a** and **47b** gave predominantly one spot by TLC (Scheme 3.1.1.3.1). Purification with a silica plug resulted in the corresponding products **48a** and **48b** in good yield.

Scheme 3.1.1.3.1.

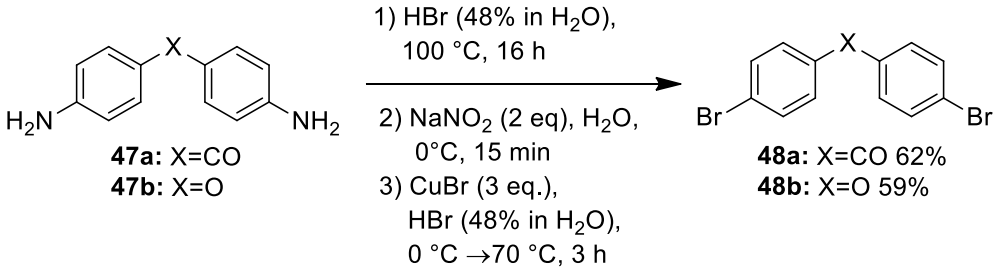

The mechanism of the Sandmeyer reaction is outlined in Scheme 3.1.1.3.2.[133] Reaction of sodium nitrite in acidic conditions at 0 °C gives a highly electrophilic nitrosonium ion, which is attacked by the amino group of an aniline, followed by loss of water, to give an aryldiazonium (**53**) ion. Controlled heating of the reaction in the presence of Cu^{I} generates an aryl radical (**55**) and nitrogen gas. The aryl radical then abstracts a bromide from $Cu^{II}Br_2$ to

regenerate $Cu^{I}Br$ and form the aryl bromide (**56**). Interestingly, the reaction uses Cu as a catalyst, but excess Cu^{I} is employed to suppress side reactions such as phenol formation or radical coupling.[134]

Scheme 3.1.1.3.2. Mechanism of Sandmeyer reaction[134,133]

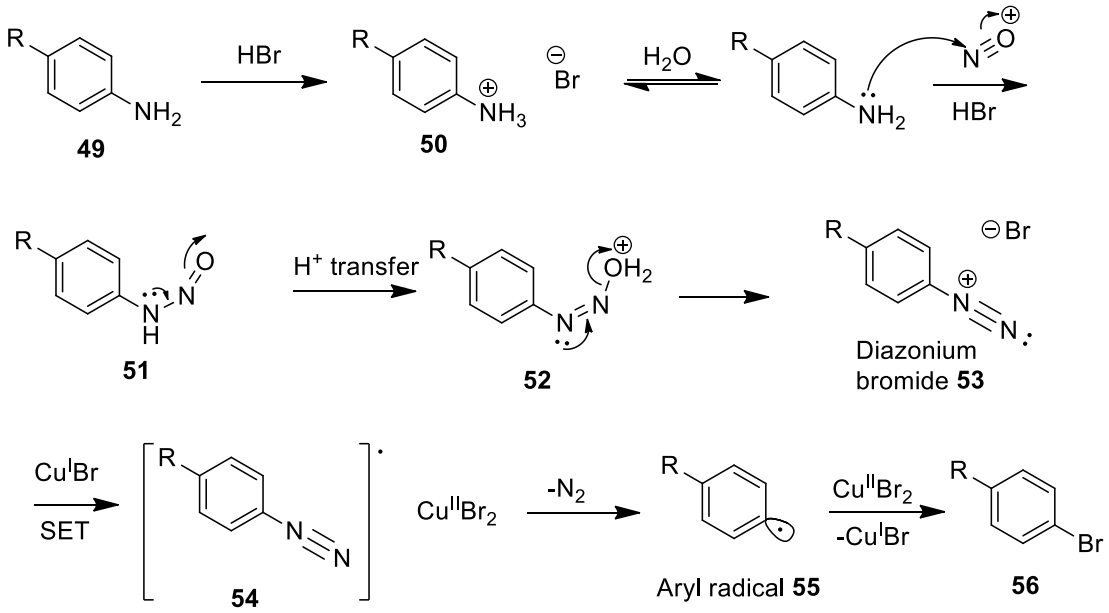

Unfortunately, in the case of compound **47c** ($X=CH_2$), the Sandmeyer conditions led to a complex mixture of products. Although we could access **48c** by reduction of ketone **48a** to **48c** under Wolff-Kishner conditions,[135] we subsequently found a more direct route to access the final salt **48c**.

Compound **48d** with the NH linker was commercially available. However, the free NH could be problematic in the subsequent Buchwald-Hartwig coupling and, thus, needed to be protected. Hence, protection of **48d** with Boc_2O using DMAP as catalyst gave **48e** in high yield (Scheme 3.1.1.3.3).

Scheme 3.1.1.3.3.

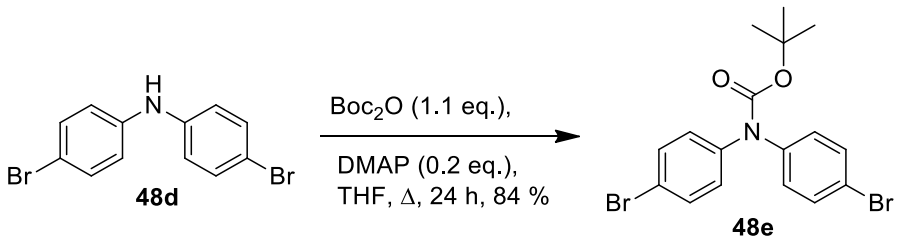

3.1.1.4 Synthesis of diaryl *bis*-2-aminopyrimidines.

With the four dibromides in hand, we turned our attention towards coupling these derivatives to 2-aminopyrimidine **57** (Scheme 3.1.1.4.1). The conditions previously developed by Shaw and Rozas,[130] were amended for diaryl bromides, using NaO^tBu as base, Pd_2dba_3 as Pd source and Xantphos as ligand in dry toluene heated at 90 °C, producing **58a** in very good yield (77%, Table 3.1.1.4.1, entry 1). However, the conditions were not general and necessitated optimisation for the rest of the compounds in the diaryl bromide family (entries 2-15).

Scheme 3.2.2.2.1. Preparation of diaryl *bis*-2-aminopyrimidines

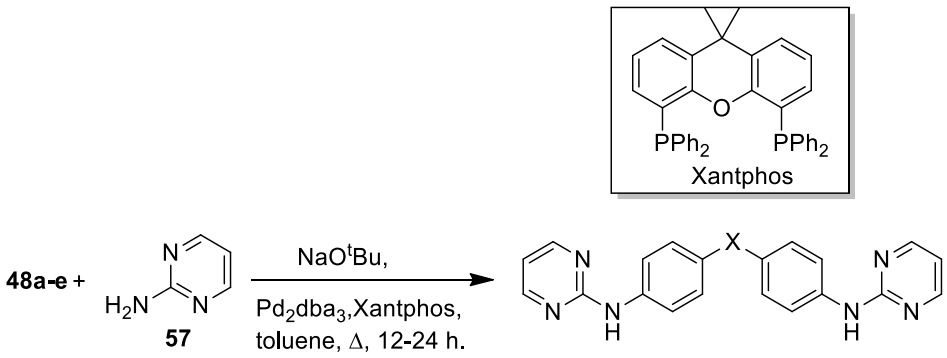

The same reaction conditions utilising **48b** gave only *mono*-coupling. To synthesise **58b**, a larger excess of **57** was employed (entry 3). Although the yield for the preparation of **58b** was low, enough compound was synthesised to carry on to the final product.

To access **58c**, the quantities of **57** and ligand and Pd were slightly increased (entries 4-6). Changing to a weaker base did not improve the reaction. Reaction of NH linker **58d** did not give a pyrimidine product, instead the starting material decomposed (entry 7). Insoluble purple solids precipitated from the reaction mixture. Dibromide **48d** may have reacted with itself to give a redox-active polyaniline. Similar compounds are known to be purple due to extensive delocalisation of radicals through the π-system. Boc-protected derivative **48e** did not decompose under initial conditions; however, the compound did not undergo coupling either, yielding only recovered starting material (entries 8 & 9). More forcing conditions triggered thermal Boc deprotection to regenerate **48d** (entry 10). This was prevented by lowering the temperature to 70 °C (entries 11 & 12). Increasing amounts of Pd_2dba_3 and ligand gave some product (entries 13 & 14). Finally, increasing temperature to 80 °C allowed isolation of **58e** in good yield (entry 15).

Table 3.1.1.4.1. Buchwald-Hartwig amination optimisation table.

Entry no.	di-bromide	$Pd_2(dba)_3$, mol%[a]	Xantphos mol% [a]	Base, eq. [a]	(**57**) eq. [a]	Yield
1	**48a** (X= CO)	4	6	NaO^tBu, 3.0	3.0	77%
2	**48b** (X= O)	4	6	NaO^tBu, 3.0	3.0	0%
3	**48b** (X= O)	4	6	NaO^tBu, 3.0	6.0	31%
4	**48c** (X= CH_2)	4	6	NaO^tBu, 3.0	3.0	0%
5	**48c** (X= CH_2)	6	9	K_3PO_4, 3.0	3.0	0%
6	**48c** (X= CH_2)	6	9	NaO^tBu, 3.0	6.0	72%
7	**48d** (X= NH)	4	6	NaO^tBu, 3.0	6.0	0%
8	**48e** (X=NBoc)	$PdCl_2(PPh_3)_2$, 4	6	NaO^tBu, 3.0	6.0	0%
9	**48e** (X=NBoc)	4	6	NaO^tBu, 6.0	6.0	0%
10	**48e** (X=NBoc)	$PdCl_2(PPh_3)_2$, 10	10	NaO^tBu, 6.0	2.0	0%
11[b]	**48e** (X=NBoc)	4	6	NaO^tBu, 2.8	2.1	0%
12[c]	**48e** (X=NBoc)	4	6	NaO^tBu, 2.8	2.1	0%
13[c]	**48e** (X=NBoc)	10	15	NaO^tBu, 2.8	2.1	0%
14[c]	**48e** (X=NBoc)	20	30	NaO^tBu, 2.8	2.1	45%
15[d]	**48e** (X=NBoc)	20	30	NaO^tBu, 5.6	4.2	63%

[a] All equivalents and mol% are based on dibromide (1 eq.). General conditions except where stated were $Pd_2(dba)_3$, toluene (3.0 mL $mmol^{-1}$) at 90 °C for 12-24 h as adjudged by TLC. [b] THF (3.0 mL $mmol^{-1}$) at 66 °C. [c] Toluene (3.0 mL $mmol^{-1}$) at 70 °C. [d] toluene (3.0 mL $mmol^{-1}$) at 80 °C.

The Buchwald-Hartwig cross-coupling occurs by oxidative insertion of a *mono*-ligated Pd^0 species (PdL) into a carbon-halide bond (Scheme 3.2.2.2.2). The Pd^{II} species is then either attacked by nucleophilic addition of an amine, followed by deprotonation (Pathway A) or activated by the base which is removed by addition of amine (Pathway B); then, reductive elimination to form the C-N bond of the product and regeneration of the *mono*-ligated Pd^0 species takes place. Alkoxide bases can activate Pd^{II} making the complex more reactive towards amines and allowing the mechanism to proceed by either pathway A or pathway B,

whereas weaker bases force the reaction to occur only by pathway A. The rate-determining step (RDS) is dependent on the C-X bond, the base used and the ease of reductive elimination of the substrate. When Shaw's cross-coupling method was developed,[130] the bulky ligand Xantphos was required for good yields, likely due to its large interacting cone angle forcing elimination at the metal centre.[136]

Scheme 3.2.2.2.2.[133]

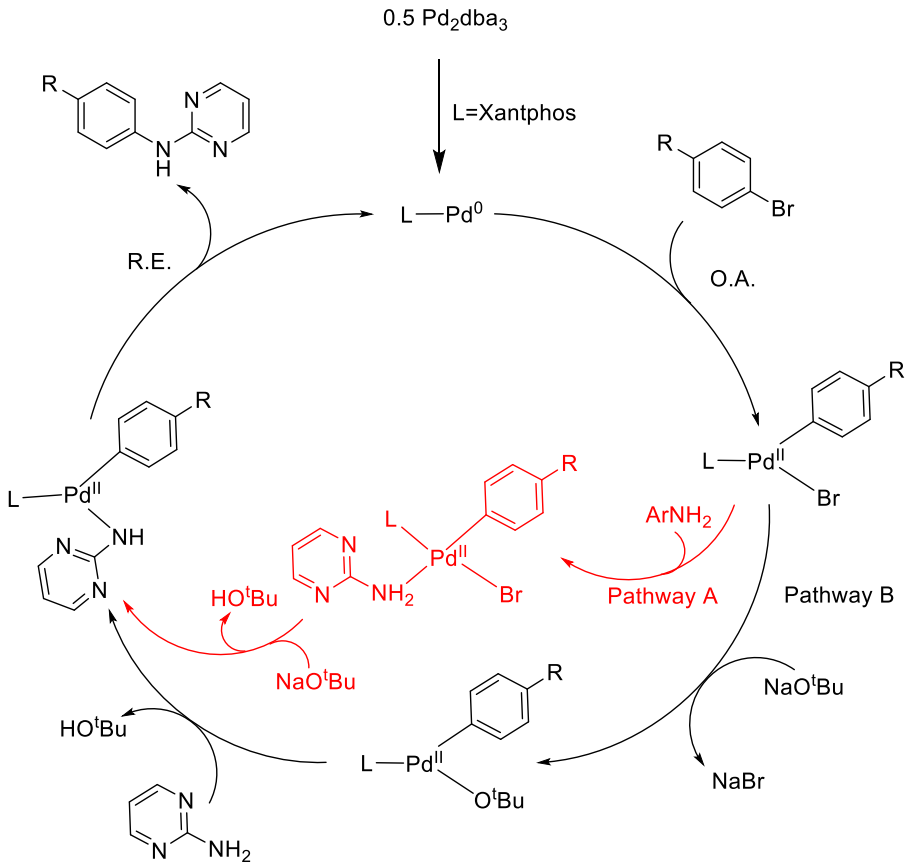

3.1.1.5 Synthesis of 2-amino-1,4,5,6-tetrahydropyrimidines.

The final step of the synthesis involved heterogeneous reduction of **58a-58e** with catalytic Pd/C in a mixture of aqueous HCl and CH_3OH. Analogous to the previous section, each compound behaved differently under the same reaction conditions (Scheme 3.1.1.5.1). Compound **58b** (X= O) gave the expected tetrahydropyrimidine hydrochloride salt **46b** in very good yields. Compound **58e** (X= NBoc) was hydrogenated to a mixture of **46d** (X= NH) and **46e**, demonstrating that under these conditions the pyrimidine reduction is faster than

Boc cleavage. Compound **46e** was converted to **46d** by stirring in 3M HCl for 16 h. Compound **58c** (X= CH_2) was converted to **46c** in poor yield; however, compound **58a** (X= CO) was also reduced in the same conditions to compound **46c**. The reduction of benzophenone-type ketones in hydrogenation is known,[137] and aided here by the presence of HCl. For this reason, we sought to access **46a** via a non-reductive process.

Scheme 3.1.1.5.1.

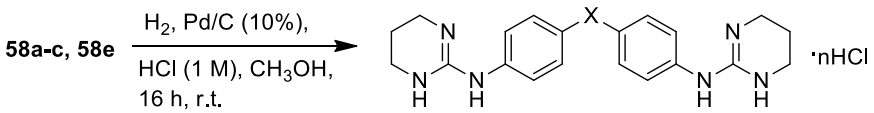

46b: X=O, n=2 (85%)
46c: X=CH_2, from **58c**, n=2 (25%)
46c: X=CH_2, from **58a**, n=2 (83%)
46d: X=NH, n=3 (57%)

To obtain compound **46a** (X= CO), we adapted a procedure commonly employed in our group to synthesise 2-aminoimidazolines, using a Hg-mediated process with tetrahydropyrimidine-2-thione **59**, (Scheme 3.1.1.5.2).[138] To improve the electrophilicity at the thiocarbonyl carbon, compound **59** was *bis*-Boc protected to give **60**. It should be noted that compound **60** is employed as a Boc-transfer reagent,[139] because the Boc carbonyl carbon is also electrophilic. In our case, using $HgCl_2$ to activate the Boc protected thione, and reacting with diamine **47a** in DMF with Et_3N as base, allowed facile preparation of **61**, albeit in poor yield. This was unsurprising as diamine **47a** possesses an electron-withdrawing carbonyl *para* to each amine that reduces the nucleophilicity of the NH_2 groups towards and has given poor yields in similar reactions in our group.[121] Deprotection of the Boc groups in anhydrous HCl in 1,4-dioxane gave *bis*-tetrahydropyrimidine **46a**. All four tetrahydropyridinium salts were fully characterised, highly water-soluble and over 95% pure by HPLC.

Scheme 3.1.1.5.2.

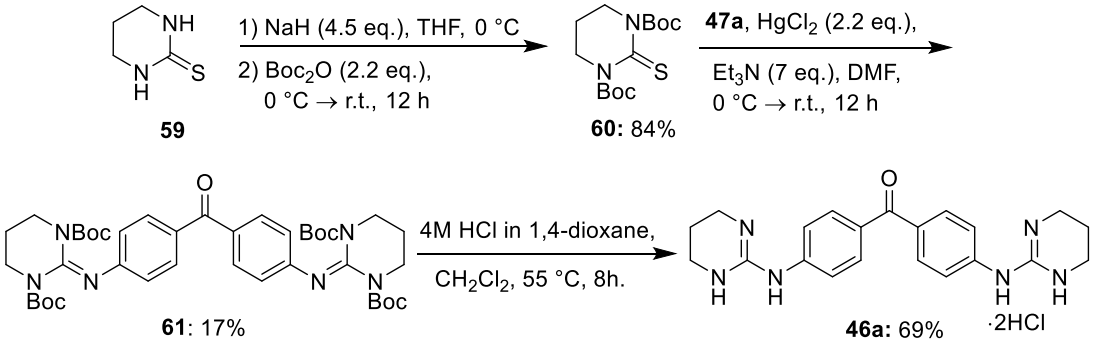

3.1.1.6 Thermal denaturation experiments on Family I.

With the *bis*-tetrahydropyrimidine hydrochloride salts in hand, we carried out biophysical experiments to assess the affinity of the compounds for DNA by thermal denaturation (discussed in Section 1.4.4). We tested affinity for both unspecific salmon testes DNA (stDNA) and an AT rich oligonucleotide poly(dAdT)$_2$. Results are shown in Table 3.1.1.6.1 and Figure 3.1.1.6.1. These outcomes follow a clear trend, with ΔT_M increasing in the order CH_2 (**46c**) < O (**46b**) < NH (**46d**) < CO (**46a**), similar to previous series of diaryl dicationic minor groove binders prepared in our lab.[120] However, when comparing the effect of the cationic moiety we observed that the 2-amino-1,4,5,6-tetrahydropyrimidine core has worse ΔT_M values than the other cations previously studied (Table 3.1.1.6.1).[121] Nevertheless, even the weakest binder of the *bis*-tetrahydropyrimidine series has clear DNA affinity (3.8 °C). The range (5.5 °C) and order of affinity of ΔT_M values obtained in this Family I for stDNA binding is similar to that of the asymmetric compounds **44a-d**, but with significantly stronger binding. Across the families, the compounds with NH or CO linkers consistently give better results than those with O or CH_2 linkers. The compounds bind to poly(dAdT)$_2$ DNA following a similar order, but the magnitude of ΔT_M is consistently larger in the AT-rich sequences than for stDNA which has only a 58.8% AT-content. This suggests that these compounds all bind to AT-rich regions of DNA such as the minor groove.

Table 3.1.1.6.1. DNA binding affinity (ΔT_M, °C) for *bis*-guanidinium-like diaromatic compounds **41** (*bis*-guanidine), **44** (guanidine/2-aminoimidazoline), **45** (*bis*-2-aminoimidazoline) and **46** (*bis*-2-amino-1,4,5,6-tetrahydrocyclohexane).

X	ΔT_M (compds **46**) stDNA & poly(dAdT)$_2$	ΔT_M (compds **41**) poly(dAdT)$_2$[a]	ΔT_M (compds **44**) stDNA[b] & poly(dA).poly(dT)[b]	ΔT_M (compds **45**) poly(dAdT)$_2$[a]
CO (**a**)	9.3 ±0.3 & 14.2 ±0.2	27.6	8.0 & 32.0	-
O (**b**)	6.2 ±0.2 & 8.0 ±0.2	22.1	7.0 & 25.3	27.1
CH_2 (**c**)	3.8 ±0.4 & 5.5 ±0.1	15.0	6.0 & 17.2	18.8
NH (**d**)	7.2 ±0.3 & 12.3 ±0.1	29.6	12.0 & 35.1	38.5

[a]Taken from reference 19; [b]Taken from reference 18.

The normalised thermal denaturation curves are shown in Figure 3.1.1.6.1 for stDNA and poly(dAdT)$_2$ strands respectively.

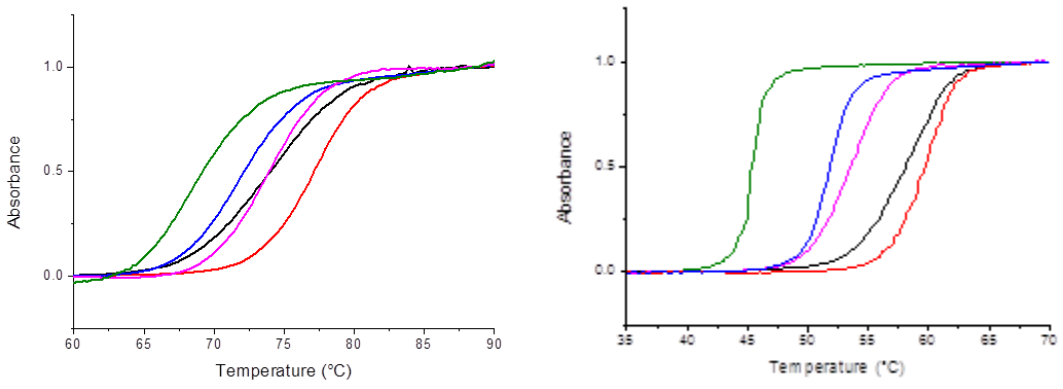

(a) (b)

Figure 3.1.1.6.1. Thermal melting plots for 150 µM of (a) ssDNA (—) and (b) poly(dA-dT)$_2$ (—), in the presence of 15 µM of compounds **46a** (—), **46b** (—), **46c** (—) and **46d** (—) in phosphate buffer, P/D =10).

3.1.1.7 Circular dichroism experiments on Family I.

In order to determine the binding mode of each compound for ssDNA (150 μM), circular dichroism (CD, discussed in Section 1.4.4) titrations of each compound were performed, increasing the concentration from 1.5 μM to 15 μM. Superimposed induced CD (ICD) spectra for each compound are shown in Figure 3.1.1.7.1. In all cases, the increasing concentration of compound induced changes in the CD spectra of DNA. These changes are indicative of DNA binding, due to chiral electronic transition moments in the DNA or compound. However, DNA does not absorb light of longer wavelength than 300 nm. Thus, any absorbance >300 nm is due to coupling of electronic transition moments between the chiral DNA and achiral ligand. Also, the right-handed helix of DNA allows for achiral groove-binding compounds to orientate themselves in a chiral helix, which will give rise to an induced CD spectrum. These strong, positive ICD peaks are indicative of groove binding. An achiral compound that intercalates into DNA bases will generally give a small negative ICD peak since the compound is not in an induced helix and is relatively far from the chiral sugars. In Figure 3.1.1.7.1, compounds **46a** and **46d** clearly show an ICD peak >300 nm, confirming that these compounds are groove binders. Compounds **46b** and **46c** do not show any ICD peaks >300 nm since the compounds do not absorb in this region. Therefore, assigning their binding mode is less trivial.

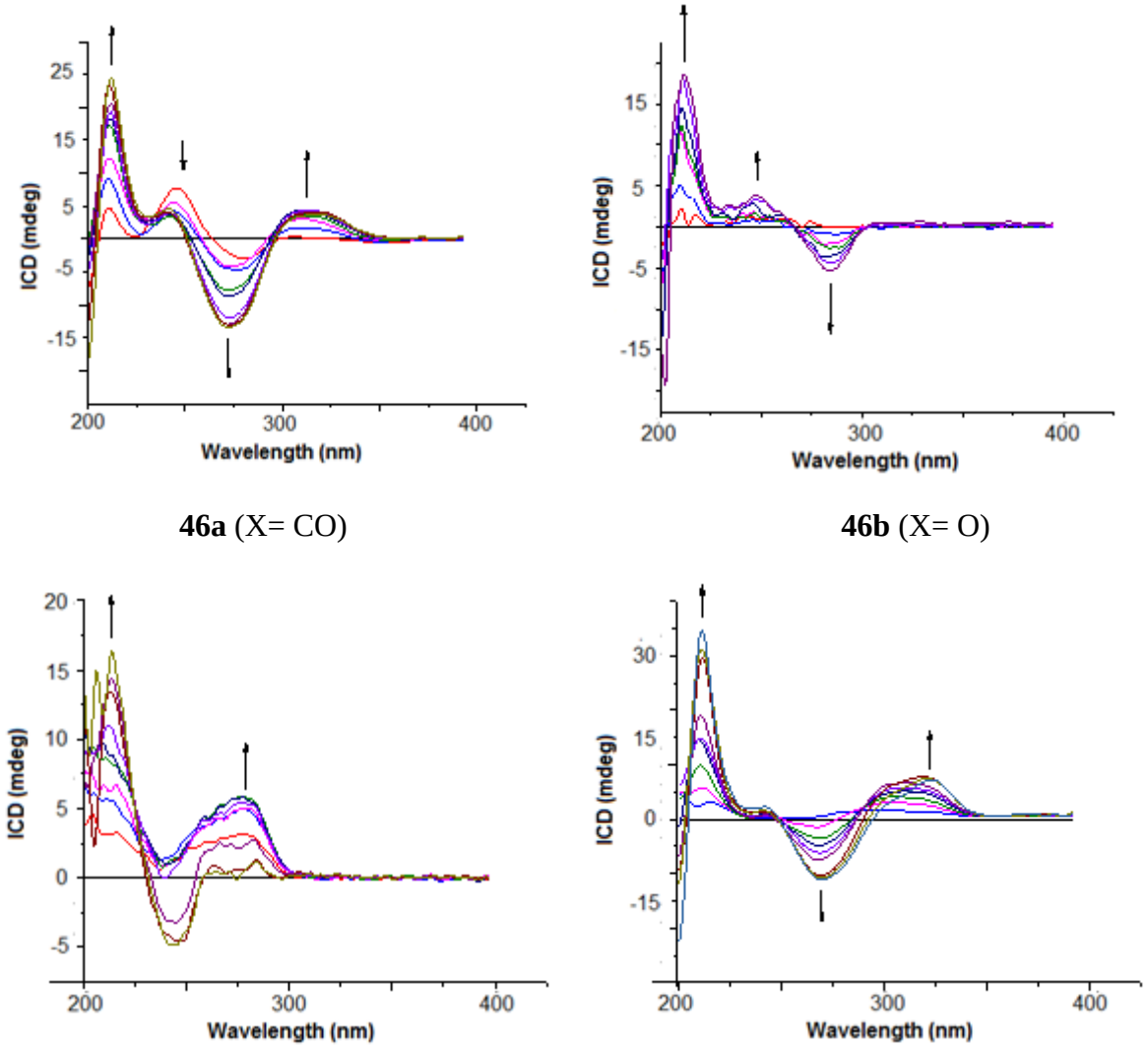

46a (X= CO) **46b** (X= O)

46c (X= CH_2) **46d** (X= NH)

Figure 3.1.1.7.1. ICD spectra obtained for compounds **46a-d** titrated with ssDNA in a concentration of 150 µM varying the Bp/D ratio from 100 to 10 through 9 additions.

The CD results from **46a** and **46d** in poly(dA.dT)$_2$ DNA (Figure 3.1.1.7.2) are very similar to those in stDNA (*i.e.* positive ICD signals), once again indicating minor groove binding (AT rich regions). Attempts to fit the data to different binding models where we could extract a binding constant were unsuccessful. The binding mode of the compounds can change upon increased occupancy in favoured pockets.

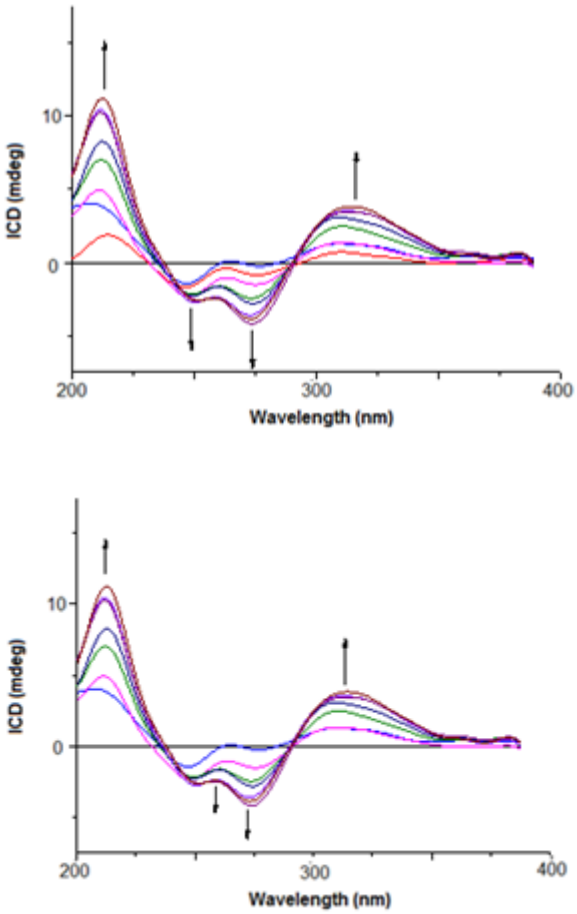

46a (X= CO) **46d** (X= NH)

Figure 3.1.1.7.2. ICD spectra obtained for compounds **46a** and 46**d** titrated with poly(dA-dT)$_2$ in a concentration of 37.5 µM varying the Bp/D ratio from 19.2 to 2.5.

Since compounds **46a** and **46d** absorb light at longer wavelength and have stronger thermal denaturation values compared to **46b** and **46c**, we hypothesised that the stronger groove binding of **46a** and **46d** was due to a more co-planar low energy conformation as found previously in our group.[123] The planar low energy conformation may fit better into its binding site in DNA and also give rise to a delocalised, lower energy chromophore. To test this hypothesis, we performed *in silico* optimisation calculations at Density Functional Theory (DFT) level.

3.1.1.8 Understanding the biophysical results of Family I.

In the crystal structure published by Glass and Dardonville (Figure 3.1.1.1.3, *Right*), lead compound **45d** is orientated so that both aryl rings are almost co-planar. This "active conformation" in **45d** is likely very similar to the active conformation of Family I. The energy penalty that these compounds pay to achieve such a binding conformation may be related to the activity of each ligand. With this in mind, we calculated the lowest energy conformations of all compounds in dicationic Family I in an aqueous environment (PCM-water) at the B3LYP/6-31G computational level.

We used B3LYP, a DFT hybrid method with exchange correlation, namely Becke's three parameter functional, with modifications from Lee, Yang and Parr.[140] DFT uses electron density to calculate energy from solving the time-independent Schrodinger equation and is much faster than Hartree-Fock (HF) *ab initio* methods that attempt to calculate wave functions.[141] In particular B3LYP has the advantages of being computationally less expensive than other functionals while retaining good correlations with experimental evidence.[142] The Pople-type 6-31G basis set is a split-valence double-zeta basis set that uses a single function of six primitive Gaussians to describe each core atomic orbital, with the valence orbitals described by two functions (double-zeta), a linear combination of three primitive Gaussians and another single Gaussian function.[143] The aqueous solvent was modelled by a polarisation continuum model PCM,[144] whereby the water molecules are not explicitly defined but rather are implicitly dealt with as a continuous dielectric medium that interacts with our molecule of interest.

The calculations were performed using Gaussian09[145] and visualised with Gaussview.[145]As can be seen from the optimised geometries of **46a-d** in Figure 3.1.1.8.1, the co-planarity of the rings follows in the order **46c** < **46b** << **46d** ≈ **46a**. This correlates with the experimental DNA thermal denaturation trends, suggesting that the function of the linker in positioning the aromatic rings in a co-planar orientation may be more important than electronic effects or H-bond accepting or donating ability for minor groove binding in this family of 2-amino-1,4,5,6-tetrahydropyrimidines.

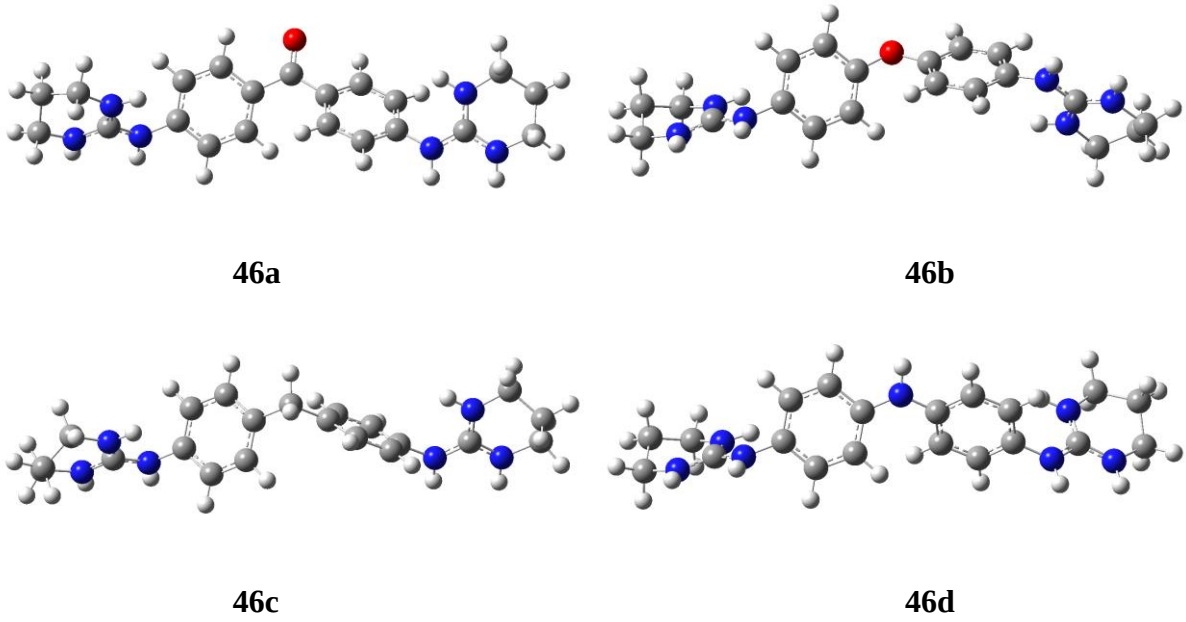

46a **46b**

46c **46d**

Figure 3.1.1.8.1. Examples of the 'front'-'front' conformers of minimum energy calculated for compounds **46a-d** at B3LYP/6-31G level.

3.1.1.9 Conclusions

Compounds in Family I were rationally designed to yield improved MGBs compared to our lead compound **45d**. Accordingly, three diaryl *bis*-(2-amino-1,4,5,6-tetrahydropyrimidinium) salts were synthesised by a Sandmeyer reaction, followed by Buchwald-Hartwig coupling and catalytic hydrogenation and a fourth derivative was synthesised by tetrahydropyrimidine-2-thione activation by Boc protection, Hg-promoted amidylation and Boc-deprotection. All four compounds were >95% pure by HPLC and were able to bind to DNA as shown by thermal denaturation, the strongest binder being the C=O linked derivative **46a**. All the diaryl *bis*-(2-amino-1,4,5,6-tetrahydropyrimidinium) derivatives demonstrated AT-selectivity and were seen to bind into the minor groove of ssDNA and poly(dA-dT)$_2$ DNA based on the CD experiments results. The DNA-binding activity of these compounds was shown to be proportional to the co-planarity of the aryl rings in their lowest energy conformation, as adjudged by calculations at B3LYP/6-31G level and UV measurements. These compounds did not bind as strongly to DNA as previous families of MGBs. The possible reason for this is

that the compounds are prevented from binding to the same pocket in the minor groove as lead compound **45d** (investigated in docking experiments) since the six-membered cations are too big. This prevents the compounds from accessing a key H-bonding interaction as shown in the crystal structure in Figure 3.1.1.1.3. Future work in MGB development will be to increase the possible amount of H-bond donors in the cation and to fix the molecules in a more planar conformation.

3.1.2 Aryl *N*-Aminoguanidines

3.1.2.1 Rationale

To enhance the minor-groove binding ability of our lead compound **3d**, we hypothesised that adding extra H-bond donors might enhance the interaction with DNA. We had observed that introducing H-bond acceptors in the cation did not improve affinity (Figure 3.1.2.1.1). Previously in the laboratory, isouronium and *N*-hydroxyguanidinium derivatives had been prepared and gave poor DNA binding results, even though the *in vitro* cytotoxicity of some of them was much improved compared to lead compound **45d**.[119] The lower pK_a of these cations (Table 3.1.2.1.1) decrease the logD (Table 3.1.2.1.1) of the compounds at physiological pH compared to **3d** and in turn may offer these molecules greater cell permeability. As a consequence of these studies and mentioned in Section 3.1, we propose now that the introduction of extra H-bond donors as in the *N*-aminoguanidine-based Family II (Figure 3.1.2.1) may enhance binding to DNA while lowering the pK_a of the molecule, allowing for increased cell permeability and cytotoxicity compared to **3d**.

Table 3.1.2.1.1. Calcualted basicity (pK_a) and lipophilicity (logD) of model compounds bearing the guanidinium, isouronium, *N*-hydroxyguanidinium and *N*-aminoguanidinium moieties, using the Marvin package.

	pKa	logD
Phenylguanidine	11.45	-0.97
Phenylisourea	8.29	0.38
Phenyl-*N*-hydroxyguanidine	9.52	0.92
Phenyl-*N*-aminoguanidine	9.16	-1.07

In addition, the *N*-aminoguanidine functional group is a known bidentate *N,N'* ligand for Pt^{II}, what can be very convenient for the preparation of the proposed Pt complexes of minor-groove binders.[146] We consider that in addition to increasing DNA affinity, the *N*-aminoguanidine functionality will allow access to a minor-groove binding Pt conjugate. This

hybrid molecule may facilitate an alternative AT-rich DNA-binding preference compared to cisplatin, potentially overcoming resistance mechanisms.

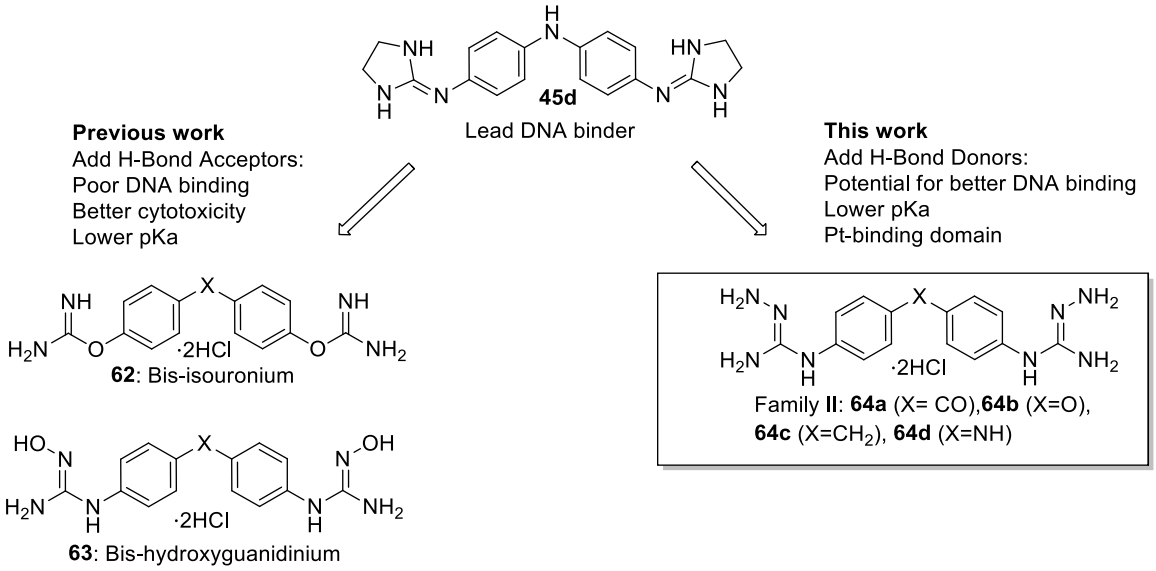

Figure 3.1.2.1.1. Rationale behind the design of Family II.

3.1.2.2 Computational Study of the Interaction of Diaryl *bis*-Cations with DNA

To assess the potential for increased DNA binding with the *N*-aminoguanidine functionality, we carried out a computational study of the interactions of a number of compounds proposed to be prepared with a model of an AT sequence, by means of docking experiments. In contrast to the docking study presented in Section 3.2.1, where the rigid-rigid approach failed to correlate well with the subsequent experiment, we choose to perform a more computationally expensive but more accurate docking experiment using a flexible-flexible approach. The eight steps (**A**-**H**) that this type of study requires are presented in Figure 3.1.2.2.1.

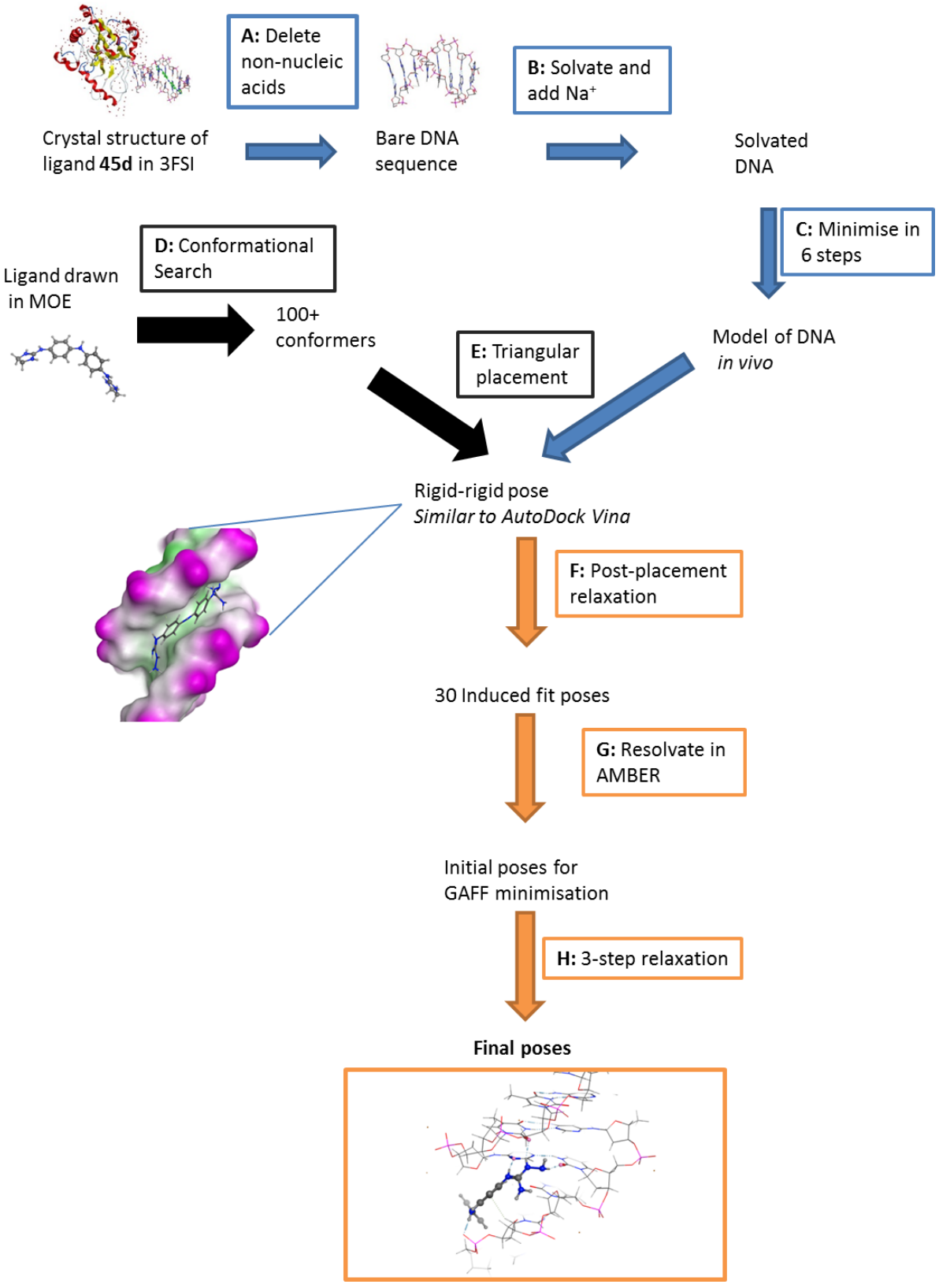

Figure 3.1.2.2.1. Docking methodology using AMBER & MOE for flexible-flexible docking.

For the step **A** we chose as DNA model the same oligomer d(CTTAATTCGAATTAAG)$_2$ from the crystal structure of Glass and Dardonville (pdb code 3FSI).[147] We then proceeded to step **B**, by removing non-nucleic acid components that were added to aid crystal growth, namely the MMLV RT protein (Moloney murine leukemia virus reverse transcriptase), ligand, solvent, acetate and metal ions leaving just the double-stranded oligomer. In step **C** water molecules were added explicitly in MOE to give a total volume of 15 Å^3, as well as Na^+ ions to balance the charge on DNA at the highest negative electrostatic potential.[148,149] The system was then carefully minimised in six stages of decreasing restraints, using the amber99SB force field, which is a molecular mechanics (MM) method (step **D**). The minimisation removes bad contacts between DNA strands and water molecules. In this way, we were able to prepare a suitable DNA template to dock our ligands.

In step **E**, the proposed DNA ligands (Figure 3.1.2.2.2) were built in MOE and minimised using the MMFF94x force field with a 0.05 gradient. A full conformational search was performed using the LowModeMD method with a minimum of 100 iterations for each compound (step **F**).[150] The conformers from this search were docked into the binding site of the minimised DNA structure, and the binding site was defined as the AATT segment. In order to generate space to dock the ligands to DNA, the solvent was removed. For the top 30 poses of each conformer, a post-placement MM forcefield refinement was carried out, allowing the receptor (DNA) to move (step **G**). A non-interacting cutoff of 12 Å was applied.

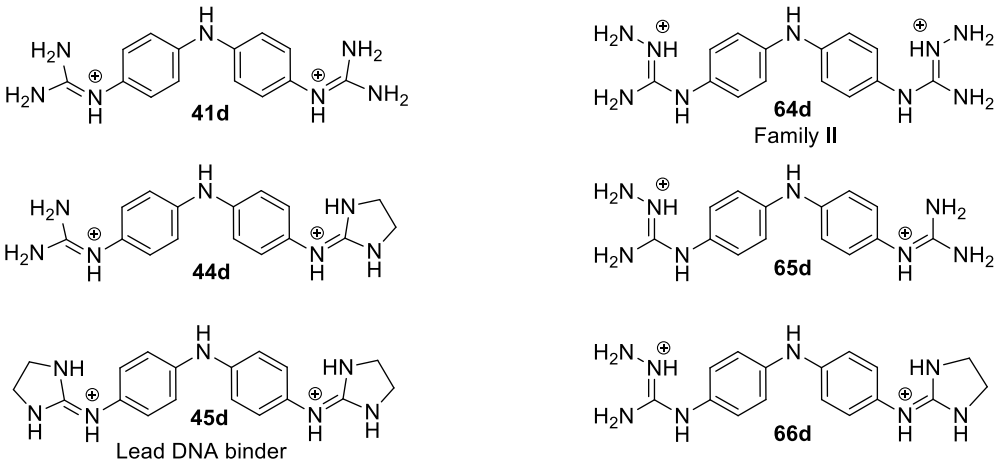

Figure 3.1.2.2.2. The six proposed ligands used in this docking study

Subsequently, the top five ranked poses for each compound docked in DNA were re-solvated in a TIP3P water box and subjected to flexible-flexible minimisation in the General AMBER Force Field (GAFF) in three stages of restraint (step **H**).[151,152] Finally, the minimised complexes were analysed using the MMPBSA/MMGBSA methodologies[153] (Molecular Mechanics Poisson-Boltzmann Surface Area/Molecular Mechanics Generalised Born Surface Area) to calculate solvated binding free energies (equation 1 where B= binding, S= solvation, V= vacuum, Com= complex, Lig= ligand and Rec= receptor).

$$\Delta G°_{B,S} = \Delta G°_{B,V} + \Delta G°_{S,Com} - (\Delta G°_{S,Lig} + \Delta G°_{S,Rec}), \quad (1)$$

The advantages of docking in AMBER 12.0 over AutoDock Vina are that the H atoms are treated explicitly rather than as a part of the adjoining atom; the solvent is treated explicitly, allowing for important water-mediated binding to be found; the initial structure used for docking is not the exact same as the solid state structure; the ligand-receptor complex is relaxed to more accurately model an induced fit; and, finally, the induced fit complex is minimised with solvent to provide a good predictor of a stable fit in solution phase.

It is also important to note that the scoring functions from AutoDock Vina and AMBER 12.0 are different. In particular, AutoDock Vina does not take into account the directionality of H-bonds or solvation effects, both of which are treated in the MMPBSA/MMGBSA methods (AMBER) mentioned above. The difference between MMPBSA and MMGBSA force fields is in the calculation of polar contribution to electrostatic solvation energy. MMPBSA uses the Poisson-Boltzmann (PB) equation to calculate the polar contribution, whereas MMGBSA uses the Generalised Born (GB) model. PB describes the electrostatic environment of a solute in a solvent containing ions whereas GB approximates this by modelling the solute as a set of spheres that interact with solvent. Generally, MMPBSA gives better approximations of the absolute energy of a system but MMGBSA gives better rankings of systems relative to each other.[154] In our study, the top five minimised poses for each of the six compounds were ranked according to free energies calculated by MMPBSA and MMGBSA. The lowest

energy poses of the docking study are shown in Table 3.1.2.2.1. The extended table of all five poses for each ligand are given in the appendix.

Table 3.1.2.2.1. Results of MMPBSA/MMGBSA analysis on lowest energy DNA-ligand complex

Entry	Compd.	Cation[a]	G (kcal mol^{-1}) PB	Ranking PB	G (kcal mol^{-1}) GB	Ranking GB
1	**41d**	Gua/Gua	-50.47	6th	-46.02	6th
2	**44d**	Gua/Imi	-52.55	5th	-49.01[b]	5th
3	**45d**	Imi/Imi	-58.42	2nd	-52.47	2nd
4	**64d**	Amgu/Amgu	-55.73	3rd	-49.10[b]	4th
5	**65d**	Amgu/Gua	-55.27	4th	-49.63	3rd
6	**66d**	Amgu/Imi	-65.84	**1st**	-58.36	**1st**

[a]Gua: guanidinium; Imi: 2-aminoimidazolinium; Amgu: *N*-aminoguanidinium. [b]This pose was different to the lowest energy pose found by MMPBSA.

With regards to the ranking of best binding interaction to least, both methods are in strong agreement: **66d** >> **45d** >> **64d** ≈ **65d** ≥ **44d** >> **41d**; and the binding interactions are in excellent agreement with previous binding results: **45d** >> **44d** > **41d**. Furthermore, the minimised poses suggest a reason for the improved binding of **66d** and **45d**. In the overlaid minimised poses of all six compounds in Figure 3.1.2.2.2, it can be observed that **66d** and **45d** are in the same binding pocket as it was **3d** in the 3FSI crystal structure. The other four compounds are in a slightly higher binding pocket, similar to Family I in the AutoDock Vina docking model in Section 3.1.1.1. It is interesting that the 2-aminoimidazolinium cations in **3d** and **66d** act like an anchor, allowing **45d** and **66d** into the lower binding pocket, but **44d**, the other compound containing an 2-aminoimidazolinium cation, binds in the same upper space as the other molecules.

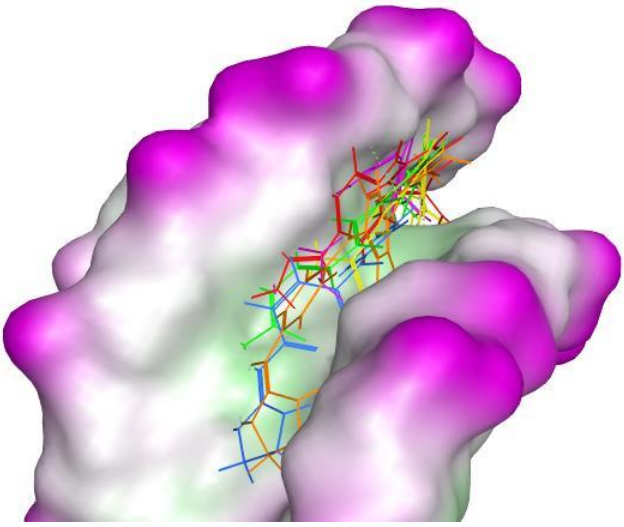

Figure 3.1.2.2.2. Superimposition of **41d** (red), **44d** (green), **45d** (blue), **64d** (yellow), **65d** (pink), **66d** (orange) in DNA oligomer after minimisation. Both **45d** and **66d** occupy a lower section of the binding pocket.

Compounds **45d** and **66d** also contain a 2-aminoimidazolinium or extra *N*-aminoguanidinium cation, which are larger than the guanidinium in compound **44d**. Presumably, for these two compounds, the combination of the interactions of the cations with DNA and the hydrophobic binding of the aryl rings with DNA results in a lower free energy of the system than any possible with the other four compounds in this study. Notably, the aryl rings are not as coplanar as in the crystal structure in 3FSI. All of the binding poses have extensive H-bond networks (Figure 3.1.2.2.3, yellow atoms) from guanidine-like NH atoms to the O atoms in nearby deoxyribose rings. The minimised pose of **64d** in the DNA oligomer is shown in detail in Figure 3.1.2.2.3.

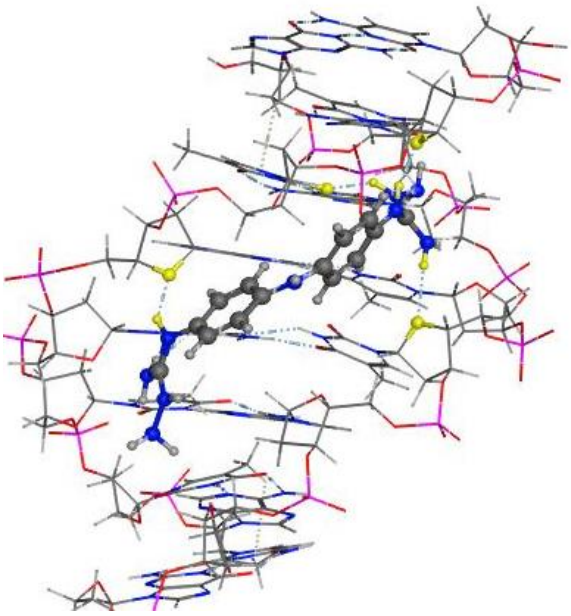

Figure 3.1.2.2.3. H-bonding networks in the minimised pose of **64d** docked in DNA oligomer.

The results presented in Table 3.1.2.2.1, indicated that aryl *N*-aminoguanidines would be good DNA MGBs. Considering the paucity of literature precedents for this type of guanidines we embarked upon the synthesis of substituted *mono*-aryl *N*-aminoguanidines (**67a-c**) and diaryl *bis*-*N*-aminoguanidines (**64a-c**) as shown in Figure 3.1.2.2.4.

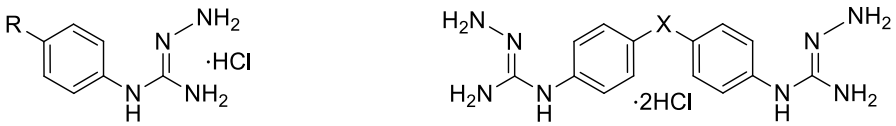

67a: R=H
67b: R=OCH_3
67c: R=NO_2

Family **II**: **64a** (X= CO),**64b** (X=O),
64c (X=CH_2), **64d** (X=NH)

Figure 3.1.2.2.4. Aryl *N*-Aminoguanidines pursued in this work.

3.1.2.3 *N*-Aminoguanidines

Since 1986, *N*-aminoguanidine (**68**) has undergone clinical trials in type II diabetes treatment under the name pimagedine, and is also a nitric oxide synthase inhibitor. First synthesised in 1892, *N*-aminoguanidine has a number of interesting chemical properties. As well as the common *mono*-cationic salt (**68**·HCl), the dicationic salt (**68**·2HCl) has been isolated. Compound **68** and its derivatives behave chemically as substituted hydrazines rather than substituted guanidines. The free base, synthesised by reaction of **68**·HCl with 1 eq. of aq. KOH, readily undergoes dimerization and oxidation to give red/pink 1,2,4,5-tetrazine-3,6-diamine (Scheme 3.1.2.3.1).[155]

Scheme 3.1.2.3.1.

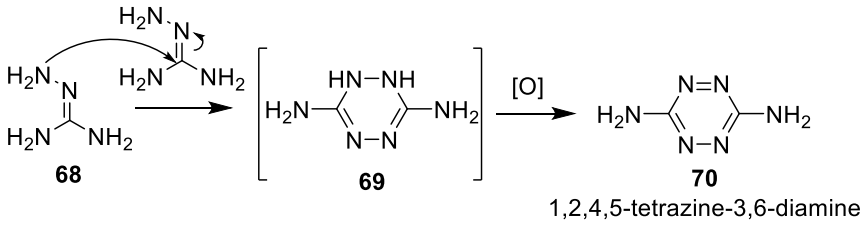

In excess of base, however, **68**·HCl undergoes basic hydrolysis to liberate ammonia, hydrazine and carbon dioxide, and has been tested as a propellant (Scheme 3.1.2.3.2).[155,156]

Scheme 3.1.2.3.2.

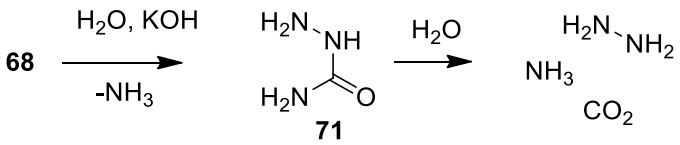

However, **68** is "extremely resistant" to acid hydrolysis and forms hydrazone-type structures with benzaldehyde (e.g. **72**) in either dilute acid or excess base; interestingly, this structure resists hydrolysis (Scheme 3.1.2.3.3).[155]

Scheme 3.1.2.3.3.

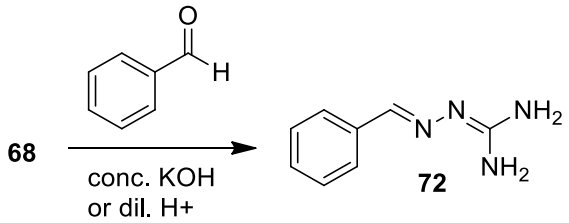

Moreover, *N*-aminoguanidine **68** reacts with benzoic acid to give **73** (Scheme 3.1.2.3.4).[155]

Scheme 3.1.2.3.4.

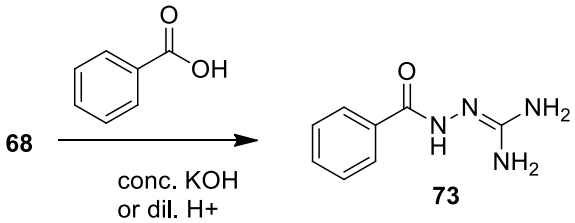

Reaction of **68** with alkyl acids produces intermediates that can further undergo cyclisation to 3-amino-1,2,4-triazoles (Scheme 3.1.2.3.5).[155]

Scheme 3.1.2.3.5.

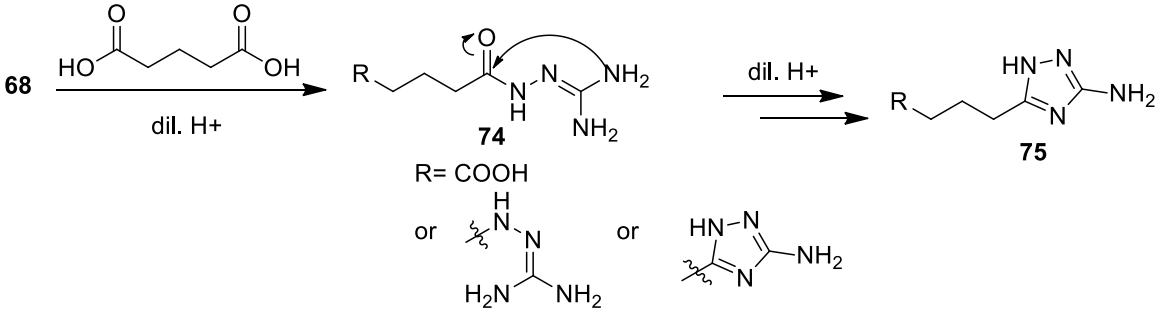

As shown in the above examples, the aminoguanidine functionality is not stable in the presence of base or oxidising agents and, furthermore, is intolerant to a range of electrophiles, including itself, in mild or neutral acidic conditions. Thus, isolation and purification of these compounds could be problematic.

3.1.2.4 Synthesis of Aryl *N*-Aminoguanidines

There are three possible structural isomers of aminophenylguanidine: (i) where the phenyl group is on the amino N atom (Figure 3.1.2.4.1, **76**), (ii) where both the phenyl and amino substituents are on the same guanidine N atom (Figure 3.1.2.4.1, **77**), and (iii) where the phenyl and amino groups are on different guanidine N atoms (Figure 3.1.2.4.1, **67a**). The potential tautomers of these compounds and their *E* and *Z* isomers have not been studied in detail.

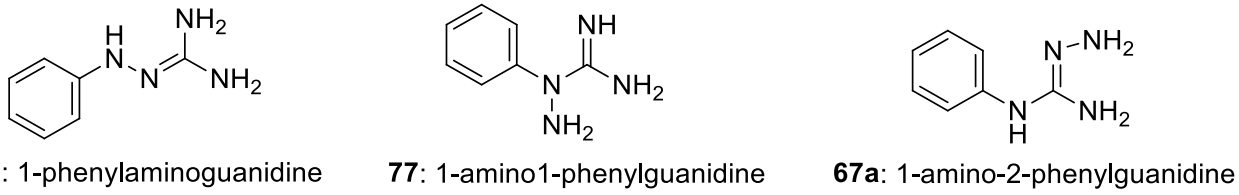

76: 1-phenylaminoguanidine **77**: 1-amino1-phenylguanidine **67a**: 1-amino-2-phenylguanidine

Figure 3.1.2.4.1. Structural isomers of aminophenylguanidine.

Various methods have been employed for the synthesis of aryl *N*-aminoguanidines. The reaction of phenylhydrazine (**78**) with cyanamide produced both **76** and **77** in equimolar amounts (Scheme 3.1.2.4.1). Their different physical and chemical properties allowed for convenient separation, either through hydrazone formation or fractional crystallisation of their corresponding HBr salts from EtOH.[155]

Scheme 3.1.2.4.1.

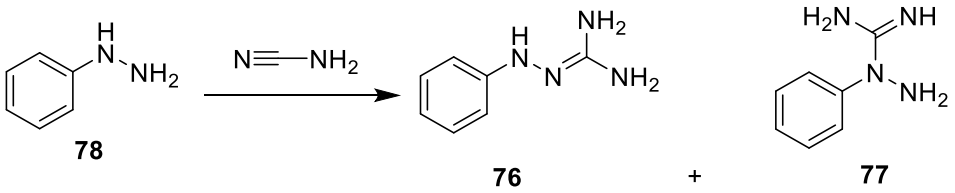

Similarly, in the 1950s, Scott, O'Donovan and Reilly from University College Cork (Ireland) developed guanylpyrazole (**79**), a guanidylating agent from **68**, and used it to make aryl *N*-aminoguanidines **76** and **77** (Scheme 3.1.2.4.2), this time isolated as their picrate salts. Interestingly, once again the compounds were isolated as a 1:1 mixture, rather than the expected kinetic product, 1-aminophenylguanidine (**76**).[157] This may be due to the α-nucleophile effect of the primary amine *N* atom of **30** imparting electron density onto its aniline-type *N* atom, which would otherwise be much less nucleophilic.

Scheme 3.1.2.4.2.

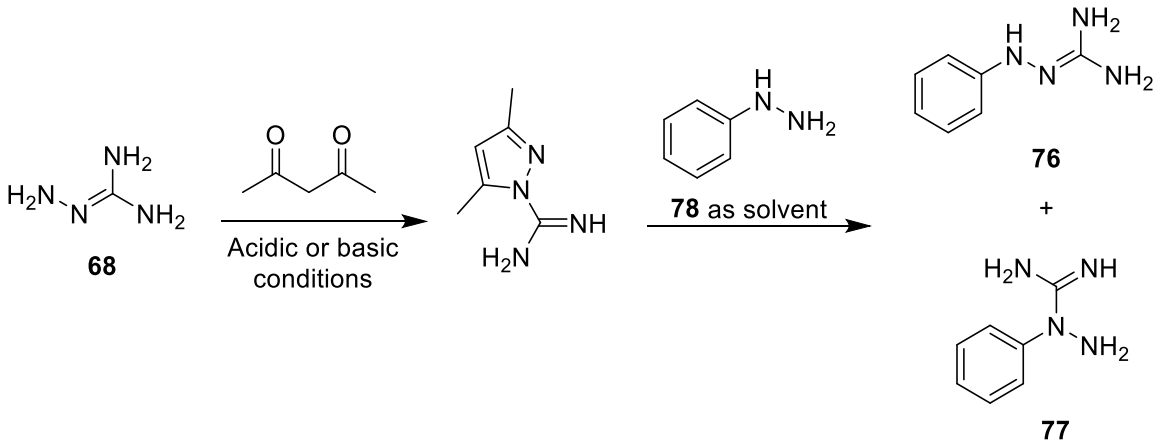

However, from the results of our docking study (Section 3.3.2), we are interested in synthesising 1-amino-2-phenyl guanidine (**67a**) and its derivatives and, thus, a number of methods reported to give the parent compound are discussed hereafter.

In an example from a patent from 1994, the authors used toxic thiophosgene and neat anhydrous hydrazine to synthesise **83**, the HI salt of **67a** in quantitative yield on a 91.5 g

scale (Scheme 3.3.4.3).[158] The ^{1}H NMR spectrum of the HI salt in DMSO-d_6 was 9.5 (br s, 0.5H), 9.0 (br s, 1.5H), 7.7 (br s, 2H), 7.4 (t, 2H), 7.2 (m, 3H), 4.8 (br s, 2H).

Scheme 3.1.2.4.3.

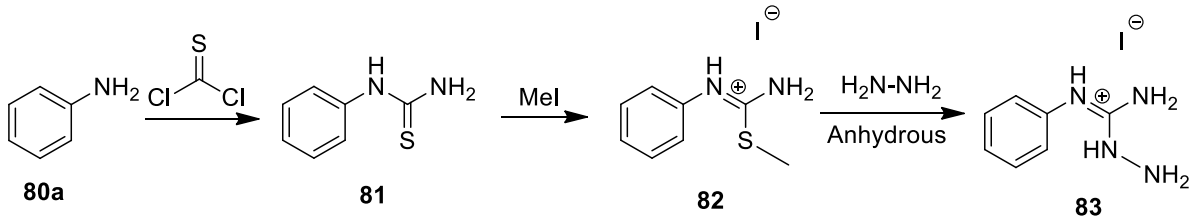

In 2002, Dobosz and Wujec published a simple synthesis of three *N*-aminoguanidine hydroiodide salts upon reaction of **80a** with *S*-methylthiosemicarbazide hydroiodide (**84**).[159] The aniline derivative was isolated in 84% (Scheme 3.1.2.4.4). However, their ^{1}H NMR spectrum in DMSO-d_6 for **83** was vastly different to the previously reported in the patent: 10.35 (br s, 1H NH), 7.83 (br s, 3H, NH), 7.20-7.60 (m, 5H, Ar), 5.72 (br s, 2H, NH).

The disparity between both ^{1}H NMR spectra may have been caused by two separate stable tautomers being formed under the two different conditions or two different protonation states of the molecule. Neither source fully characterised the compound but subsequent synthetic steps in each case proceeded as expected for structure **67a**.

Scheme 3.1.2.4.4.

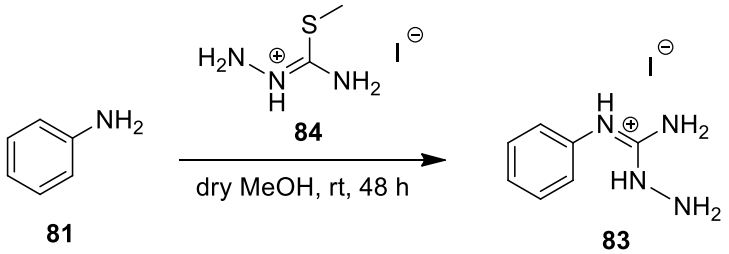

This last simple procedure, avoiding the need for toxic thiophosgene or hydrazine, was ideal for our synthesis.

In our hands, the reaction shown in Scheme 3.1.2.4.4 did not occur as the authors reported. With the aim of synthesising *N*-aminoguanidines by using Dobosz and Wujec's method, we methylated thiosemicarbazide with MeI in excellent yield (Scheme 3.3.5.1, 84%).[160]

Scheme 3.1.2.4.5.

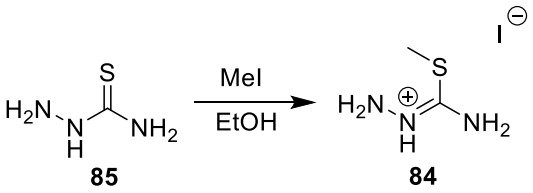

85 **84**

The reaction between **81** and **84** (Scheme 3.1.2.4.6) went to completion, but the ^{1}H NMR spectra of the crude product obtained did not resemble that of **83** as reported by Dobosz and Wujec. However, peaks corresponding to those in the patent report for **83** were present. Attempts at isolation through crystallisation led to degradation. Heating the reaction to 40 °C, to reflux or under microwave conditions, in order to produce predominantly **83**, gave rich mixtures of unidentified compounds.

Scheme 3.1.2.4.6.

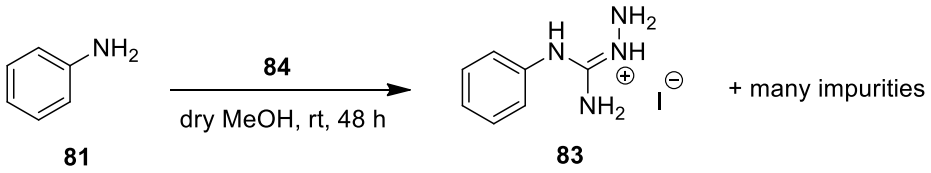

81 **83**

Since the isolation of **83** proved difficult, we searched for methods that produced protected aryl *N*-aminoguanidines. Marletta's group published a method to form Cbz-protected aryl *N*-aminoguanidines. In their paper they gave examples of converting 4-bromoaniline and 3,5-dimethylaniline into their corresponding Cbz-protected aryl *N*-aminoguanidines.[161] The group never published a deprotection step for these compounds but used Pd-catalysed reduction to

deprotect alkyl Cbz-protected *N*-aminoguanidines to give their acetate salts (Scheme 3.1.2.4.7).

Scheme 3.1.2.4.7.

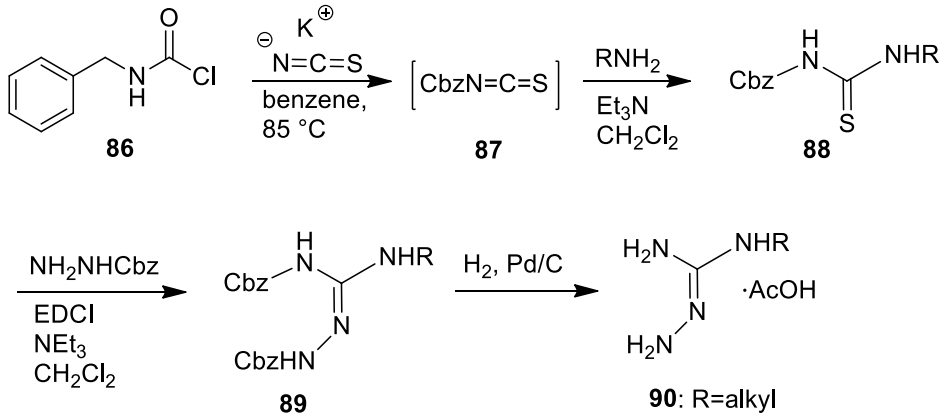

A previous student in our group was unable to replicate this procedure. With or without direct isolation of intermediate **87**, they could not detect evidence for the formation of thiourea **88**.[162] Therefore, we decided to modify this procedure to produce Bn-protected thioureas, which would lead to Cbz- and Bn-protected *N*-aminoguanidines (Scheme 3.1.2.4.8).

Scheme 3.1.2.4.8.

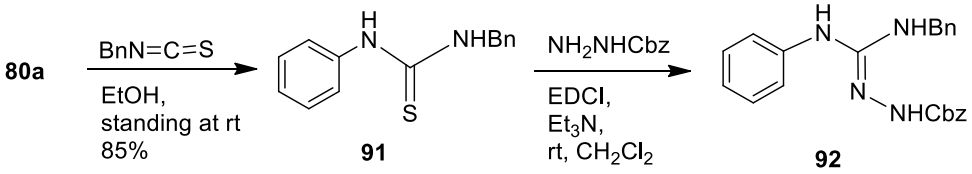

Gratifyingly, the facile preparation of thiourea **91** enabled us to access a more electron-rich thiourea than **88**,[163] which would facilitate formation of the intermediate carbodiimide upon addition of coupling reagent EDCI. Unfortunately, compound **92** was very difficult to isolate as it had similar polarity to the other starting material, benzyl carbazate, $CbzNHNH_2$. On account of the purification difficulties on a small scale and irreproducibility on a slightly larger scale, this route was abandoned. Next, we decided to focus on a method based on

previous work in the group towards synthesis of *N*-hydroxyguanidines.[119] This *N*-aminoguanidylation method employing Boc-protection (Scheme 3.1.2.4.9) was developed in tandem with the previous Cbz-protected method and was ultimately successful in creating **67a**.

We sought to introduce the *N*-aminoguanidine group by converting our anilines into *N*-aryl-*N'-tert*-butoxycarbonyl thioureas and then reacting hydrazine or a protected hydrazine with this activated thiourea in the presence of thiophilic Hg^{2+}. Deprotection of this moiety would lead to formation of the *N*-aminoguanidine hydrochloride salt (Scheme 3.1.2.4.9) analogous to structurally similar *N*-hydroxyguanidines constructed in our group. In order to test this methodology, we applied it to the synthesis of simple *mono*-aryl systems before extending the methodology to diaryl *bis*-*N*-aminoguanidines (Scheme 3.1.2.4.9).

Scheme 3.1.2.4.9.

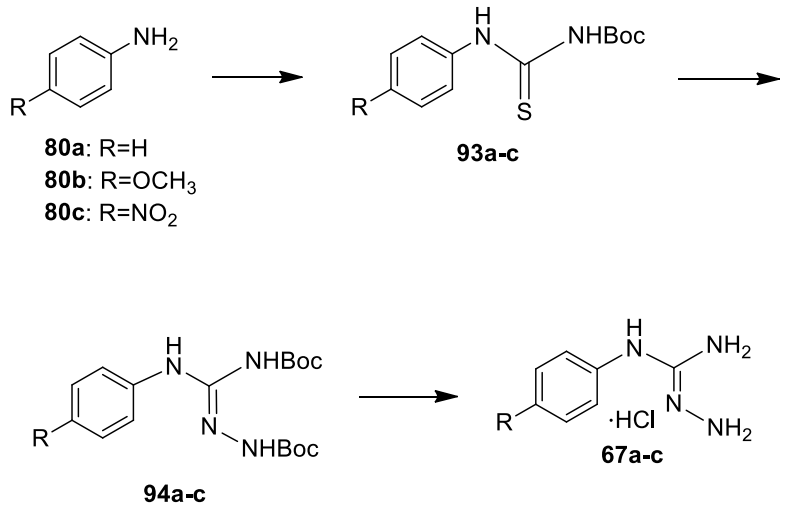

Since other substituted thioureas were not commercially available, we synthesised aryl substituted thioureas by *in situ* reaction of anilines with an activated thiourea. Thiourea, **95**, was Boc-protected by reaction with Boc_2O and excess NaH in THF to give product **96** in 62% (Scheme 3.1.2.4.10).[164]

Scheme 3.1.2.4.10.

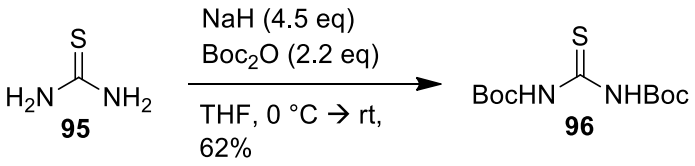

Further deprotonation of **96** and reaction with trifluoroacetyl anhydride provided an electrophile **97** which was attacked with anilines **80a-c** to form substituted thioureas **93a** and **93b** (see scheme in Table 3.1.2.4.1).[164] Unfortunately, when the electron-withdrawing NO_2 group was present at the phenyl ring, aniline **80c** did not react with **96**, even upon heating to 45 °C after 2 days. We chose to omit **93c** from further studies.

Table 3.1.2.4.1.

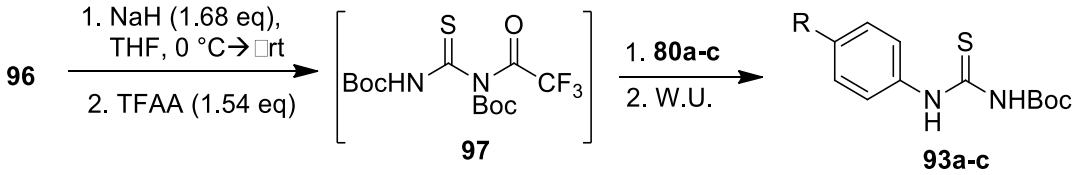

Entry	Compound	R	Yield
1	**93a**	R = H	52%
2	**93b**	R = OMe	78%
3	**93c**	R = NO_2	0%

With thioureas **93a** and **93b** in hand, we turned our attention to the synthesis of protected *N*-aminoguanidine. In order to test different protecting groups we synthesised Boc-protected hydrazine **98** from freshly distilled hydrazine hydrate in 75% yield (Scheme 3.1.2.4.11).

Scheme 3.1.2.4.11.

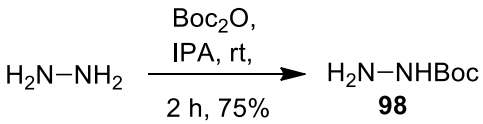

We then carried out test *N*-aminoguanidylations on thiourea **93a** using either commercially available $CbzNHNH_2$ or $BocNHNH_2$, **98** (Scheme 3.3.6.3.3). The product spot was clearly less polar than the reactant spots by TLC in hexane/EtOAc mixtures. With hydrazine **98**, the reaction went to completion by TLC whereas with hydrazine $CbzNHNH_2$ significant amounts of starting material remained (Table 3.1.2.4.2). Product **93a** was isolated in 89% yield on a 0.2 mmol scale but upon scale up to 2.0 mmol thiourea, the yield was lower.

Table 3.1.2.4.2.

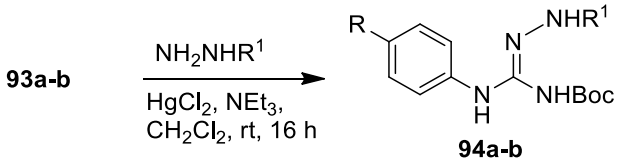

Entry	Compound	R	R^1	Yield
1	**94a**	H	Boc	61%
2	**94b**	OCH_3	Boc	57%

Interestingly, these protected *N*-aminoguanidines gave very broad NMR signals in the aromatic region as visualised by both ^1H and ^{13}C NMR experiments. From previous work in the Rozas group on Boc-protected trisubstituted guanidines,[165] we rationalised that trisubstituted *N*-aminoguanidines are amorphous and contain six tautomers and various rotamers that interconvert on an NMR timescale. Each of the three positions of the neutral guanidine functionality may contain a localised double bond, as either the *E*- or *Z*- isomer. Under a variety of conditions, the TLC was one spot and the mass was found by mass spectrometry and also the IR spectra were consistent with the structures of **94a** and **94b**. Marletta reported trisubstituted 1-aryl-2-Cbz-3-Cbz-aminoguanidines with all aryl peaks in

one multiplet spanning only 0.12 ppm in the ^{1}H NMR and were able to provide all ^{13}C NMR peaks.[161] However, it is possible that in this molecule, the Cbz groups have a single low energy conformation that is not possible with the bulky *tert*-butyl substituents on the corresponding Boc-derivatives.

Deprotection of *bis*-Boc protected *N*-aminoguanidines **45a** and **45b** was achieved by heating in dry HCl. Similar to the deprotection of the amorphous trisubstituted guanidines in the Rozas group, the salts gave rise to ^{1}H and ^{13}C NMR signals in D_2O that were in agreement with the expected structure. Mass spectrometry and IR spectroscopy also allowed us to confirm the identity of **67a** and **67b** as the compounds shown in Table 3.1.2.4.3. Interestingly, the compound seemed to degrade in DMSO-d_6 so direct comparison with the previous syntheses of the HI salt of **67a** were not possible.

Table 3.1.2.4.3.

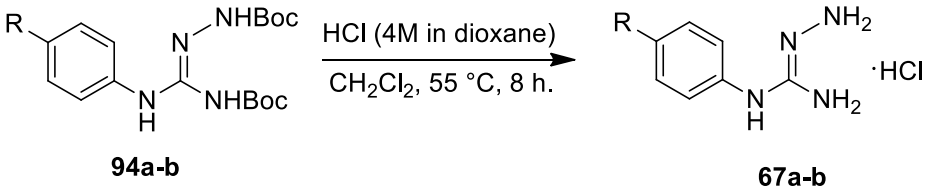

94a-b **67a-b**

Entry	Compound	R	Yield
1	**67a**	H	61%
2	**67b**	OCH_3	76%

3.1.2.5. Test reactions on diaryl *bis*-*N*-aminoguanidines

Having achieved the synthesis of 1-amino-2-arylguanidinium salts **67a** and **67b**, we extended this methodology to the preparation of diaryl *bis*-thioureas. The proposed synthesis is outlined below (Scheme 3.1.2.5.1).

Scheme 3.1.2.5.1.

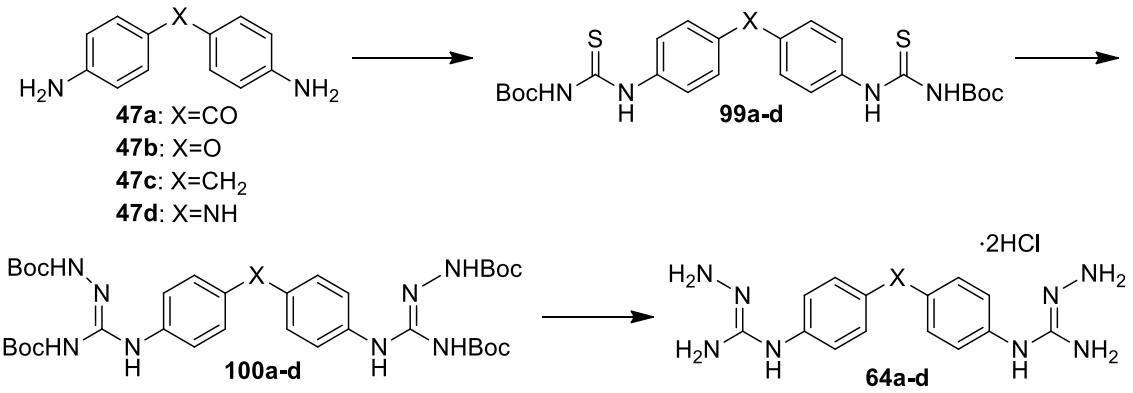

The substrates for the reaction, diaminoanilines **47a-c**, were commercial but **47d** was not. Compound **47d** was prepared in two steps: NAS (nucleophilic aromatic substitution) and reduction (Scheme 3.1.2.5.2). The anion of 4-nitroaniline (**101**) was reacted with 1-fluoro-4-nitrobenzene (**102**) to generate *bis*(4-dinitrophenyl)amine (**103**) in 67% yield,[166] which was reduced to give **47d**. Initially, we attempted $SnCl_2$-mediated reduction to diamine **47d**. Isolation of **47d** after the $NaHCO_3$ quench proved difficult since the diamine is water-soluble. Pd-cataylsed hydrogenation was used instead, with filtration of the product through two sheets of fluted filter paper and copious EtOH washings affording NMR-pure **47d**, in 24% yield, which required storage under Ar.

Scheme 3.1.2.5.2.

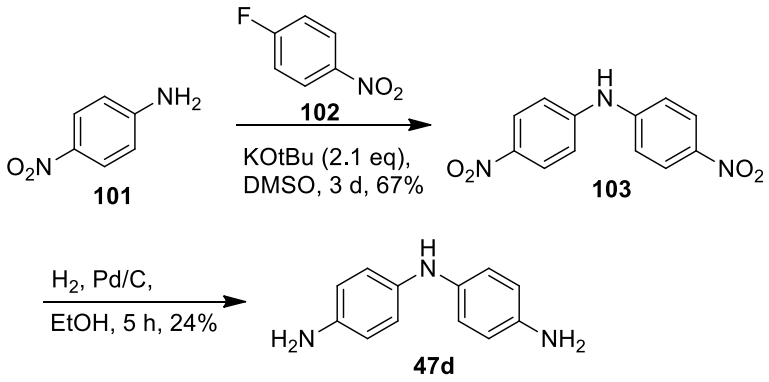

With **47d** in hand, we applied the same methodology described for the aniline systems to create *bis*-thioureas. The yields depended on the electron-donating ability of the X linker. Electron-rich NH linker **47b** gave the product in very good yield, while the O-linked (**47d**)

and CH_2–linked (**5c**) compounds gave lower yields. Unsurprisingly, CO-linked compound **5a** gave the worst result, with only 16% yield after stirring for eight days.

Scheme 3.1.2.5.3.

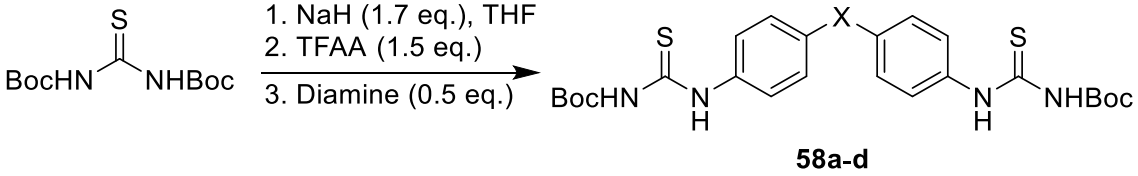

Entry	Compound	X	Yield
1	**58a**	CO	16%
2	**58b**	O	67%
3	**58c**	CH_2	44%
4	**58d**	NH	85%

Unfortunately, the *N*-aminoguanidylation reaction was poor yielding compared to the *mono*-aryl family. With this in mind, we explored many conditions to optimise the reaction. Previously in the group, a $CuCl_2$-mediated guanidylation reaction was developed.[167] This reagent performed similarly to or better than $HgCl_2$ in *mono*-guanidylation reactions so we investigated its effect in this reaction. However, $CuCl_2$ did not improved the results obtained with $HgCl_2$. On a test scale, we were only able to isolate product from the reaction of strongly electron-withdrawing CO linker **99a** with **98** in the presence of $HgCl_2$ (Scheme 3.1.2.5.4). Although the yield of the reaction was low (21%), we demonstrated that it is possible to synthesise Boc-protected diaryl *bis*-thioureas using our methodology. Notably, the NMR spectra showed distinct peaks for the compound of interest.

Scheme 3.1.2.5.4.

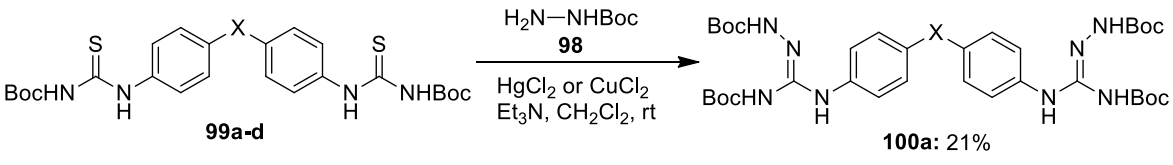

3.1.2.6 Conclusions and Future work

In an effort to improve the binding strength of our MGBs, we completed a comprehensive flexible-flexible docking study between families of MGBs previously synthesised by us and proposed families incorporating the 1-aryl *N*-aminoguanidinium cation. These *N*-aminoguanidine families showed excellent results in the docking studies, giving very close binding energy to compounds **44d** and **45d** but with improved pharmacokinetic properties, including lower calculated pK_a. Their synthesis, however, proved non-trivial. *N*-Aminoguanidines possess a rich chemistry, and are likely to decompose into many compounds, hampering their isolation in high purity. The NMR spectra of the Boc-protected *N*-aminoguanidines are convoluted by possible rotamers, in some cases broadening the spectra beyond use. However, analysis by TLC and mass spectrometry gave an indication that the products were formed and were pure. Deprotection of the Boc groups gave assignable spectra. Furthermore, a small family of diaryl *bis*-thioureas were synthesised and one member of the Boc-protected diaryl *bis*-aminoguanidine family was synthesised. The coordination chemistry of the aryl *N*-aminoguanidines will be explored in Section 3.2.1.9. Future work will include scaling these reactions up to isolate the deprotected salts of Family II.

3.1.3 Malonate-derived MGBs

As mentioned in the Objectives section, we aimed to create a strongly DNA-binding, highly water-soluble organic dication, based on our lead compound **45d**, which would incorporate a Pt-binding moiety (Figure 3.1.3.1). The proposed complex (**68**) should include: (i) a diprotonated diaryl guanidinium that can bind strongly to the DNA minor groove and (ii) a linker that binds to Pt but can be released *in vivo* to give an aquated cisplatin-type moiety. With this objective in mind, we chose to use a malonate ligand as a linker (reviewed in Section 3.2.1.1) to give target complexes such as **69**.

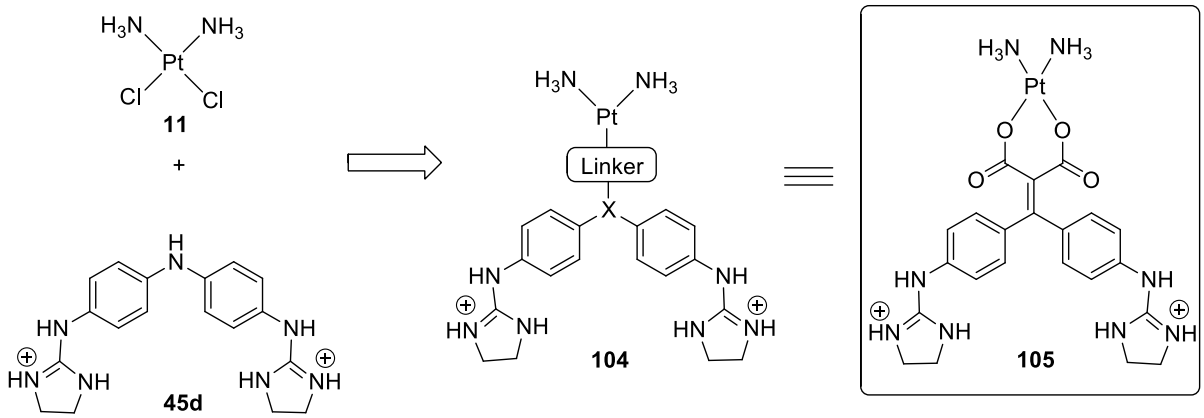

Figure 3.1.3.1. Target compound incorporating cisplatin and MGB.

To create the proposed complex **105**, we would have to synthesise malonate-derived ligand **106** and then, couple the dicarboxylate to an activated Pt species. Related to **105**, compounds **106** and **107** could also be synthesised to probe the orientation of the linker (Figure 3.1.3.2).

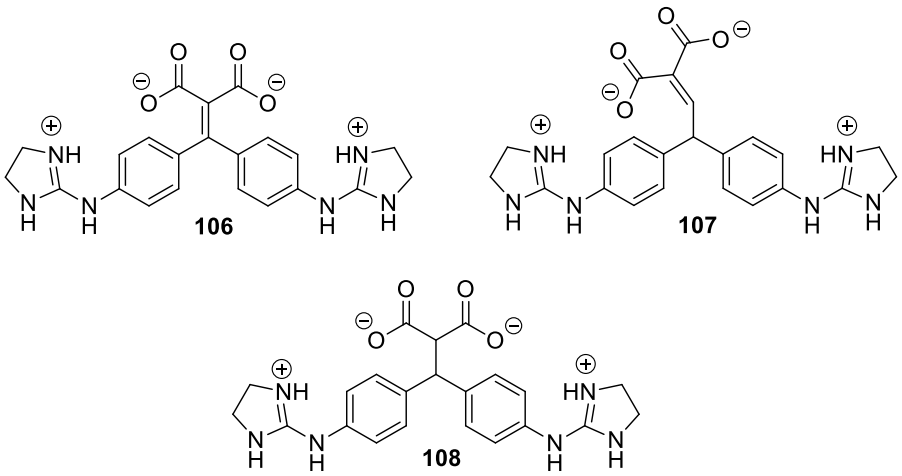

Figure 3.1.3.2. Proposed MGB-malonate derivatives.

First, the DNA-binding activity of malonate-derived diaryl *bis*-aminoimidazolinium salts was explored using *in silico* docking. Then, we synthesised the most promising compounds and evaluated their biophysical properties. The design, synthesis and biological activity of a second generation of malonate-containing DNA binders was also pursued. Finally, the complexation of **106** and related compounds with Pt was attempted (see Section 3.2.2).

3.1.3.1 Computational Study

In order to assess whether previous MGBs, developed in the group, would retain their activity when linked to a Pt-binding malonate moiety, *in silico* docking experiments of these ligands to DNA were carried out. Three malonate derivatives were selected, with linkers that vary in unsaturation and distance to the MGB (Figure 3.1.3.2). Thus, structures **106**, **107** and **108** were optimised using the Gaussian09 package,[145] in a PCM water solvation model[144] (at B3LYP/6-31G level).[141,140,143] Similarly to Sections 3.2 and 3.3, we chose the crystal structure of **45d** within the minor groove of an oligonucleotide resolved by Glass *et al.*[129] as template for the docking studies. Then, using AutoDock Vina,[128] the ligands were docked into the minor groove formed by the oligomer of the oligo crystal structure.

Three different dockings were performed:

i) '*crystal fixed*'- by using the ligands in a rigid-rigid approach, fixing the dihedral angles between the aryl rings, and the dihedral angle between the aryl rings and the 2-

aminoimidazolinium rings to the same values observed in compound **45d** within the crystal, this leaves only the malonate group free to rotate;

ii) '*crystal flexible*'- a flexible-rigid approach where the conformations from the crystal were used as an initial guess, with all bonds freely rotatable in the binding site of the rigid DNA octamer, and

iii) '*optimised flexible*'- a flexible-rigid approach where the optimised ligands were used as an initial guess, with all bonds freely rotatable in the binding site of the rigid DNA octamer.

Docking scores, which are an approximation of the binding enthalpy, were calculated using the AMBER forcefield (Table 3.1.3.1.1).[128] In general, those docking poses (*i.e.* complex structures) using the ligands with fixed dihedral angles scored a much better binding than when using optimised ligands. It was clear from these results that the unsaturated malonate ligand **107** was not able to orientate itself in the optimal docking configuration within the DNA octamer so its synthesis was discarded.

Table 3.1.3.1.1. Docking scores (kcal/mol) of best poses from malonate ligands (**106**-**108**) in DNA compared to those of the MGB (**45d**) which had been crystallised with the DNA oligomer

Orientation	45d	106	107	108
Crystal fixed	-11.0	-9.7	-6.8	-10.0
Crystal Flexible	-8.2	-7.4	-7.4	-7.5
Optimised Flexible	-8.6	-8.1	-8.1	-7.7

On the other hand, compounds **106** (Figure 3.1.3.1.1) and **108** provided good docking results across the board. Their synthesis and biological activity is outlined below.

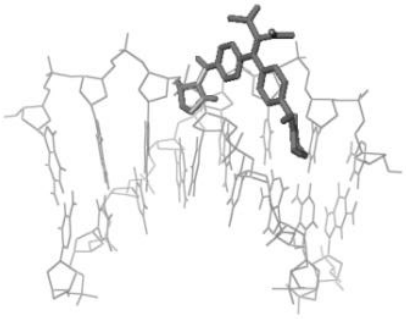

Figure 3.1.3.1.1. Docking model of **106** in DNA oligomer, visualised in AutoDockTools.

3.1.3.2 Retrosynthesis

The retrosynthesis of compound **105**, presented in Scheme 3.1.3.2.1, was straightforward; diamminoplatinum complexes with malonates are known to form by addition of the malonate ligand to iodoplatin (**10**) and $AgNO_3$ in water[168] so disconnection of the Pt-O bonds to form **106** was a clear choice. Since malonate groups can undergo decarboxylation in acidic conditions,[169] it was decided to protect them as the diethyl ester. In our lab, guanidylation by reaction of thiourea-like compounds with aryl amines is carried out routinely. For this reason, we performed a simultaneous functional group interconversion to the Boc-protected iminoimidazoline (**109**), where compounds of this type are commonly prepared by reaction of the dianiline (**110**) with Boc-protected imidazolidine-2-thione (**111**). Finally, disconnection of the malonate moiety left diethyl malonate and a dianiline with an electrophilic benzylic carbon, here we chose 4,4'-diaminobenzophenone (**47a**).

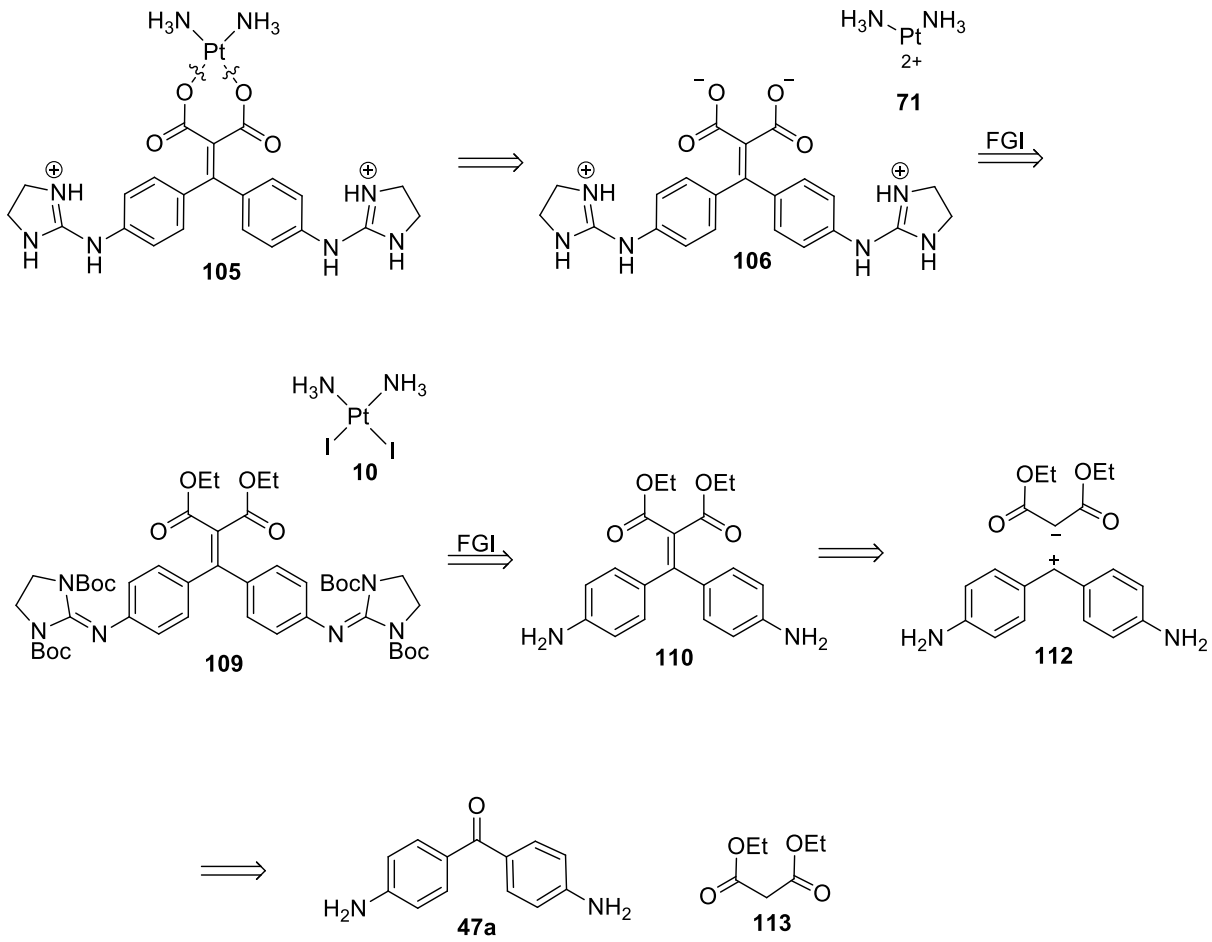

Figure 3.1.3.2.1. Retrosynthesis of **105**.

3.1.3.3 Attempted synthetic routes

The forward synthesis began with nucleophilic attack of diethylmalonate (**113**) on commercial benzophenone **47a**, to form a C=C double bond that could be easily reduced by sodium cyanoborohydride.[168] Following Griffith's procedure,[168] ketone **47a** and **113** were heated in ethanol at reflux with 10 mol% pyridine as a base and 10 mol% benzoic acid to activate the ketone. Regrettably, no reaction was evident by TLC or ^{1}H NMR analysis after 48 hours. The reaction was repeated without benzoic acid with identical results. Exchange of the base and solvent with either sodium hydride or sodium ethanoate and THF also gave no positive result. The complete lack of reaction, especially with a base as strong as sodium hydride, implied that deprotonation was not the problem. Thus, we thought to activate the ketone with a Lewis acid to make it more electrophilic. Activation of a carbonyl group with equimolar amounts of titanium chloride ($TiCl_4$) and pyridine has worked previously for the

reaction of poorly reactive aryl aldehydes with di-*tert*-butyl malonate.[170] In this case, reaction with benzophenone **47a** again proved fruitless.

Removal of the electron-donating aniline amino groups should improve electrophilicity of the carbonyl. Thus if the Boc-protected 2-iminoimidazolidine (**114**) was synthesised first and subsequently reacted with malonate there would be no electron-donating groups and the reaction might proceed (Scheme 3.1.3.3.1). However, attack by malonate in the presence of the same variety of bases yielded no new compound.

Scheme 3.1.3.3.1.

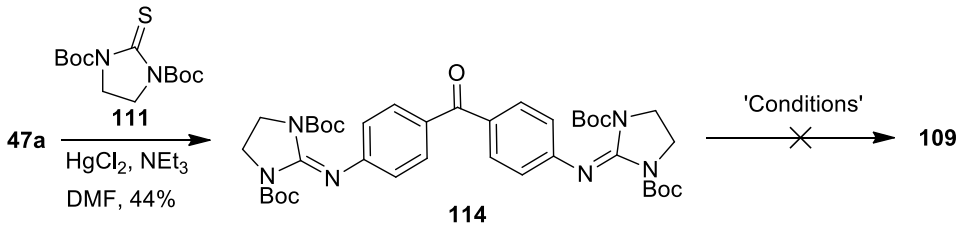

Simple Boc-protection of the dianiline to reduce the nucleophilicity of the amines was another alternative. Unfortunately, Boc-protection of benzophenone **47a** with di-*tert*-butyldicarbonate and DMAP gave no reaction,[171] presumably because of deactivation by the electron-withdrawing carbonyl group (Scheme 3.1.3.3.2).

Scheme 3.1.3.3.2.

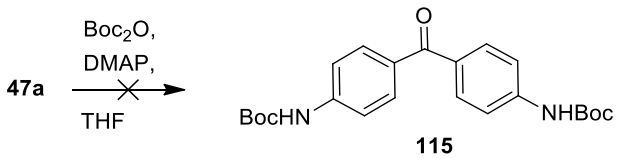

Another synthetic route to key intermediate **74** that would avoid any problems with the electron-donating amines would be the nucleophilic aromatic substitution (NAS) of diethyl 1,1-di(4-fluorophenyl)methylenemalonate (**116**) with a nitrogen nucleophile such as sodium

phthalamide or sodium azide. The corresponding retrosynthetic scheme is shown in Figure 3.1.3.3.1.

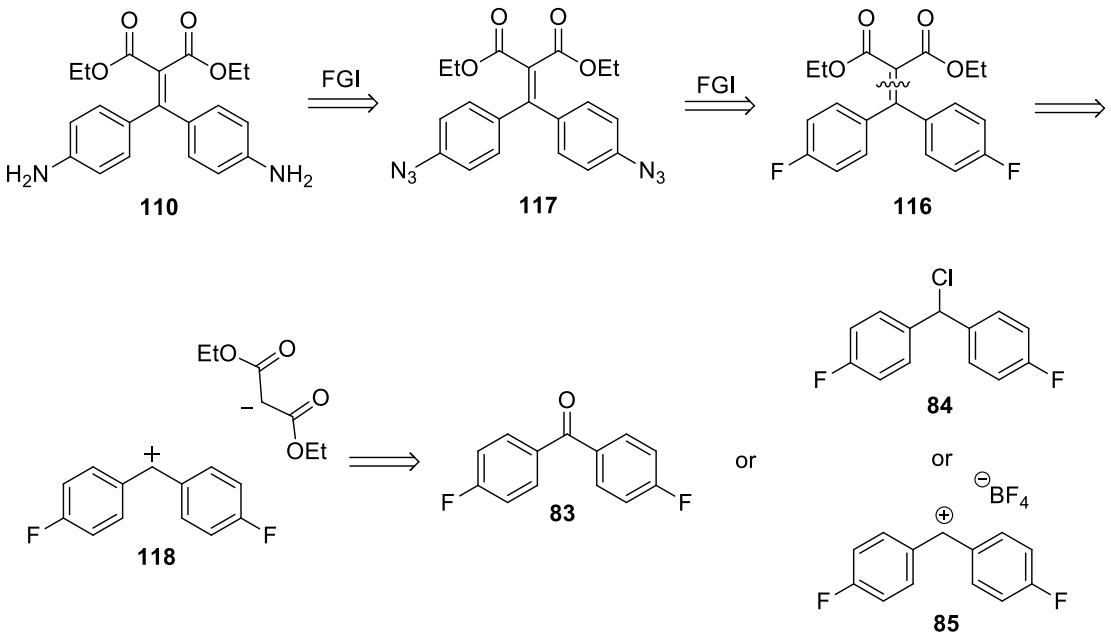

Figure 3.1.3.3.1. Retrosynthesis of **110** with azide NAS on **116** as the key step.

Similar to previous attempts, diethyl malonate did not react with 4,4'-difluorobenzophenone, **119**, in any of the reaction conditions used previously. Reduction was attempted to access the alcohol, which can be converted into a more reactive electrophile, *i.e.* the tetrafluoroborate salt or alkyl halide. Gratifyingly, reduction of **119** with $NaBH_4$ in CH_3OH furnished alcohol **122** in an excellent yield (98%).[172] Following Mayr's procedure,[173] synthesis of a benzylium tetrafluoroborate salt **121** was attempted (Scheme 3.1.3.3.3).

Scheme 3.1.3.3.3.

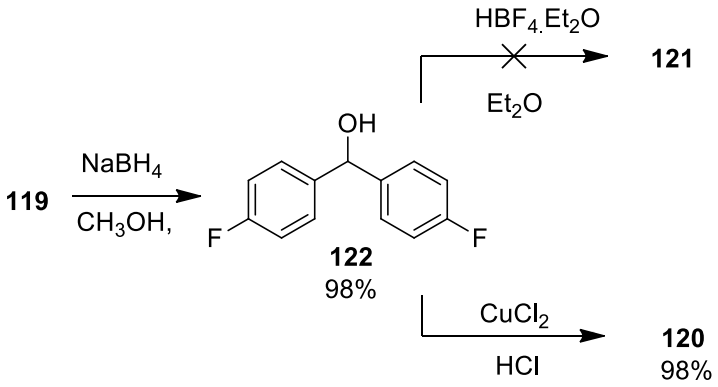

The reaction mixture turned black but did not precipitate out of diethyl ether as described in the literature. However, using Narsaiah's procedure,[172] chlorination of **122** with $CuCl_2$ in refluxing HCl yielded the alkyl chloride **120**. Narsaiah used piperazine as a nucleophile to displace chloride. Unfortunately, analogous malonation of **120** in THF with K_2CO_3 or NaOEt as base did not occur, even at reflux for 48 hours (Scheme 3.1.3.3.4).

Scheme 3.1.3.3.4.

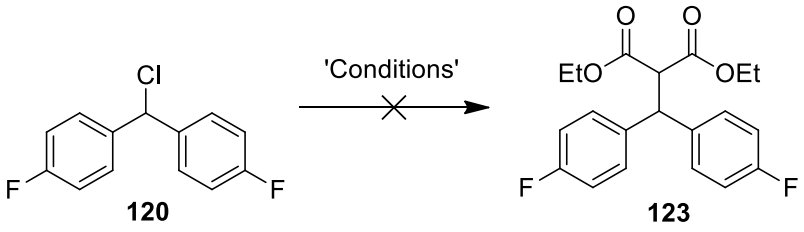

3.1.3.4 Dibromo route

The failure of the previous methodologies prompted us to revise our route towards key intermediate **110**. The addition of diethyl malonate to a sterically-congested doubly benzylic carbon was not optimal. Figure 3.1.3.4.1 shows an alternative synthetic route involving the formation of the malonate group in two steps by a disconnection at the C-C single bond, to give known compound **128**. For ease of synthesis we used bromide handles on the aryl rings

in the hope that we could later functionalise the aryl rings with transition metal-catalysed cross-coupling.

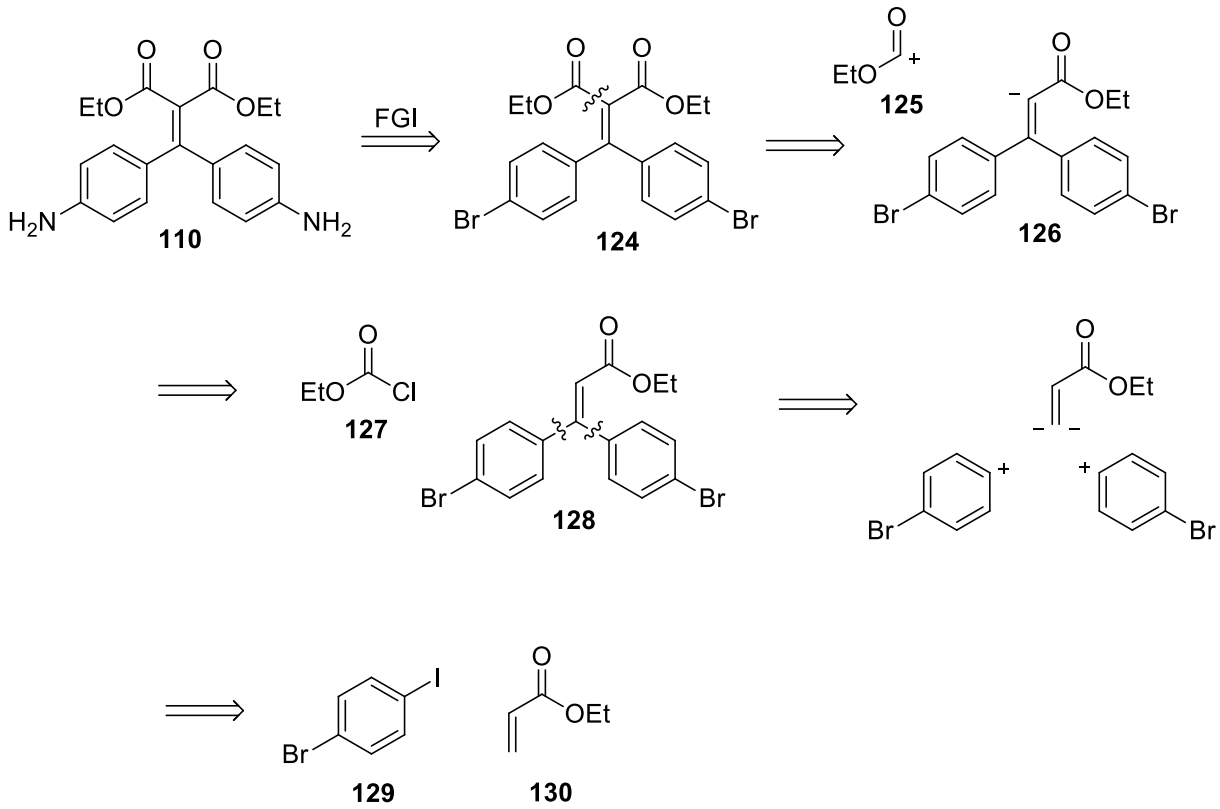

Figure 3.1.3.4.1. Retrosynthesis of **110** by forming the malonate functionality in two steps.

Known compound **128** had previously been synthesised in high yield in an acid-mediated Heck reaction.[174] In our hands, the procedure was amenable to scale-up, producing up to 2.3 g in 90% yield (Scheme 3.1.3.4.1). Ethyl acrylate (**130**) required distillation immediately prior to use in order to remove the radical inhibitor present in the commercial product.

The anion of **128** (compound **126**) was quenched in an ethereal solution of ethyl chloroformate to generate malonic ester derivative **124**. The procedure by Forn[175] and coworkers for the synthesis of similar *bis*-aryl malonic ester derivatives was modified, using LDA (lithium diisopropyl amide) instead of *n*-BuLi to prevent lithium-halogen exchange. To our delight, the reaction proceeded in good yield, even after scale-up to 2.3 g of **128** (64% yield, Scheme 3.1.3.4.1).

Scheme 3.1.3.4.1.

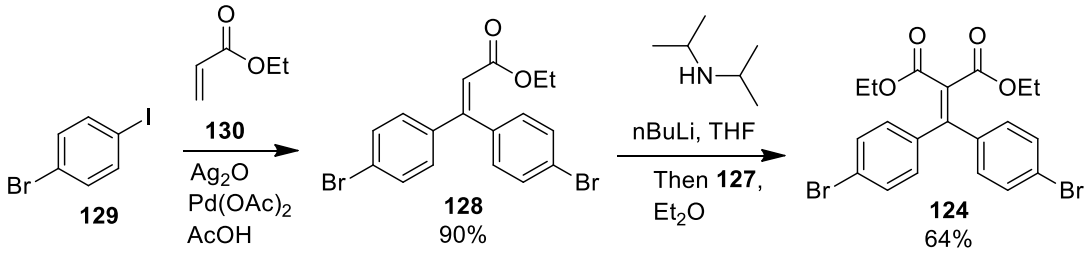

Palladium-catalysed cross-coupling reactions to exchange the aryl bromo groups of **124** with amino or guanidino N atoms were less straightforward. Pd-catalysed coupling of aryl halides to ammonia has been recently reviewed, albeit using a very expensive Josiphos ligand (**131**, Figure 3.1.3.4.2) and gaseous ammonia.[176]

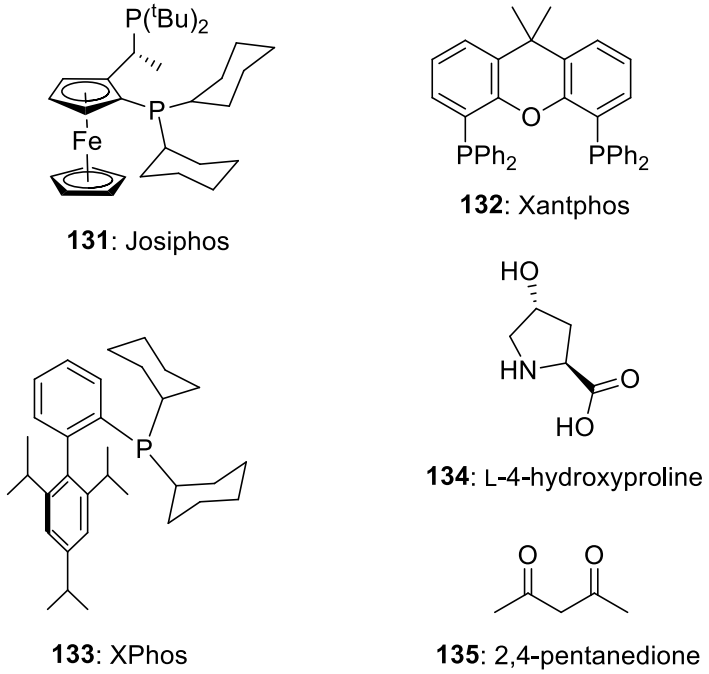

Figure 3.1.3.4.2. Ligands used in cross-coupling reactions.

Attempts at Buchwald-Hartwig coupling with 2-aminopyrimidine (**57**)[130] and Xantphos (**132**) were unsuccessful (entry 1, Table 3.1.3.4.1). We later tried *tert*-butylcarbamate (**136**, see Section 3.1.3.10) which gave moderate yield (entry 2, Table 3.1.3.4.1).[177]

Table 3.1.3.4.1. Conditions for cross-coupling of diaryl bromides with amines.

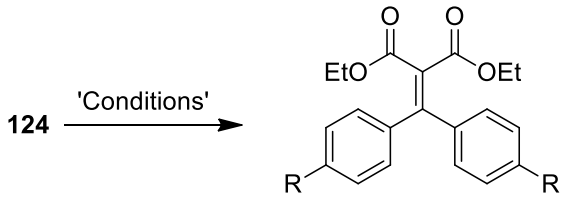

137: R=NH(2-pyr)
138: R=NHBoc
110: R=NH_2

Entry	Metal precursor	Base	Ligand	Temperature/ solvent	Additive	Yield[a]
1	$Pd_2(dba)_3$ or $PdCl_2(PPh_3)_2$ or $Pd(PPh_3)_4$	NaO^tBu or KO^tBu or K_3PO_4 or Et_3N	**132**	90 °C / toluene	**57**	0%
2	$Pd(OAc)_2$	Cs_2CO_3	**133**	100 °C / dioxane	**136**	**138**: 41%
3	$Cu(acac)_2$	Cs_2CO_3	**134**	rt or 90 °C, DMF	Aq. NH_4OH	0%
4	CuI	K_3PO_4	-	rt, DMF	Aq. NH_4OH	0%
5	CuI	K_2CO_3	**135**	55 °C, DMSO	Aq. NH_4OH	**110**: 48%

[a]Isolated yield after chromatography.

In contrast, direct coupling of aryl halides with ammonia in the presence of Cu and low-cost ligands has been an area of intense research over the past decade.[178] We investigated a number of Ullmann-type coupling reactions with ammonia (35% in water). The coupling of Zhao (entry 3, Table 3.1.3.4.1)[179] and room temperature couplings of Taillefer (entry 4, Table 3.1.3.4.1)[180] proved fruitless but the reaction of Ma and co-workers[181] gave *bis*-amino compound **110** in good yield (entry 5, Table 3.1.3.4.1). Optimisation of the reaction conditions was carried out. The best yields were recorded using thin sealed tubes at least 80% full of solvent and submerged in an oil bath. The parts of the tubes protruding from the bath were wrapped strongly in aluminium foil for insulation. These precautions allowed us to minimise the amount of liquid or gaseous ammonia condensed in the headspace. Additional equivalents of aqueous ammonia were detrimental to the yield, presumably since water can add *via* Michael addition to the double bond, giving the observed side product

dibromobenzophenone **48a** and diethyl malonate (**113**) by TLC and ^{1}H NMR analysis (Scheme 3.1.3.4.2). Analogous formation of diaminobenzophenone **47a**, although likely, was not observed since **5a** is highly polar and water-soluble.

Scheme 3.1.3.4.2.

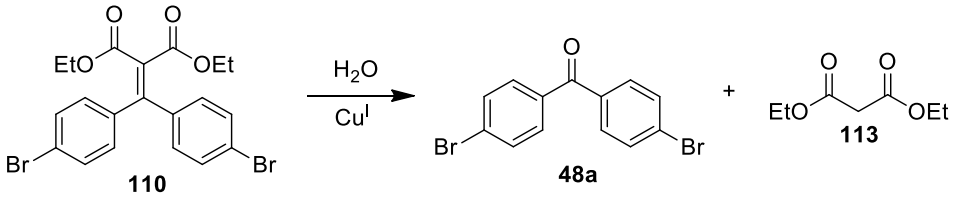

Degassing of the aqueous ammonia to prevent O_2-mediated oxidation of Cu^I to Cu^{II} was also inferior in terms of yield. We attributed this to the undesired removal of gaseous NH_3 from the reaction mixture. Unsurprisingly, using dry, degassed DMSO from a sealed bottle as solvent improved the yield. However, stoichiometric amounts of Cu^II and ligand were also detrimental to the reaction yield. When the reaction was scaled up to use 2.1 g of compound **124**, key intermediate **110** was isolated in 35% yield.

3.1.3.5 Conversion of diamine to target molecules

The key intermediate **110** was brought through guanidylation and deprotection (Scheme 3.1.3.5.1). We attempted both $CuCl_2$-mediated and $HgCl_2$-mediated guanidylation but the Hg-promoted conditions gave no side products, meaning simpler purification using flash chromatography on neutral alumina. As is well known in our group, *bis*-Boc-protected 2-iminoimidazolidines are highly unstable to silica chromatography. Crystallisation of these intermediates is often not possible and although significant amounts of degradation (>10%) occur upon alumina chromatography, this is often the best method of purification. The ^{1}H NMR-pure intermediate **109** was deprotected in dry HCl to give salt **139**. The salt is stable to water and, if necessary, its free base (liberated using fresh NaOEt in EtOH) can be columned on silica using CMA (80 mL $CHCl_3$: 20 mL MeOH : 3 mL aq. NH_4OH) after packing with 100% $CHCl_3$ and washing with dry HCl to reconstitute hydrochloride salt **139**.

Scheme 3.1.3.5.1.

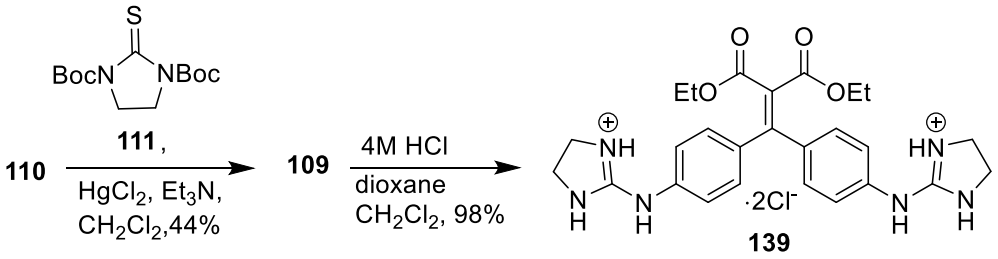

In order to explore the potential of the saturated derivative of **139**, the β-unsaturated diester was reduced with Pd/C to give compound **140** (Scheme 3.1.3.5.2). Standard reducing conditions (10% w/w of Pd/C with balloon of H_2 at 3 atm) overnight gave no reaction. Addition of extra Pd/C (to 100% w/w) also did not give any reaction, even up to 100 psi. However, when the pressure of H_2 was increased to 300 psi (20 atm) overnight, the ^{1}H NMR spectrum of the crude mixture showed product formation. To drive the reaction to completion, the reaction required stirring for three days under these conditions.

Scheme 3.1.3.5.2.

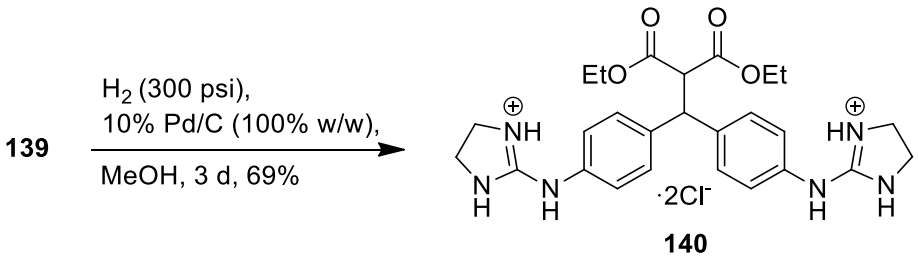

Double bonds of aryl-substituted unsaturated malonic esters are difficult to reduce. Other methods include very expensive sterically demanding frustrated Lewis acid/Lewis base pairs[182] or potentially toxic sodium cyanoborohydride.[168] Since we were producing a small amount (20 mg) of the final product **140** we reasoned that stoichiometric Pd was justified. While the ^{1}H NMR was clean, the product was further purified on reverse phase silica to ensure >95% purity by HPLC.

Scheme 3.1.3.5.3.

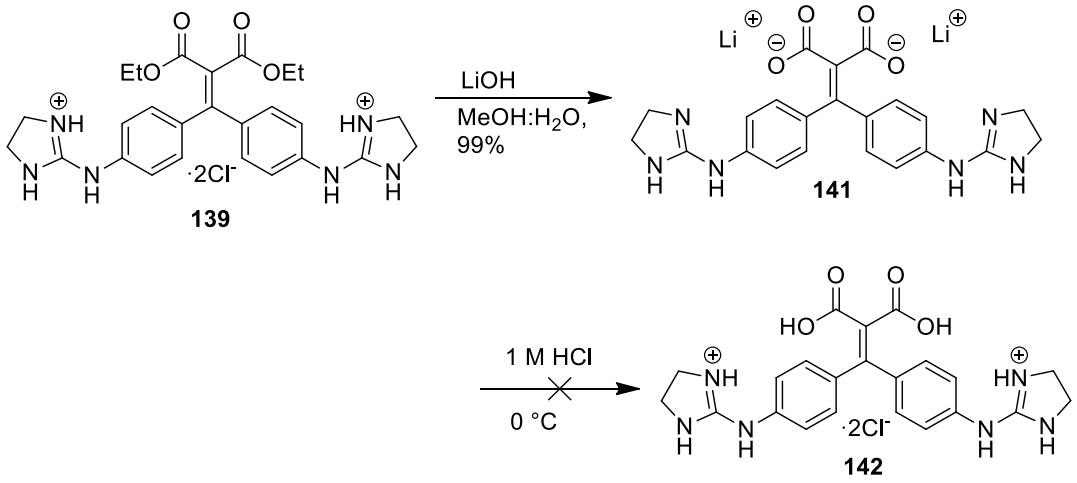

We also attempted the synthesis of malonic acid derivatives **142** and **144** using a number of conditions (Scheme 3.1.3.5.3 and Scheme 3.1.3.5.4). Unfortunately, these compounds were unstable to acid, even dilute HCl at 0 °C. The products degraded upon rotary evaporation with concomitant formation of a red solid. Although purification on reverse phase silica was possible, these compounds did not pass HPLC purity, even upon drying at room temperature *in vacuo*. We decided that these were not amenable for testing since the thermal denaturation experiment requires compounds stable to aqueous solution at up to 90 °C.

Scheme 3.1.3.5.4.

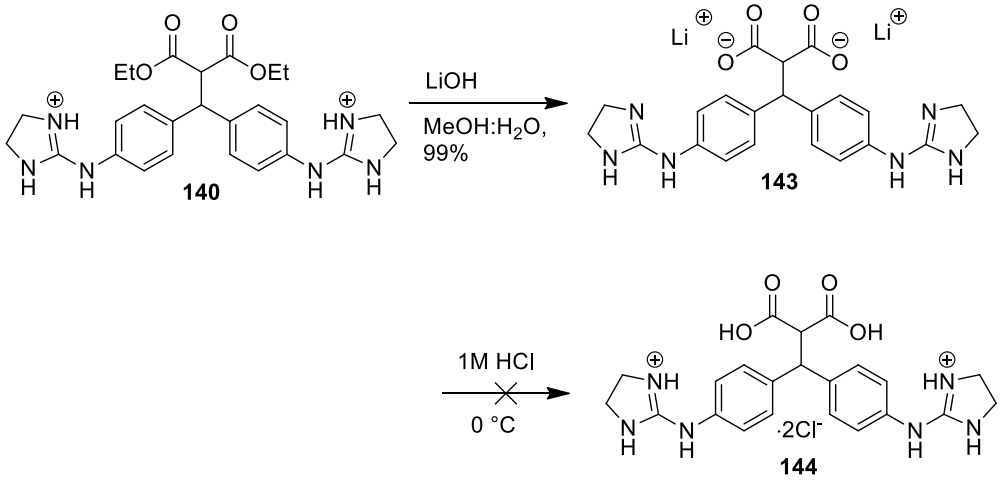

3.1.3.6 Biophysical studies

Compounds **139** and **140** were tested for DNA binding by thermal denaturation using unspecific salmon testes DNA (Figure 3.1.3.6.1). As expected from the docking results for compound **106**, compound **139** seems to be a DNA binder even though it only increased the thermal denaturation of stDNA by 3.6 °C. Compound **140**, on the other hand, had no effect on DNA thermal denaturation (ΔT_M = 0 °C).

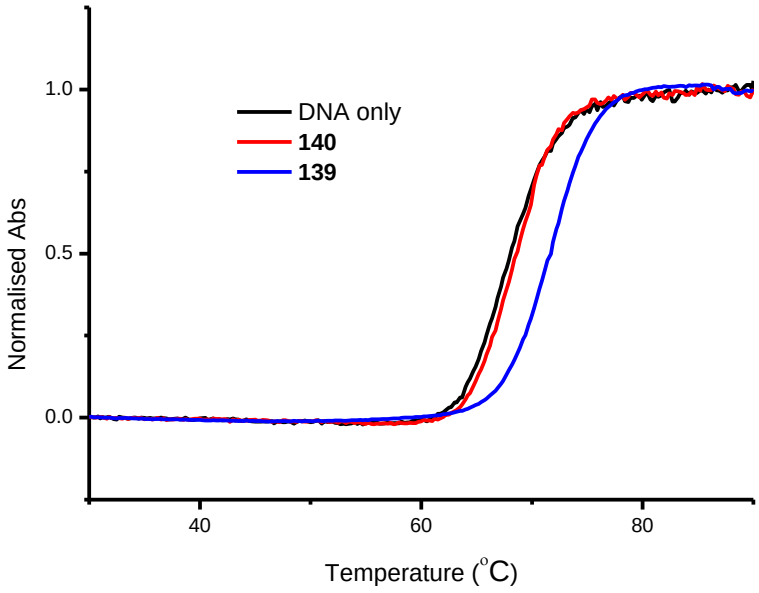

Figure 3.1.3.6.1. Thermal denaturation curve of stDNA (150 μM) alone (**black**), in the presence of **139** (**blue**, 15 μM) and **140** (**red**, 15 μM).

Interestingly, compound **139** was selective for poly(dAdT)$_2$ tracts (ΔT_M = 8.8 °C, Figure 3.1.3.6.2), suggesting that **139** is a MGB.

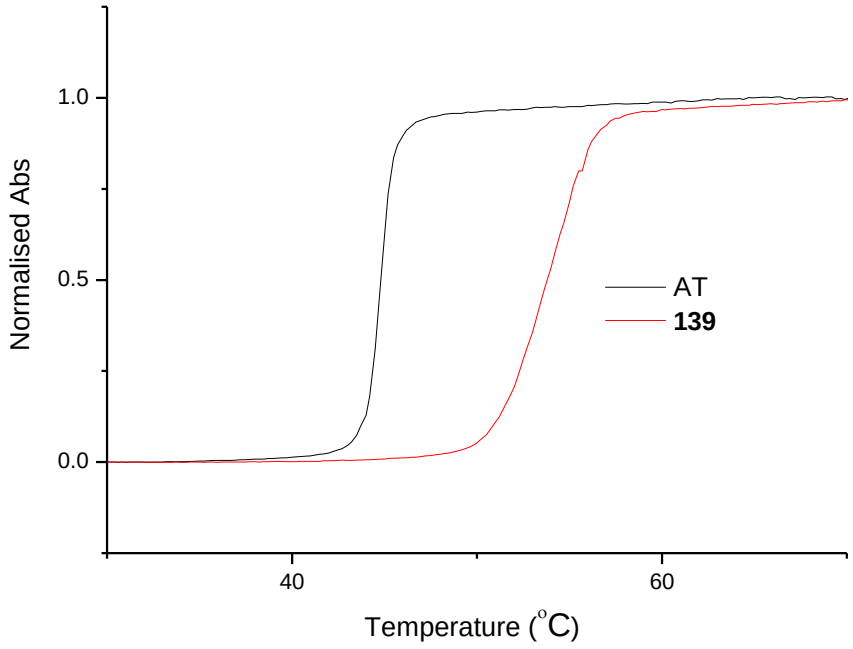

Figure 3.1.3.6.2. Thermal denaturation curve of poly(dAdT)$_2$ DNA (150 μM) alone (**black**), and in the presence of **139** (**red**, 15 μM).

To confirm that **139** binds into the minor groove, we carried out circular dichroism (CD) titrations of **139** with both stDNA and poly(dAdT)$_2$(Figure 3.1.3.6.3). In stDNA, the induced peak (3 mdeg) at 300 nm with lower concentrations of **139** indicates groove binding. However, at highest concentration of **139** (P/D = 0.4), this peak disappears and a negative peak (-4 mdeg), indicative of intercalation is present instead. The small magnitude of the signal and high concentration of drug may also indicate electrostatic binding to the phosphates perpendicular to the minor groove.

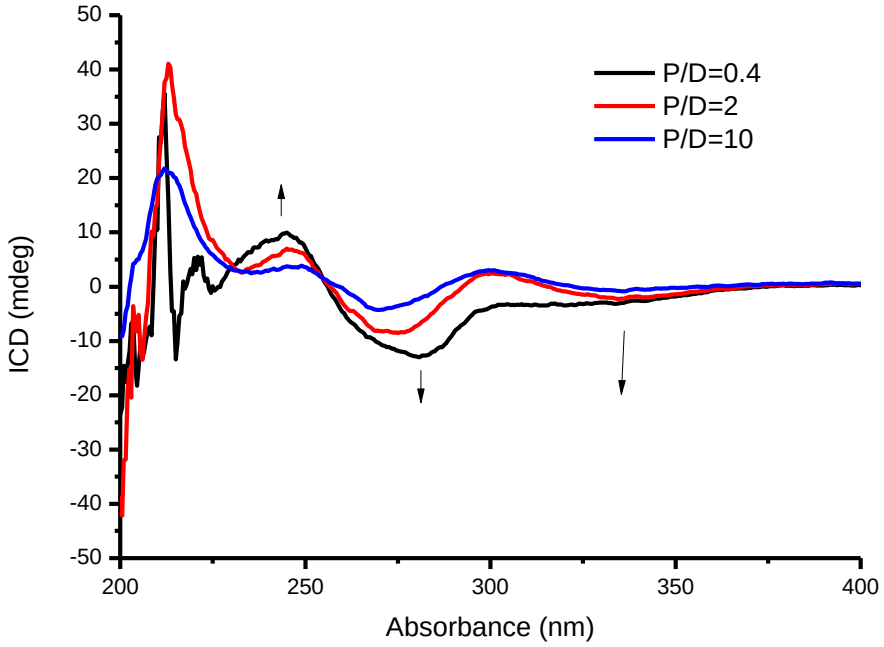

Figure 3.1.3.6.3. Induced CD spectrum of stDNA while increasing **139**.

The titration of increasing amounts of **139** into poly(dAdT)$_2$ DNA (Figure 3.1.3.6.4) gave a very clear increase in the magnitude of peaks at 250 nm and 290 nm and a decrease at 270 nm. In this concentration range there is no red or blue shift in these peaks, implying that there is only one mode of binding. The presence of the induced peak at 290 nm indicates that **139** is binding into the groove.[183] Since AT-rich regions disfavour intercalation, which is usually strongest between GG motifs, it makes sense that in poly(dAdT)$_2$ DNA, compound **139** is binding only in the minor groove. Also the small size of the minor groove in AT-rich tracts (3-4 Å in diameter) compared to average DNA minor grooves (6 Å in diameter) allows for more hydrophobic interactions to occur and enthalpically-favoured displacement of tightly-bound water molecules.[184]

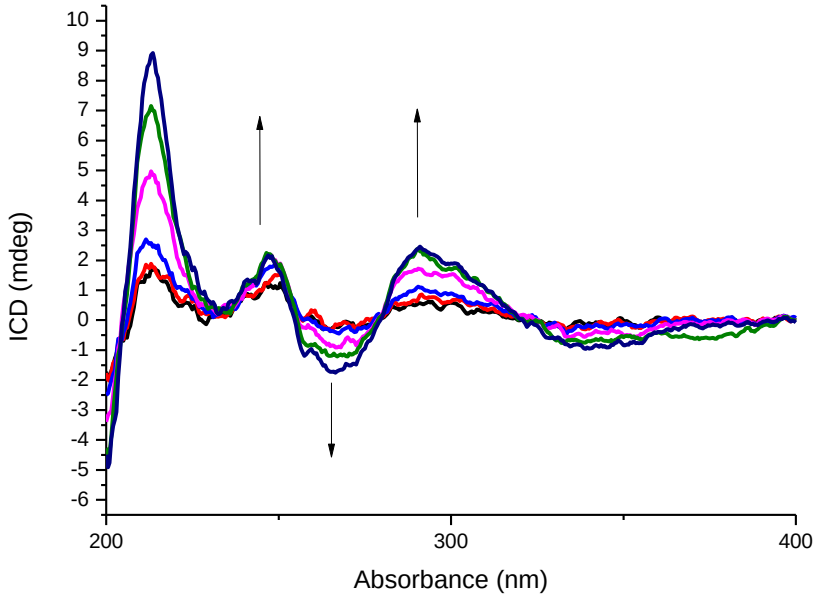

Figure 3.1.3.6.4. Induced CD spectrum of poly(dAdT)$_2$ DNA with increasing **139**.

3.1.3.7 Computational Rationalisation

To rationalise the difference in binding between the two compounds **139** and **140**, we carried out calculations in an model of aqueous solvation (PCM-water) at the B3LYP/6-31G(d,p) computational level to find the energy-minimised conformations of each compound. These low energy conformations (Figure 3.1.3.7.1) showed that the angle between the planes of the aryl rings were 69.8° and 68.2° for **139** and **140**, respectively. The single point energies (calculated at the B3LYP/6-311G(d,p) level in PCM/water) of these conformations compared to the conformations where the aryl rings were coplanar were lower in energy by 108.5 kJ mol^{-1} and 64.5 kJ mol^{-1} for **139** and **140** respectively. This means that the more coplanar structure (**139**) would fit better in the minor groove of DNA than the less coplanar one (**140**).

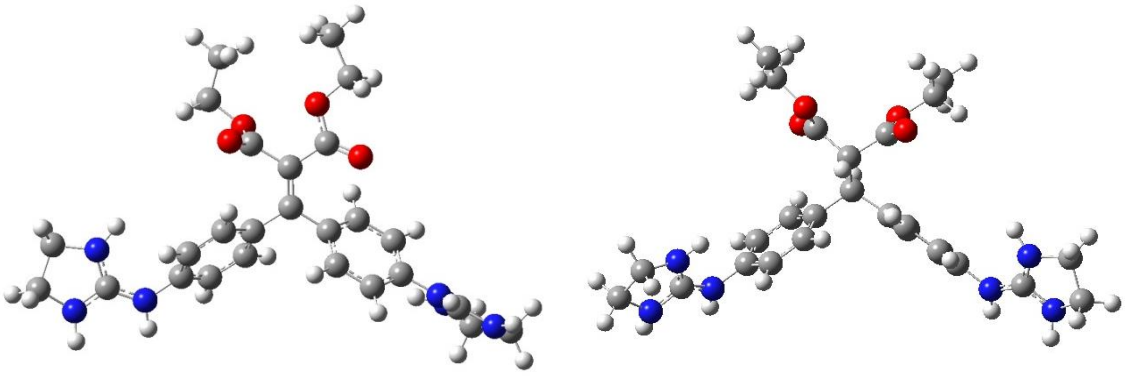

Figure 3.1.3.7.1. Energy-minimised conformations of **139** (left) and **140** (right) at the B3LYP/6-31G (d,p) computational level.

Considering that the synthesised *bis*-2-aminoimidazolinium malonate derivatives **139** and **140** possess a protected malonate group and that the DNA affinity of **139** and **140** was proportional to the planarity of the aromatic rings in their lowest energy conformations, the next step was to fix these aryl rings in a coplanar environment to improve DNA binding.

3.1.3.8 Fluorene synthesis

In order to redesign the compounds to increase DNA affinity, we reasoned that restricting **140** in a coplanar environment with respect to the aryl rings (**145**, Figure 3.1.3.8.1) should increase DNA binding. However, we were aware from previous results in the group[124] that the tricyclic core could change the binding mode to intercalation. Thus, we also decided to synthesise the 'parent' 3,6-disubstituted 9*H*-fluorene **146** in order to develop a SAR of the MGBs.

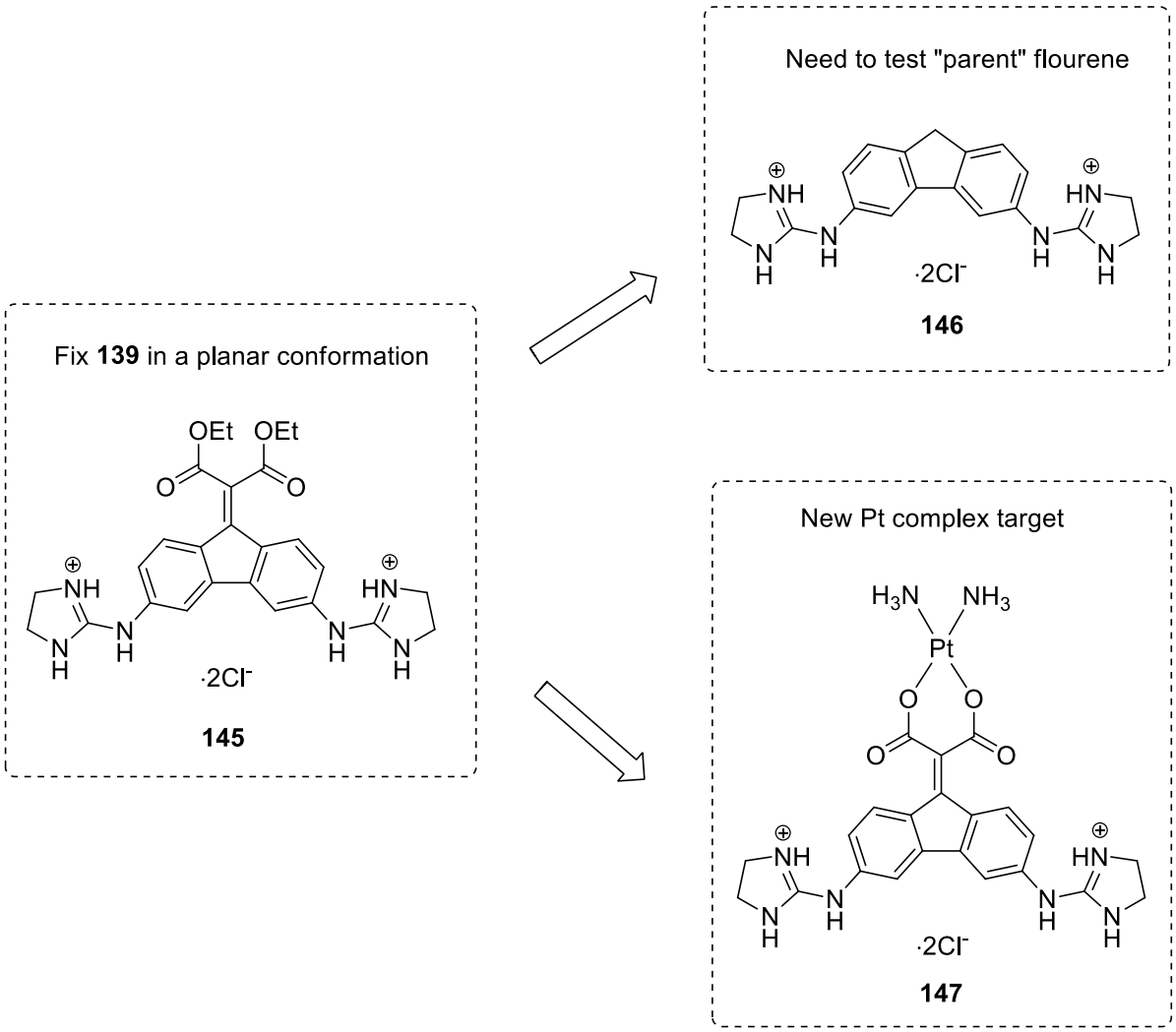

Figure 3.1.3.8.1. Rationale behind the synthesis of the conformationally planar family.

As mentioned in Section 1.5.7, very strong DNA binding was observed when tricyclic 2,7-guanidine-like 9*H*-fluorene **39** was used. The change in DNA binding mode from minor groove binding to intercalating was attributed to the two lowest energy conformations, **39a** and **39b**. The conformationally restricted molecule **40** also had very strong binding to DNA. Guanidylated acridine derivatives **3** and **4** (Section 1.4.3) displayed very strong DNA affinity too. Moreover, Wilson and Boykin have synthesised *bis*-amidine and *bis*-imidazole carbazole derivatives with very high affinity for calf thymus DNA (Figure 3.1.3.8.2).[185,186] Although shorter than our molecule **146**, compounds **148** and **149** were clearly identified as MGBs by CD and NMR experiments.

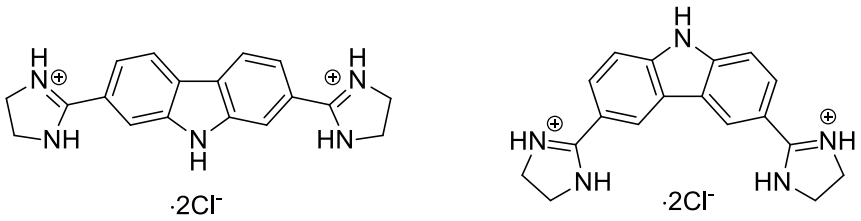

148 **149**

Figure 3.1.3.8.2. Boykin and Wilson's carbazoles.

These results supported our idea that locking the *bis*-guanidine-like compounds in a planar tricycle does not necessarily force the compounds to become intercalators.

3.1.3.9 Attempted cyclisation

Both compounds **145** and **146** can be synthesised from 3,6-diamino-9*H*-fluorenone (**154**) by standard guanidylation chemistry similar to that presented in Section 3.1.3.5 (Figure 3.1.3.9.1). Although **154** is known, the low-yielding laborious 5 step procedure from 2,7-diamino-9*H*-fluorenone was not attractive.[187] Thus, we attempted the preparation of **154** through an EAS (electrophilic aromatic substitution) with a nitrile (**156**), similar to Yu and Velasco's synthesis of fluorenones.[188] We envisioned that biaryl **156** could be accessed through Suzuki coupling of commercial **160** and known **161**.

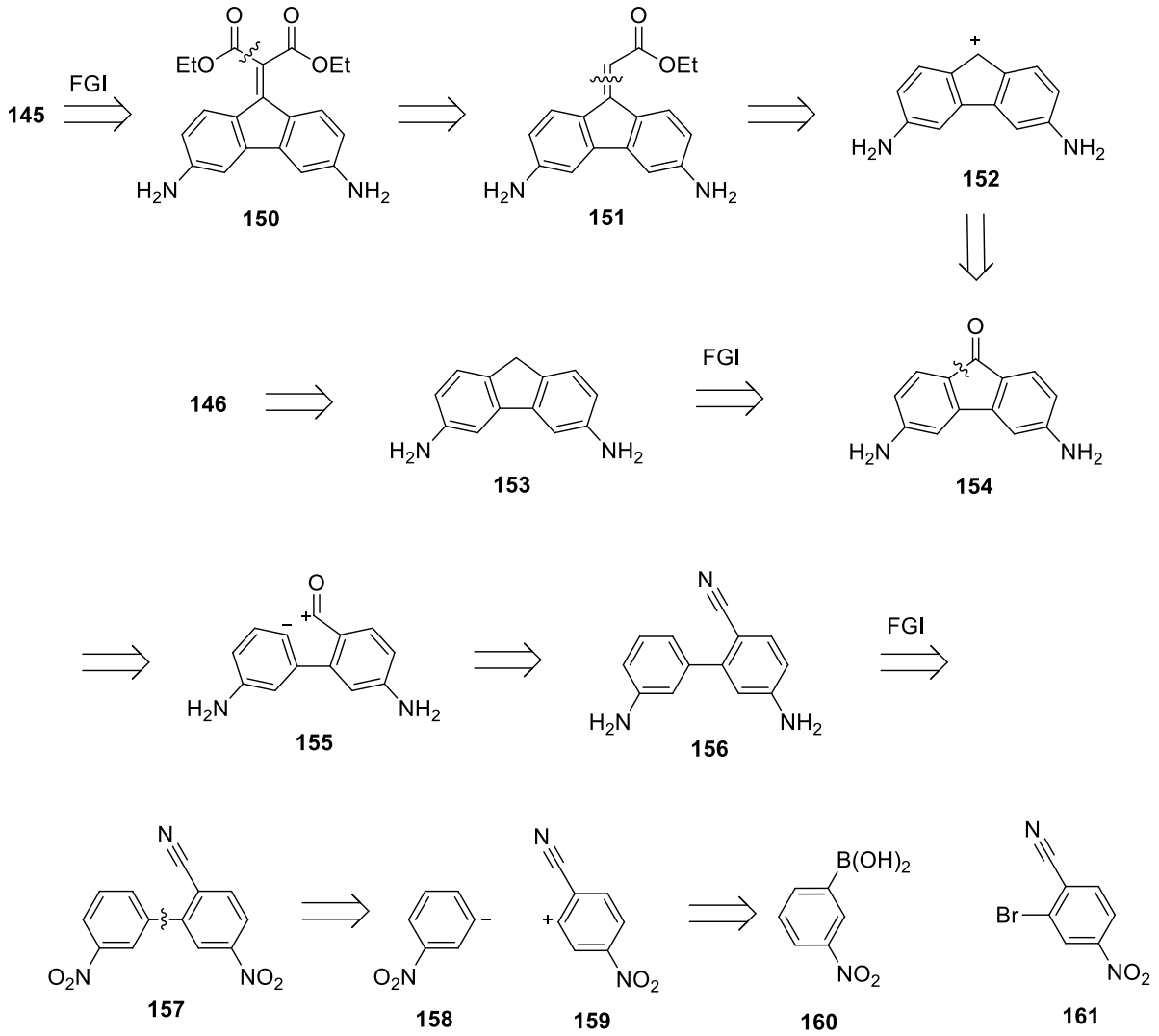

Figure 3.1.3.9.1. Retrosynthesis of compounds **145** and **146** *via* key intermediate **154**.

The trisubstituted bromide **161** was synthesised by a nitrile-directed Pd^{II}-catalysed C-H activation of 4-nitrobenzonitrile with NBS (*N*-bromosuccinimide) and catalytic TsOH in air (Scheme 3.1.3.9.1).[189]

Scheme 3.1.3.9.1

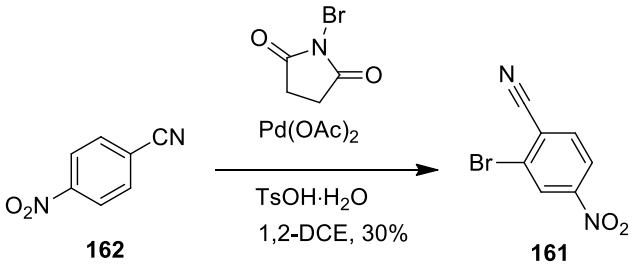

We were unable to replicate the excellent yield reported (93%), especially at large scale (700 mg). Nonetheless, the trisubstituted product was synthesised in sufficient quantity to carry on. The reaction is likely to pass through a Pd^{II}/Pd^{IV} catalytic cycle, and is not reduced to Pd^{0} which would quickly insert into the Ar-Br bond of **161**, destroying the product.

The Suzuki-Miyaura coupling of **161** and **160** following a procedure reported in a patent,[190] afforded coupled product **157** in good yield (60%). Optimisation including using KF, heating at reflux overnight, longer and shorter reaction times in the microwave, and different ligand concentrations allowed us to isolate the product (Scheme 3.1.3.9.2).

Scheme 3.1.3.9.2.

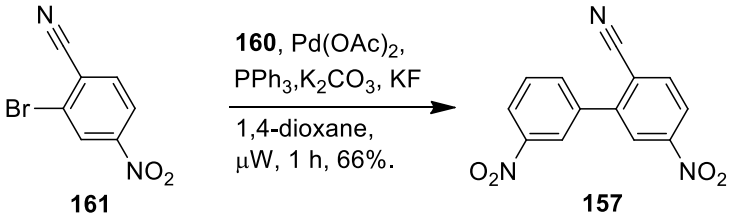

Unsurprisingly, due to the strong electron-withdrawing nature of the nitro group, attempted cyclisation of the dinitro derivative was futile (Scheme 3.1.3.9.3).

Scheme 3.1.3.9.3.

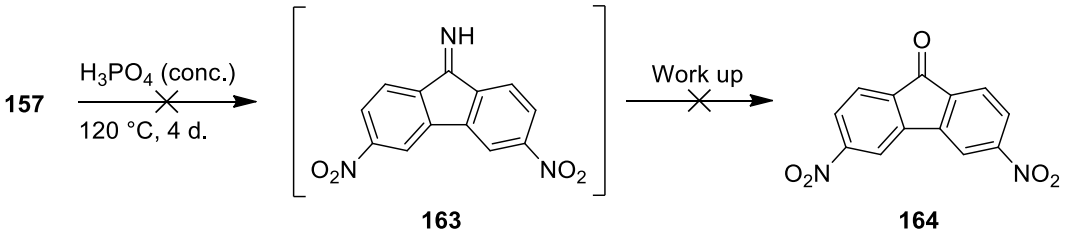

In a different approach, we expected that reduction of compound **157** to diamino compound **156** would result in the *in situ* cyclisation of the ring directly to **154**, similar to the first reported Friedel-Crafts reactions.[169] However, the use of Fe gave mostly uncyclised reduction product **156**, together with unreacted starting material **157**.[191] The reduction of **157** with $SnCl_2$ was very clean, giving complete conversion to **156**, and did not require further purification (Scheme 3.1.3.9.4).[192]

Scheme 3.1.3.9.4.

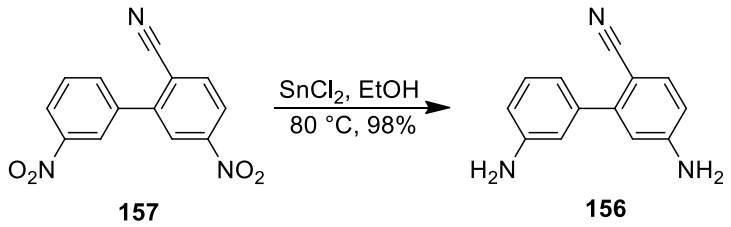

As shown in Table 3.1.3.9.1, the attempted ring closing of **156** to **154** did not work, presumably since Lewis acid coordination to the amines deactivated the ring. Even reaction in nitromethane at high temperature was not enough to close the ring.

Table 3.1.3.9.1. Attempted cyclisations of 156.

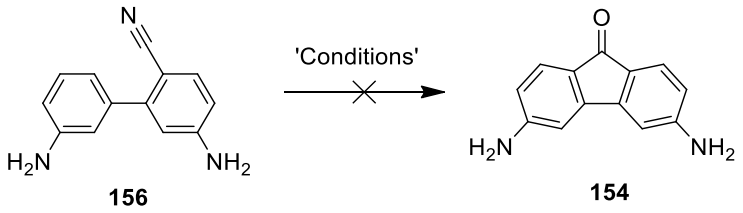

156 **154**

Entry	Lewis Acid	Solvent at relfux	Yield[a]
1	-	AcOH	0%
2[188]	-	H_3PO_4[b]	0%
3	H_2SO_4 (1M)	H_2O	0%
4[193]	-	H_2SO_4[b]	0%
5	Fe	AcOH	0%
6[194]	$Sc(OTf)_3$ (0.1 eq)	$MeNO_2$	0%
7	$CuCl_2$ (0.1 eq)	$MeNO_2$	0%
8	$CuCl_2$ (1.0 eq)	$MeNO_2$	0%
9[194]	-	$MeNO_2$	0%

[a]Yield after aqueous work-up. [b]Solvent heated to 120 °C

Finally, we decided to convert the amines to more amenable functional groups for ring closing. Sandmeyer conditions could afford us a dibromo compound more ammenable to cyclisation, giving us a five step procedure to access **165** from commercial starting materials. Instead, we used the known two step procedure from 9,10-phenanthraquinone (**166**) to synthesise **165**.

3.1.3.10 New attempt for the preparation of key intermediate 165

The procedure used to prepare dibromide **165** is outlined in Scheme 3.1.3.10.1 and Scheme 3.1.3.10.2 below.[195] The radical-mediated bromination of 9,10-phenanthraquinone (**166**) in nitrobenzene at reflux gave **167** in very good yields: 80% on a 3.86 g scale and 76% on a 10 g scale with respect to **130**.

Scheme 3.1.3.10.1.

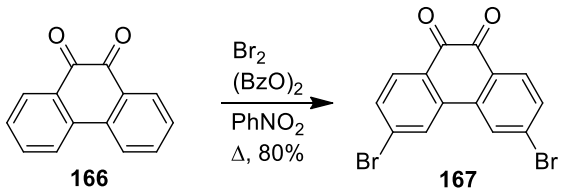

Dibromo intermediate **167** was insoluble in many solvents. Thus, upon cooling of the reaction mixture in nitrobenzene and washing with copious amounts of hexane, **167** was isolated without the need for further purification. Ethanol had been used in the synthesis of **167** previously,[196] but in our experience, much of the product was lost in the ethanolic layer (as visualised by TLC). Isolated **167** was then used in a green chemistry reaction with H_2O_2 and I_2 in various solvents to attempt to oxidise **167** to **165** without the use of $KMnO_4$.[197] However, none of these reactions showed evidence of product formation by TLC. Thus we used the known procedure with $KMnO_4$.[196]

Scheme 3.1.3.10.2.

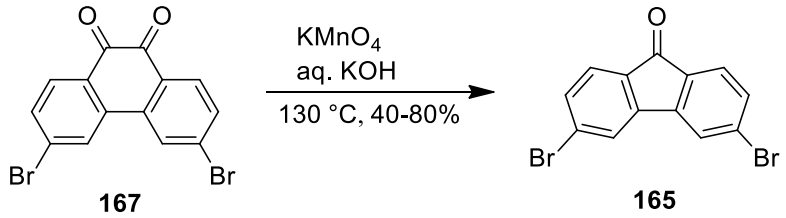

In this procedure, the synthesis of **165** was severely hampered by its insolubility.[195,196] Noted for its difficult workup,[198] the filter cake obtained after quenching (Scheme 3.1.3.10.2) required upwards of ten iterations of resuspension in H_2O and refiltration to isolate the product. The filter cake would routinely block, and thus, the entire process took three days of labour-intensive work. Quenching with sodium bisulfate ($NaHSO_3$), while removing metal salts more effectively than H_2O alone, further increased the clogging of the filter cake. The highly exothermic delayed reaction upon addition of $KMnO_4$ (6.8 eq.) in portions, was tricky to control on scaling up and the safest scale to work on was deemed to be 1.8 g. As

previously mentioned, smaller scales increased the practicality of the filtration. The final product (**165**) was soluble enough to get a dilute ^{1}H NMR in $CDCl_3$, consistent with the literature. Although the purity was an issue, to our delight subsequent reactions yielded products that could be easily isolated in a very pure state.

3.1.3.11 Synthesis of key diamine intermediate 153

With intermediate **165** in hand, we then focussed on amination to arrive at key intermediate **153** in the synthesis of diaminofluorene **146**. Unfortunately, the previously successful Cu conditions did not work well with this substrate (entry 1, Table 3.1.3.11.1). Many other Cu-catalyed conditions were used, but to no avail (entry 2, Table 3.1.3.11.1). However, without the malonate groups of **124**, Pd-conditions worked excellently. Hartwig's amination using NHMDS (sodium hexamethyldisilazane) followed by acidic work-up (entries 3 and 4, Table 3.1.3.11.1) gave complete conversion of starting materials but no isolated product. Conditions for coupling protected amines (Cbz, entry 5 and Boc, entry 6, Table 3.1.3.11.1) afforded highly organic-soluble Boc-protected **168** (Table 3.1.3.11.1).

Table 3.1.3.11.1.

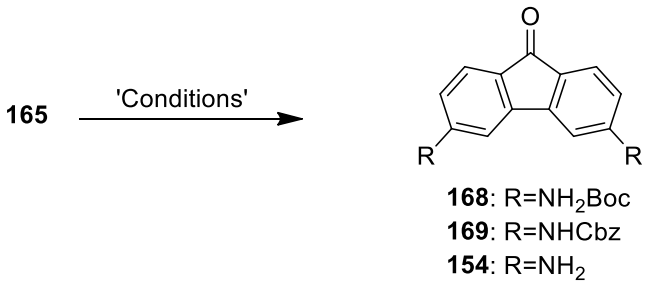

Entry	Metal precursor	Base	Ligand	Temperature/ solvent	Additives	Yield[a]
1[181]	CuI	K_2CO_3	**134**	55 °C, DMSO	Aq. NH_4OH	0%
2[180]	$Cu(acac)_2$	Cs_2CO_3	**134**	90 °C/ DMF	Aq. NH_4OH	0%
3[199]	$Pd_2(dba)_3$	NaO^tBu	**BINAP**	90 °C/ toluene	NHMDS	0%
4	$Pd_2(dba)_3$	NaO^tBu	**133**	90 °C/ toluene	NHMDS	0%[b]
5[177]	$Pd(OAc)_2$	Cs_2CO_3	**133**	100 °C / dioxane	$CbzNH_2$	**169**: 10%
6	$Pd(OAc)_2$	Cs_2CO_3	**133**	100 °C / dioxane	**145**	**168**: 75%

[a]Isolated Yield. [b]100% Conversion of starting material.

Deprotection of **168** in dry HCl yielded **154** as the neutral free base (Scheme 3.1.3.11.1). Stirring in conc. HCl at 100 °C was insufficient to protonate the aniline and the NH_2 groups did not exchange with D_2O. Interestingly, hydrogenation of either ketone **154** or **169** to give fluorene **153** with Pd/C similar to Section 3.1.1.5 gave a complex mixture of products, presumably due to the possible resonance forms of **154** being reducible.

Scheme 3.1.3.11.1.

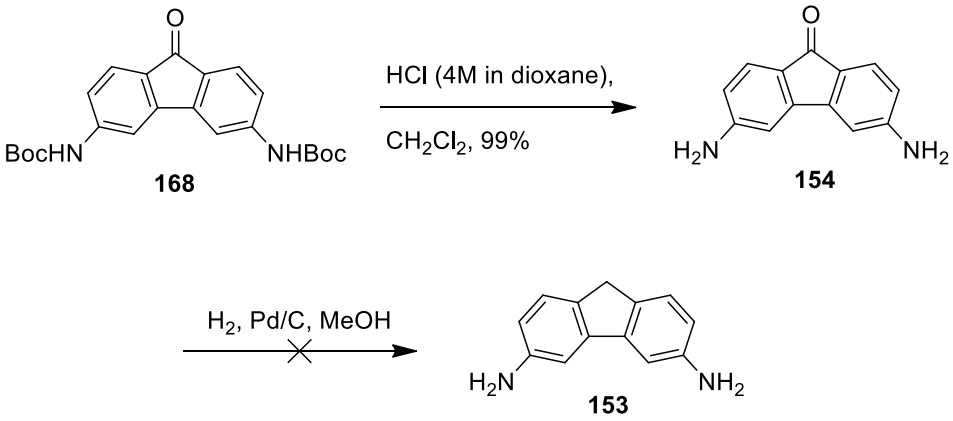

Instead, reduction of Boc-protected **168** under the same conditions proceeded cleanly to give **170** (Scheme 3.1.3.11.2). Compared to other hydrogenation reactions, the relatively low yield achieved for compound **170** (67%) can be explained by the *in situ* Boc-deprotection of **170** to **154**, followed by degradation of **154** as above. Subsequent facile Boc deprotection gave key diamine intermediate **153** as its hydrochloride salt.

Scheme 3.1.3.11.2.

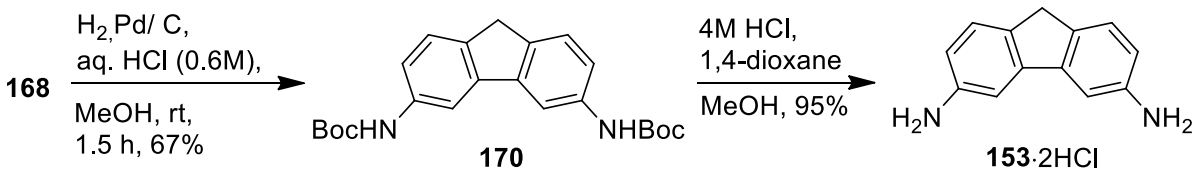

3.1.3.12 Synthesis of key diamine intermediate150

With key intermediate **153** synthesised, we turned our attention to the key intermediate in the preparation of malonate **145**, diamine **150**. Following a similar synthetic route as for **110**, dibromoketone **165** was converted to unsaturated ester **172** in good yield (82%) by a Wittig reaction (Scheme 3.1.3.12.1). Again, the separation of the product from poorly soluble starting material **165** was straightforward.

Scheme 3.1.3.12.1.

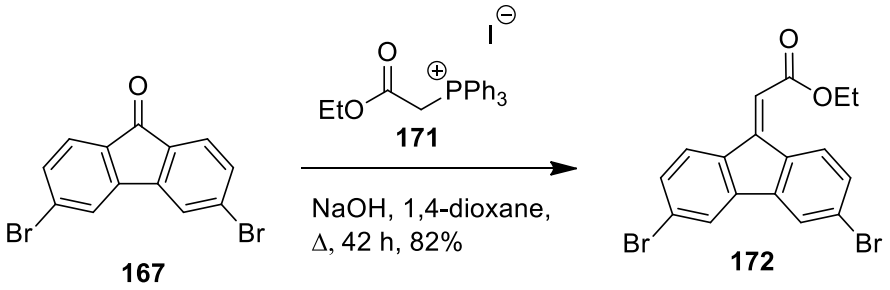

Unfortunately, the deprotonation step (Scheme 3.1.3.12.2) did not produce the expected symmetrical product **173** under identical conditions to **124**. In fact, the anion reacted to give side products before the ethyl chloroformate quench (as visualised by TLC). The two asymmetrical products were not identified.

Scheme 3.1.3.12.2.

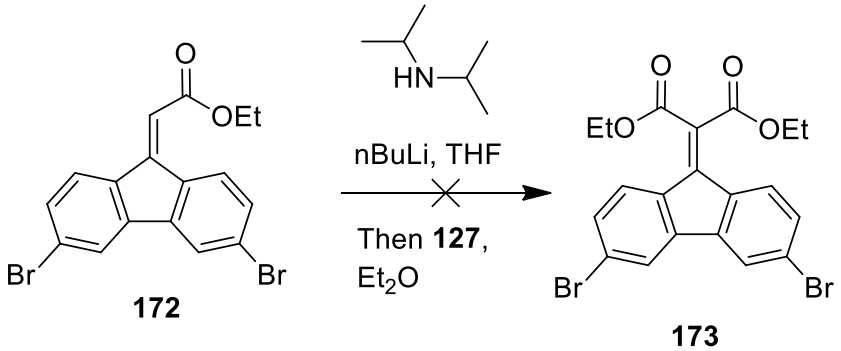

Luckily, in contrast to difluorobenzophenone **119,** the reaction of diethyl malonate (**113**) with ketone **165** and $TiCl_4$ gave malonate **173** directly (Scheme 3.1.3.12.3). Solvent switch to CCl_4 was key.[200] Notably, the reaction when carried out in a glass stopper-sealed Schlenk tube did not work and the best yields were obtained when using rubber septa to seal the flask. Presumably, this was to let O_2 into the reaction, preventing the well-studied reduction of Ti^{IV} to Ti^{III}, Ti^{II} or Ti^0. Like the pinacol reaction outlined in Wang's publication,[201] pyridine may play a role as a ligand for Ti.

Scheme 3.1.3.12.3.

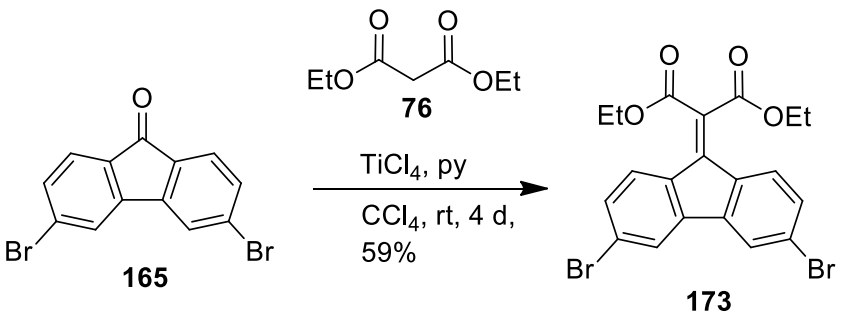

Similar to the preparation of **168**, Cu coupling reactions on dibromide **173** did not work; however, Pd chemistry worked excellently, giving **174** in 83% yield (Scheme 3.1.3.12.4). Deprotection of **174** as before gave hydrochloride salt **150** without the need for further purification.

Scheme 3.1.3.12.4.

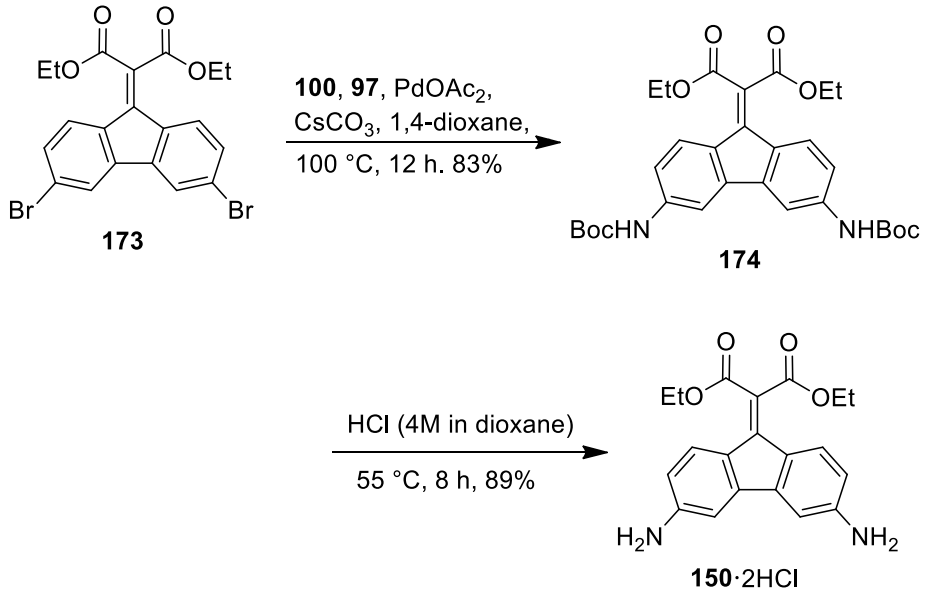

3.1.3.13 Conversion of diamines to 2-aminoimidazolinium salts

With diamine hydrochloride salts **150** and **153** in hand, the final reactions to make aimed salts **145** and **146** were guanidylation and deprotection. Guanidylation in both instances gave moderate yields (39 and 46%), due to the difficulty in separating *mono*- and di-guanidylated products from the alumina columns (Scheme 3.1.3.13.1).

Scheme 3.1.3.13.1.

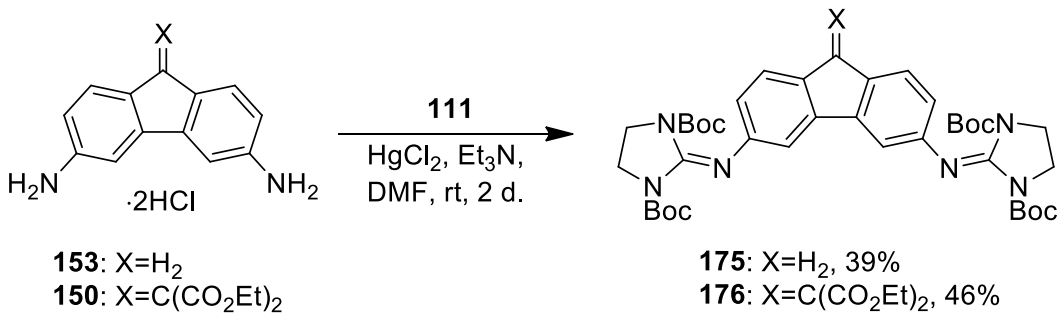

Salt formation using anhydrous HCl in dioxane was also straightforward and high-yielding (89-98%). Purification by reverse phase silica column was difficult, but after three slow

columns, the products eluted in 100% H_2O in greater than 95% purity by HPLC (Scheme 3.1.3.13.2).

Scheme 3.1.3.13.2.

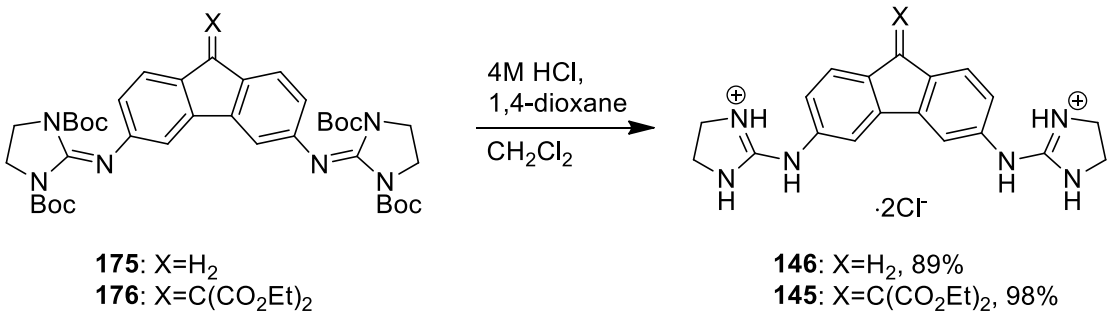

175: X=H_2
176: X=$C(CO_2Et)_2$

146: X=H_2, 89%
145: X=$C(CO_2Et)_2$, 98%

3.1.3.14 Biophysical studies

Compounds **145** and **146** were tested for DNA binding by thermal denaturation and by CD on both salmon testes DNA and poly(dAdT)$_2$ DNA (Table 3.1.3.14.1). The normalised thermal denaturation curve in stDNA is shown in Figure 3.1.3.14.1.

Table 3.1.3.14.1. ΔT_M values obtained for the fluorene-based DNA binders.

	ssDNA	poly(dAdT)$_2$
145	8.0 ± 0.5 °C	1.0 ± 0.5 °C
146	10.3 ± 0.5 °C	19.5 ± 0.5 °C

As can be seen in Figure 3.1.3.14.1 and Table 3.1.3.14.1, both compounds **145** and **146** bind strongly to stDNA, giving ΔT_M measurements of 8.0 °C and 10.3 °C, respectively. These results compare similarly to 2,7-*bis*-(2-aminoimidazoline)-9*H*-fluorene **39** (9 °C), showing excellent binding to DNA. Moreover, compared to our initial malonate-derived **139**, fluorene-based malonate derivative **145** has 2.2-fold increase in binding strength (assuming the size of the binding site is similar- Section 1.4.4).

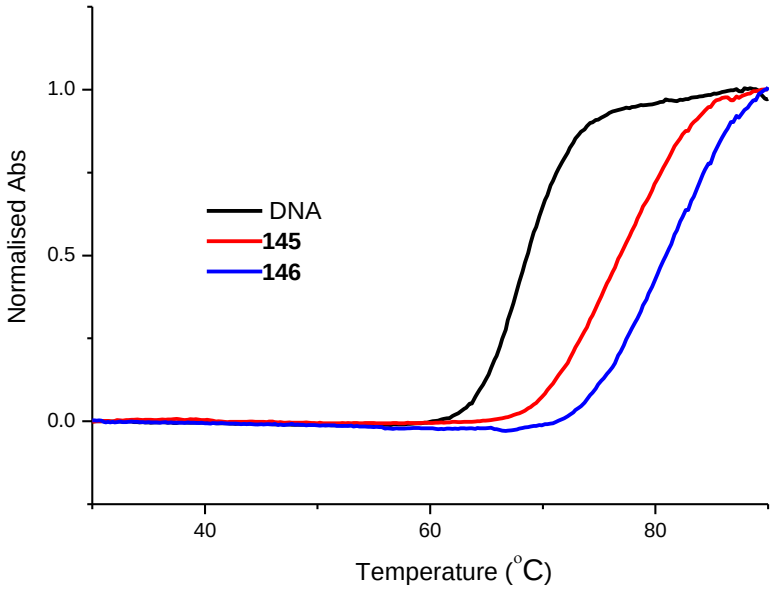

Figure 3.1.3.14.1. Thermal denaturation curve of stDNA (150 μM) alone (**black**), in the presence of **145** (**red**, 15 μM) and **146** (**blue**, 15 μM).

Compounds **145** and **146** were also tested for their affinity towards poly(dAdT)$_2$ DNA and the results are shown in Figure 3.1.3.14.2 and Table 3.1.3.14.1.

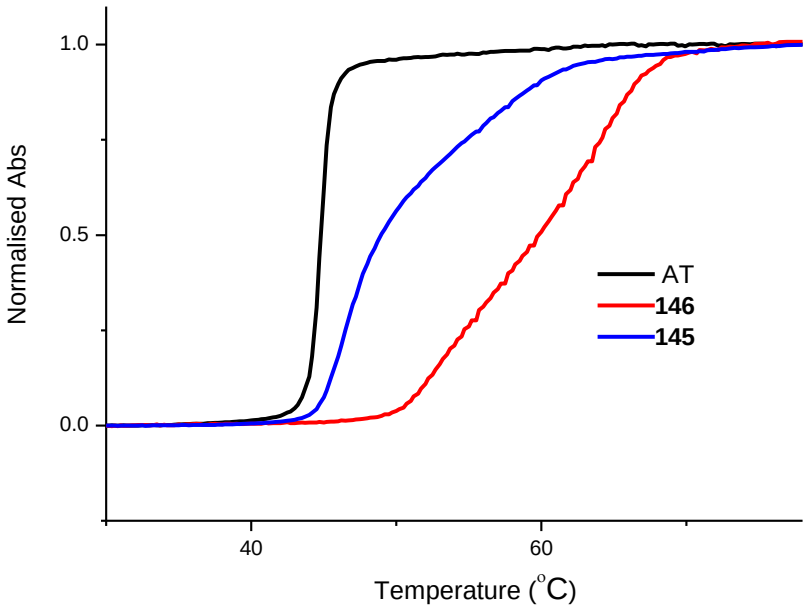

Figure 3.1.3.14.2. Thermal denaturation curve of poly(dAdT)$_2$ DNA (150 μM) alone (**black**), in the presence of **145** (**blue**, 15 μM) and in the presence of **146** (**red**, 15 μM).

As is obvious from the graph, compound **145** has very different binding to poly(dAdT)$_2$ DNA than stDNA. The ΔT_M value in poly(dAdT)$_2$ (1 °C) shows that **145** requires G or C bases for strong DNA binding. On the contrary, **146** gave a ΔT_M value of 19.5 °C, demonstrating that **146** interacts preferentially with A and T bases. These results compare well to 2,7-*bis*-(2-aminoimidazoline)-9*H*-fluorene **39**, which also bound stronger to poly(dAdT)$_2$ DNA (ΔT_M =26 °C), indicating possible minor groove binding.

In order to explore the DNA binding mode of compounds **145** and **146**, we performed CD measurements using both stDNA and poly(dAdT)$_2$ DNA. The induced CD spectra of **146** in stDNA (Figure 3.1.14.3) and poly(dAdT)$_2$ DNA (Figure 3.1.3.14.4) are given below.

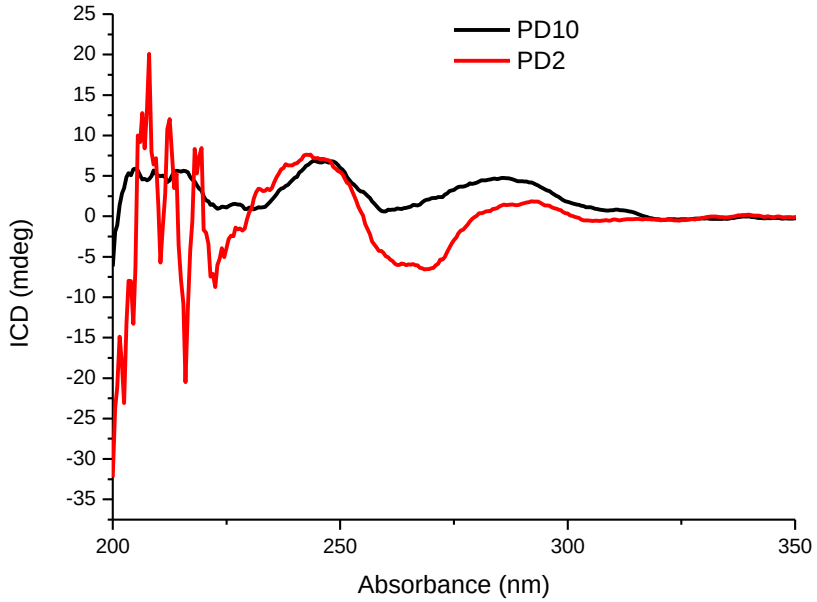

Figure 3.1.3.14.3. Induced CD spectrum of stDNA while increasing **146**.

From Figure 3.1.3.14.3, we can see that there is a small induced peak at 310 nm at a P/D ratio of 10, but with increasing drug (P/D=2) this peak disappears. We can conclude that there are concentration-dependent binding modes of **146** in stDNA. At a low concentration, there is a clear minor groove-binding mode as seen by the induced peak. However, this is masked at a higher concentration, probably by non-specific phosphate binding. The induced CD spectrum of **146** with poly(dAdT)$_2$ DNA is shown in Figure 3.1.3.14.4.

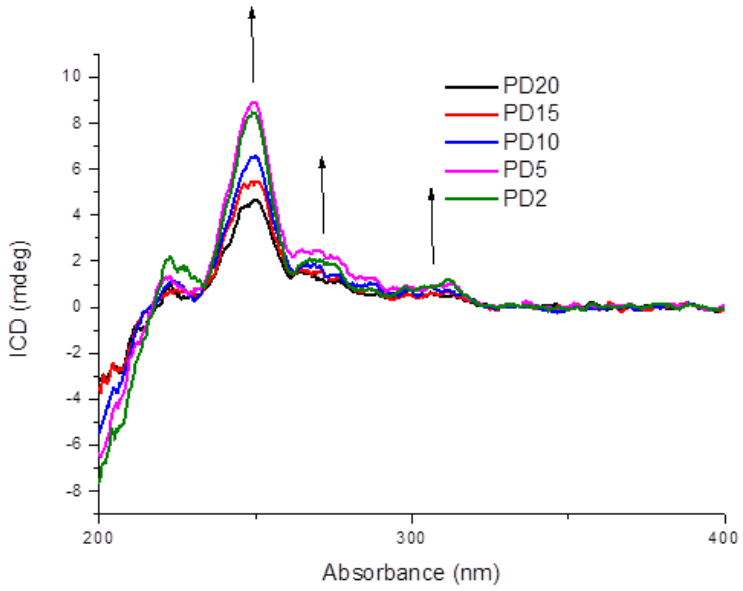

Figure 3.1.3.14.4. Induced CD spectrum of poly(dAdT)$_2$ DNA with increasing **146**.

In this induced CD spectrum, the induced peak at 310 nm increases with addition of **146**; and thus, the likely binding mode seems to be minor-groove binding. However, the magnitude of the induced peak is much smaller than would be expected for pure minor groove binding (see Section 3.2.4). For this reason, we can assume that phosphate binding or intercalation is likely competing with minor groove binding.

Experiments with the malonate-derived fluorene **145** in stDNA gave the induced CD spectra shown in Figure 3.1.3.14.5.

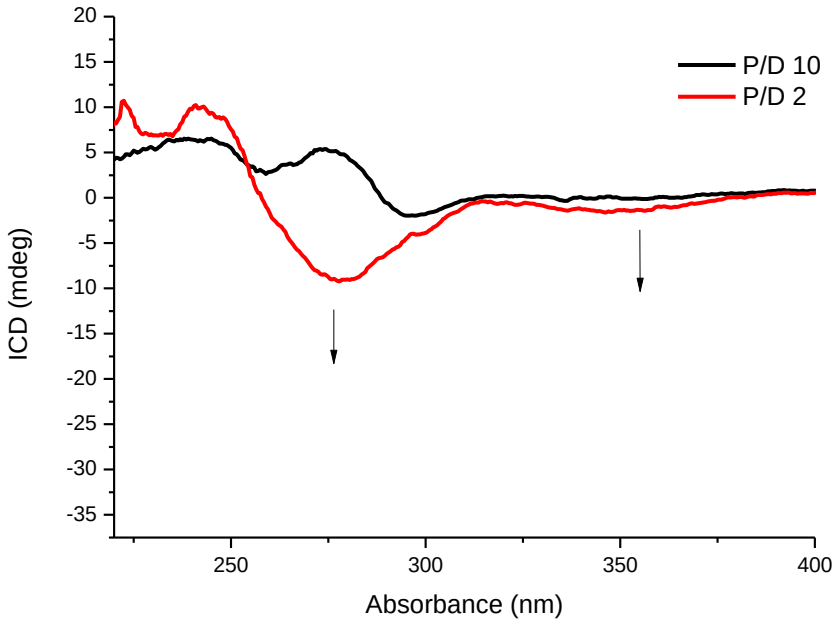

Figure 3.1.3.14.5. Induced CD spectrum of stDNA while increasing **145**.

The induced CD spectrum of **145** with stDNA showed a clear preference for intercalation. The induced trough at 350 nm is indicative of pure intercalation. The interaction of **145** with poly(dAdT)$_2$ DNA shows similar patterns (Figure 3.1.3.14.6).

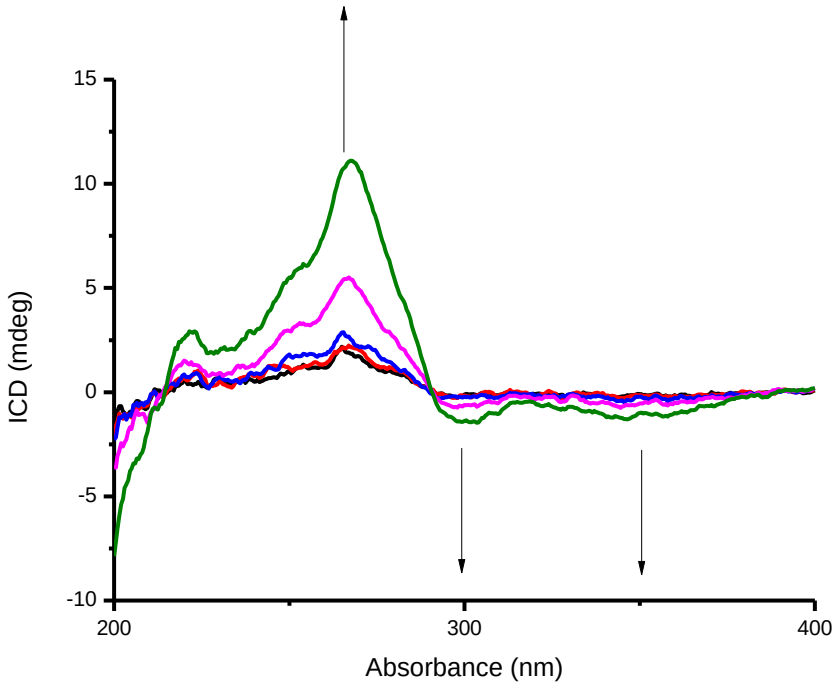

Figure 3.1.3.14.6. Induced CD spectrum of poly(dAdT)$_2$ DNA with increasing **145**.

Again, the induced CD spectrum of poly(dAdT)$_2$ DNA with **145** showed two clear induced troughs at 300 nm and 350 nm. This confirmed that **145** intercalates into poly(dAdT)$_2$ DNA and stDNA. Although our original plan was to use **145** to bring Pt to the DNA minor groove, the thermal denaturation and CD experiments showed that this compound, although a stronger stDNA binder than **145**, is unlikely to bind into the minor groove.

3.1.3.15 Conclusions

The objective of this chapter was to present the development of malonate-containing DNA binders that would have good affinity for the DNA minor groove. We have created DNA-binding malonate-derived **139** that binds to the minor groove (ΔT_M = 8.8 °C for poly(dAdT)$_2$ DNA). In an effort to increase DNA binding, we synthesised 9*H*-fluorene-based malonate compound **146** that binds to DNA. The affinity for stDNA was more than doubled but malonate-containing **145** did not bind strongly to poly(dAdT)$_2$ DNA indicating that it did not bind to the minor groove. This mode of binding cannot be attributed to its planar fluorene core since fluorene-derived compound **146** binds strongly to poly(dAdT)$_2$ DNA (ΔT_M = 19.5 °C) and has a measurable amount of minor-groove binding activity as well as preference for AT regions over GC regions.

Compounds **139**, **145** and **146** will be tested for cytotoxicity to cancer cells. We will also discuss methods of converting **139** and **145** to Pt-containing agents.

3.2 Pt-guanidine complexes

As stated in the introduction, a major aim of this project is to combine *bis*-guandinium-like MGBs with Pt^{II} systems to produce DNA-binding compounds with anti-cancer activity. We anticipated that these dual-acting agents would avail of different transporters to cisplatin and bind in the DNA minor groove where they would form alternative adducts with DNA compared to cisplatin.

We conceived of two different possible families of Pt-MGB complexes: (i) those where the metal is bound directly to a guanidine N atom and (ii) those where the MGB scaffold is modified to incorporate a well-studied Pt ligand, e.g. malonate (Figure 3.2.1). Investigations into the binding mode of Pt with *mono*-aryl guanidines will be discussed in Section 3.2.1, whereas Pt complexes of MGB-derived malonate ligands will be discussed in Section 3.2.2.

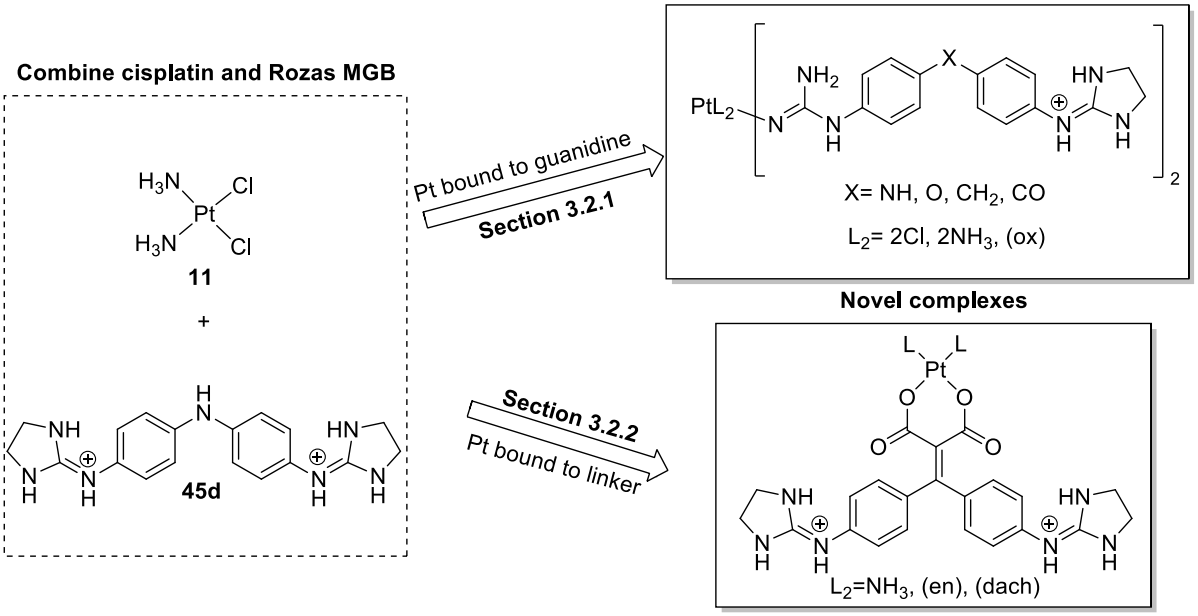

Figure 3.2.1. Two possibilities of connecting a cisplatin-type moiety to the Rozas MGB scaffold

3.2.1 Pt complexes of guanidines

Coordination complexes of Pt with *mono*-substituted aryl guanidines are not known in the literature. In this section we will explore the rich chemistry of aryl guanidines with different Pt precursor species, leading to Pt complexes of MGBs (Figure 3.2.1.1).

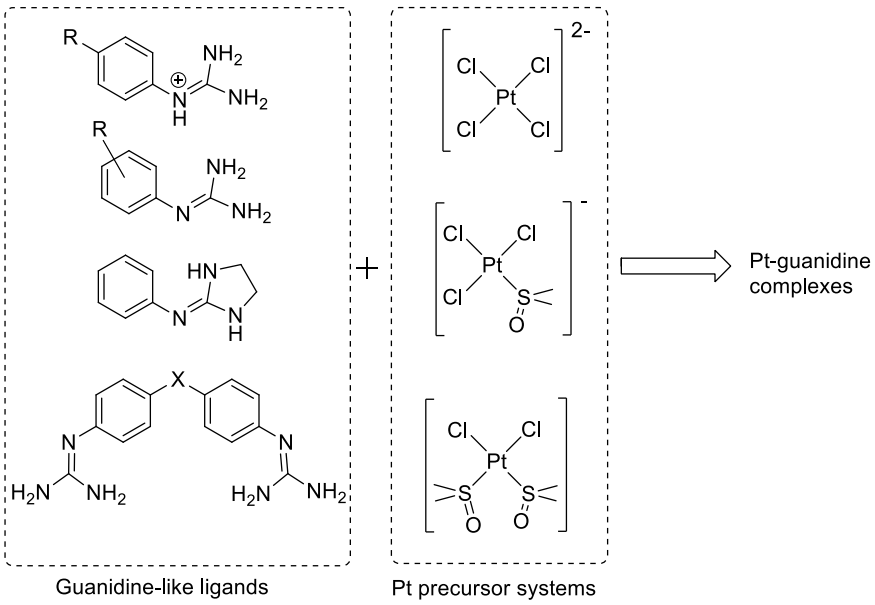

Figure 3.2.1.1. Guanidine like ligands and Pt precursors in this work.

As shown in Section 1.5.1, cisplatin and other compounds that contain Pt-N bonds are excellent anti-cancer agents. A comprehensive review detailing the synthesis of Pt complexes bound to alkyl amines was published in 2014 by Wilson and Lippard.[94] Our interest lies in creating Pt complexes with aryl N ligands, specifically with *mono*-aryl guanidines.

3.2.1.1 Review of Pt-guanidine complexes

Guanidines have a rich coordination chemistry.[202] Metal complexes with neutral guanidine (**177**), anionic guanidinate (**178**) and dianionic guanidinate (**17**) ligands are known. Substituted guanidinate anions are stabilised by resonance delocalisation (Figure 3.2.1.1.1), as well as by electron-withdrawing ligands.

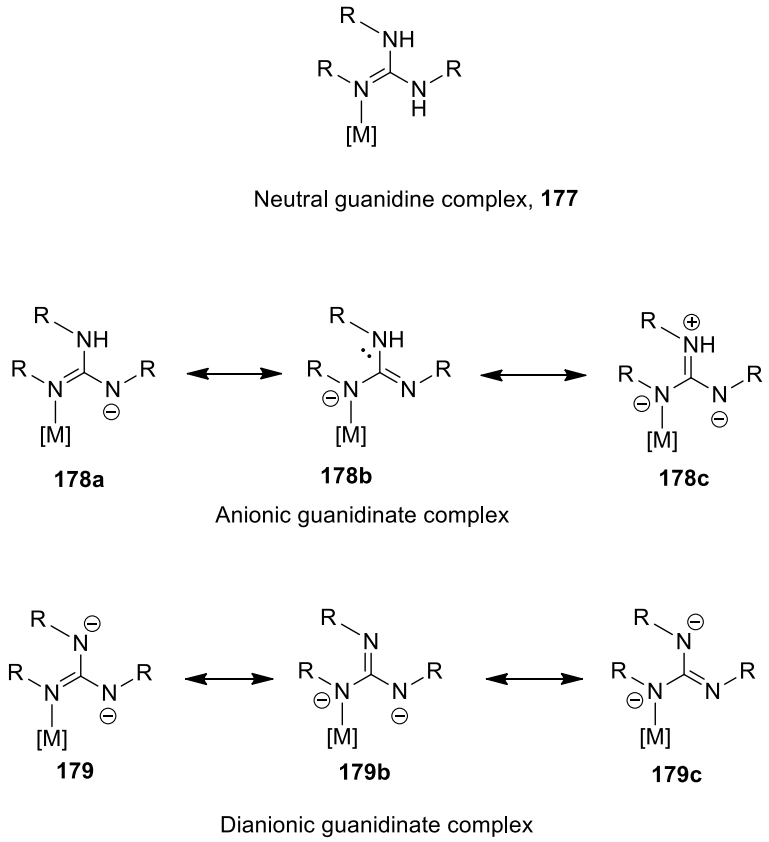

Figure 3.2.1.1.1. Resonance forms of neutral and anionic guanidine ligands.

Like with amidine complexes, the predominant method to form Pt-guanidine complexes described in the literature is by the attack of gaseous ammonia onto stable Pt-cyanimide complexes. However, only disubstituted alkyl amines are accessible by this method (Scheme 3.2.1.1.2).[102]

Scheme 3.2.1.1.2.

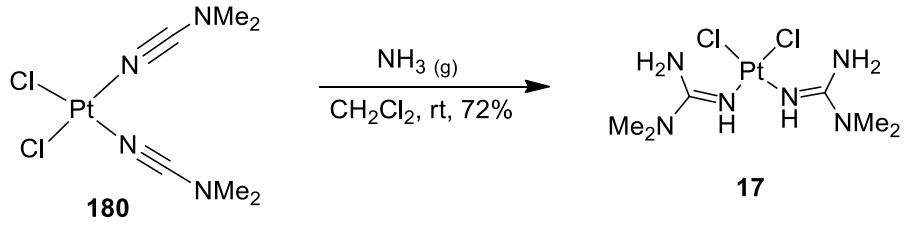

Similarly to amines, a neutral guanidine (**181**) can be used as a nucleophile to attack Pt-nitrile complexes (**182**) to give iminoguanidine derivative **183** (Scheme 3.2.1.1.3).[203] Interestingly, **183** does not form a six-membered chelate because *bis*-chelation would lead to loss of delocalisation of the Me_2N lone pair into the rest of the molecule.

Scheme 3.2.1.1.3.

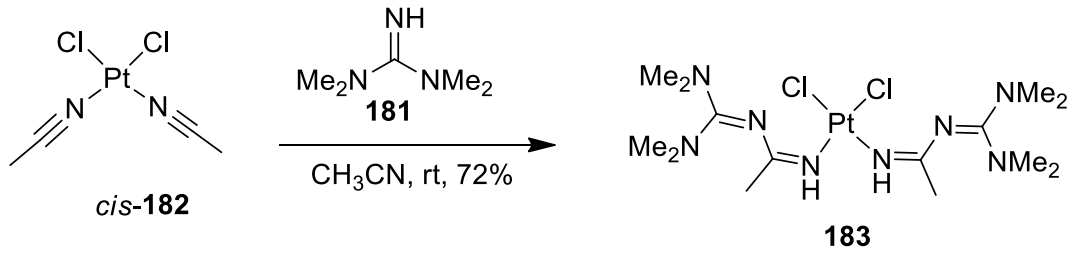

There are, however, complexes of guanidines with Pt created by direct Pt-N bond formation. The amino acids arginine (**184a**) and canavanine (**184b**) were complexed to *tert*-pyridine complex [PtCl(terpy)]Cl (**185**) to give *mono*-coordinated **186a** and **168b**, as well as paddlewheel complexes **187a** and **187b** (Scheme 3.2.1.1.4). The bimetallic complex was stabilised by π-π interactions between the terpy ligands. The reaction was carried out in water at pH = 9 over four days.

Scheme 3.2.1.1.4.

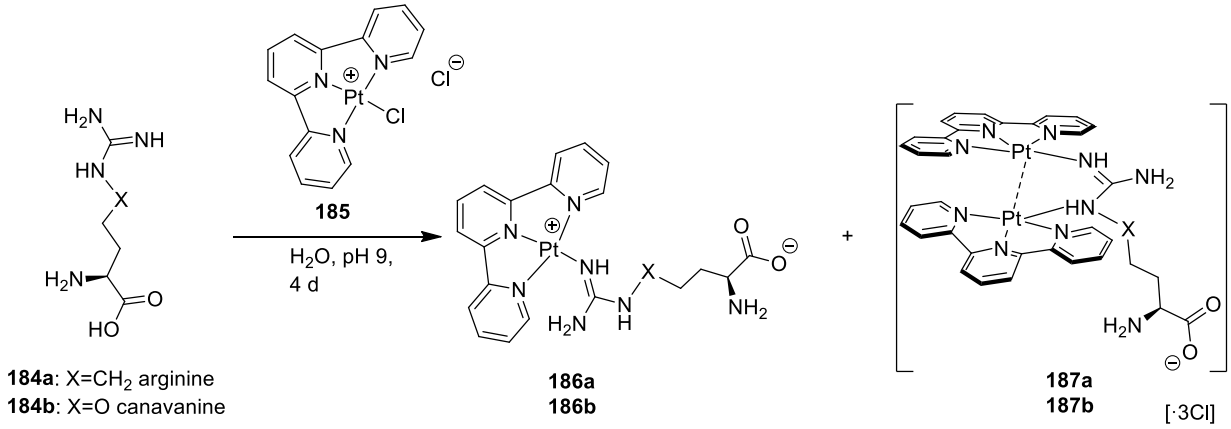

Another alkyl guanidine, the superbasic bicyclic guanidine ligand 1,5,7-triazabicyclo[4.4.0]dec-5-ene (TBD, also known as 1,3,4,6,7,8-hexahydro-2*H*-pyrimidino[1,2-*a*]pyrimidinate or hpp, **188**) was complexed to Pt under mild conditions by Himmel's group (Scheme 3.2.1.1.5).[204] The Pt source **189** was dissolved in CH_2Cl_2 with **188** to produce *cis*-**190**. The authors used an unusual method to access the *trans*-isomer by converting the ligand **188** into its tetrachloroplatinate salt (**191**) by reaction of **188** (3 eq.) with K_2PtCl_4 (**5**). The salt was then reacted with the lithium guanidinate **192** (4 eq.) in dry THF and quickly formed *trans*-**193** by initial attack on the tetrachloroplatinate. The guanidinate, a stronger σ-donor than neutral guanidine, facilitated the *trans*-complex formation. Protonation from the weakly acidic counter-cation produced *trans*-**190**.

Scheme 3.2.1.1.5.

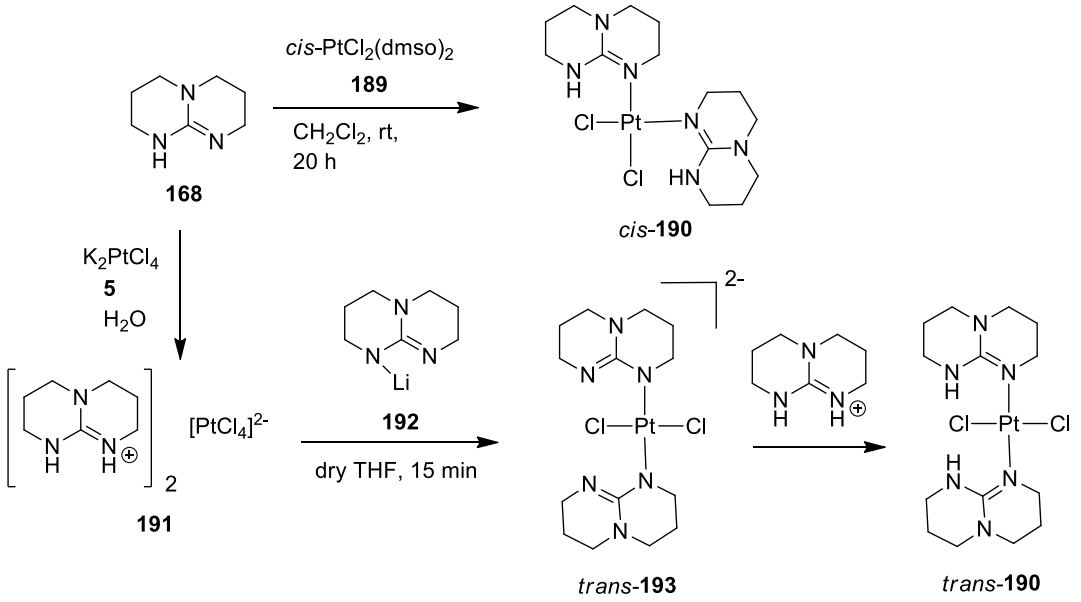

Of substantial importance was the synthesis of mononuclear triarylguanidine Pt complexes, disclosed by Elumalai *et al.* in 2013.[205] By reacting **189** with *ortho*-substituted triarylguanidines (**194**) in the presence or absence of NaOAc, the authors were able to isolate the cyclometalated (**195**) or non-cyclometalated (**196**) complex. Interestingly, a solvent switch from MeOH to toluene was also required to prevent cyclometalation. To achieve complexation to the bulky free base, the toluene solution was heated for 3 h (Scheme 3.2.1.1.6).

Scheme 3.2.1.1.6.

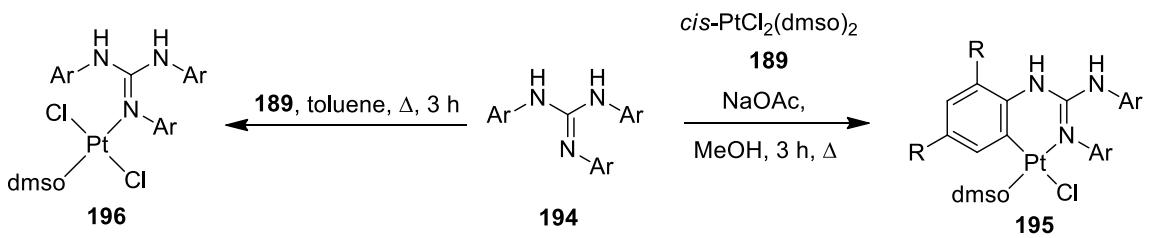

A similar ligand, triphenylguanidine (**197**) was used to form the air-stable four-membered Pt^{II} complex (**199**) in Scheme 3.5.2.6.3 with cycloocta-1,4-diene (cod).[206] The additive, Ag_2O,

removed Cl ligands from the Pt source **198**, generating AgCl and also providing free coordination sites on the metal. Also, Ag_2O acted as a base, forming H_2O and the guanidinate dianion upon complexation of the ligand to Pt.[207] The water stability of the complex **199** is notable. Additionally, unlike **195**, complex **199** does not cyclometalate to produce a six-membered platinacycle. The absence of a strong π-acceptor ligand and the difficulty in breaking a Pt-N bond to form the necessary intermediate are probable factors that prevent cyclometalation. The Pt-N guanidinate bond must indeed be very strong since the highly-strained four-membered ring does not protonate.

Scheme 3.2.1.1.7.

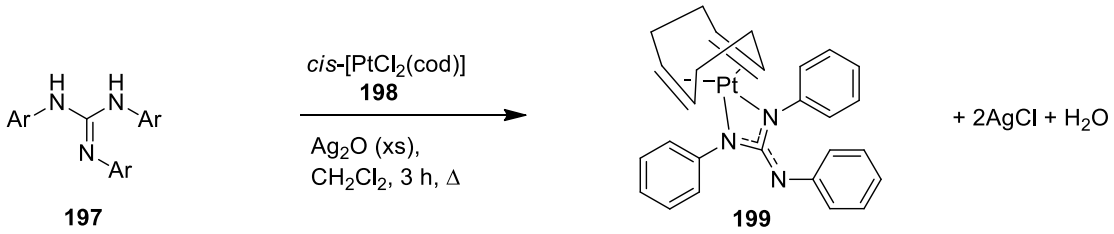

An article presenting the synthesis of 1-aryl-2,3-di(isopropyl)guanidine complexes was published at the end of 2015; the authors describe the preparation of these complexes by heating the guanidine free base in toluene with *cis*-[$PtCl_2(dmso)_2$] (Scheme 3.2.1.1.8).[208] The corresponding cyclometalated complex was not observed.

Scheme 3.2.1.1.8.

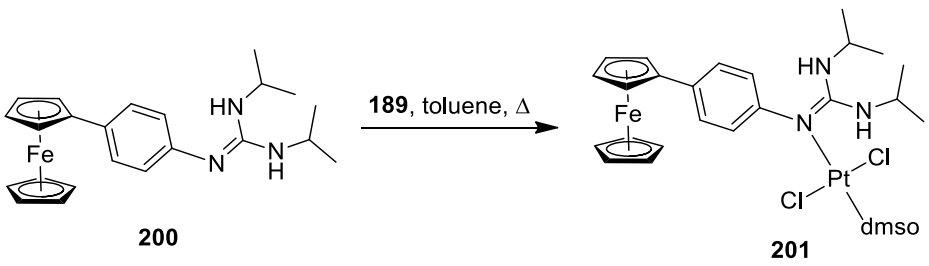

3.2.1.2 Synthesis of arylguanidine ligands

As mentioned before, our goal was to create complexes of *mono*-aryl guanidines and diaryl *bis*-guanidines (where the guanidines are mono substituted) to produce cytotoxic agents. Since complexation of guanidines with Pt can be carried out by direct reaction of the guanidine ligands with a Pt precursor complex, we first turned our efforts to synthesising neutral aryl guanidine-based ligands. The aryl guanidinium salts were prepared *via* the *bis*-Boc-protected guanidines (**203a-e**) by conditions previously used in Rozas' group, namely guanidylation of the appropriate aniline (**202a-j**) with *N,N'-bis(tert*-butoxycarbonyl)-*S*-methylisothiourea (**204**) and Et_3N in CH_2Cl_2 or DMF at 0 °C initially and warming to room temperature (Table 3.2.1.2.1).

Table 3.2.1.2.1. Synthesis of Boc-protected guanidines.

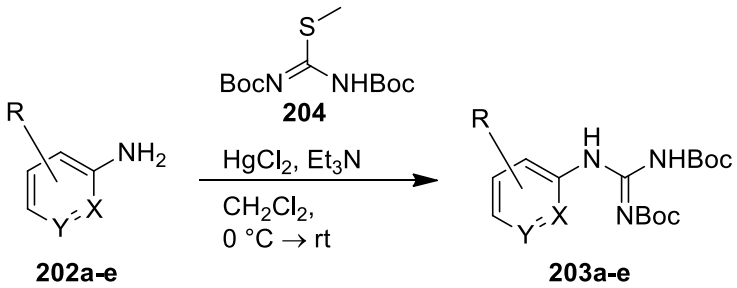

202a-e 203a-e

Cpd	R	X	Y	Yield[a]
203a	H	CH	CH	76%
203b	*p*-OMe	CH	CH	84%
203c	H	N	CH	84%
203d	H	CH	N	85%
203e	*o*-NH_2	CH	CH	98%

[a]Isolated yield after column chromatography

To explore the effect of constraining the aryl guanidine in a five-membered ring, we also prepared 1,3-[di-(*tert*-butoxycarbonyl)]-2-(iminophenyl)imidazolidine **205** in 65% yield after recrystallisation (Scheme 3.2.1.2.1).

Scheme 3.2.1.2.1.

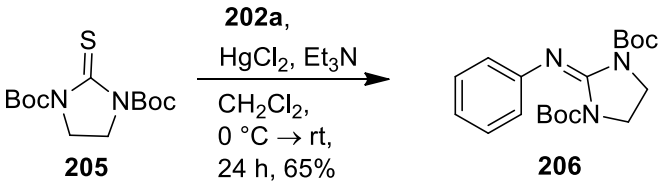

Additionally, benzylguanidine **208** was prepared from nucleophilic benzylamine **207**. The literature route from electrophile **199** in THF gave an inseparable mixture of highly polar salts.[209] However, standard Hg chemistry similar to that described above and silica gel chromatography afforded *bis*-Boc-protected benzyl guanidine **198** (Scheme 3.2.1.2.2).

Scheme 3.2.1.2.2.

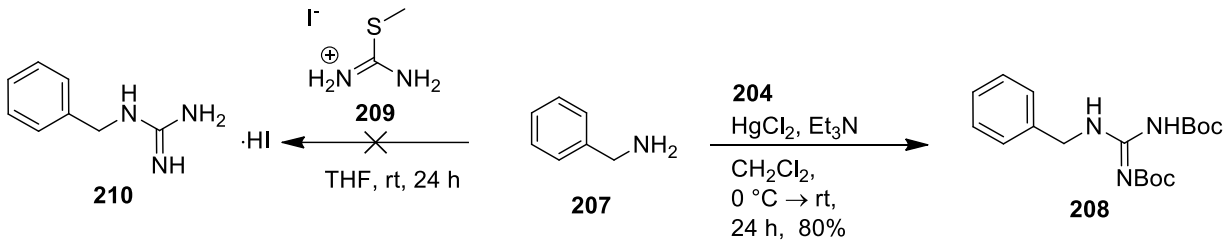

Deprotections of most Boc-protected intermediates proceeded smoothly with HCl dioxane solutions, producing the corresponding HCl salts (Table 3.2.1.2.2).

Table 3.2.1.2.2. Synthesis of guanidinium salts.

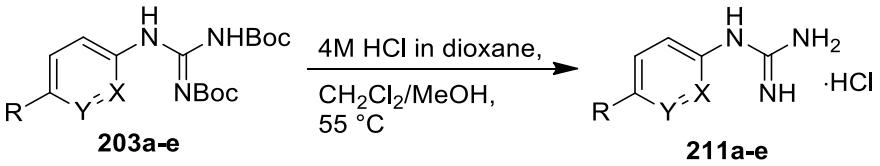

Cpd	R	X	Y	Yield[a]
211a	H	CH	CH	92%
211b	*p*-OMe	CH	CH	99%
211c	H	N	CH	75%
211d	H	CH	N	94%
211e	*o*-NH_2	CH	CH	Decomposition[b]

[a]Isolated yield. [b]See text.

However, Boc-protected *ortho*-amino phenylguanidine **203e** decomposed under the HCl conditions. Using the Lewis acid $SnCl_4$ to deprotect **203e** at rt provided **211e** in high yield (Scheme 3.2.1.2.3). The removal of Sn byproducts is known to be problematic,[210] but in this case was easily achieved by trituration and decantation of the crude gum with hexanes until a crystalline solid was obtained.

Scheme 3.2.1.2.3.

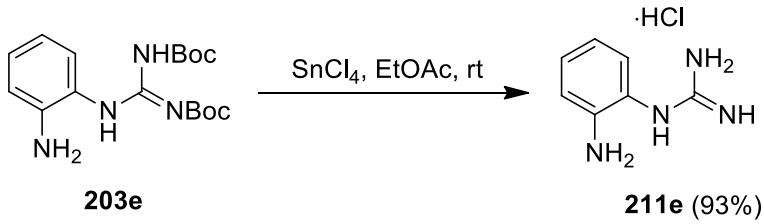

The Boc deprotection of both **196** and **198** was achieved using the usual HCl deprotection method (Schemes 3.2.1.2.4).

Scheme 3.2.1.2.4.

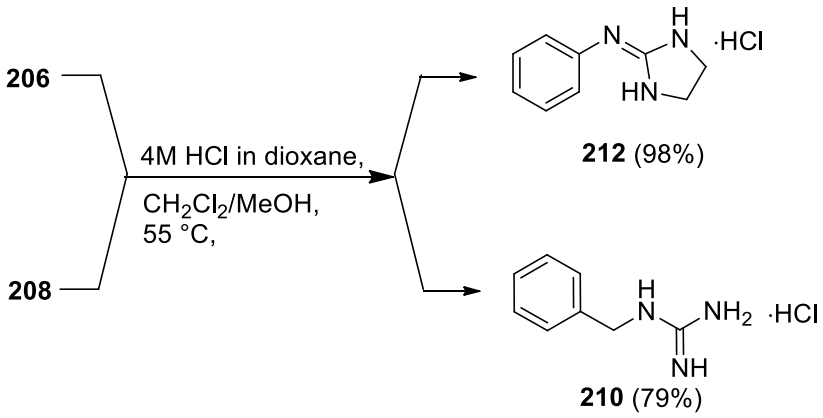

3.2.1.3 Free base formation

With the aim of forming the corresponding Pt complexes, the free base of the arylguanidines prepared was required and, hence, we explored a number of extraction systems and bases to isolate the free base **213a** (Table 3.2.1.3.1). However, the yields obtained were not ideal, since the neutral guanidine was soluble in water. A breakthrough came with an article by Yamada *et al.* where they described the formation of the free base of guanidine in ethanol using sodium ethoxide as a base.[211] We optimised the procedure accordingly to give quantitative formation of the corresponding free base **213a**.

Table 3.2.1.3.1.

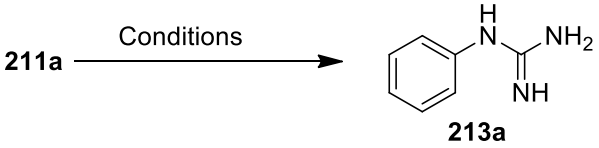

Base	Solvent	Yield[a]
NH_4OH (5 eq.)	CH_2Cl_2/H_2O	0%
KO^tBu (5 eq.)	CH_2Cl_2/H_2O	66%
KOH (pH 13)	CH_2Cl_2/H_2O	41%
NaOEt (1.0 eq.)	EtOH	92%[b]
NaOEt (1.1 eq.)	EtOH	100%

[a]Isolated yields. [b]Mixture of **213a** with **211a** (8% by ^{1}H NMR).

With these conditions in hand, we converted a selection of guanidinium salts to the corresponding free bases (Table 3.2.1.3.2). Not just to probe changing electron density on the aryl ring (as with the *para*-OMe substituent in **213b**), the chosen salts gave a diverse range of possible metal-binding domains, *e.g*. pyridine N (**213c**, **213d**), *ortho*-NH_2 (**213e**) as well as the guanidine N to compare where Pt would bind and in what coordination mode.

Table 3.2.1.3.2. Yields of free bases.

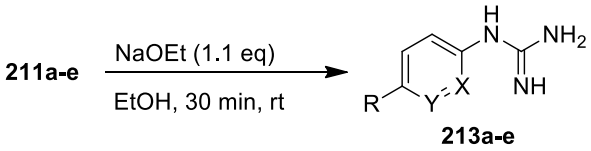

Cpd	R	X	Y	Conversion[a]
213a	H	CH	CH	100%
213b	*p*-OMe	CH	CH	100%
213c	H	N	CH	100%
213d	H	CH	N	100%
213e	*o*-NH_2	CH	CH	100%

[a]% conversion by ^{1}H NMR. Isolated yield was 104-110% due to excess NaOEt (visible by ^{1}H NMR).

The effect of the imidazolidine-2-imine moiety on Pt binding was also assessed by synthesising free base **214** (Scheme 3.2.1.3.1).

Scheme 3.2.1.3.1.

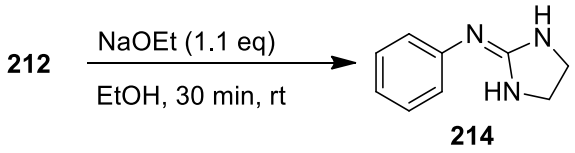

Finally, to assess if the aryl ring has an effect on Pt binding when the guanidine N is not delocalised into the ring, we synthesised the free base of benzylguanidine, **208** (Scheme 3.2.1.3.2).

Scheme 3.2.1.3.2.

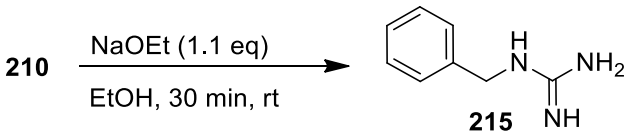

3.2.1.4 Diaryl bis-guanidine MGB ligand synthesis

With conditions for the synthesis of monoaryl guanidines in hand, we turned our attention to creating the corresponding MGBs. The diaryl *bis*-guanidine salts had been previously synthesised in our group, thus, following the methodology developed by Rodríguez and Rozas, the Boc-protected species **216a-b** were prepared (Table 3.2.1.4.1).[212]

Table 3.2.1.4.1. Yields of Boc-protected diaryl intermediates.

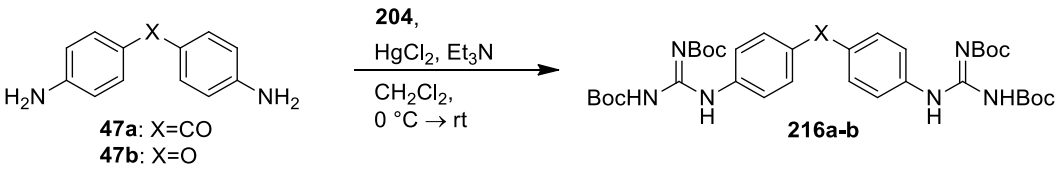

Cpd	X	Yield[a]
216a	CO	10%
216b	O	57%

[a]Isolated yield after column chromatography

The Boc groups were removed using a 4M solution of HCl in dioxane (Table 3.2.1.4.2).

Table 3.2.1.4.2. Yields of diaryl hydrochloride salts.

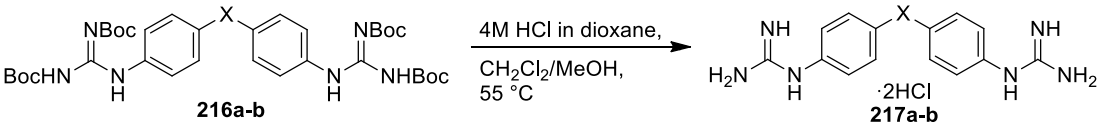

Cpd	X	Yield[a]
217a	CO	88%
217b	O	99%

[a]Isolated yield

Next, these salts were treated with 2.2 equivalents of fresh NaOEt to furnish the free bases **218a-b** (Table 3.2.1.4.3), which were used as ligands for Pt complexes.

Table 3.2.1.4.3. Yields of free bases **218a-b**.

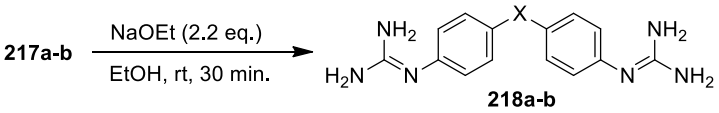

Cpd	X	Conversion[a]
218a	CO	100%
218b	O	100%

[a]% conversion by ^{1}H NMR. Isolated yield was 104-110% due to excess NaOEt (visible by ^{1}H NMR).

3.2.1.5 Reaction with K_2PtCl_4: Salt formation

With our arylguanidine ligands (generally formed *in situ*) in hand, we attempted to complex them to commercial Pt source K_2PtCl_4 (**5**). Initially, we reacted phenylguanidine ligand **213a** with **5** in the presence of KOH at pH = 9 and pH = 13 at room temperature and at reflux and in all cases a black precipitate of Pt^0 was the major product.

Then, following the procedure of Aitken *et al.* in their aminoguanidine complexation reaction (as discussed in Section 3.2.1.9),[146] we attempted to complex aryl guanidine hydrochloride salts **211a** and **211b** (5 eq.) with K_2PtCl_4 (**5**, 1 eq.) in water without the presence of base.

Precipitates of **219a** and **219b**, which were soluble only in DMSO, formed instantly (Scheme 3.2.1.5.1). Conductivity measurements in DMSO clearly demonstrated that ions in solution were only the unchanged guanidinium cation and chloride anions. The 'new' compounds were similar to **211a** and **211b** by ^{1}H and ^{13}C NMR in DMSO-d_6, but contained two peaks in the ^{195}Pt NMR spectrum. These peaks were attributed to *cis*- and *trans*- isomers of $[PtCl_2(dmso\text{-}d_6)_2]$. Thus, the precipitate formed in H_2O were the di(arylguanidinium) tetrachloroplatinate salts **219a** (82%) and **219b** (75%), as confirmed by elemental and IR spectroscopy on the solid sample. When this compound was dissolved in DMSO it reacted to form two equivalents of arylguanidinium chloride and one equivalent of $PtCl_2(dmso)_2$ as a mixture of isomers in solution.

Scheme 3.2.1.5.1.

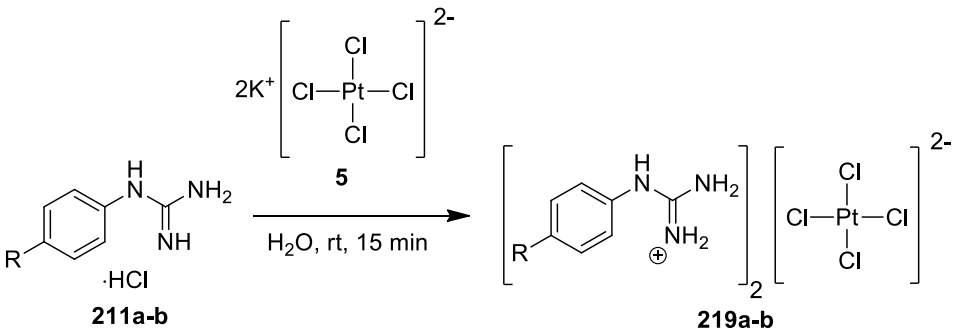

These complexes are similar to guanidinium salt $[TBD]_2[PtCl_4]$ **191**. However, **191** was recrystallised from hot water, whereas these complexes were insoluble even in boiling water. Also, addition of KOH to **219a** or **219b** in water led to decomposition to Pt^0.

We reattempted complexation with K_2PtCl_4 (**5**) with our library of isolated free base ligands. Unfortunately, reaction of the free bases **213a**, **213b** and **214** with **5** in MeOH or H_2O at room temperature in subdued lighting conditions (the solution was wrapped in aluminium foil and used in a darkened fumehood) led to decomposition to Pt^0 (Scheme 3.2.1.5.2). Therefore, in order to synthesise stable Pt^{II} complexes of guanidines, we evaluated other platinating agents.

3.2.1.6 Reaction with $PtCl_2(dmso)_2$: Cyclometalation

The platinum complex *cis*-$[PtCl_2(dmso)_2]$ (**189**) was shown to form Pt^{II} complexes with guanidine N atoms (Section 3.2.1.1).[204,205,208] Its synthesis proceeded easily by leaving excess DMSO (3 eq.) to stand overnight in an aqueous solution of **5**, followed by filtration and washing of the crystalline material with water, EtOH, and Et_2O (Scheme 3.2.1.6.1).[213]

Scheme 3.2.1.6.1.

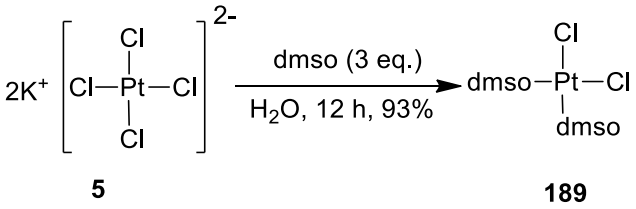

5 **189**

Initially, two equivalents of **213a** with **189** were mixed in THF or $CHCl_3$ at reflux but only starting materials were recovered. When the reaction was carried out in MeOH at room temperature, a mixture of inseparable products formed (as visualised by ^{1}H NMR in DMSO-d_6). When the reaction was carried out with only one equivalent of **213a** in MeOH at reflux, the reaction gave two products, **211a** and **220a**. High temperature ^{1}H NMR experiments were carried out on a sample of the crude mixture, demonstrating satellite peaks at 6.3 ppm (NH) and 8.0 ppm (CH) (Figure 3.2.1.6.1).

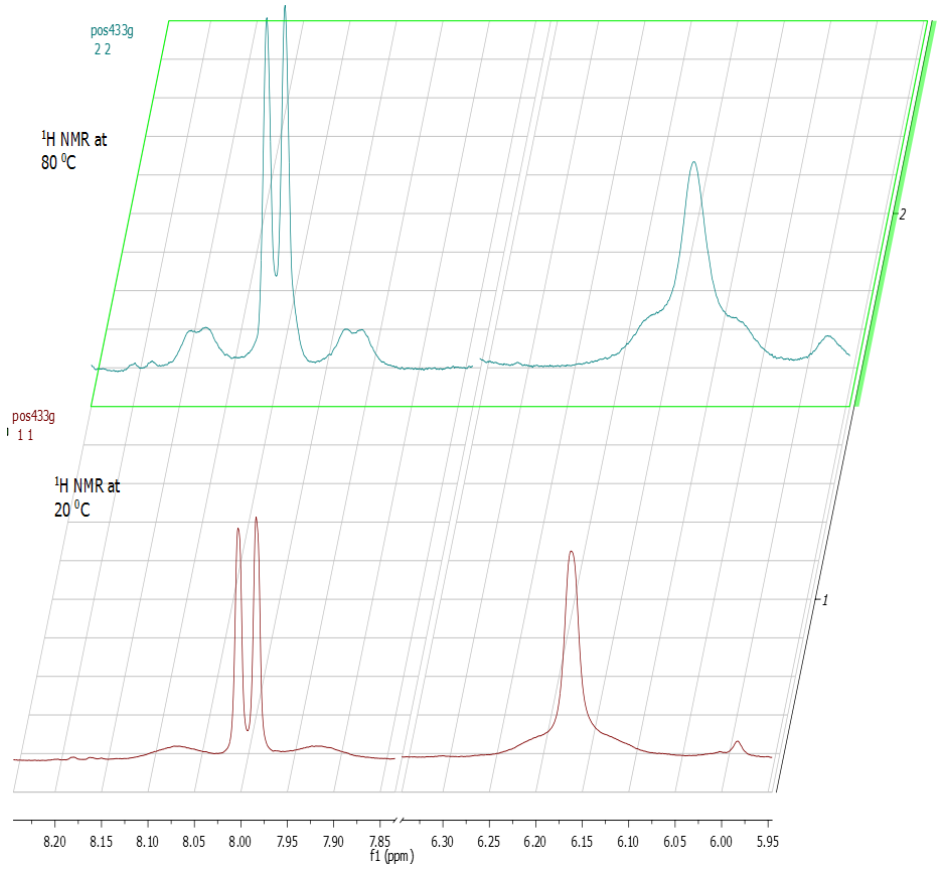

Figure 3.2.1.6.1. High temperature ^{1}H NMR experiments in DMSO-d_6 on a mixture of **209a** clearly demonstrating presence of satellite peaks around the nearest neighbours to Pt . From bottom to top, the temperatures are 20 °C (**red**) and 80 °C (**blue**).

The reaction mixture was filtered through cotton wool to remove insoluble materials. The solvent was removed in vacuo and the product was dissolved in the minimum amount of DMSO and precipitated out by addition of water. The fine solid was isolated by centrifugation and characterised by NMR spectroscopy and IR. The ^{1}H NMR spectrum of **220a** gave four aromatic C-H peaks (integrating to one proton each), two NH peaks and one NH_2 peak. From TOCSY and nOESY experiments, an outline of the structure could be proposed (Figure 3.2.1.6.2).

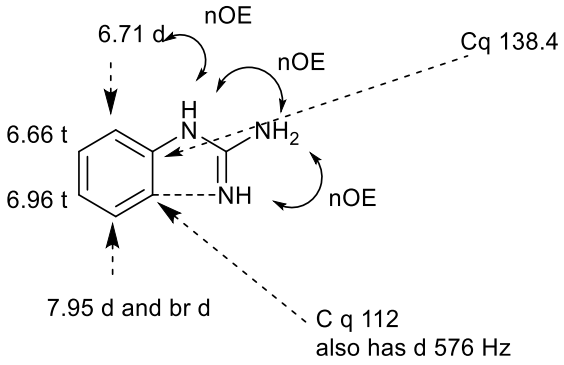

Figure 3.2.1.6.2. Partial structure of **220a** consistent with NMR data.

We figured that in the dotted line between the aryl ring and imine-type NH in Figure 3.2.1.6.2, there must be a Pt atom, because of the satellite peaks on the C-H, N-H and quaternary carbon surrounding this line. Furthermore, there is evidence from the ^{13}C NMR spectrum of coordinated DMSO-d_6 and the IR spectrum of the isolated solid also contains an S-O stretch at 1091 cm^{-1}. Low resolution mass spectrometry showed an $[M+H]^+$ peak at 443.02, with a characteristic isotope splitting pattern for Pt and matching a calculated formula of $[C_9H_{15}ClN_3OPtS]^+$. From this we could confidently assign the fourth ligand as Cl. Although we had no direct evidence of the arrangement of the Cl and dmso ligands relative to the aryl guanidine, we inferred from the literature that dmso will not bind *trans* due to the strong *trans*-effect of the cyclometalated group. Taking all this data into account the structure of cyclometalated **220a** shown in Scheme 3.2.1.6.2 was proposed.

Scheme 3.2.1.6.2.

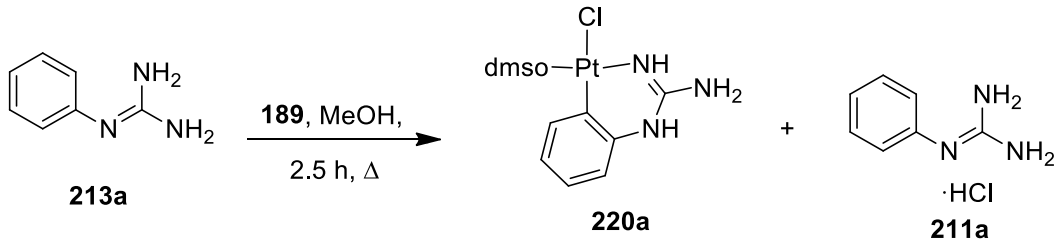

In summary, the reaction in Scheme 3.2.1.6.2 produced cyclometalated product **220a** and guanidinium salt **211a** from the reaction of two equivalents of free base **213a** with excess of

89 (*cis*-[$PtCl_2(dmso)_2$]). The fact that we have used the privileged cyclometalation Pt source **189** and carried out the reaction at a relatively high temperature strongly supported the formation of such a platinacycle. Moreover, a second equivalent of free **213a** can act as a bridging base, similar to NaOAc, in order to facilitate cyclometalation. To regenerate free base **213a**, we added one equivalent of NaOMe. The optimised conditions for this reaction are shown in Scheme 3.2.1.6.3.

Scheme 3.2.1.6.3.

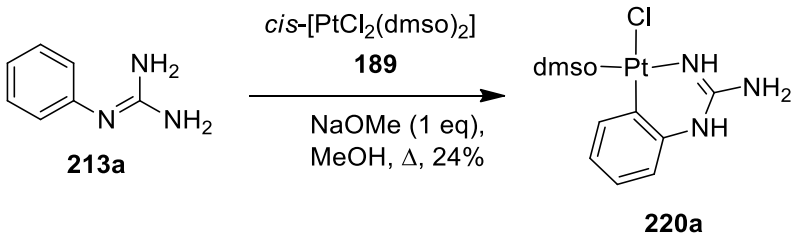

To our satisfaction, the crude NMR spectrum of the reaction mixture was very clean, showing only the signals corresponding to compound **220a**. The reaction mixture was purified by repeated precipitation from a concentrated DMSO mixture with water. Crystals of suitable quality for X-ray crystallography were grown in darkness at room temperature over a period of three months by slow evaporation of water into a concentrated DMSO solution of **220a**. Gratifyingly, the structure confirmed our solution phase assignment (Figure 3.2.1.6.3).

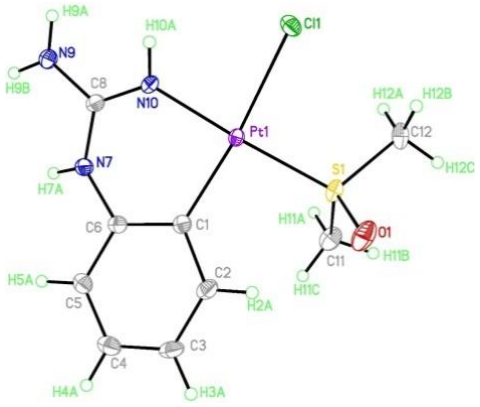

Figure 3.2.1.6.3. Crystal structure of the asymmetric unit in **220a**. Displacement ellipsoids are at 50% probability.

Complex **220a** crystallised in an orthorhombic unit cell (0.71 Å resolution). The relative configuration of the ligands was confirmed to be SP-4-4 (square planar 4-coordinate with the highest priority ligand, in this case Cl, *trans* to the fouth priority ligand, C). The strong *trans*-effect of C was demonstrated by the long Pt-Cl bond (2.4 Å). The N-Pt-C and Cl-Pt-S angles around Pt were 89° and 93° respectively, close to the ideal bond angle of 90° for a square planar complex. The crystal is stabilised by intermolecular H bonds between the dmso O atom and a H atom on the NH_2.

Changing the ligand to **214** gave complex **221** (Scheme 3.2.1.6.5) and under identical conditions for crystallisation as those used with **220a**, suitable crystals for X-ray crystallography of complex **221** were formed (Figure 3.2.1.6.4).

Scheme 3.2.1.6.5.

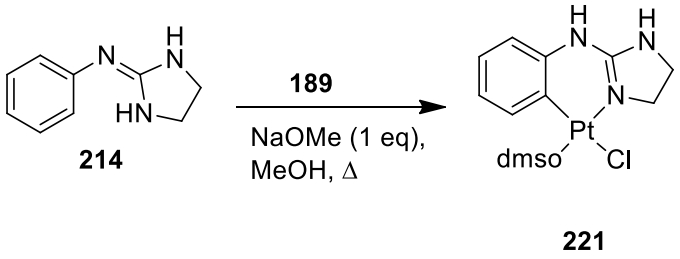

214 **221**

The crystal structure of **210** was very similar to that of **209a**. The Pt-Cl bond length was 2.4 Å, and the N-Pt-C and Cl-Pt-S angles were 87° and 88°. The unit cell was orthorhombic (0.71 Å resolution), in the space group Pbca, identical to **209a**. The main difference in the crystal packing was that **210** contained an intermolecular H bond between the dmso O^1 atom and the aniline $N^{7'}H$ of another molecule.

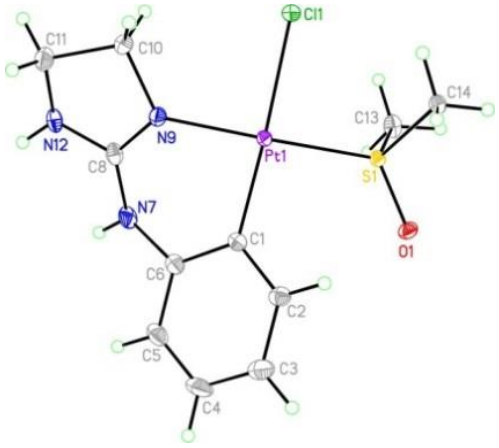

Figure 3.2.1.6.4. Crystal structure of the asymmetric unit in **210**. Displacement ellipsoids are at 50% probability.

The reaction of **189** with **213b** to create **220b** in 2.5 h gave a clear cyclometalation pattern by ^{1}H NMR (satellite peaks around broad NH signal at 5.99 ppm and satellite peaks doublet, although free base and side products were also observed in the spectrum of the crude . The reaction mixture was purified and set up for crystallisation, but no pure compound was found. A solvent swap for DMSO revealed that cyclometalation was much slower for the formation of **220b** without presence of MeOH. ^{1}H NMR spectra of the reaction were taken for two days, but even after 48 h full conversion was not achieved. Conversion was estimated at 15%.

Interestingly, compounds **213c** and **213d** (pyridinyl-2-guanidine and pyridinyl-3-guanidine), under similar conditions to those in Scheme 3.2.1.6.3, yielded a yellow precipitate after 2.5 h. After 30 min, the ^{1}H NMR spectrum of the crude showed conversion of the signals corresponding to the free base to new broad signals. After 2.5 h, the product obtained was insoluble in all common solvents (toluene, CH_2Cl_2, $CHCl_3$, H_2O, 1M HCl (aq), DMSO, DMF, nitrobenzene, THF) and did not react with PPh_3. However, the precipitate decomposed in concentrated HCl. This result will be discussed in detail in Section 3.2.1.10.

Unfortunately, the reaction of **215** (benzylguanidine) with **189** did not give a reaction as determined by ^{1}H NMR. Initially, no evidence of cyclometalation (satellite peaks or appearance of a doublet at 8 ppm) was observed. Compared to free base **215**, the aromatic peaks broadened considerably and the benzyl CH_2 almost disappeared upon addition of **189**. Upon heating for 3 h, there was no change in the ^{1}H NMR spectrum. However, after 12 h, the ^{1}H NMR spectrum showed what could be a triplet at 8.28 ppm, as well as a broad singlet integrating for 4H at 7.27 ppm, 2H at 6.29, 1H at 5.54 ppm and 3H at 4.27 ppm. However,

due to the broadening of the signals, it was difficult to make conclusive assignments. The reaction mixture was allowed to crystallise as with previous complexes, but no product was isolated.

Interestingly, reaction of **213e** with **189** produced an isolable bimetallic species (**222**, Scheme 3.2.1.6.5). Small purple crystals of suitable quality for X-ray diffraction were grown from a mixture of DMSO and H_2O over a period of six weeks.

Scheme 3.2.1.6.5.

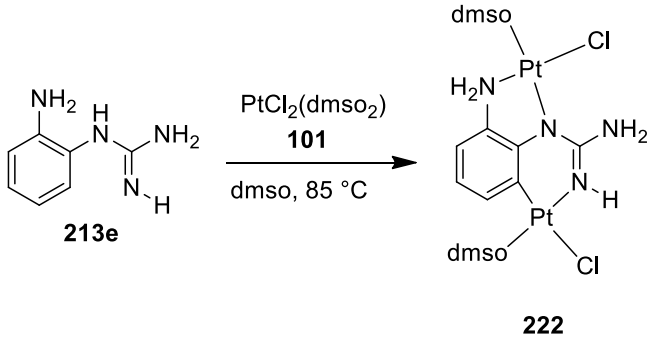

Complex **222** crystallised in a monoclinic unit cell ($P2_1$ space group, 0.81 Å resolution) and was refined as an inversion twin (Figure 3.2.1.6.5). Due to the close proximity of both Pt atoms, H atoms could not be located. Some bond lengths, especially C-N bond lengths differ significantly between both structures of the inversion twin. For these reasons, we could not unambiguously assign the geometry of the N atoms. This may be an artefact of the experiment; however, when the refinement in the centrosymmetric space group $P2_{1/n}$ was used, there were large residuals of *ca.* 4.4 e^-/Å (compared to 1.45 e^-/Å in $P2_1$).

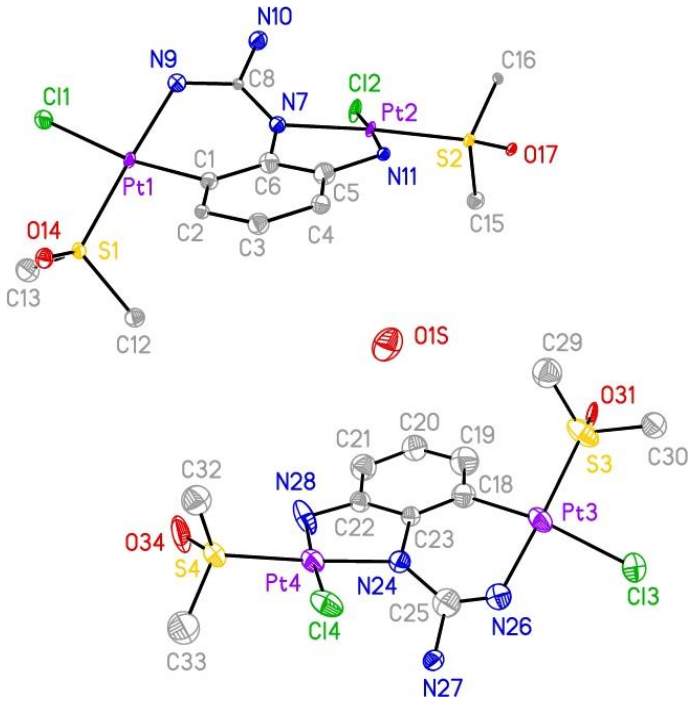

Figure 3.2.1.6.5. Crystal structure of **222**. Displacement ellipsoids are at 50% probability.

The binuclear structure of **222** in the solid state was interesting; however, in a solution of DMSO-d_6 at rt the compound degraded to give a mixture of signals, suggesting that the complex is unstable to DMSO-d_6. Once again, the compound was insoluble in other solvents.

The three cyclometalated Pt complexes, **220a**, **221** and **222**, were tested for activity in HL-60 leukemia cells (Section 3.3). Also the complexes **220a** and **221** were investigated for generation of ROS (reactive oxygen species, Section 3.2.11). Our next synthetic aim was then to create non-cyclometalated Pt-arylguanidine complexes and assess their stability and cytotoxicity. For this reason we investigated another Pt precursor complex.

3.2.1.7 Reaction with K_2PtI_4: Cyclometalation to Pt^{III} complex

Similar to the synthesis of cisplatin, we utilised K_2PtI_4 (**6**) as a precursor to create Pt-N bonds. The electron-rich ligand **213b** was chosen to be tested with this agent since its cyclometalation reaction had shown to be slow (see Section 3.2.1.6). Thus, KI (6 eq.) was added to a solution of **5** in H_2O at 55 °C for 30 min to give **217** *in situ*.[110] The reaction was cooled to room temperature, then the free base **213b** (2 eq.) was added and the reaction stirred for 15 min. The brown precipitate formed was isolated by filtration and washed with

water; then, it was dissolved in hot EtOAc, purified by slow diffusion of Et_2O into the EtOAc solution and filtered. Crystals suitable for X-ray diffraction were grown from a standing solution of the filtrate to give **223** (Scheme 3.2.1.7.1).

Scheme 3.2.1.7.1.

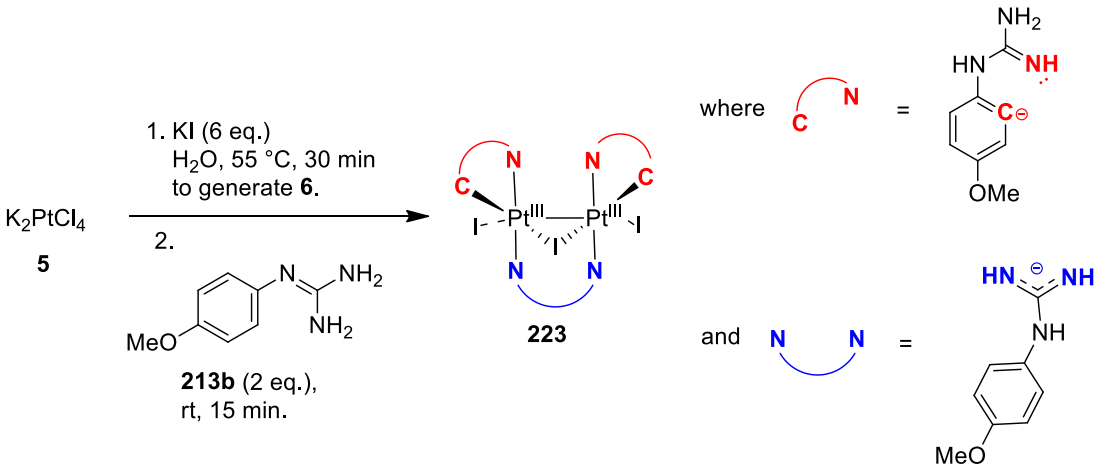

The crystal structure of **223** ($P2_{1/c}$, monoclinic, 0.78 Å resolution) was notable for many features (Figure 3.2.1.7.1). First, the dinuclear structure $[Pt_2(ArGua)_3I_3]$ contained a Pt-Pt bond (2.61 Å), with each Pt bound to one axial I atom (Pt-I = 2.77 Å and 2.74 Å) and one bridging I atom (Pt-I = 2.80 Å and 2.82 Å, Pt-I-Pt = 55°). Moreover, each Pt atom was bound to cyclometalated ligand **213b** (**C**-Pt-**N** = 87° and 90°) and a bridging guanidinate derivative of **213b** (each Pt-**N** bond = 2.02 Å). The environment around each Pt is distorted octahedral, which is unknown for Pt^{II} or Pt^{IV}. Additionally, there are two solvent pores in the crystal (Et_2O and H_2O). The three negatively-charged guanidine ligands and three I ligands require a +6 overall charge. From this charge balance and the almost symmetrical nature of the complex, we can assume the Pt atoms are both in a +3 oxidation state.

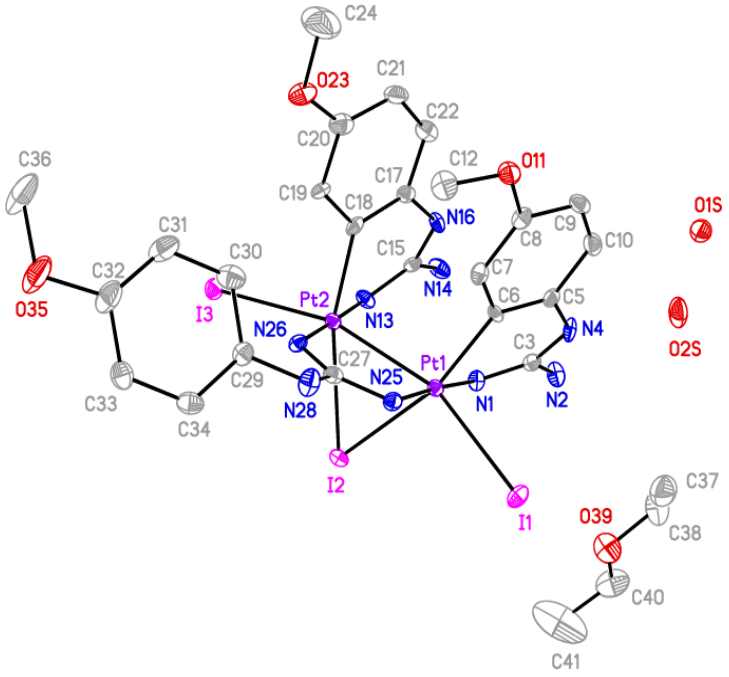

Figure 3.2.1.7.1. Crystal structure of the asymmetric unit in **223**. Displacement ellipsoids are at 50% probability.

Most Pt^{III} complexes are bimetallic, stabilising the unpaired radicals in a Pt-Pt bond. Also, these bimetallic Pt^{III} complexes have a distorted octahedral geometry, similar to that of **223**. Some literature examples of Pt^{III} complexes are given in Figure 3.2.1.7.2.

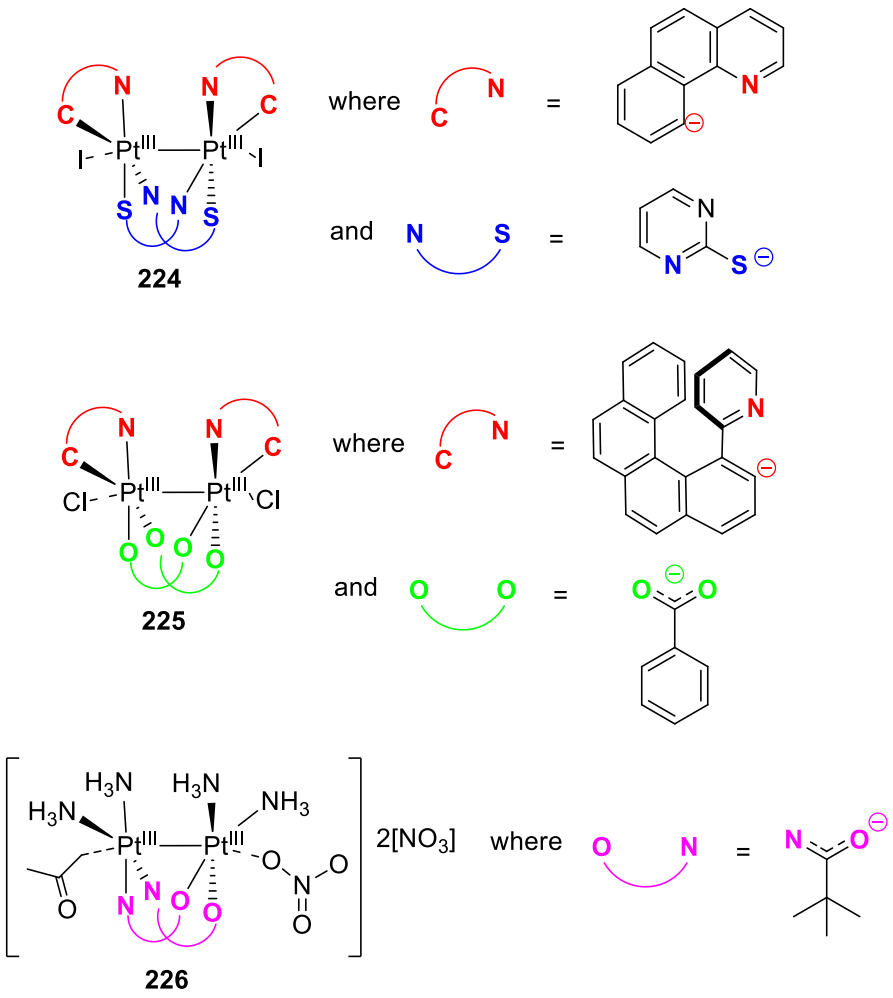

Figure 3.2.1.7.2. Structures of binuclear organo-Pt^{III} complexes **224**[214], **225**[215] and **226**.[216]

Lippard and coworkers isolated a binuclear Pt^{III} complex with anti-cancer activity;[217] however, compound **223** is insoluble in water. The ^{1}H NMR in DMSO-d_6 showed some impurities, suggesting that in solution the complex either decomposes or exists as a mixture of species. For these reasons, we did not fully isolate the complex or synthesise derivatives. Therefore, the use of yet another Pt^{II} precursor complex was explored to prepare a non-cyclometalated Pt-arylguanidine complex.

3.2.1.8 Reaction with K[PtCl$_3$(dmso)]: No Cyclometalation

We searched the literature for milder conditions to prevent cyclometalation of aryl compounds coordinated by an N atom. The diphenyl imine complexes in Scheme 3.2.1.8.1 were synthesised as luminescent compounds,[218] based on work by Kukushkin.[219] The authors were able to control Pt complexation of benzophenone imine **227** by either heating with **189** in toluene to give platinacycle **228** or stirring with K[PtCl$_3$(dmso)] (**230**) at room temperature in a biphasic mixture of CH_2Cl_2 and water to give non-cyclometalated **229**. The ligand **227** and product **229** are partitioned into the organic phase (CH_2Cl_2 cannot participate in the reaction as a ligand), whereas the Pt source **230** and any free DMSO are sequestered in the aqueous phase. The authors were able to show that **229** can be transformed into **228** in the solid state by releasing HCl, demonstrating that heat is necessary for complexation in the absence of solvent participation. Complex **228** was also converted to acac (acetylacetone) derivative **231** by reaction with 2,4-pentanedione and Na_2CO_3 in toluene. The bidentate anion replaced a neutral dmso and anionic Cl^- in order to retain a neutral charge on the complex while changing the luminescent properties of **231** compared to **229**.

Scheme 3.2.1.8.1.

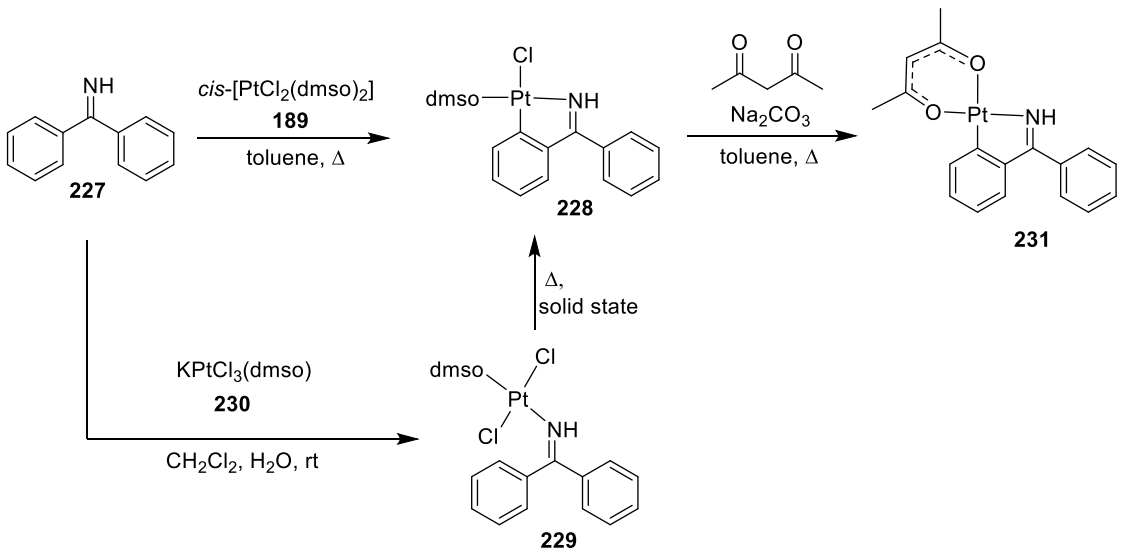

Following this example, we synthesised K[$PtCl_3$(dmso)] (**230**) *in situ*, followed by addition of water-soluble ligand **214** and CH_2Cl_2 at room temperature to obtain *trans*-dichloro complex **232** after evaporation of the organic layer at room temperature and quick chromatography on silica (Scheme 3.2.1.8.2). Crystals suitable for X-ray crystallography were grown over 12 h by slow diffusion of Et_2O into a concentrated solution of **232** in CH_2Cl_2 (Figure 3.2.1.8.1). Pure **232** was not soluble in CH_2Cl_2 and decomposed in dmso; thus, all ^{1}H NMR experiments were carried out in DMF-d_7 in which the complex is stable for at least 7 days. Unfortunately, biochemical assays of cytotoxicity on cancer cell lines are incompatible with high percentages of DMF; hence, since **232** did not dissolve in aqueous media and decomposed to Pt^0 when heated, it was not possible to evaluate its effect on cell viability.

Scheme 3.2.1.8.2.

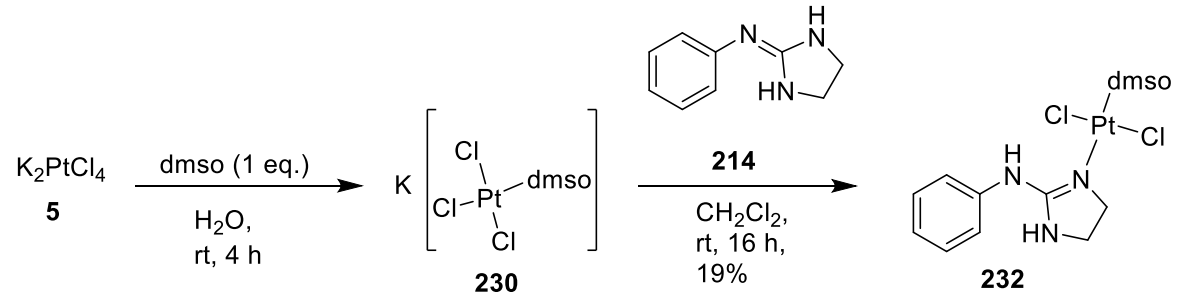

The crystal structure of complex **232** again demonstrated that dmso binds to Pt *trans* to the guanidine N. The compound crystallised in a orthorhombic unit cell (resolution = 0.71 Å) and $P2_12_12_1$ space group. The crystal packing is stabilised by an intermolecular H bond between the dmso O^1 of a molecule and the aniline-type N^6H of another molecule. The Pt-Cl bond lengths are both 2.31 Å and the Cl-Pt-Cl angle is 175° whereas the N-Pt-S angle is 179°.

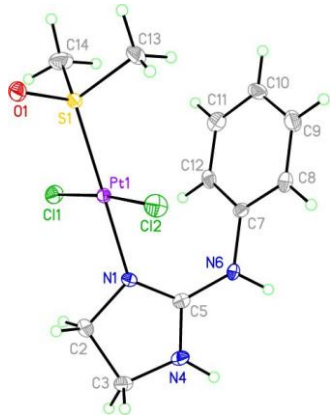

Figure 3.2.1.8.1. Crystal structure of the asymmetric unit in **232**. Displacement ellipsoids are at 50% probability.

The ^{1}H NMR spectra of compound **232** in DMF-d_7 confirmed that the solution structure is the same as in solid state. Two separate broad NH singlets, three signals for the *ortho*-, *meta*- and *para*-H atoms in the aryl ring and two distinct 2H triplets in the alkyl region as well as a 6H peak for coordinated dmso, all were in agreement with the structure shown above for **232** (Figure 3.2.1.8.2). There is no NOE between the dmso protons and any other protons on the molecule, suggesting that dmso is *trans* to the 2-aminoimidazoline ligand. High resolution mass spectrometry (ESI$^-$) confirmed a molecular mass in agreement with the molecular formula $C_{11}H_{17}Cl_2N_3OPtS$.

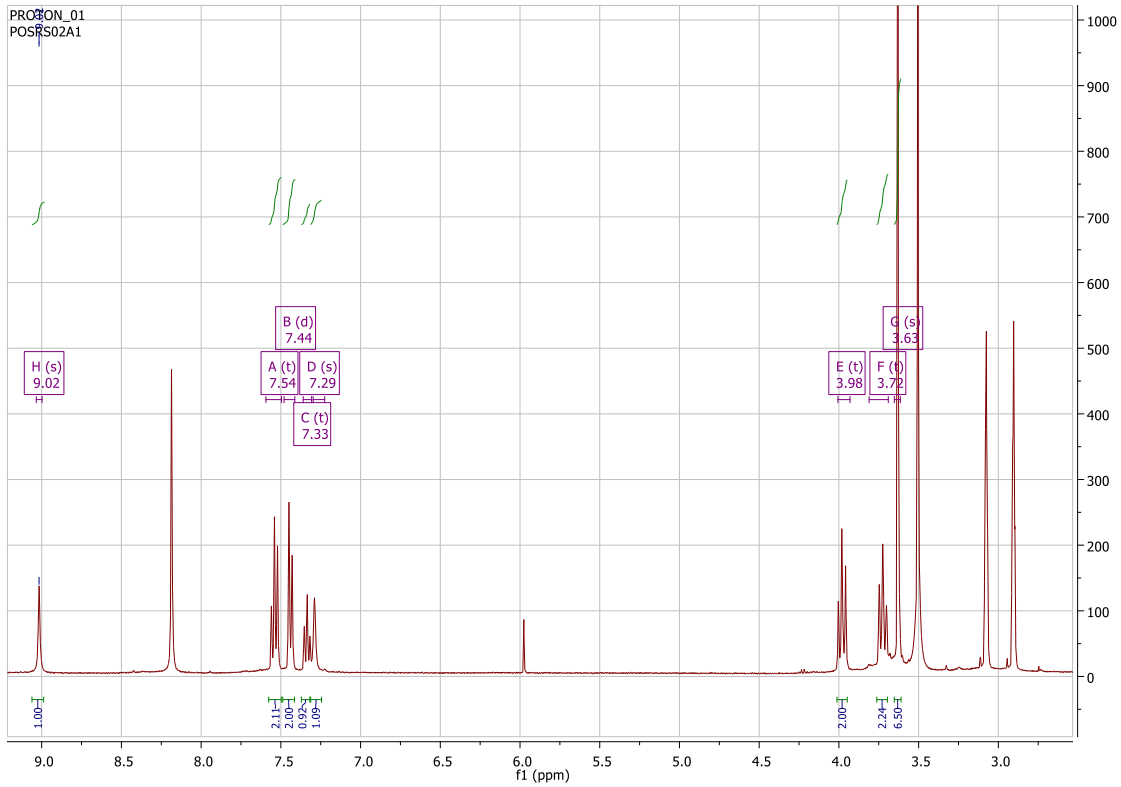

Figure 3.5.3.6.2. ^{1}H NMR spectrum of **232** in DMF-d_7, showing agreement with the crystal structure.

To further explore the limits of non-cyclometalation, two equivalents of free base **214** were reacted with **230** (Scheme 3.2.1.8.3). When the crude reaction mixture from the organic layer was evaporated and re-dissolved in acetonitrile, crystals suitable for X-ray crystallography were isolated (Figure 3.2.1.8.3). To our surprise, the isolated structure was the iminoguanidine complex **233**, which is the result of a reaction with a molecule of acetonitrile.

Scheme 3.2.1.8.3.

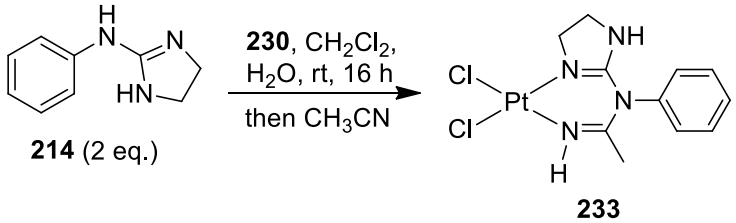

The crystal structure (Figure 3.2.1.8.3) of **233** is in a monoclinic unit cell (0.66 Å resolution), with space group $P2_{1/c}$. The Pt-Cl and Pt-N bond lengths are 2.31 Å and 1.98 Å, respectively and the N-Pt-N and Cl-Pt-Cl angles are 88° and 89°, respectively. The three C-N bond lengths around the guanidine C atom are 1.30 Å (N1-C5), 1.35 Å (N4-C5), 1.39 Å (C5-N6), and the C-N bond lengths around the amidine C atom are 1.39 Å (N6-C7) and 1.28 Å (C7-N8). Clearly, the C-N bonds coordinated to Pt are the shortest, implying that the guanidine/amidine double bonds are more localised on these atoms (the CN triple bond in the acetonitrile solvate is much shorter, 1.13 Å). The other three C-N bonds to the guanidine or amidine C atom are intermediate in length between single and double bonds, demonstrating some degree of resonance. The C-N bonds to the imidazole CH_2 groups (1.45 Å and 1.48 Å) and to the aryl ring (1.45 Å) are clearly single bonds.

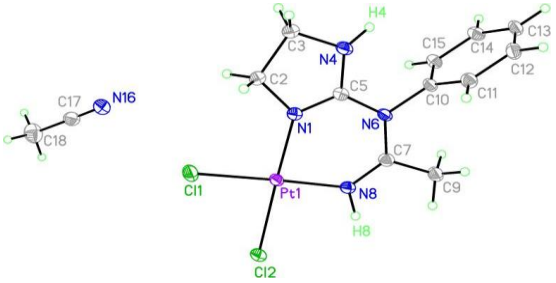

Figure 3.2.1.8.3. X-ray crystal structure of the asymmetric unit in **233**. Displacement ellipsoids are at 50% probability.

Our proposed mechanisms for the acetonitrile insertion are given in Scheme 3.2.1.8.4. We do not know whether the acetonitrile first coordinates to **232** and then undergoes nucleophilic addition of coordinated 2-aminoimidazoline (Path A) or whether the coordinated acetonitrile is attacked by free 2-aminoimidazoline (Path B). We ruled out attack of coordinated 2-aminoimidazoline on uncoordinated acetonitrile for steric reasons and also considering the lack of precedence in the literature for nucleophilic attack on unactivated nitriles. In contrast, the strongly electrophilic properties of metal-acetonitrile complexes have been comprehensively reviewed.[220]

Scheme 3.2.1.8.4.

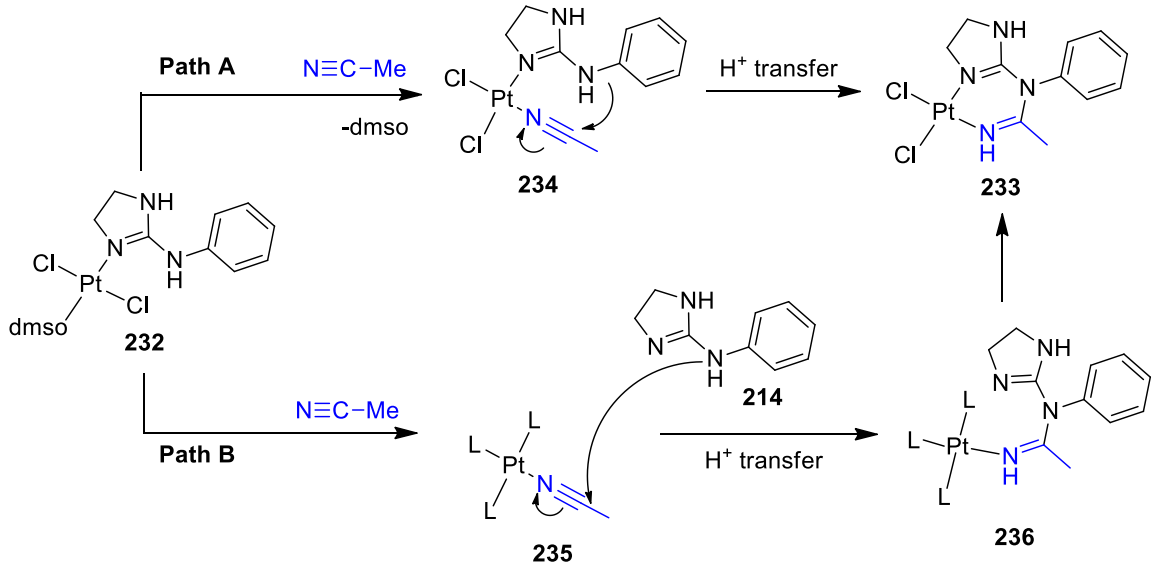

To investigate whether the mechanism could more likely proceed via Path A or Path B, we synthesised acetonitrile complex **182** and reacted it with free base **214**. Similarly, we reacted **232** with acetonitrile (Scheme 3.2.1.8.5). However, we were unable to isolate complex **233** again. We did observe by TLC that **232** decomposed in the presence of acetonitrile. Since **233** itself is highly unstable (decomposed in CD_2Cl_2, CD_3CN, DMSO-d_6 and DMF-d_7 at room temperature) we reasoned that decomposition of **232** in acetonitrile was tentative evidence of Path A.

Scheme 3.2.1.8.5.

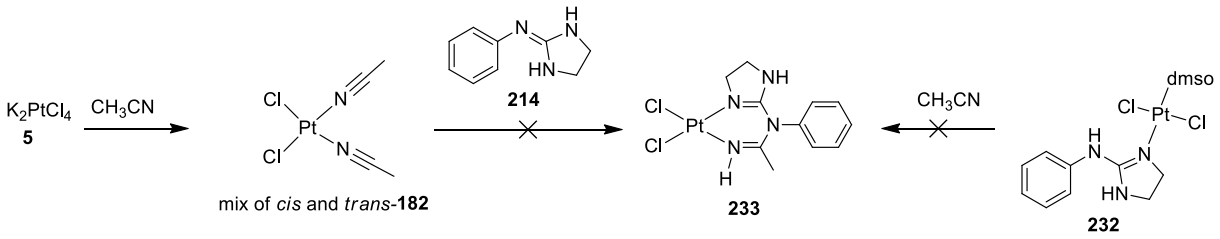

Upon reaction of benzonitrile with **232**, no reaction occurred after 48 h, suggesting that benzonitrile is not electrophilic enough to react with the 2-aminoimidazoline N atom and also not electrophilic enough to react with the Pt centre, even upon reflux. Regardless, due to its

insolubility in H_2O and instability at rt, neither **233** nor its derivatives would make useful drug candidates.

Instead, we focussed our efforts on synthesising more non-cyclometalated complexes similar to **232** (Scheme 3.5.3.6.5). Unfortunately, free bases **213a** and **213b** did not dissolve in the biphasic H_2O/CH_2Cl_2 solvent system at room temperature as used in Scheme 3.5.3.6.1. Free base **214** was ideal in the solvent system because it dissolved in H_2O whereas its non-cyclometalated complex dissolved in CH_2Cl_2. Free bases **213a** and **213b** were both insoluble in H_2O. The only common water-immiscible solvent we found that would solubilise **213a** and **213b** was nitromethane (CH_3NO_2). However in this solvent, a mixture of many compounds was observed by ^{1}H NMR experiments of the crude reaction mixture. Attempts at crystallisation failed and these compounds degraded on silica. Instead of a biphasic system, we changed to a single solvent system, using either MeOH or THF with isolated **230,** K[$PtCl_3$(dmso)]. Similar to CH_3NO_2, when all reactants were in the same phase, the reaction gave a mixture of many compounds (as adjudged by ^{1}H NMR). In MeOH especially, there was a large amount of cyclometalated product as adjudged by ^{1}H NMR (DMSO-d_6).

Scheme 3.5.3.6.5.

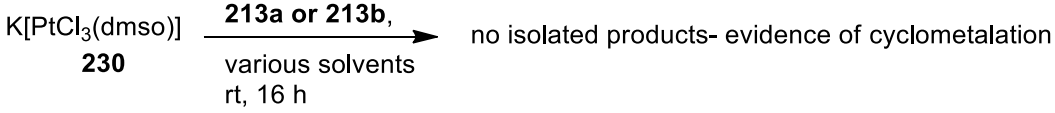

We did not attempt any further synthesis with the monoaryl guanidine ligands and Pt precursors other than K_2PtCl_4, K_2PtI_4, K[$PtCl_3$dmso], *cis*-[$PtCl_2$(dmso)$_2$] or [$PtCl_2(CH_3CN)_2$]. Before turning our attention to the preparation of MGB-derivatives of cisplatin, we first investigated the feasibility of *mono*- and bi-dentate *N*-amino-*N*'-arylguanidine complexes of Pt, in terms of synthesis, stability and water solubility.

3.2.1.9 Pt-aminoguanidine complex synthesis

To develop alternate Pt-based anticancer agents we used the *N*-amino-*N'*-arylguanidinium salts prepared as Pt ligands. We hypothesised that these simple aryl ligands may change the

specificity of cisplatin-like compounds for DNA in new cell types, broadening the efficacy of cisplatin much like the *N*,*N*'-bidentate 1,2-diaminocyclohexane (DACH) ligand allowed oxaliplatin to be efficacious in colorectal cancers. Furthermore, the *N*-aminoguanidine moiety would also allow for *mono*- and bi-dentate complex formation that could be used to attach Pt to the *bis*-guanidine-like MGBs to give a strongly DNA-binding dual action agent.

Our hypothesis was inspired by Aitken's synthesis of *N*-aminoguanidine-derived Pt^{II} complexes.[146] Using just one equivalent of *N*-aminoguanidine HCl with K_2PtCl_4, they isolated compound **237**, a charge-neutral complex with *N*-aminoguanidinium as a monodentate ligand (Scheme 3.2.1.9.1).

Scheme 3.2.1.9.1.

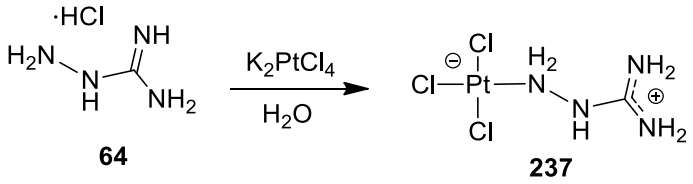

These authors were unsuccessful in displacing chloride to generate the expected 5-membered chelate despite adding base or silver compounds to force the reaction. Instead, any efforts resulted in precipitation of black Pt^0. However, when using a large excess of ligand (5 eq.) the authors succeeded in forming the *bis*-ligated species **238** (Scheme 3.2.1.9.2). This time, upon neutralisation with stoichiometric base and $AgNO_3$, the authors obtained the *bis*-chelated dicationic species **239**.

Scheme 3.2.1.9.2.

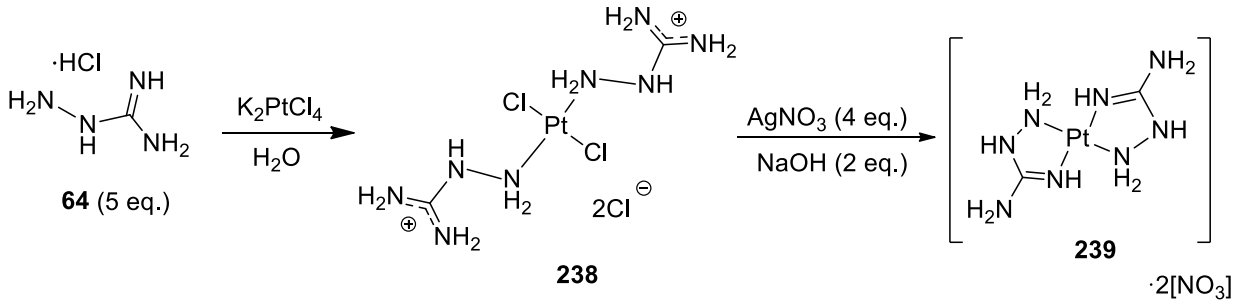

From the above results, the authors noticed that chelation occurred only on the *S*-ligated Pt complex **238** and not the trichloro-Pt complex **237**. Thus, they synthesised the more reactive K[$PtCl_3$(dmso)] (**230**) as a Pt-precursor and reacted it with compound **64**. The reaction proceeded directly to give chelate complex **241**, presumably *via* the dichloro intermediate **240** (Scheme 3.2.1.9.3).

Scheme 3.2.1.9.3.

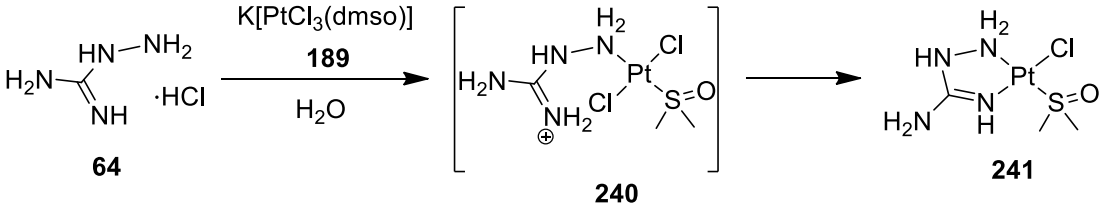

Considering the similarity of our compounds **67a** and **67b** to the parent compound **64**, we applied the same conditions to **67b** as Scheme 3.2.1.9.2 above. However, the pK_a difference and steric effects may impart different reactivity towards Pt on the *N*-aminoguanidine scaffold compared to Aitken's. To our delight, reaction of **67b** with K_2PtCl_4 in analogous conditions to those in Scheme 3.2.1.9.2, on a test scale yielded complex **242** as detected by mass spectrometry and ^{1}H NMR in DMF-d_7 (Scheme 3.2.1.9.4).

Scheme 3.2.1.9.4.

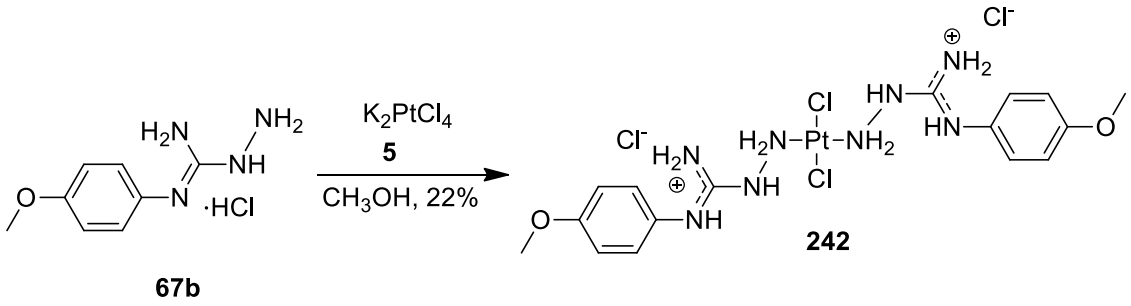

Conditions analogous to Schemes 3.2.1.9.1 and 3.2.1.9.3 lead to black Pt^0 precipitate in our hands. However, using [$PtCl_2$(dmso)$_2$] (**189**) as Pt source and forming the free base of **67b**,

by reaction with fresh sodium ethoxide in ethanol, allowed us to form **244** and characterise the compound by ^{1}H NMR and mass spectrometry (Scheme 3.2.1.9.5). Unfortunately, any effort to purify the compound from the reaction mixture was not possible on such a small scale.

Scheme 3.2.1.9.5.

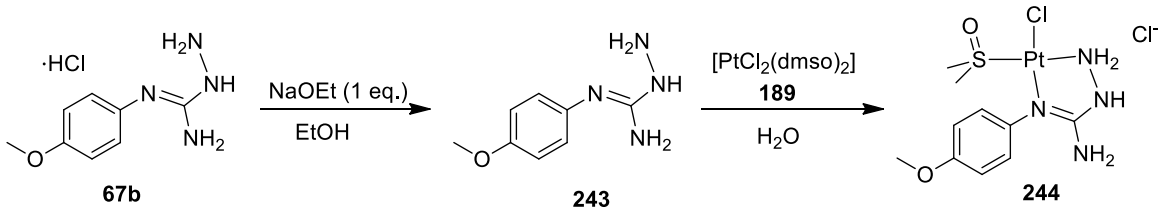

Notably, complexes **242** and **244** were soluble in water, along with their impurities. This preliminary data validated our assumption that non-cyclometalated Pt complexes of *N*-amino-*N'*-arylguanidines may be useful drug candidates, with improved physical properties over currently administered drugs such as cisplatin. Moreover, Pt complexes of *N*-amino-*N'*-arylguanidine-containing MGBs may prove to be a promising avenue of research in the future.

With isolated Pt complexes of monoaryl-guanidines **220a**, **221**, **222**, **223, 232** and **233** as well as Pt complexes of *mono*-aryl-*N*-aminoguanidines **242** and **244** in hand, we next turned our attention to synthesising Pt complexes of MGB-like diaryl bis-guanidine ligands **218a** and **218b**.

3.2.1.10 Reaction of diaryl *bis*-guanidine MGB ligands with Pt complexes precursors

When the free bases of the *bis*-guanidinium diaryl systems (**218a-b**) were exposed to conditions for cyclometalation previously used, an insoluble yellow precipitate was formed in both cases instead of cyclometalation (Scheme 3.2.1.10.1). Similar to what was observed with compound **213d**, the precipitates did not dissolve in any common solvent and decomposed in conc. HCl to give a black solid (Pt^{0}) and the corresponding HCl salt of the

ligand (see Section 3.2.1.6). Neither addition of coordinating ligands PPh_3 nor dmso (120 °C) were successful in breaking up the precipitates.

Scheme 3.2.1.10.1.

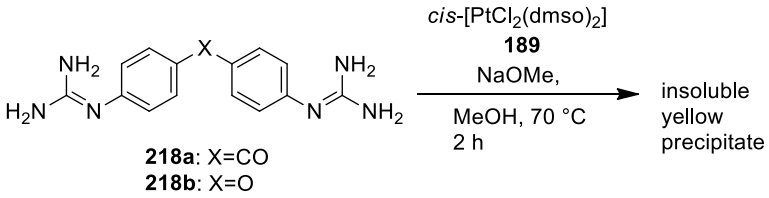

Free bases **213d** and **218a-b** have two N atoms capable of forming *bis*-Pt complexes by coordinating with one N atom of another ligand and, hence, these oligomers may continue to polymerise until they precipitate out of solution as the yellow precipitate. In an attempt to measure these intermediates, we removed NaOMe, changed solvent to DMSO-d_6 and ran an NMR tube reaction of **218a** and **218b** to understand the process. Gratifyingly, with no MeOH or methoxide present, both cyclometalation reactions of **218a** and **218b** with **189** progressed to completion (Scheme 3.2.1.10.2).

Scheme 3.2.1.10.2.

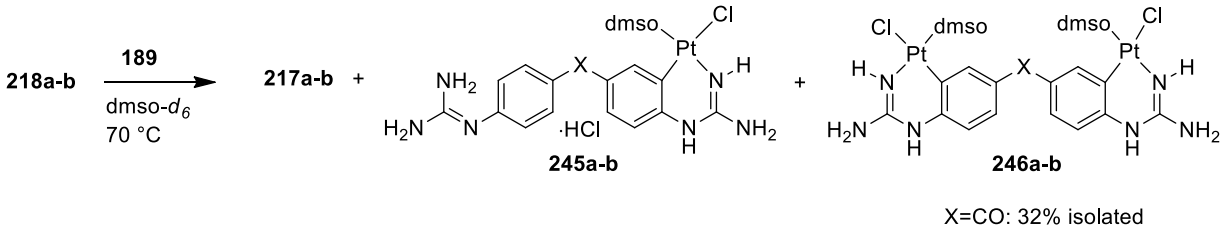

To confirm this, the reaction was followed by ^{1}H NMR as indicated in the spectra shown in Figure 3.2.1.10.1.

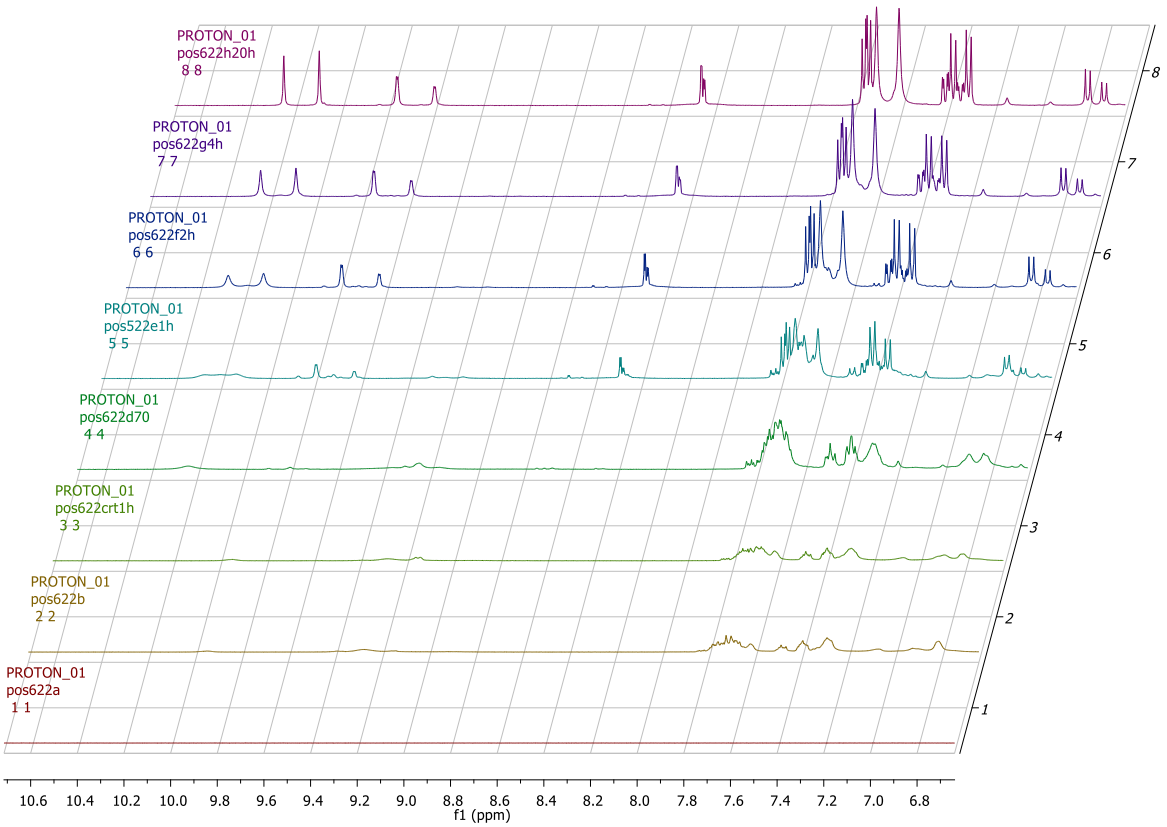

Figure 3.2.1.10.1. Overlay of ^{1}H NMR spectra from reaction of **218a** (X=CO) with **189**.

The reactions produced a 1:1:1 mixture of HCl salts **217a-b**, the *mono*-cyclometalated products **245a-b** and the *bis*-cyclometalated products **246a-b**. The mixture was fully characterised by ^{1}H NMR (Figure 3.2.1.10.2) and ^{13}C NMR.

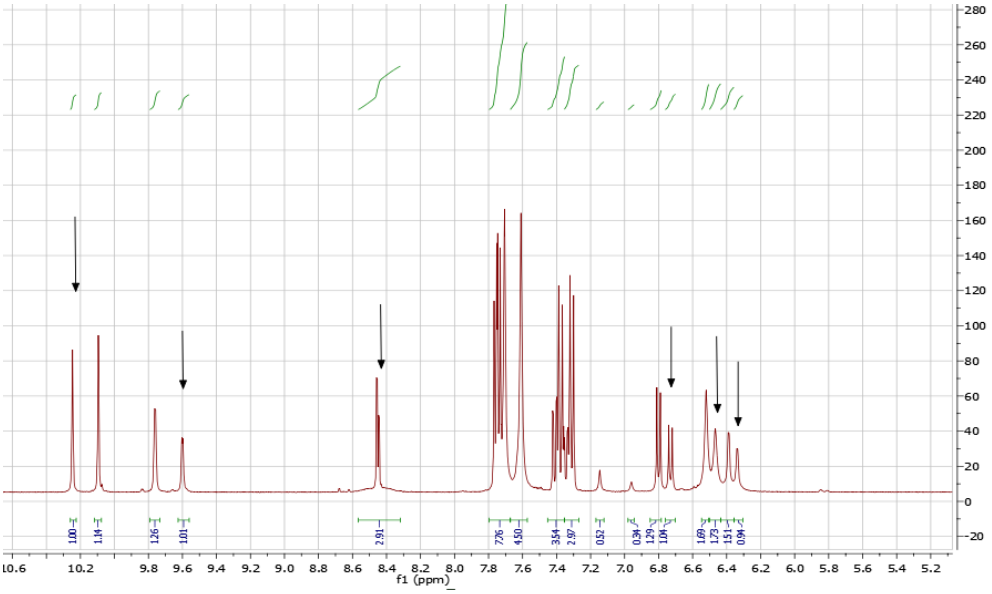

Figure 3.2.1.10.2. Mixture of ^{1}H NMR spectra from reaction of **218a** with **189**. Peaks due to **245a** are marked by arrows.

Isolation of the complexes proved difficult since all three species were water soluble. Repeated dissolution of the crude mixture in DMSO, followed by precipitation with H_2O and filtration gave a filtrate from which carbonyl-linked **246a** crystallised**.** Despite repeated attempts, purification of **245a**, **245b** or **246b** did not yield adequate material for characterisation. However, the X-ray structure of **246a** was in agreement with the solution structure (Figure 3.2.1.10.3).

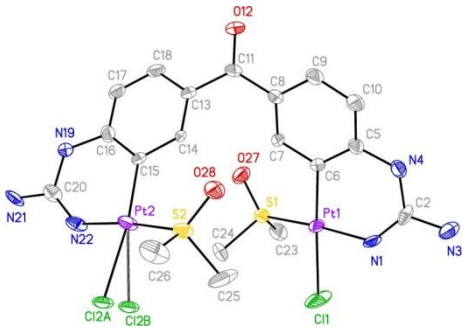

Figure 3.2.1.10.3. Crystal structure of the asymmetric unit in **246a**. Displacement ellipsoids are at 50% probability.

The binuclear complex crystallised in an orthorhombic unit cell (0.80 Å resolution, $Pna2_1$ space group). The crystal was refined as a two-component twin. Restraints and constraints were used to model the disorder in the Cl position (72%/18% occupancy). Four water molecules per unit cell were found but their respective H atoms were not located.

We attempted to create non-cyclometalated Pt complexes of our MGBs, with the hope that the isolated complexes would be water soluble, since the mono-Pt complexes would have one guanidinium cation. With this in mind, we performed many variations of the biphasic reaction from Scheme 3.2.1.8.2. Unfortunately, we could not isolate any product from these reactions. When we switched to a *mono*-phasic system (MeOH) with $K[PtCl_3(dmso)]$ (**230**) and free base **217a**, we were again able to isolate cyclometalated **246a** after crystallisation from aqueous solution (Scheme 3.2.1.10.3). Moreover, a sample suitable for X-ray diffraction was found (Figure 3.2.1.10.4).

Scheme 3.2.1.10.4.

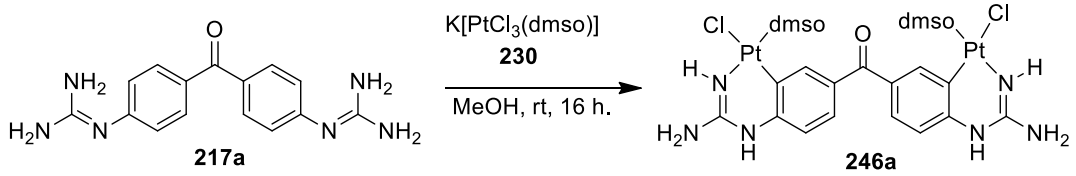

In this case, **246a** crystallised as a triclinic unit cell (Pī space group, 0.78 Å resolution) with two water molecules per molecule of **247a**. The Pt-N bonds were 2.00 and 2.01 Å. The Pt atoms were both square planar. Within the platinacycles, the C-Pt-N angles were both 89°. However, the C-Pt-S angle was 98° in both cases. The overall molecule showed a helical twist. The Pt-Pt distance was 6.09 Å and the angle between the planes of the square planar Pt geometries was 37°. The dihedral angle between the planes of each benzene ring was 50°. In this case there were no partially occupied atoms. All H atoms on **246a** were located.

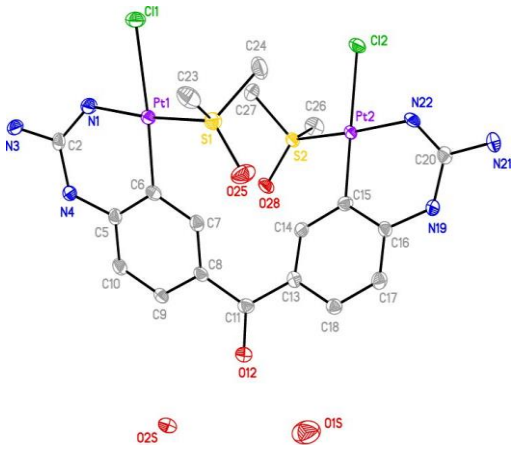

Figure 3.2.1.10.4. Crystal structure of the asymmetric unit in **246a**. Displacement ellipsoids are at 50% probability.

This work showed that the MGBs are likely to cyclometalate, even at room temperature. Thus, non-cyclometalated Pt-MGB complexes bound *via* a guanidine, even if isolated from a reaction mixture, would likely decompose under biological conditions. With this in mind, we tested some of the cyclometalated complexes for possible ROS generation as a method of causing cell death.

3.2.1.11 ROS generation experiment

Since cyclometalated complexes of Pt have been shown to generate singlet oxygen ($^1O_2$),[221] we investigated if complexes **220a** and **211** could generate $^1O_2$. The strongly absorbing compound 1,3-diphenyl-2-benzofuran (DPBF, **247**, λ_{max} = 418 nm in DMSO) is known to react with $^1O_2$ destroying the chromophore. The decrease in absorbance at 418 nm can then be used as a measure of how much $^1O_2$ is produced (Scheme 3.2.1.11.1).[222]

Scheme 3.2.1.11.1.

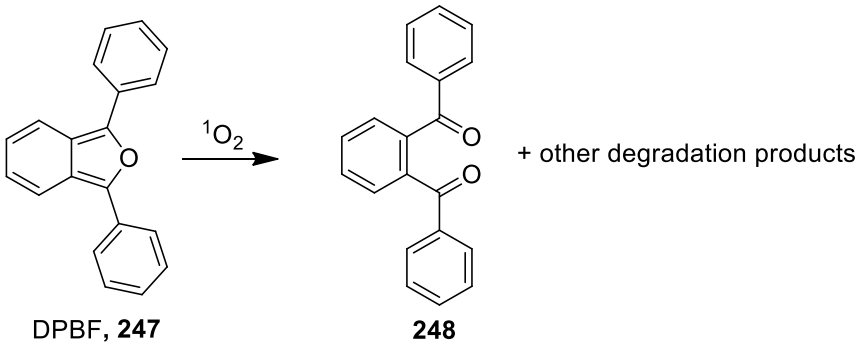

In an open air atmosphere, there is a background reaction of light with triplet oxygen ($^3O_2$) to excite the molecule to $^1O_2$.[223] We used white light at an intensity that decreased the intensity of DPBF (**247**, 100 mM) absorption at 418 nm by 10% after 30 min (Figure 3.2.1.11.1a). This ensured that enough light was present to generate $^1O_2$, but not too much that it would mask $^1O_2$ generation from our complexes. The experiment was run in DMSO to ensure that **220a** and **221** (both 150 μM) were fully solubilised. As can be seen from Figure 3.2.1.11.1b and 1c, the decrease in intensity at 418 nm was very similar in either the presence or absence of Pt complex.

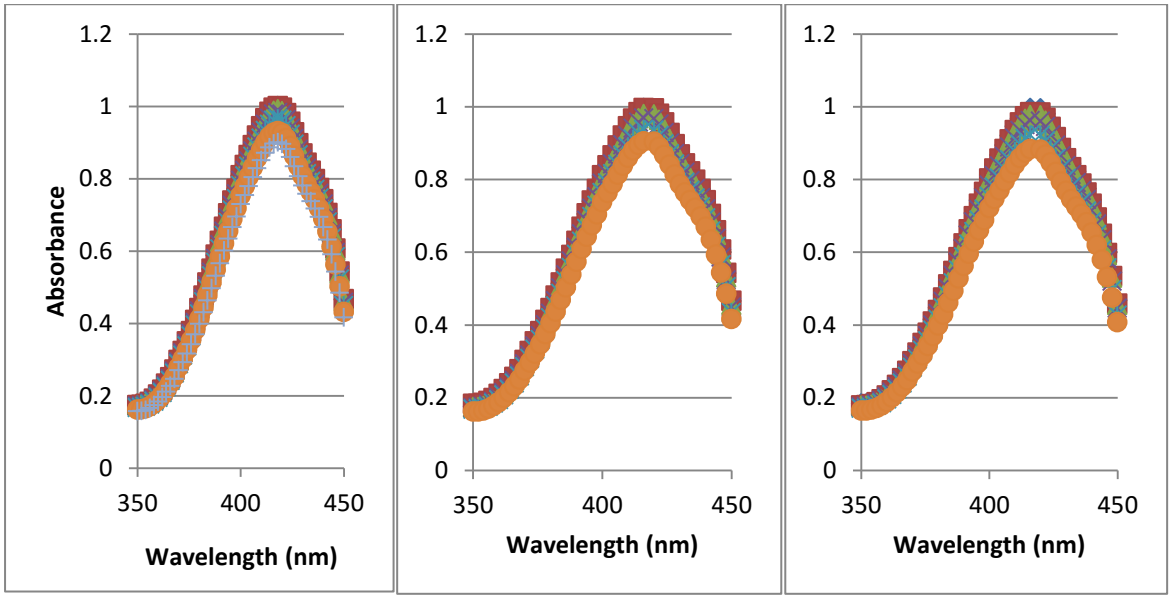

Figure 3.2.1.11.1. Graph showing decrease in concentration of DPBF in the presence of white light and a) DMSO only, b) **220a** in DMSO, c) **221** in DMSO at time points of 0, 2, 5, 10, 15, 20, 30 min.

The combined normalised results are shown in Figure 3.2.1.11.2. Each compound shows a linear degradation of **247** over time. All three systems and conditions (**247** alone, **247** with **220a** and **247** with **221**) gave very similar results. The slope of **247** alone (-0.0033 min^{-1}) and **247** with **220a** (-0.0031 min^{-1}) are almost identical. The slope of **247** with **221** (-0.0037 min^{-1}) gives a measurably stronger, albeit very slight improvement in $^1O_2$ generation. From this data, we can conclude that **220a** does not generate $^1O_2$ and that **221** may generate a small amount of $^1O_2$ at a relatively high concentration (150 μM), but for therapeutic purposes both are inactive.

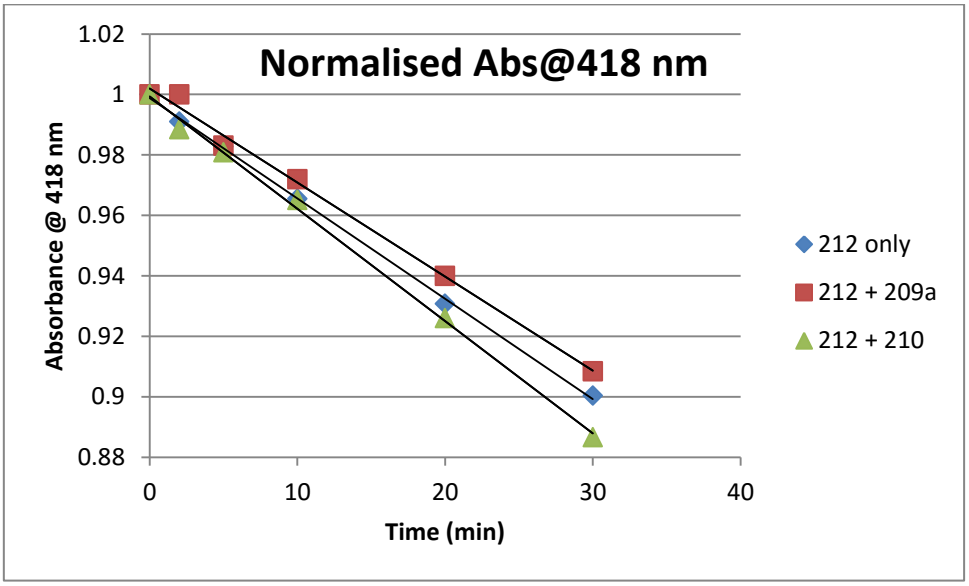

Figure 3.2.1.11.2. Graph of change in DPBF (**227**) absorbance vs. time in the presence of DMSO (blue diamond, slope= -0.0033 min^{-1}), **220a** (red square, slope= -0.0031 min^{-1}) and **221** (green triangle, slope= -0.0037 min^{-1}). All linear fits (R^2=0.999). Each data point is an average of two runs.

Studies on known $^1O_2$-generating Pt complexes indicate that HOMO (highest occupied molecular orbital)-LUMO (lowest unoccupied molecular orbital) interactions are crucial for the stabilisation of the platinacycle triplet state. Similar complexes to **220a** and **221** have a HOMO that is centred on the metal and the platinated aryl ring. We can infer that in **220a** and **221**, the HOMO is localised in a similar manner. Thus, the difference should be in the LUMO. In $^1O_2$-generating Pt complexes, there is a low-lying LUMO on the heterocycle (usually pyridine) bound to Pt *via* the N atom (Figure 3.2.1.11.3).[221,224] In complexes **220a**

and **221**, this low-energy LUMO is not present, which prevents the long-lived triplet metal-to-ligand charge-transfer (^{3}MLCT) required to generate $^1O_2$.[225]

249

Figure 3.2.1.11.3. HOMO (middle) and LUMO (right) of photoactive Pt complex **249**.[224]

Although **220a** and **221** do not generate $^1O_2$, they may cause a cytotoxic effect. Their cytotoxicity in HL-60 leukemia cells will be discussed in Section 3.3.2. In the following section we will focus on connecting our MGB motif to Pt^{II} *via* a malonate linker.

3.2.2 Pt malonate complexes

Since we had greatly improved our knowledge of guanidine ligands binding to Pt (Section 3.2.1), we followed up by reacting our malonate-derived DNA binders (Section 3.1.3) with Pt in the presence of guanidine-like moieties with the hope of creating Pt complexes of DNA binders coordinated via the malonate group. The malonate group is widely used as a ligand for Pt^{II}. Section 3.2.2.1 will give a brief outline of the use of malonates to combine Pt with other drugs to create dual action agents and examine the effect of the malonate group on the efficacy of the original drug. The rest of the section will be devoted to our experience with creating Pt-O bonds to the malonate group.

3.2.2.1. Review of Pt malonate complexes

Dicarboxylates have been extensively used as ligands for both Pt^{II} and Pt^{IV} and there are many different approaches to the synthesis of their complexes (Figure 3.2.2.1.1).[94] In this section, we will focus solely on Pt^{II} dicarboxylate complexes (**255**). Generally, a nitrate or sulfate salt of a *cis*-di(amino)di(aqua)Pt complex (**251**) is generated in situ from its corresponding *cis*-diiodo complex (**250**) and, then, reacted with a metal salt of the carboxylate (typically also generated *in situ*). Alkali metals such as Na^+ or K^+ are purely used as counterions to generate the dicarboxylate form of the ligand (**254**) required for complexation. However, other dicarboxylate salts can be used to precipitate out the counterion of **251** and further enhance the reactivity of the species. These include Ba^{2+} salts that precipitate out oxalates and sulfates, Ca^{2+} salts that precipitate out oxalates and Ag^+ salts that are widely used to precipitate out halides. These salts can be prepared from the free diacid or diester of the ligand (Scheme 3.2.2.1.1).

Scheme 3.2.2.1.1.

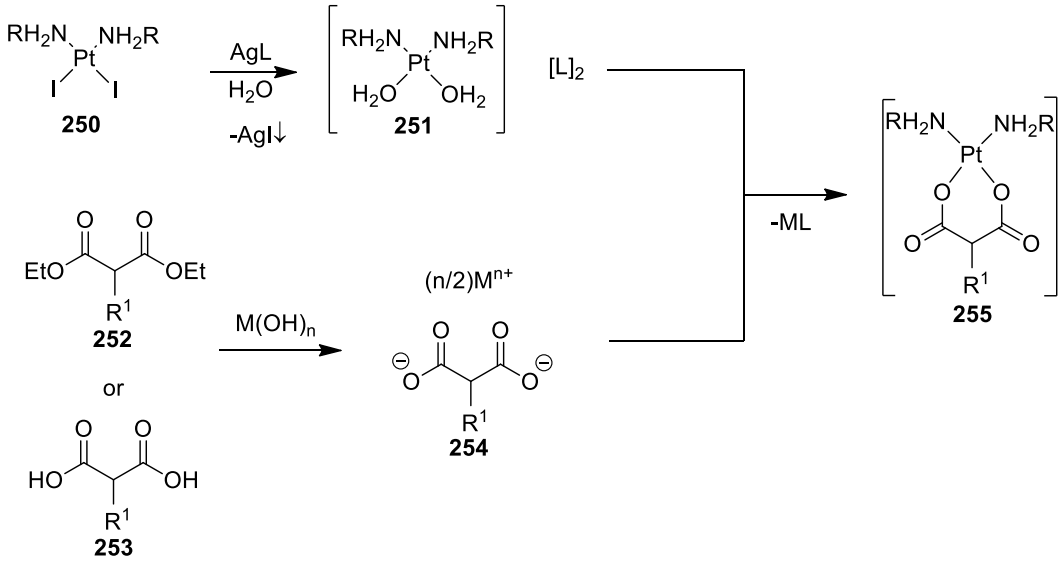

Rochon and Massarweh recommended that the $BaSO_4$ precipitation method ($M=Ba^{2+}$, $L=[SO_4]^{2-}$) to prepare Pt complexes gave much better yields and cleaner reactions compared to the "KNO_3" method.[226] However, in a patent, Sohn and Kim gave a brief guide for choosing one method over another.[227] In their experience, if the Pt complex is sparingly soluble in water, the use of the dicarboxylate barium salt with $[Pt(NH_3)_2(OH_2)_2][SO_4]$ results in the water-soluble Pt complex and the insoluble $BaSO_4$ that precipitates out. However, if the final compound is not water-soluble, then, the authors recommend using the dicarboxylate potassium salt with $[Pt(NH_3)_2(OH_2)_2][NO_3]_2$ so that the KNO_3 biproduct remains in solution while the Pt complex precipitates out of the aqueous solution, or upon addition of acetone or alcohols.

Many drug conjugates were mentioned in Section 1.5.5, *e.g.* **27**, **30**-**33**, and many of them were prepared by the "$NaNO_3$" method. As a representative example, the synthesis of Marmion's SAHA derivative **33** is shown in Scheme 3.2.2.1.2.[110] The authors used two equivalents of base to form the dianion of **256**, added this to a freshly prepared solution of the Pt precursor **257** (1.95 eq.) to form **33**, which precipitated out of solution. Unfortunately, while the cytotoxicity was similar to carboplatin, the compound lost its HDAC inhibitory properties by conjugation of the malonate group.[110]

Scheme 3.2.2.1.2

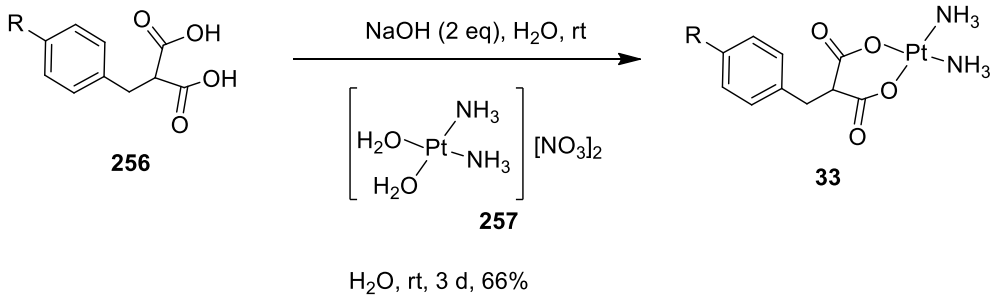

In Siddik's group, gadolinium dual-acting anticancer agent **259** was synthesised from **258** without the use of a hydroxide base (Scheme 3.2.2.1.3).[228] This was possible because **258** already contained an acetate ligand and a *mono*-anionic malonic acid derivative. Upon reaction with $NaNO_3$, the NaOAc that was produced *in situ* was able to deprotonate the free acid. Excess nitrate coordinated to the Gd^{3+} centre allowing the malonate-containing side arm to coordinate to the Pt precursor **257**. The markedly different shapes of **258** and **259** allowed for their separation by a C-18 SPE (solid phase extraction) cartridge (10 mL). Compound **259** eluted in 40% v/v 40 mM aq. KNO_3 in MeOH and was desalted by passing through another C-18 SPE column, eluting in 95% MeOH with 5% aq. HNO_3 (10 mM).[228] Complex **259** was better than carboplatin alone as cytotoxic agent in lung cancer and ovarian cancer cells. Drugs were incubated for 5 days because it took 3 days to release Pt from the malonate linker. The compound retained the cancer-targeting action of the original Gd compound, proving that attaching the malonate linker did not alter the original function of the drug. The authors also synthesised an oxaliplatin derivative.[229]

Scheme 3.2.2.1.3.

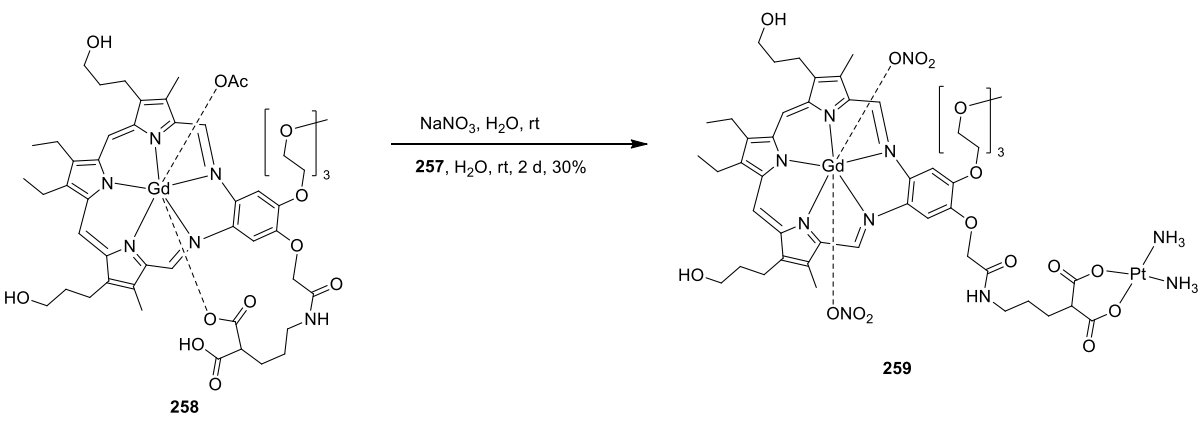

Considering the breadth of malonate-bound Pt complexes in the literature, we were eager to explore the complexation of our malonate-containing molecules **139** and **145** with Pt.

3.2.2.2. Attempts to prepare cisplatin-like complexes

We initially focussed on reacting dicarboxylate derivatives of **139** with Pt precursors **257** and **262**. The highly water-soluble dicarboxylate derivatives **151**, **271**, and **272** were easily prepared (Scheme 3.2.2.2.1) and all gave the same ^{1}H NMR spectrum.

Scheme 3.2.2.2.1.

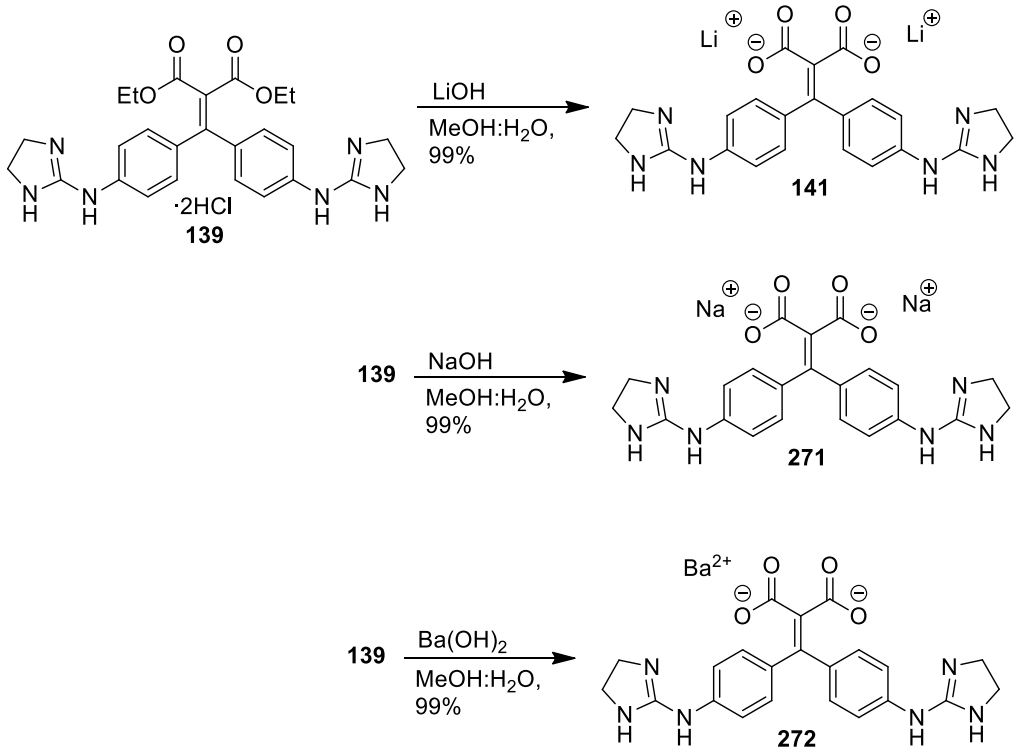

As stated in Section 3.1.3.5, attempts to create the free acids were unsuccessful. Instead, we directly used the carboxylates **141** and **271** with Pt precursor **257** (Scheme 3.2.2.2.2). However, only decomposition to Pt^{0} was observed. Also of note, the starting ligand was not recovered, in any form, from these reactions. We also tried buffered conditions, namely

AcOH, HCl, KPO_3H_2 and TsOH, all at pH 5-7, but decomposition occurred in all cases. The salts **106** and **221** could not dissolve in any solvent other than H_2O so we could not carry out the reaction in alcohols, acetone, DMF or even DMSO.

Scheme 3.2.2.2.2.

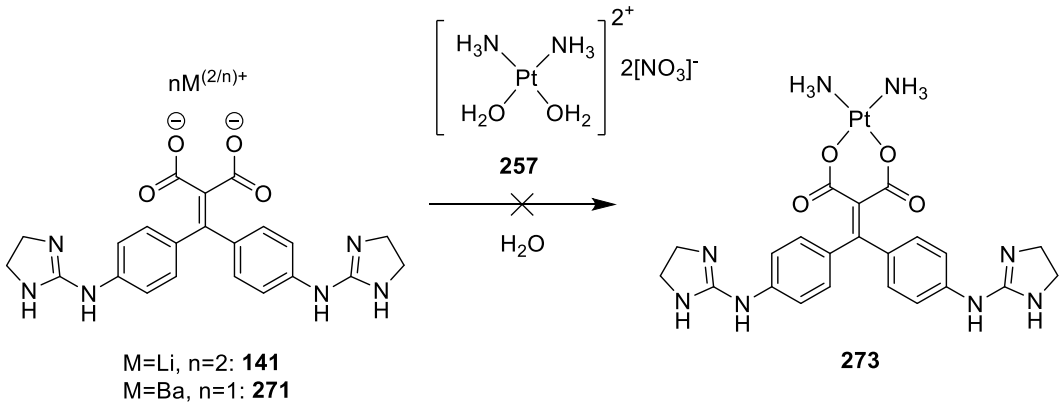

The patent literature gives many examples of preparation of Pt complexes of malonate-derived ligands with pendant primary, secondary or tertiary amines by judicious choice of buffer system, one example of which is shown in Scheme 3.2.2.2.3.[230] Keeping the reaction at pH 5-7 allowed the pendant amine to stay protonated, preventing interaction with Pt, while the malonate group was activated as the dicarboxylate. Other acids used were hydrobromic acid, phosphoric acid, acetic acid, benzoic acid, citric acid and tartaric acid.[230] It was interesting that compound **263** was isolated in the presence of acetate ions.

Scheme 3.2.2.2.3.

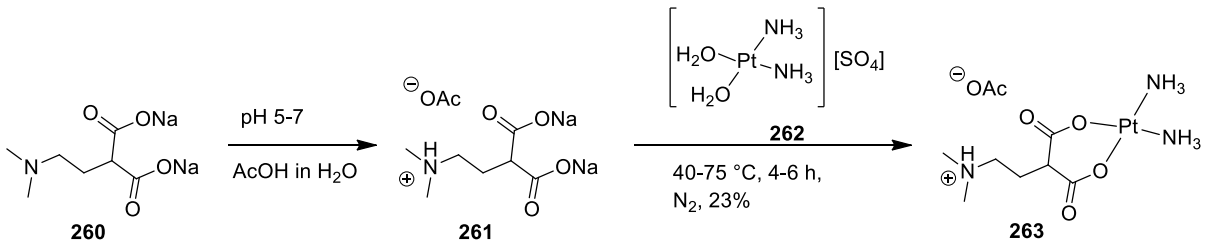

When we tried the $BaSO_4$ method by reacting Ba complex **272** with **262,** the same decomposition occurred (Scheme 3.2.2.2.4). Changing concentration (0.005 M to 0.05 M) and temperature (0° C to rt to 50° to 80 °C) gave the same results. Since **262** had a low aqueous solubility we could not perform the reaction at a higher concentration than 0.05 M. The corresponding fluorene derived malonate ligands also gave the same results for both the $BaSO_4$ and the $NaNO_3$ methods of complexation with **262** and **257**, respectively.

Scheme 3.2.2.2.4.

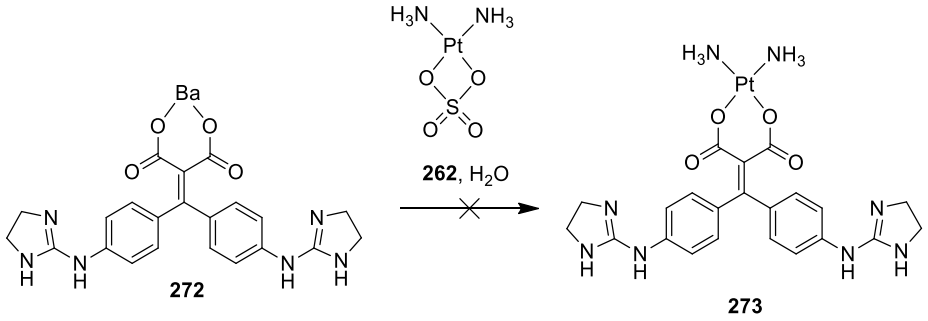

Taking inspiration from Rochon and Massarweh,[226] we attempted to synthesise the Ag complex **274** in order to directly react that with iodoplatin **6** (Scheme 3.2.2.2.5). However, the reaction degraded to an insoluble red/brown precipitate. In Rochon and Massarweh's article, the authors used the carboplatin leaving group 1,1-cyclobutanedicarboxylate as their dicarboxylate ligand. In our case, the ligand may react with $AgNO_3$ by decarboxylation similar to the Hunsdiecker reaction[231] or oxidation (by reduction of Ag^I to Ag^0).[232] Ag salts of carboxylates have a complex coordination chemistry.[226] In addition, silver malonate complexes are known to decompose to brown Ag nanoparticles.[233]

Scheme 3.2.2.2.5.

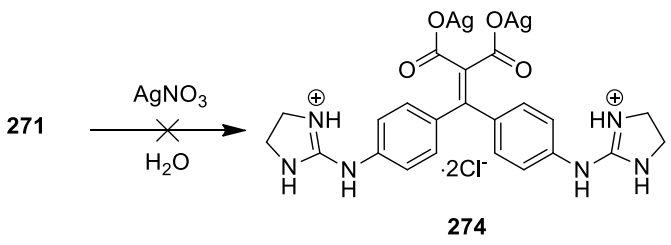

Since we could not isolate compounds using the above methods, we set up a number of test reactions on model substrates. We considered that either the Pt or Ag precursors were reacting with the guanidine-like 2-aminoimidazolinium moiety or with the *tetra*-substituted alkene. We synthesised diphenylmethylene malonate **277** to assess the coordination chemistry of the diphenylmethylenemalonate ligand with Pt precursor **257** under our complexation conditions. Dicarboxylate salt **277** was prepared in two steps from the low-yielding Ti^{IV}-mediated coupling with diethyl malonate (**113**) to give **276**, followed by quantitative ester deprotection (Scheme 3.2.2.2.6).

Scheme 3.2.2.2.6.

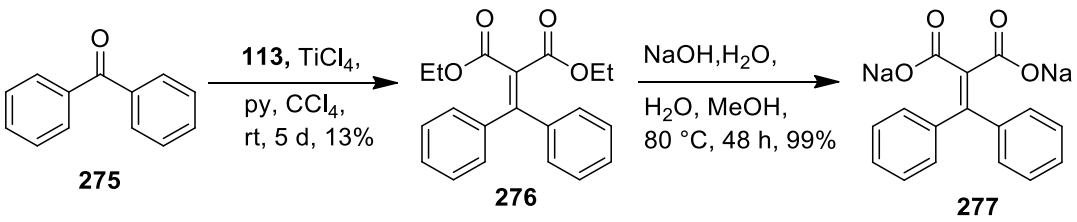

The complexation reaction of **277** with **257**, however, gave the same black Pt^0 precipitate (Scheme 3.2.2.2.7). From this result, it was possible to conclude that neither the 2-aminoimidazolinium moiety nor any buffer system or counterion was the main problem in the complexation reaction. Either the starting ligand (*i.e.* **277**) is attacked by the Pt or precursor, causing decomposition or the reaction to form **278** occurs, but the Pt complex is unstable and undergoes decomposition.

Scheme 3.2.2.2.7.

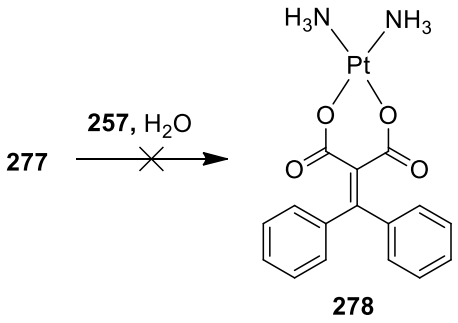

Since dicarboxylate groups are widely used as Pt ligands, some problems have been recorded in the literature. Lee's group have shown that dmso ligands can remove an amine from the coordination sphere of Pt in diamine malonate complexes (Scheme 3.2.2.2.8).[234] When the diamine ligands were connected as a more stable bidentate ligand, the amines remained chelated and instead the dmso ligand removed one of the carboxylate ligands in the chelate. Of interest to us is the fact that the double bond of the methylenemalonate group did not interfere with the reaction.

Scheme 3.2.2.2.8.

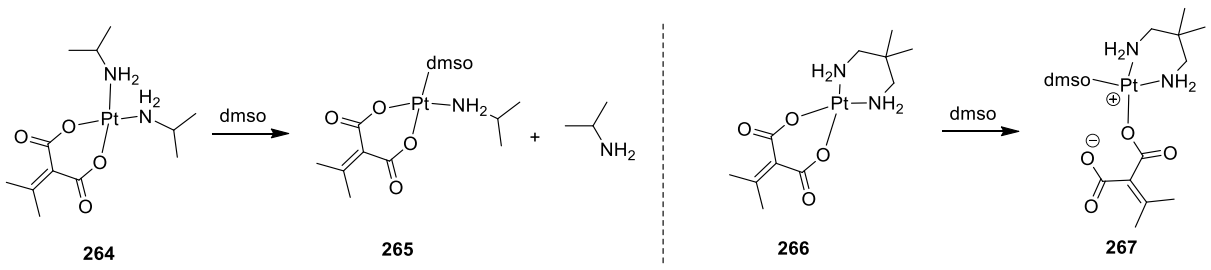

Interestingly, when **268**, the unsaturated barium dicarboxylate salt of itaconic acid, was exposed to **269** or other bidentate amine ligands, the η^2-complex **270** was formed (Scheme 3.2.2.2.9).[235] The H bond between a free carboxylate O atom and ligand NH atom was seen in the crystal structure. High temperature ^{1}H NMR experiments in D_2O up to 70 °C proved that this unusual linkage isomer was the only compound present in solution also. The stability of the complex was ascribed to the formation of a five-membered ring and six-membered H

bonded ring over the unfavourable formation of a seven-membered [*O,O'*] isomer. The other option, a four-membered [*O,O'*] chelate with both O atoms from the same carboxylate is rarely observed in Pt chemistry, but is implicated in disassociative substitution mechanisms.[236] The Pt-alkene bond has been well studied. The first organoplatinum complex, $K[PtCl_3(H_2C{=}CH_2)]$ (Zeise's salt), was discovered in 1830.[237]

Scheme 3.2.2.2.9.

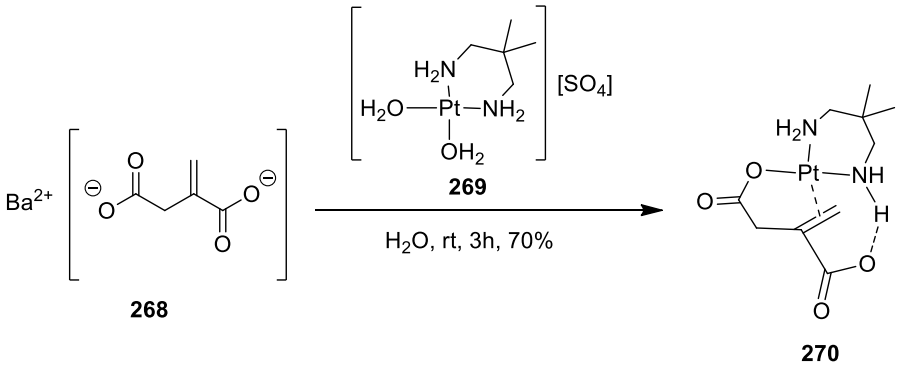

In order to better understand the complexation of our *bis*-2-aminoimidazolinium malonate derivatives we reduced the unsaturated ester double bond to give sodium salt **279** and attempted to react this with **257** under normal room temperature conditions for four days (Scheme 3.2.2.2.10). Unfortunately, there was no reaction, with ligand **279** being recovered fully and identified by ^{1}H NMR analysis. No black Pt^0 precipitate was observed either, suggesting that consumption of ligand and formation of reduced Pt are coupled.

Scheme 3.2.2.2.10.

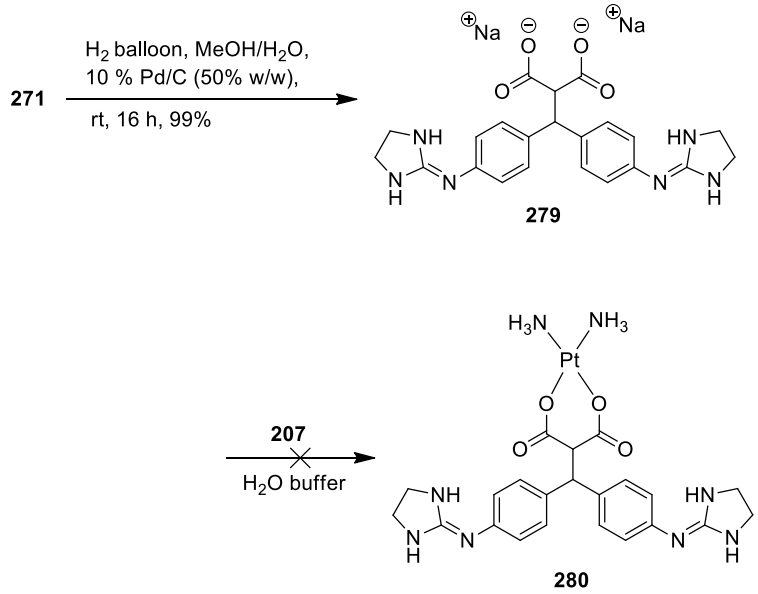

From computational experiments (Section 3.1.3.7), we inferred that the unsaturated ligand **279** would likely be similar to saturated diester **140** in its conformation and that specifically the malonate groups would likely arrange in a conformation where the carboxylate units would be far from each other in space, aided by steric crowding of both aryl groups, and in a coplanar conformation that is necessary for chelation. Thus, their lack of reaction compared to Marmion's monoaryl **256** (Scheme 3.2.2.1.2) is understandable. We reckoned that more forcing conditions (higher temperature, even longer reaction time) may allow us to access **280**, but we were more interested in finding stable complexes of unsaturated ligand **271** since **280** is likely to be a very weak DNA binder.

We did envisage that a saturated version of the fluorene ligand **260** may indeed be a strong DNA binder. Thus, ligand **282** was prepared and its complexation attempted with **262** (Scheme 3.2.2.2.11).

Scheme 3.2.2.2.11.

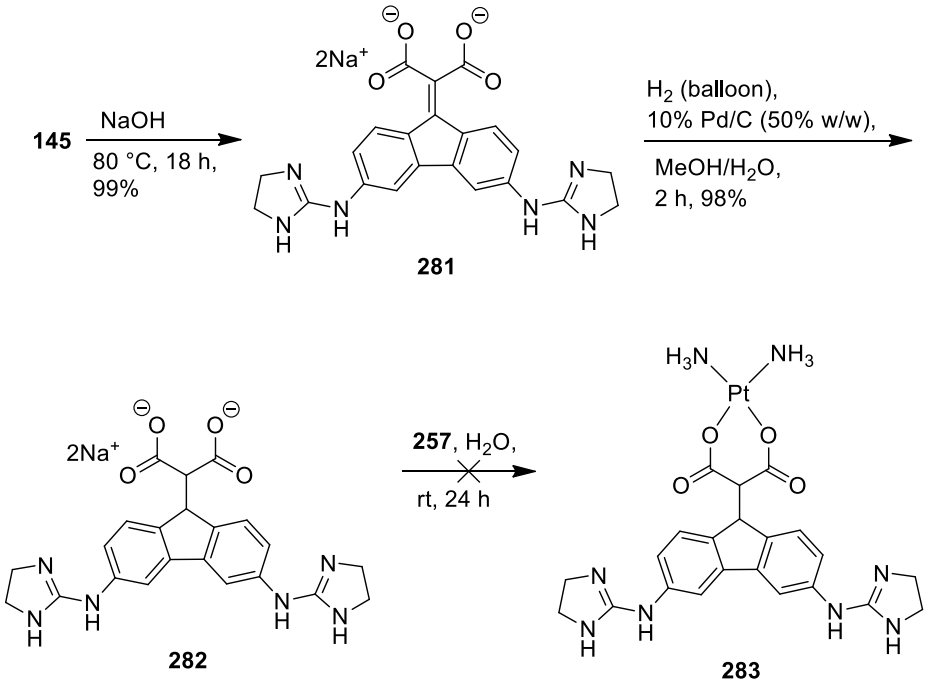

Again, the reaction to synthesise **283** did not proceed, but no decomposition was observed. In any case, this result (Scheme 3.2.2.2.11) was very useful since it reasonably confirmed that complex **273** was unstable and likely degraded after complexation. It has been noted that addition of small amounts of NH_4Cl (0.25 mol%) during complexation can prevent decomposition of the diammine Pt complex.[238] In our hands, NH_4Cl addition did not prevent decomposition (Scheme 3.2.2.2.12). As a result, we thought about creating more stable, chelated *N* ligands for Pt instead of the two *cis*-diammine groups.

Scheme 3.2.2.2.12.

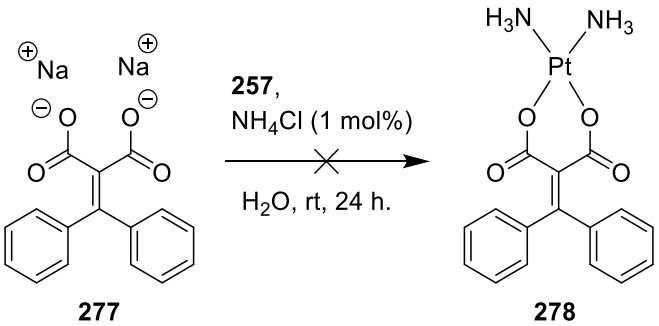

3.2.2.3 Attempts to prepare Oxaliplatin-like complexes

The chelated bidentate diamine (or tridentate *tris*-pyridine) motif is used in many anticancer Pt complexes in the literature instead of the diammine (two ammonia) ligands (including oxaliplatin, lobaplatin, heptaplatin, compounds **16**, **26, 30-31** and **34-37**). The widespread use of chelating diamines implies that these more stable complexes were easier to handle than the *cis*-diammine derivatives. Furthermore, reactions with biologically relevant substrates demonstrated that cisplatin can lose NH_3 ligands instead of Cl ligands.[239,240] Considering that the methylenemalonate Pt complexes **264** and **266** contained bulky isopropylamine or stable chelated amine ligands respectively, we extended the scope of our target molecules to include oxaliplatin-type derivatives of **284** and **285** (Figure 3.2.2.3.1). The two amine groups of dach (1,2-diaminocyclohexane) are permanently orientated in a configuration suitable for chelation.

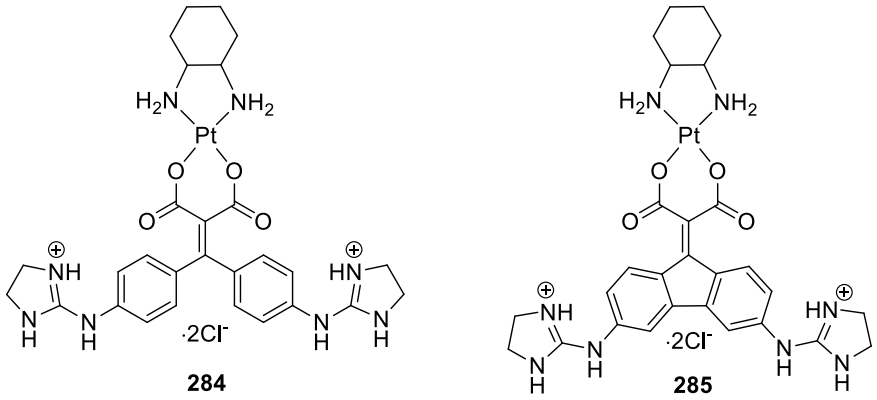

Figure 3.2.2.3.1. Novel oxaliplatin-derived targets of our DNA-binding **139** and **145**.

Sohn's group had previously synthesised very similar fluorene-type complexes (Figure 3.2.2.3.2).[241] The crystal structure of the fluorene derivative **287** shows that the fluorene is perpendicular to the plane of the Pt(dach) moiety, since keeping the carboxyl groups in the plane of the ring would be sterically demanding.

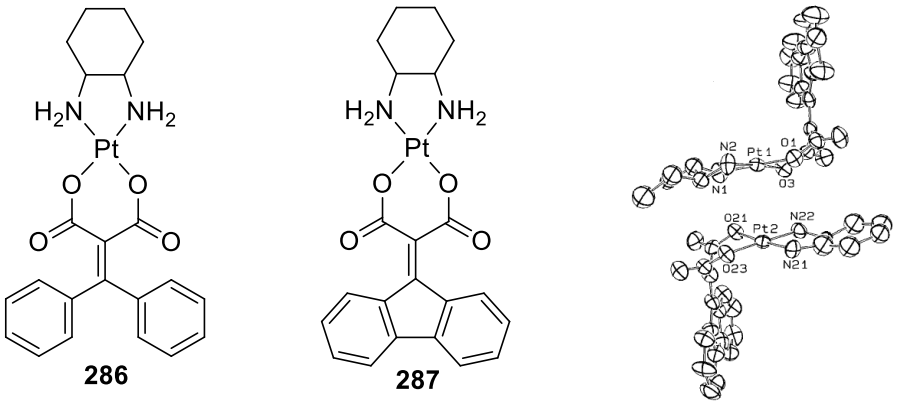

Figure 3.2.2.3.2. Structures of Sohn's oxaliplatin derivative and crystal structure of **287**.[241]

Therefore, we synthesised the Pt precursor **289** containing the dach ligand (**288**) according to a procedure by Siddik (Scheme 3.2.2.3.1).[229]

Scheme 3.2.2.3.1.

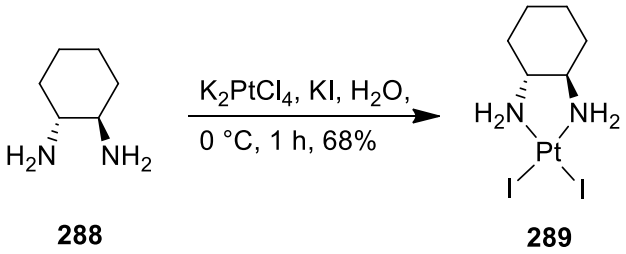

Reaction of flexible ligand **272** with the activated sulfate **290** gave uncoordinated salt **291** (as adjudged by ^{1}H NMR) after filtering off $BaSO_4$ instead of the expected **279** (Scheme 3.2.2.3.2).

Scheme 3.2.2.3.2.

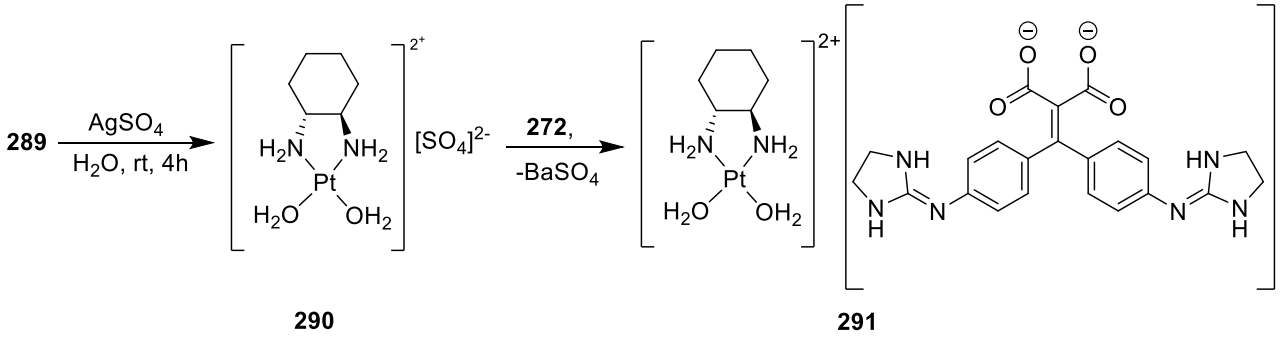

However, using the corresponding fluorene ligand **292**, we were able to isolate complex **285** (Scheme 3.2.2.3.3).

Scheme 3.2.2.3.3.

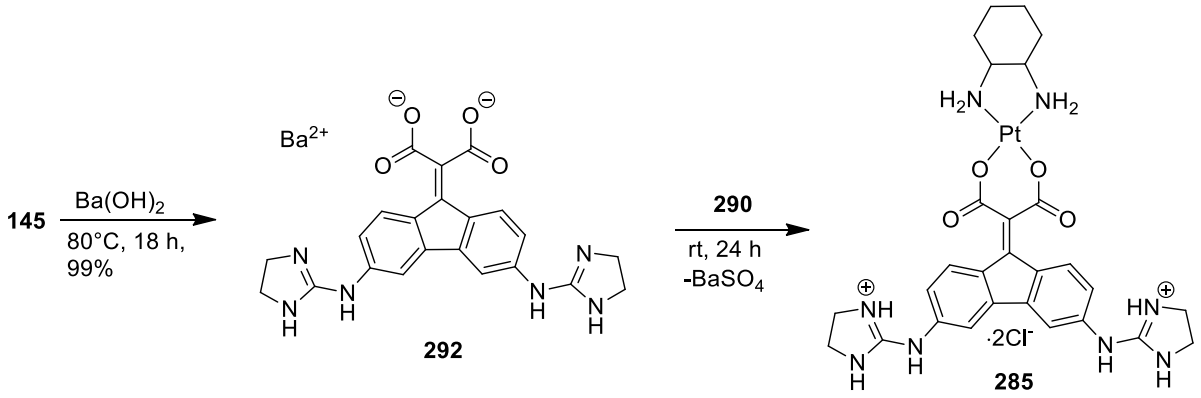

A comparison of the ^{1}H NMR spectra of the starting materials and product is given in Figure 3.2.2.3.3. Clearly, the aromatic region is very different to that of **145** and the ^{1}H NMR spectrum of the cyclohexane ring is unchanged, similar to other complexes of dach.[229] No NOE was observed between the protons on the fluorene core and the protons on the dach ligand. Even though the compound was not found by mass spectrometry, we are currently screening conditions for crystallisation of **285** to unambiguously prove that the compound has been synthesised.

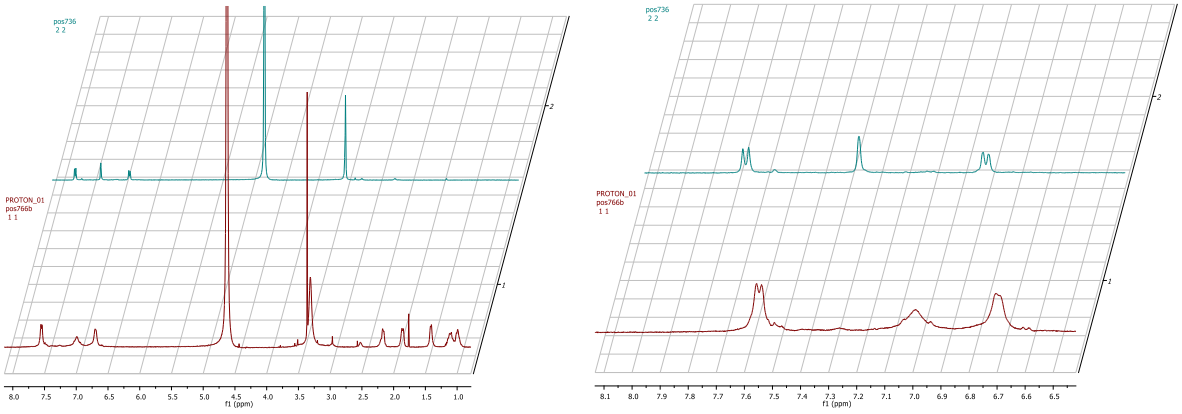

Figure 3.2.2.3.3. *Left:* Full ^{1}H NMR spectrum of **279** (top, **blue**) and **285** (bottom, **red**) in D_2O. *Right:* Expansion in the aromatic region.

3.2.3. Conclusions

We have investigated three main possibilities by which we could conjugate our diaryl *bis*-guanidine-like MGBs with Pt, namely *via* the guanidine, *via* an aminoguanidine or *via* a malonate linker.

Firstly, the rich chemistry of aryl guanidines with Pt was explored. We demonstrated by NMR, IR, mass spectrometry, X-ray crystallography and elemental analysis that Pt can bind to aryl guanidines and their derivatives by a monodentate Pt-N bond, by cyclometalation, and by chelation *via* an iminoguanidine. The coordination mode most stable to aqueous conditions was cyclometalation since the Pt-C bond is rather strong. Further work with these complexes will include testing the activity of cyclometalated complexes **220a**, **221**, **222** and **246a** on cancer cell lines to determine if these novel compounds cause cytotoxicity. We were able to demonstrate that strong binding of arylguanidines to Pt depends on the Pt precursor.

Secondly, we assessed *N*-amino-*N'*-arylguanidines as potential Pt binders. We found preliminary evidence by NMR, IR and mass spectrometry not only that these ligands do form complexes with Pt^{II}, but also that these complexes are water-soluble and do not form cyclometalated complexes. This initial study gives hope for the development of stable, water-soluble Pt-MGB complexes connected *via* an *N*-aminoguanidine.

Thirdly, we pursued the complexation of our diaryl *bis*-aminoimidazoline malonate-derived DNA binders with Pt^{II}. Unfortunately, this goal was much more difficult than expected.

However, we proved that the ammine ligands on our complexes were labile and led to decomposition of the metal centre to Pt^0. By using a Pt precursor based on oxaliplatin's dach ligand, we were able to isolate a Pt compound bound to our fluorene-derived ligand. Further work is underway to unambiguously characterise this compound that will then be tested in cancer cell lines for cytotoxicity.

3.3 Cell cytotoxicity

3.3.1 Cell cytotoxicity introduction

This chapter presents the results and discussion of the cytotoxicity assays of the organic DNA binders and their Pt complexes as potential anti-cancer therapeutics. We have assessed whether these compounds cause cell death in HL-60 (human promyelocytic leukemia) cells, which are easy to handle (because they grow quickly and generally do not adhere to each other) and serve as a useful generic test of cytotoxicity. Moreover HL-60 cells are susceptible to chemotherapy, making them an ideal cell line for cytotoxicity screening.[242] These cells are routinely used in cancer screens for DNA binders and Pt-containing compounds. Our group has reported cytotoxicity studies on many families of *bis*-guanidinium-like and related diaryl compounds in HL-60 cells, enabling comparison with the organic DNA-binding agents synthesised in this work (see Section 3.3.2).

A reliable, non-toxic method of counting live cells is essential to measure cytotoxicity. Common methods include ^{3}H-labelled thymidine incorporation or absorbance assays such as 3-(4,5-dimethylthiazol-2-yl)-2,5-diphenyltetrazolium bromide (MTT) or water-soluble tetrazolium (WST) methods. However, these methods suffer from radioactive waste disposal issues, solubility problems or cell toxicity. We used the AlamarBlue® fluorescence assay (Figure 3.3.1.1) based on the reduction of reazurin to strongly fluorescent resorufin in a metabolically active cell.

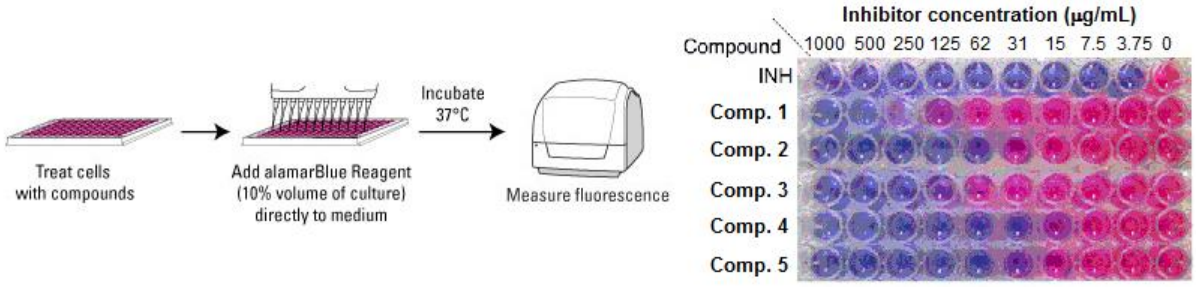

Figure 3.3.1.1. Protocol for AlamarBlue® cell viability assay.[243,244]

Reazurin is non-toxic, water soluble and passively diffuses across the cell membrane.[245] In a metabolising cell, dark blue reazurin is reduced to pink resorufin (Scheme 3.3.1.1) by a variety of enzyme-mediated processes. Resorufin in excited at 544 nm and the emission at

590 nm is measured. The fluorescence of resorufin is directly proportional to the number of live cells.

Scheme 3.3.1.1.

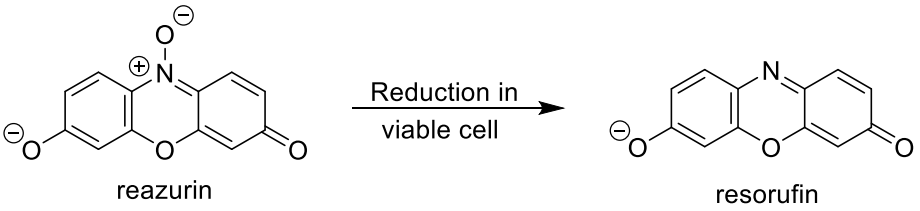

3.3.2 Cytotoxicity of the prepared organic DNA minor groove binders

As mentioned, in order to measure the cytotoxicity of our compounds we used the AlamarBlue® assay. We initially trialled the same conditions as in our previous work[119] (40,000 HL-60 cells per well) for our organic DNA binders compounds **46a**, **46b**, **139**, **140**, **145** and **146**. A screen of these compounds at 100 μM over 72 h gave five active compounds (**46a**, **46b**, **119, 145** and **146**). Unexpectedly, the compounds did not kill cells in a dose-dependent manner; shown in Figure 3.3.2.1 is a graph of compound **145** showing that there is no difference between cell death caused at 50 μM or 75 μM and also that slightly more viable cells are present at 100 μM than the previous two concentrations. The trend for **139** was similar. Thus, the compounds behave more like a straight line than a typical dose-response curve.

Table 3.3.2.1. IC_{50} values for organic DNA binders in HL-60 cells (10,000 cells per well). The DNA thermal melting results are given for reference.

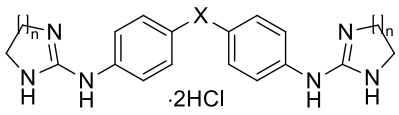

46a: n=2, X= CO
46b: n=2, X= O
139: n=1, X= $C=C(CO_2Et)_2$
140: n=1, X= $CH-CH(CO_2Et)_2$

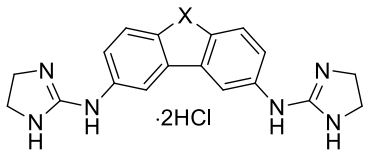

145: X= $C=C(CO_2Et)_2$
146: X= CH_2

Compd.	**IC_{50} ± SEM (μM)[a]**	**ΔT_m stDNA (°C)**	**ΔT_m poly(dAdT)$_2$ (°C)**
145	66.88 ± 3.1	8.0	1.0
46b	45.70 ± 0.8	6.2	8.0
146	52.15 ± 2.7	10.3	19.5
139	17.65 ± 1.4	3.6	8.8
46a	94.55 ± 1.5	9.3	14.2
140	> 100	0	
Furamidine	12.10 ± 1.9		

[a]Cells were seeded at a density of 5 x 10^4 cells/ mL in a 96-well plate and treated with the compounds dissolved in ddH_2O at 10 μM, 25 μM, 50 μM, 75 μM and 100 μM. Furamidine was used as a reference and tested in the same manner. Once treated, cells were incubated for 72 h at 37 °C after which they were treated with AlamarBlue® and left in darkness in an incubator for 5 h. The resulting fluorescence was read using a plate reader from which percentage viability was calculated. IC_{50} values were calculated using Prism GraphPad 5 software from at least three independent experiments performed in triplicate.

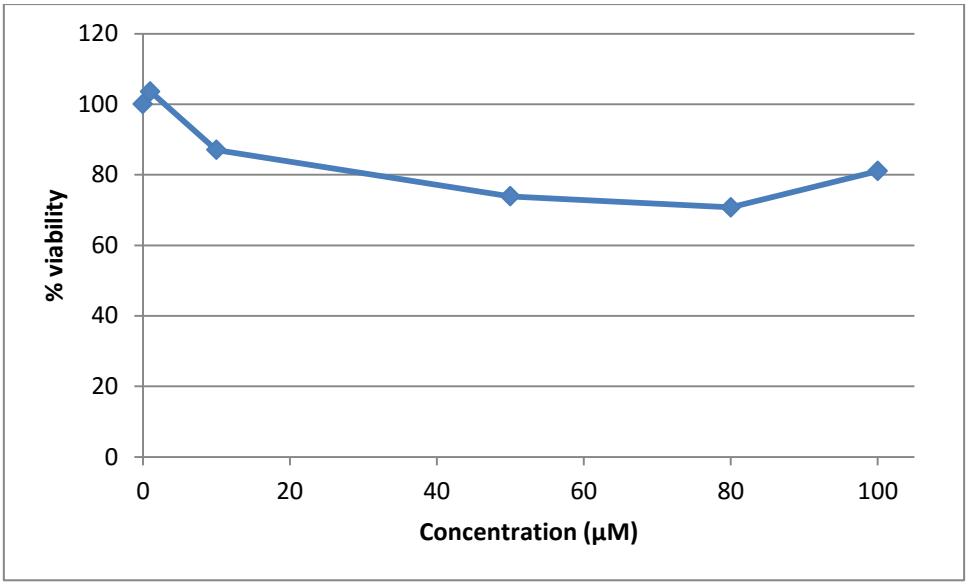

Figure 3.3.2.1. Graph of percentage cell viability (40,000 HL-60 cells per well) vs. drug concentration (**145**).

Since these results were not very coherent, we repeated the AlamarBlue® assays with 10,000 HL-60 cells per well and, this time, there were clear dose-response curves for the active compounds (Figure 3.3.2.2) and we were able to determine the corresponding IC_{50} values of the organic DNA minor groove binders (Table 3.3.2.1).

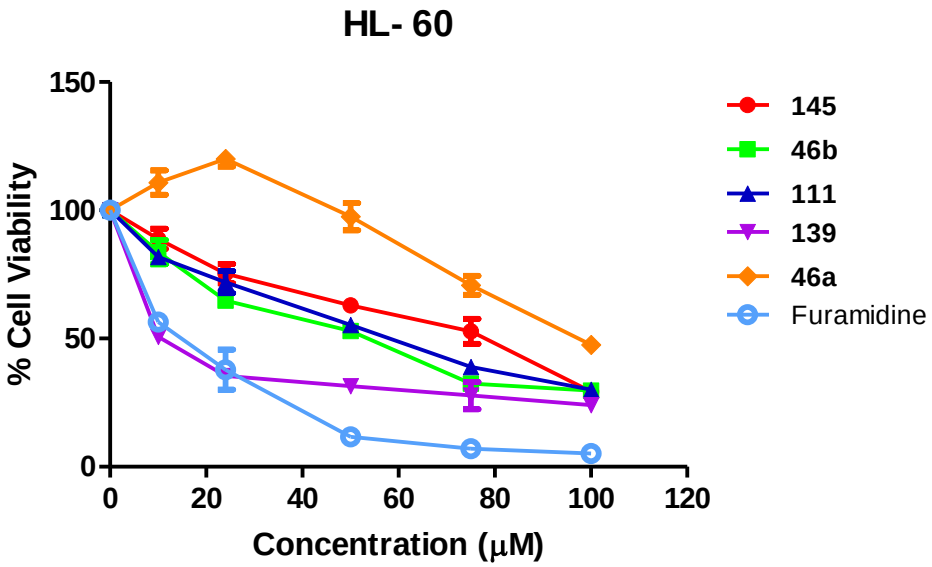

Figure 3.3.2.2. Graph of percentage cell viability (10,000 HL-60 cells per well) vs. drug concentration**.**

Similar to previous families, the linker in the 2-amino-1,4,5,6-tetrahydropyrimidine family had a substantial effect on cytotoxicity; thus, the compound with the O linker (**46b**, IC_{50} = 46 μM) seems to be much more cytotoxic than that with the CO linker (**46a**, IC_{50} = 95 μM). These data correlate well with previous work demonstrating the improved cytotoxicity of O-linked diaryl *bis*-hydroxyguanidinium compounds over their corresponding CO linked-compounds.[162] In fact, the *bis*-guanidinium and *bis*-2-aminoimidazolinium derivatives all had IC_{50} values greater than 100 μM.[162] The increased cytotoxic effect of our *bis*-1,4,5,6-tetrahydropyrimidine family over these stronger DNA binders could be due to increased permeability of the more lipophilic cations. The reason because the O linker is clearly preferred over the better DNA-binding CO linker could be that the biological target of these compounds is not DNA, and that the O-linked diaryl system binds stronger to a different biological target. Whether this is due to the difference in the preferred conformation of the aryl rings (almost coplanar for **46a** but closer to perpendicular for **46b**) or a favourable H-bonding interaction to the O atom of **46b** or less steric clash with **46b** compared to **46a** is beyond the scope of this study.

Previously, we had not explored the chemical space above the linker in terms of DNA minor groove binding. Now, we can see that increasing in this direction steric bulk with esters has an effect on cell growth, but can both increase or decrease cytotoxicity depending on the saturation of the connection to the ester. Thus, the saturated malonate ester was not active in HL-60 cells (**140**, IC_{50} > 100 μM), whereas, the methylenemalonate ester gave the best cytotoxicity of the series (**139**, IC_{50} = 18 μM), very close to the value obtained for the known DNA MGB furamidine (IC_{50} = 12 μM).

The results obtained for the fluorene-based derivatives gave an insight into the effect of compound planarity in cytotoxicity. The parent derivative 3,6-*bis*-2-aminoimidazoline-9*H*-fluorene (**146**, IC_{50} = 52 μM) was more cytotoxic than the 9-malonate-derivative 3,6-*bis*-2-aminoimidazolinefluorene (**145**, IC_{50} = 67 μM).

The cytotoxicity of the malonate-derived compounds can be compared. Once again, these results do not correlate with thermal denaturation values (Table 3.3.2.1), suggesting that DNA is not necessarily the only biological target of these compounds. Both unsaturated malonate compounds (**140** and **146**) were active in HL-60, but the most flexible compound **139** gave the best cytotoxicity. Although all three compounds have similar lipophilicity (give the logP for each of them here), their polar surface area may be different and may passively diffuse across the cell membranes to a different extent. It is unusual that compound **140** is not at all active in HL-60 cells. Considering that the molecule has more freedom of rotation, it is possible that it is unable to reach its most active conformation. Interestingly, fixing the rings to make them coplanar (**145**) decreased the activity but did not destroy it. However, removing the malonate group from this fluorene (**146**) increased activity, implying that in the case of the fluorene rings, substitution at the linker is not favoured. Perhaps the esters in fluorene **145** are more restricted and are not able to achieve the same interactions with their target as **139**.

3.3.3 Cytotoxicity of Pt compounds

Water-stable Pt compounds **220a**, **221**, **222** and **246a** we tested against HL-60 cells for a cytotoxic effect. These compounds were dissolved in DMSO and tested in cells at a final concentration of 0.1% DMSO, which had no effect on cell viability. Since our compounds crystallised out of DMSO/H_2O solutions over a period of months, were stable for at least one year in DMSO-d_6 at room temperature (as adjudged by ^{1}H NMR) and could be heated to 80 °C in DMSO-d_6 and cooled to room temperature without a noticeable change in the ^{1}H NMR spectrum, we were confident that DMSO would not interfere with the cytotoxicity measurements over three days at 37 °C.

The compounds were assessed for their effect on cell growth by the AlamarBlue® assay and the results are shown in Table 3.3.3.1. For purposes of comparison with previous work,[119] and also with the organic DNA MGBs from Table 3.3.2.1, we calculated IC_{50} values using 10,000 (Figure 3.3.3.1) and 40,000 cells per well. Compounds **220a** and binuclear **221** showed no activity, while binuclear **246a** had weak cytotoxicity (IC_{50} = 101 μM with 10,000 cells per well and IC_{50} > 100 μM with 40,000 cells per well). Pt-2-Aminoimidazoline complex **221** was clearly the most active in both conditions (IC_{50} = 55 μM with 10,000 cells per well and IC_{50} = 65 μM with 40,000 cells per well). This promising result shows that the five-membered 2-aminoimidazoline ring is important for activity. Furthermore, the cytotoxicity of Pt complex **221** is similar to the fluorene ligand **146** and compares well to the bioactive *mono*- and *bis*-isouronium and hydroxyguanidinium families previously tested in our group.[119] Although the IC_{50} value of this compound is moderate, there are many options to derivatise it in the future to enhance its cytotoxicity.

Table 3.3.3.1. IC_{50} values calculated for Pt complexes in HL-60 cells using the AlamarBlue® assay.

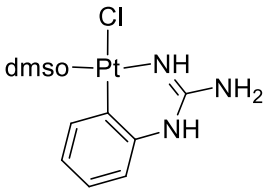

220a

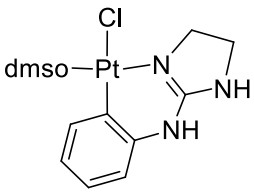

221

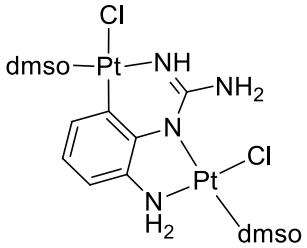

222

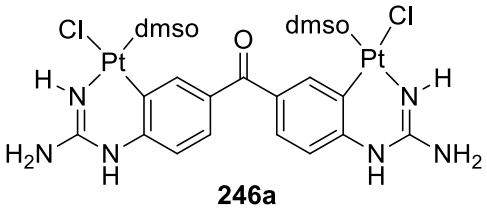

246a

Compd.	**IC_{50} ± SEM (μM)[a] 10,000 cells per well**	**IC_{50} ± SEM (μM)[b] 40,000 cells per well**
220a	> 100	> 100
221	55.29 ± 3.0	66.82 ± 5.9
246a	100.81 ± 3.4	> 100
222	> 100	> 100
Carboplatin	12.62 ± 1.7	N/A

[a]Cells were seeded at a density of 5 x 10^4 cells/mL in a 96-well plate and treated with the compounds dissolved in 0.1 % DMSO in ddH_2O at 10 μM, 25 μM, 50 μM, 75 μM and 100 μM. Carboplatin (dissolved in ddH_2O) was used as a reference and tested in the same manner. Once treated, cells were incubated for 72 h at 37 °C after which they were treated with AlamarBlue® and left in darkness in an incubator for 5 h. The resulting fluorescence was read using a plate reader from which percentage viability was calculated. IC_{50} values were calculated using Prism GraphPad 5 software from at least three independent experiments performed in triplicate. [b]As note a but cells were seeded at a density of 4 x 10^5 cells/mL.

The weak cytotoxicity of **246a** may be due to the two Pt-guanidine moieties in the molecule transferring two molecules of Pt into the cell per molecule of **246a**. Considering that the free organic ligand has no activity in HL-60 cells,[162] we were very happy to see that attaching a Pt moiety to the MGB had a measurable cytotoxic effect. Further work is needed to elucidate possible targets of **221**.

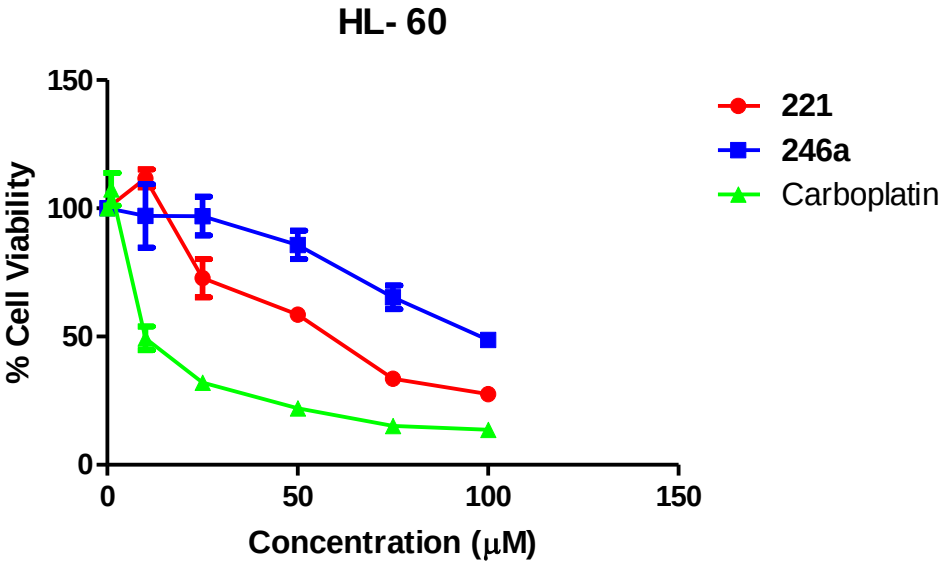

Figure 3.3.3.1. Graph of percentage cell viability (10,000 HL-60 cells per well) *vs* concentration.

3.3.4 Conclusions

In this work a number of organic ligands and organometallic complexes were synthesised with the hope of creating anticancer agents. In this chapter, the compounds were screened for their effect in cell growth by treatment on the leukemia HL-60 cell line. Some structure-activity conclusions can be drawn. Firstly, the 2-amino-1,4,5,6-tetrahydropyrimidinum cation seems to be more cytotoxic than the guanidinium or 2-aminoimidazolinium cations but not as cytotoxic as the isouronium or *N*-hydroxyguanidinium cations. This is likely due to cell transport issues. The pK_{aH} of the 1,4,5,6-tetrahydropyrimidinium compounds is similar to the pK_{aH} of the guanidinium or 2-aminoimidazolinium compounds ($pK_{aH} \approx 10$),[246] but the larger lipophilicity of the pyrimidinium cation (Section 3.1.1.1) will allow the compounds to cross membranes more easily. The isouronium and *N*-hydroxyguanidinium molecules have $pK_{aH} \approx 8$, hence, their unionised form should be present in appreciable amounts in the cell media, facilitating passive diffusion across membranes.[162] Secondly, the identity of the linker between the aromatic systems is very important with regards to the cytotoxic effect. The O linker is generally better than the CO linker across many different cations. Also, the diethyl methylenemalonate linker can substantially improve cytotoxicity of the diaryl *bis*-2-aminoimidazolinium compounds but not for the fluorene derivatives. Thirdly, forcing the

compounds into a planar conformation also improves cytotoxicity on the molecules. Finally, adding a cyclometalated Pt atom increases cytotoxicity as well.

Considering the good cytotoxicity results obtained with the lead organic ligand **104** in HL60 cancer cells, future work could include testing the compound on other cell lines and assessing the form of cell death induced by the compound (*i.e.* apoptosis, necroptosis or oncosis).

In general, future biochemical work with these compounds should include an *in silico* or *in vitro* screen for other possible drug targets. Direct DNA binding is unlikely to be the major mechanism of action of these organic ligands. A screening assay on different kinase pathways may be beneficial since similar *meta/para*-substituted diaryl *bis*-guanidines synthesised in our group act by interfering with the RAF/MEK pathway.[247] Another option would be to assess if, for example, a fluorescent derivative of **146** can be localised in a subcellular compartment (as viewed by confocal microscopy), helping to narrow the search for a target and to prove the cell permeability of these molecules.

With regards to our lead Pt complex **210**, future work could include substituting the aryl or 2-aminoimidazoline rings to help finding a SAR (structure-activity relationship) as well as increasing water solubility. Another option would include changing the Cl and DMSO ligands for other halides, sulfoxides and bidentate anionic or neutral groups to aid solubility.

The biological results from this project showed that we succeeded in increasing the cytotoxicity of our previous lead compound **45a**. We also showed that attaching Pt gave a measurable increase in cytotoxicity of the MGB, validating our initial hypothesis.

4.0 Conclusions and Future Work

4.1 Conclusions

The objectives of this work were to enhance the DNA-binding and anti-cancer activity of *para*/*para*-substituted diaryl *bis*-guanidiniums and *bis*-2-aminoimidazoliniums by improving the lipophilicity and H-bonding ability of the molecules, as well as by preparing Pt complexes of these molecules. We also aimed to create novel stable complexes of Pt with arylguanidines in order to investigate their cytotoxicity in cancer cells. From the work presented in this thesis we can make some interesting conclusions.

4.1.1 Synthesis

The synthesis of a small family of diaryl *bis*-1,4,5,6-tetrahydropyridinium diaryl derivatives was successfully carried out by two different routes depending on the linker. We developed Buchwald-Hartwig amination conditions based on previous work in the group by Shaw, followed by hydrogenation to access final salts.[130] The carbonyl linker was unstable to hydrogenation so we utilised a modified Hg-mediated guanidylation method from previous work in the group by Dardonville.[210]

Additionally, we developed a family of malonate-based diaryl and fluorenyl *bis*-2-aminoimidazolinium salts using a variety of metal-catalysed and metal-mediated reactions. Various synthetic routes were scouted in order to create the target compounds, utilising a wide range of chemistry methodologies. These target compounds allowed us to assess the effects of planarity on DNA binding and cytotoxicity. Furthermore, we were able to probe the effect of the diethyl malonate group on DNA binding and cytotoxicity.

We created a small family of *N*-amino-*N*'-arylguandinium salts by developing a Hg-mediated coupling of $BocNHNH_2$ with *N*-aryl-N'-Boc-thioureas and subsequent deprotection. We extended this methodology towards the synthesis of diaryl *bis*-aminoguanidines. We also proved that complexation of *N*-amino-*N*'-arylguandines with Pt precursors is possible, although these complexes are insoluble in water.

Moreover, we investigated a wide variety of Pt^{II} complexes with aryl guanidines, showing a range of possible binding modes such as monodentate, bidentate and bridging. We discovered a facile synthesis of binuclear Pt^{III} complexes of arylguanidines and an *in situ* activation of

Pt-arylguanidine complexes with acetonitrile to create a bidentate aryl iminoguanidine complex. The cyclometalated Pt^{II} complexes were particularly stable to aqueous environments and were tested for anti-cancer activity. We extended our cyclometalation methodology to create a water-stable conjugate incorporating two Pt^{II} molecules and a diaryl *bis*-guanidine MGB.

Moreover, we explored the coordination chemistry of the malonate-derived ligands with Pt^{II} to develop potentially cytotoxic conjugates. After many troubleshooting experiments and exploration of different conditions, we developed a small scale synthesis of a Pt^{II}-containing oxaliplatin-based conjugate of the fluorene-based DNA binder.

4.1.2 Biophysical Measurements

We assessed the interaction of the water-soluble *bis*-guanidinium-like compounds with salmon testes DNA (stDNA) and poly(dAdT)$_2$ by DNA thermal denaturation and circular dichroism (CD) experiments. We found that the effect on the DNA thermal denaturation of the *bis*-2-amino-1,4,5,6-tetrahydropyridinium compounds was not as high as previous *bis*-guanidine-like compounds developed in the group. Stronger affinity for poly(dAdT)$_2$ over stDNA and induced signals above 300 nm in CD experiments demonstrated that these compounds retained the minor groove binding ability observed in previous families. Furthermore, we were able to correlate the thermal denaturation data with the coplanarity of the aryl rings following optimisation at the B3LYP/6-31G level.

The biophysical measurements of the fluorene- and malonate-derived *bis*-2-aminoimidazoliniums were more difficult to interpret. The DNA thermal denaturation experiments showed that the saturated malonate-derived compound did not bind to DNA, whereas the unsaturated compound was a relatively good binder with selectivity for AT-rich sequences. By incorporating the malonate ester in a planar fluorene scaffold, the selectivity was reversed. Removing the malonate group from the fluorene-based *bis*-2-aminoimidazolinium restored the AT selectivity. The CD data showed that the groove-binding ability of the fluorene- and malonate-derived *bis*-2-aminoimidazolinium compounds was not as clear as with previous families. The mode of binding may incorporate some groove binding or phosphate binding as well as intercalation. In particular, the fluorene-based malonate-derived *bis*-2-aminoimidazolinium molecule was a clear intercalator in

poly(dAdT)$_2$ DNA. However, this derivative was a stronger stDNA binder than the diaryl unsaturated malonate-derived *bis*-2-aminoimidazolinium DNA binder. Thus, compounds **139** and **145** are promising carriers for Pt systems while bringing the metal to either AT-rich or GC-rich areas on DNA separately.

4.1.3 Cell Cytotoxicty

Of the non-metal containing compounds tested in HL-60 cancer cells, almost all were cytotoxic. The more lipophilic diaryl *bis*-2-amino-1,4,5,6-tetrahydropyridinium family were more active than the guanidinium or 2-aminoimidazolinium compounds. Those compounds containing an unsaturated malonate group were also more cytotoxic than previous guanidine-like dervatives, being the malonate-containing compound **139** the most cytotoxic derivative (IC_{50} = 18 μM). While the fluorene-derived compounds **145** and **146** were also cytotoxic, they were not as good as **139**.

The water-stable Pt^{II} complexes were also tested for cytotoxic activity in the HL-60 leukemia cell line. The cyclometalated phenyl-2-aminoimidazoline-derived compound **221** was the most cytotoxic (IC_{50} = 55 μM). This promising lead is structurally very different from currently investigated anticancer metal complexes. The other active metal complex was the binuclear cyclometalated *bis*-guanidine diaryl derivative **246a**. Although it possesses very weak activity (IC_{50} = 101μM), the free ligand is completely inactive. This result showed that attaching Pt to a MGB increased its cytotoxic effect, confirming a major objective of the project.

In summary, we have created a range of arylguanidine-like compounds that have a much better anticancer effect than our lead *bis*-guanidinium and *bis*-2-aminoimidazolinium compounds developed previously in the Rozas group.

4.2 Future work

With regard to the results outlined above, a number of possibilities for further investigation can be suggested. These are presented below with reference to synthesis, biophysical testing and biochemical evaluation.

4.2.1. Synthesis

The restriction of the diaryl *bis*-2-iminoimidazolidinium motif in a planar fluorene scaffold changed the unique MGB characteristics of these molecules with respect to DNA binding. It could be interesting to investigate the restriction of the diaryl *bis*-2-iminoimidazolidinium motif to bias the planar conformation of the diaryl system but retain some degree of rotational freedom. Two examples of this are outlined in Figure 4.2.1.1.

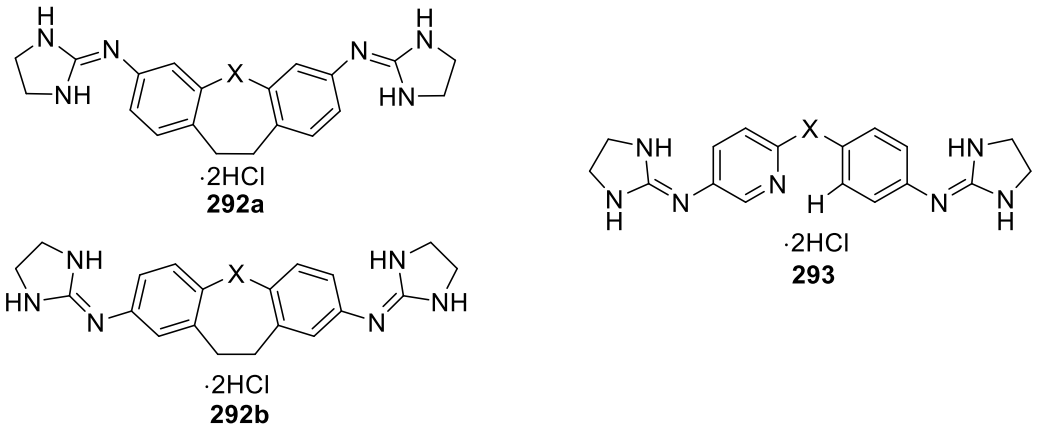

Figure 4.2.1.1. Potential conformationally restricted diaryl compounds with possibly enhanced MGB activity.

Also it would be interesting to investigate the uptake of these compounds into cells by synthesising potentially fluorescent molecules such as **294** (Figure 4.2.1.2). This compound could be synthesised from 3,6-*bis*-(*tert*-butoxyamino)fluorenone by a Wittig reaction and subsequent Boc-deprotection, guanidylation and salt formation.

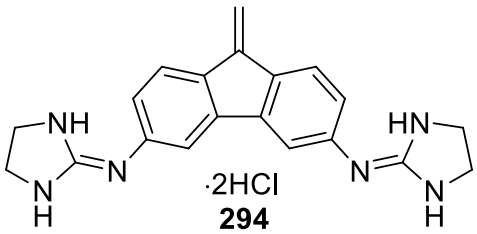

Figure 4.2.1.2. Potentially fluorescent possible DNA binder **294**.

Furthermore, it would be desirable to complete the synthesis of symmetrical *bis*-*N*-aminoguanidinium and asymmetrical *N*-aminoguanidinium/2-aminoimidazolinium families of potential DNA binders. These molecules could be assessed for DNA binding and cytotoxicity to investigate the predictions made by our modelling study.

With regards to the cyclometalated Pt complexes, it would be worth carrying out a SAR study based on the cytotoxic compound **221** (Figure 4.2.1.3). The aryl ring and imidazolidine ring could be substituted in many positions. Furthermore, the Cl and dmso ligands on the metal could be exchanged for more water-soluble ligands.

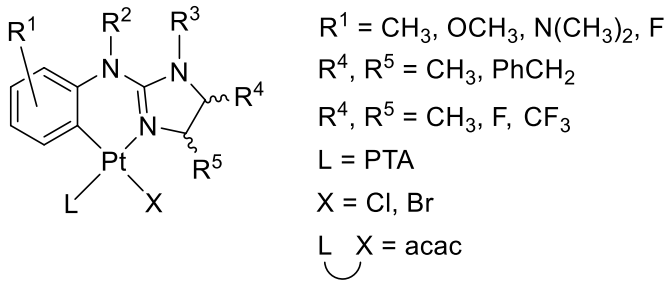

Figure 4.2.1.3. Substitution of **221** to generate potential SAR.

Another synthetic aim to be pursued is the synthesis of other Pt complexes such as **285** and to find a synthetic pathway to access **284**. One possible route could consist in the reaction of malonate derived *bis*-2-aminoimidazolinium esters **139** and **145** directly with Pt precursor **289**. In the presence of aquated Pt precursors, esters have unexpectedly broken under aqueous or DMF solvents to give carboxylates.[248,249] These findings could be exploited to our advantage. Another possibility could be to create MGB with different linkers, such as **295**, **296** and **297** (Figure 4.2.1.4) which can conjugate to Pt systems easily.

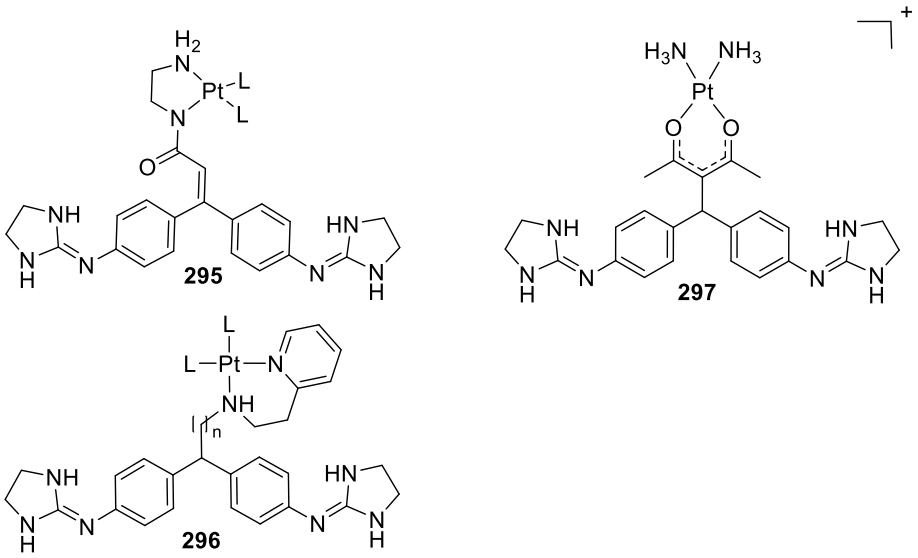

Figure 4.2.1.4. Other possible linkers to conjugate Pt systems with 2-iminoimidazolidine-based MGB.

Instead of forming the metal-ligand bond in the final step, outer-sphere ligand conjugation reactions with Pt^{II} complexes bearing free acids, azides or thiophilic maleimides could be availed of. These complexes are used to couple with ligands that have a suitable appendage, namely amines, alkynes or thiols respectively.[94] One possible idea could be to combine a Pt-malonate complex bearing a free amine (**302**)[230] with a carboxylic acid derived from a DNA binder (**301**) to create dual-acting agent **303** (Scheme 4.2.1.1).

Scheme 4.2.1.1.

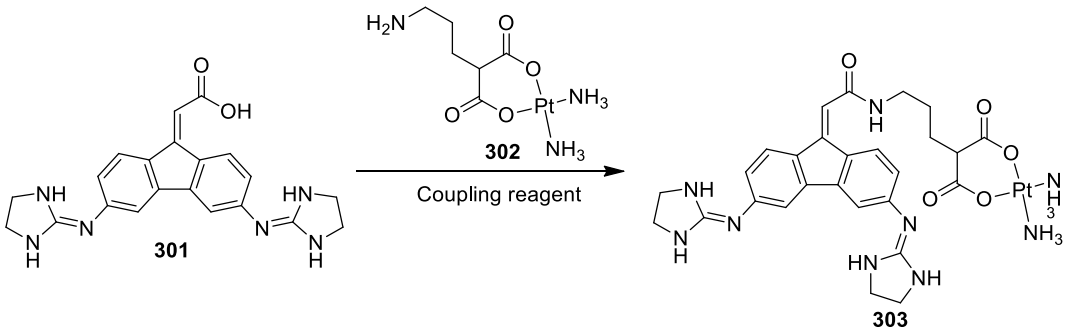

Another option it could be to use Pt as a linker between the diaryl groups and create a photoactive MGB such as **304** (Figure 4.2.1.5).

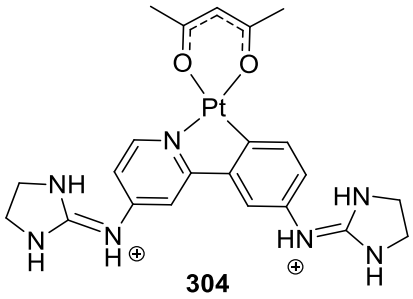

Figure 4.2.1.5. Potentially photoactive Pt^{II} complex containing high energy HOMO (Pt-Ar) and low energy LUMO (pyridine ring) containing water soluble DNA binding *bis*-2-aminoimidazolidinium cations.

Finally, it could be possible to synthesise a *mono*- or di-substituted Pt^{IV} complex based on a carboxylate salt of an MGB derivative (Figure 4.2.1.6).

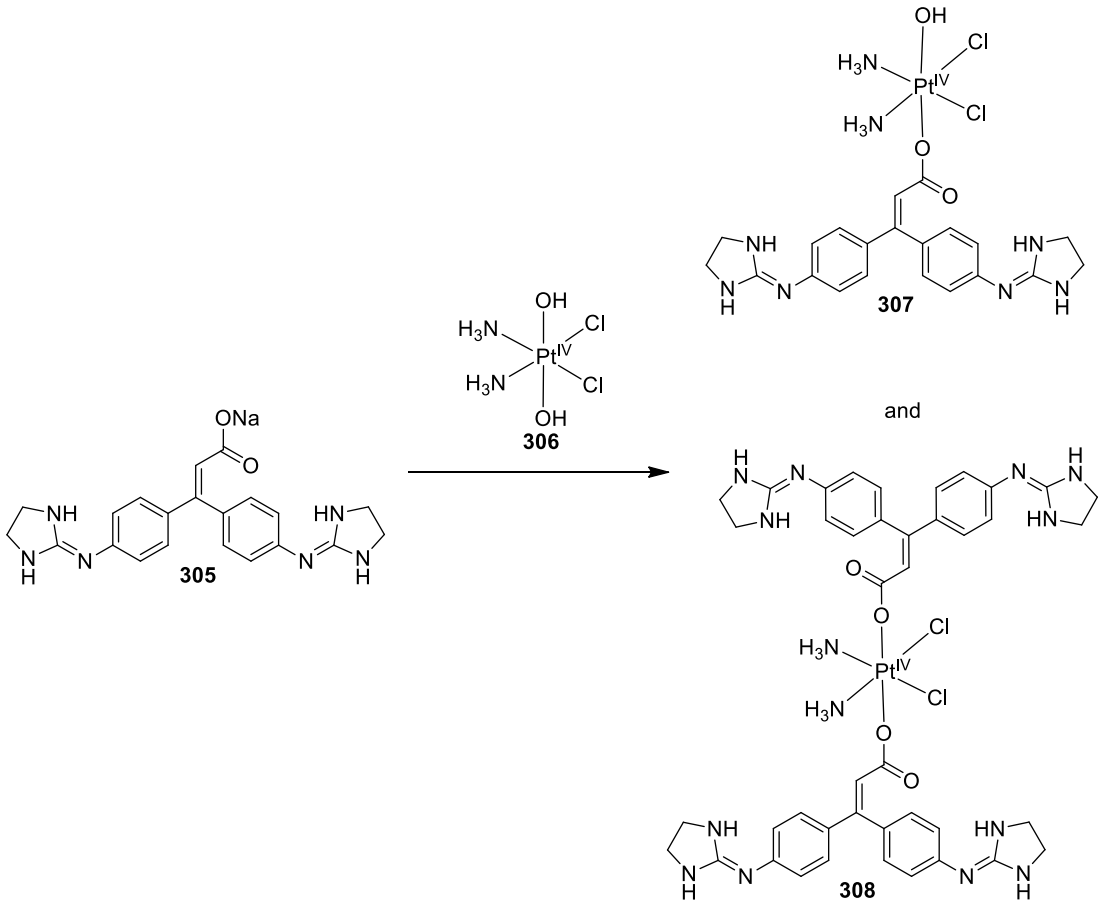

Figure 4.2.1.6. Mono- and di-substituted Pt^{IV} complexes of potential MGBs.

4.2.2. Biophysical Measurements

Future biophysical measurements on compounds synthesised in this thesis should include linear dichroism (LD) in order to get a better understanding of the mode of binding of the fluorene- and malonate-derived *bis*-aminoimidazolinium compounds with DNA. The Pt-MGB conjugate **285** should be assessed for DNA binding by thermal denaturation and CD measurements to test the effect, if any, of Pt(dach) on the binding mode of the compound compared to **221**.

4.2.3. Biochemical Testing

Future biochemical work on existing compounds should be centred around the bioactive ester **139** and platinacycle **221**. Both of these compounds should be tested for cytotoxicity in a range of cell lines including MCF-7 (breast) and Kelly (neuroblastoma) cell lines and their mechanism of cell death should be explored. Furthermore, Pt-MGB conjugate **285** should be screened for its cytotoxic effect on HL-60 cells and, if found active, then also on MCF-7 and Kelly cells.

Compound **221** should also be tested for Pt localisation in organelles *via* electron microscopy or differential centrifugation to understand the mechanism of cell death more in depth. The novel structure of this compound may induce cell death by specifically targeting cancer cells. We need to screen platinacycle **221** for activity against cisplatin-resistant cell lines, as well as non-cancerous tissue to explore selectivity. We could also test **221** on models of metastasis *in vitro* and *in vivo* to assess if **221** has any anti-metastatic effect.

Finally, since many related MGBs are active against trypanosomal diseases, all of these compounds could be tested on various species of parasite.

Chapter 5: Experimental

5.1 Synthetic Chemistry

5.1.1 Materials and Methods

All commercial chemicals were obtained from Sigma-Aldrich or Fisher and were used without further purification. Phosphate buffer solutions contained 10 mM K_2HPO_4/KH_2PO_4 adjusted to pH 7 and were prepared using Millipore water. Deuterated solvents for NMR use were purchased from Apollo. Dry DMF, DMSO and 1,4-dioxane were purchased from Sigma-Aldrich or Fisher. THF was dried over 4 Å molecular sieves (activated under vacuum by heating with a heat gun for 30 min) for at least 24 h before use. All other dry solvents were prepared using standard procedures, according to Vogel, with distillation prior to use. Chromatographic columns were run using Silica gel 60 (230-400 mesh ASTM). Solvents for synthetic purposes were used at general purpose reagent (GPR) grade. Analytical TLC was performed using Merck Kieselgel 60 F_{254} silica gel plates. Visualisation was by UV light (254 nm) or by staining with I_2, $KMnO_4$, ninhydrin or cerium ammonium molybdate. NMR spectra were recorded in Bruker DPX-400 Avance spectrometers and operating at 400.13 MHz and 600.1 MHz for ^{1}H-NMR and 100.6 MHz and 150.9 MHz for ^{13}C-NMR and were referenced to the internal solvent signals. For ^{195}Pt-NMR, the spectrometer was operated at 86.04 MHz and was referenced to an external sample of K_2PtCl_4 (-1600 ppm). For ^{19}F-NMR, the spectrometer was operated at 376.20 MHz and was referenced to an external sample of trifluorotoluene (-63.72 ppm). NMR data were processed using MestReNova software. HRMS spectra were measured on a Micromass LCT electrospray TOF instrument with a WATERS 2690 autosampler with methanol as carrier solvent. APCI (atmospheric pressure chemical ionisation) spectra were measured on a micrOTOF-QIII with a direct insertion probe (DIP). Melting points were determined using a Stuart Scientific Melting Point SMP1 apparatus and are uncorrected. Infrared spectra were recorded on a Perkin Elmer Spectrum One FT-IR Spectrometer equipped with a Universal ATR sampling accessory. Microanalysis was performed using an Exeter Analytical CE 440 elemental analyser. HPLC purity analysis was carried out using a Varian ProStar system equipped with a Varian Prostar 335 diode array detector and a manual injector (20 μL). UV detection was performed at 245 nm and peak purity was confirmed using a purity channel. The stationary phase consisted of an ACE 5 C18-AR column (150 x 4.6 mm), and the mobile phase used the following gradient system, eluting at 1.0 cm^3/min: aqueous formate buffer (30 mM, pH 3.0) for ten minutes, linear ramp

to 85% methanol buffered with the same system over 25 minutes, held at 85% buffered methanol for ten minutes.

5.1.2. General Procedures

Method A: Boc deprotection reaction.[164]

The appropriate Boc-protected 2-amino-1,4,5,6-tetrahydropyrimidine, 2-aminoimidazoline, guanidine or amine (1.0 eq., 0.47 mmol) was added to a 4 M solution of HCl in dry 1,4-dioxane (6.0 eq. per Boc group, 5.64 mmol) and the solution was brought to 0.2 M concentration by addition of CH_2Cl_2. The solution was stirred at 55 °C until the TLC showed a single highly polar spot (typically 7 h). After 2 h, a small amount of CH_3OH was added if necessary to solubilise the compound. Upon completion, the reaction was then partitioned between water (3 mL) and dichloromethane (3 × 5 mL). The aqueous layer was concentrated under vacuum to give the deprotected compound as a HCl salt.

Method B: Pd-catalysed hydrogenation of 2-aminopyrimidines to 2-amino-1,4,5,6-tetrahydropyrimidinium salts.

To a solution of the appropriate *bis*-2-aminopyrimidine diaromatic derivative (0.136 mmol) in degassed CH_3OH (1 mL), was added Pd/C (10%, 82 mg) and aq. HCl (1 M, 0.5 mL). The mixture was stirred vigorously under a balloon of H_2 for 16 h, diluted with CH_3OH, filtered and concentrated to directly yield the *bis*-(2-amino-1,4,5,6-tetrahydropyrimidinium) dichloride salts.

Method C: Buchwald-Hartwig coupling of aryl bromide and 2-aminopyrimidine.

To a vacuum-dried mixture of $Pd_2(dba)_3$ (21.7 mg, 0.023 mmol), Xantphos (27.4 mg, 0.047 mmol), NaO^tBu (170 mg, 1.776 mmol), 2-aminopyrimidine (169 mg, 1.776 mmol) and the appropriate dibromide (0.592 mmol) under an atmosphere of Ar at 90 °C, was added dry toluene (1.5 mL) and the mixture was stirred for 16 h. The flask was cooled and diluted with EtOAc (50 mL), filtered through Celite® and separated with H_2O (20 mL). The aqueous

layer was extracted again with EtOAc (2 × 20 mL) and the combined organic layers were washed with brine and dried over Na_2SO_4. The solvent was removed in vacuo and purified by silica gel chromatography in a hexane/EtOAc mixture.

Method D: Sandmeyer reaction to synthesise arylbromides.

The appropriate diamine (3.289 mmol) was heated in HBr (48% in H_2O, 5 mL) at 100 °C for 12 h until a solution was formed. Upon cooling to 0 °C, a solution of $NaNO_2$ (480 mg, 6.958 mmol) in H_20 (5 mL) was added dropwise. This solution was in turn added dropwise to a solution of CuBr (1.400 g, 9.676 mmol) in HBr (48% in H_2O, 5 mL) and the solution was heated slowly to 70 °C over 2 h and stirred at 70 °C for up to 3 h until evolution of gas ceased. To dissolve organic solids that precipitated, it was necessary to add Et_2O (0.5 mL) as the mixture reached 50 °C. The mixture was cooled and diluted with EtOAc (20 mL) and H_2O (20 mL). The layers were separated and the aqueous layer was extracted with EtOAc (2 × 20 mL). The organic phases were combined and washed with saturated $NaHCO_3$ (2 × 20 mL), H_2O (2 × 20 mL) and brine (2 × 20 mL). The organic layer was dried over $MgSO_4$, solvent was evaporated and purified on silica gel to yield the appropriate dibromide.

Method E: Boc protection of thiourea-like compounds.[212]

Under atmosphere of Ar, dry THF (300 mL) was added to vacuum-dried NaH (60% in mineral oil, 3.75 g, 93.5 mmol). The suspension was brought to 0 °C and the appropriate thiourea or thione (20.7 mmol) was added in one portion. After stirring for 10 min at rt, the mixture was cooled to 0 °C and di-*tert*-butyldicarbonate (9.94 g, 45.6 mmol) was added. Stirring was continued at 0 °C for 30 min and then the viscous liquid was stirred for 16 h at rt. Saturated $NaHCO_3$ (50 mL) was added dropwise to quench the reaction. Following dilution with H_2O (150 mL), the product was extracted with EtOAc (3 × 75 mL) and the combined organic layers washed with brine (40 mL) and dried over $MgSO_4$. Upon removal of solvent, the Boc-protected compound was recrystallised from hexane: EtOAc (4:1).

Method F: Synthesis of *N*,*N*'-disubstituted thioureas.[125]

To a solution of *N*,*N*'-di-*tert*-butoxycarbonylthiourea (1.0 eq., 3.6 mmol) in dry THF (36 mL) under N_2 at 0 °C was added NaH (146 mg, 3.65 mmol, 60% in mineral oil). After stirring at rt for 1 h, TFAA (770 μL, 5.57 mmol) was added to give a yellow solution. The stirring continued at rt for a further 1 h and then the appropriate amine was added and the reaction was stirred for 12-24 h at rt. Upon completion of the reaction (as adjudged by TLC), the solution was quenched by dropwise addition of H_2O (20 mL) and was extracted with EtOAc (3 × 20 mL). The combined organic layers were washed with brine (20 mL) and dried over $MgSO_4$. The solvent was removed under vacuum and the crude solid was purified by flash chromatography on Et_3N-treated silica using a gradient of EtOAc in hexanes.

Method G: Synthesis of Boc-protected 1-amino-2-arylguanidines.

To a solution of the respective substituted thiourea (1.0 eq., 2.0 mmol), NEt_3 (0.9 mL, 6.2 mmol) and Boc-protected hydrazine **50** (262 mg, 2.0 mmol) in CH_2Cl_2 (5 mL) at 0 °C, was added $HgCl_2$ (272 mg, 2.2 mmol) and the reaction was stirred for 1 h at 0 °C followed by further stirring for 16-24 h at rt. When starting material was consumed (as adjudged by TLC) the mixture was diluted with EtOAc (20 mL), filtered through Celite® and added to H_2O (20 mL). The biphasic mixture was separated and the aqueous layer was further extracted with EtOAc (3 × 20 mL). The combined organic layers were washed with brine (20 mL) and dried over $MgSO_4$. The solvent was removed under vacuum and the crude solid was purified by flash chromatography on Et_3N-treated silica using a gradient of EtOAc in hexanes.

Method H: Synthesis of Boc-protected disubstituted diaryl *bis*-thioureas.

To a suspension of NaH (8.7 eq., 318 mg, 8.0 mmol, 60% in mineral oil) in dry THF (15 mL) under N_2 at 0 °C was added *N*,*N*'-di-*tert*-butoxycarbonylthiourea (4.4 eq., 1.11 g, 4.02 mmol). After stirring at rt for 1 h, TFAA (1.96 mmol, 0.60 mL, 1.8 mmol) was added to give a yellow solution. Stirring was continued at rt for a further 1 h and then the appropriate amine was added (1.0 eq, 0.92 mmol), and the reaction was stirred for 12-24 h at rt. Upon completion of the reaction (as adjudged by TLC), the solution was quenched by dropwise

addition of H_2O (20 mL) and was extracted with EtOAc (3 × 20 mL). The combined organic layers were washed with brine (20 mL) and dried over $MgSO_4$. The solvent was removed under vacuum and the crude solid was purified by flash chromatography on Et_3N-treated silica using a gradient of EtOAc in hexanes.

Method I: Synthesis of Boc-protected diaryl *bis*-(2-iminoimidazolidine) compounds.[212]

The appropriate dianiline (1.0 eq., 1.28 mmol), Boc-protected thione **77** (2.0 eq., 2.57 mmol) and Et_3N (7 eq., 9.0 mmol) was dissolved in CH_2Cl_2 or DMF (5 mL) and cooled to 0 °C. To this was added $HgCl_2$ (2.5 eq., 3.21 mmol) and the resulting mixture was stirred for 16 h at rt. If the reaction did not go to completion (as adjudged by TLC) a further 0.1 eq. of $HgCl_2$ and Et_3N were added. Upon completion, the reaction mixture was diluted with EtOAc (20 mL) and filtered through a pad of Celite®. The filter cake was rinsed with EtOAc (30 mL) and water (60 mL) was added to the filtrate. The mixture was separated and the aqueous phase was extracted with EtOAc (2 × 30 mL). The combined organic layer was washed with brine (2 × 30 mL), dried over Na_2SO_4, and concentrated under vacuum. The crude product was purified by flash chromatography on neutral alumina, eluting with the appropriate gradient of hexane/ EtOAc.

Method J: Synthesis of Boc-protected *bis*-amino diaryl compounds using the Buchwald-Hartwig reaction.[177]

To a vacuum-dried mixture of $Pd(OAc)_2$ (0.06 eq., 0.018 mmol), Xphos (0.18 eq., 0.054 mmol), Cs_2CO_3 (2.8 eq., 0.84 mmol), *tert*-butyl carbamate (2.4 eq., 0.72 mmol) and the appropriate dibromide (1.0 eq., 0.30 mmol) in a Schlenk tube under Ar, was added dry 1,4-dioxane (2.4 mL) and the mixture was stirred at 100 °C for 2-16 h. The flask was cooled, diluted with EtOAc (50 mL), and separated with H_2O (20 mL). The aqueous layer was extracted again with EtOAc (2 × 20 mL) and the combined organic layers were washed with brine (10 mL) and dried over Na_2SO_4 and filtered through two layers of filter paper. The product was concentrated under vacuum and purified by silica gel chromatography, eluting with a hexane/EtOAc mixture.

Method K: Synthesis of metal dicarboxylate salts.

To a solution of the appropriate diethyl ester (1.0 eq., 0.12 mmol) in a 1:1 MeOH/H_2O mixture (1 mL), was added the appropriate metal hydroxide (7 eq., 0.87 mmol) and the reaction was stirred for 5-24 h at 70 °C. When the reaction was complete (as adjudged by ^{1}H NMR), the solvent was evaporated to give a crude solid.

Method L: Synthesis of Boc-protected guanidines.[212]

The appropriate aniline (1.0 eq., 1.47 mmol) was dissolved in dichloromethane or *N*,*N*-dimethylformamide at rt with *N*,*N*-di(*tert*-butoxycarbonyl)-*S*-methyl thiourea, (1.0 eq., 1.47 mmol) and Et_3N (3.1 eq., 4.55 mmol). To this was added $HgCl_2$ (1.1 eq., 1.62 mmol) and the resulting mixture was stirred for 16 h at rt. If the reaction did not go to completion (as adjudged by TLC) a further 0.1 eq. of mercury chloride and Et_3N were added. Upon completion, the reaction mixture was diluted with EtOAc (20 mL) and filtered through a pad of Celite®. The filter cake was rinsed with EtOAc (30 mL) and water (60 mL) was added to the filtrate. The mixture was separated and the aqueous phase was extracted with EtOAc (2 × 30 mL). The combined organic layer was washed with brine (2 × 30 mL), dried over Na_2SO_4, and concentrated under vacuum. The crude product was purified by silica gel column chromatography, eluting with the appropriate gradient of hexane/ ethyl acetate.

Method M: Synthesis of platinum-aminoguanidine complexes and guanidinium tetrachloroplatinate salts.[146]

Potassium tetrachloroplatinate (1.0 eq., 0.40 mmol) was dissolved in water (1 mL) resulting in a pink solution. This was added to the appropriate guanidinium chloride (5.0 eq., 2.00 mmol) in water (1 mL) and stirred for 15 min at rt. Precipitation occurred and the liquid was then evaporated to dryness for up to 3 days on a clock glass in a vacuum desiccator containing activated silica gel to give crystals. These were washed with H_2O (2 mL), EtOH (2mL) and Et_2O (2 mL) to yield the final product.

Method N: Synthesis of guanidine and 2-imino-imidazolidine free bases.

A portion of Na metal (1.2 eq., 0.6 mmol) was cut into small pieces and carefully dissolved in EtOH (0.5 mL) under a constant flow of Ar and stirred for 30 min to give a solution of fresh NaOEt (1.2 eq., 0.6 mmol). This solution was added to a solution of the appropriate guanidinium or 2-amino-imidazolinium salt (1.0 eq., 0.5 mmol) in EtOH (0.5 mL) and stirred for 1.5 h. The mixture was allowed to stand for 30 min and cooled to 0 °C. NaCl was filtered off through filter paper and the filtrate was evaporated under vacuum to give the appropriate free base which was used without further purification.

Method O: Synthesis of Cycloplatinated arylguanidine and 2-arylaminoimidazoline complexes.

A suspension of *cis*-[$PtCl_2(dmso)_2$] (1.0 eq., 0.888 mmol), the appropriate free base (1.0 eq., 0.888 mmol) in DMSO (1 mL) or in a fresh NaOMe solution (1.1 eq., 1.00 mmol in MeOH, 24 mL) was heated to 80 °C for 2-48 h. MeOH was removed *in vacuo* and the solid was dissolved in a minimum of DMSO (*ca.* 1 mL), filtered through cotton wool and precipitated using H_2O (5-30 mL). The fine solid was collected by centrifugation (8000 rpm), re-dissolved in DMSO (0.2 mL) and precipitated with H_2O if necessary. The powder was dried at rt *in vacuo* overnight at *ca.* 10 mbar.

5.1.3 Synthesis and Characterisation

cis-[Diamminediiodoplatinum] (6)

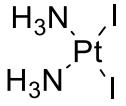

To a solution of K_2PtCl_4 (0.50 g, 1.2 mmol) in deoxygenated distilled H_2O (5 mL) at 55 °C was added KI (1.20 g, 7.23 mmol) and the solution was stirred in the dark for 20 min, followed by slow addition of NH4OH (aq., 35%) until the solution turned yellow. The reaction was stirred for 10 min, resulting in a yellow precipitate. The precipitate was filtered and washed twice each with H_2O, EtOH and Et_2O and then vacuum dried at rt to give a yellow powder (501 mg, 86%). [227]

ν_{max} (ATR)/cm^{-1}: 3263 (NH), 3165(NH), 2518, 2049, 1596, 1500, 1290, 1262, 737.

% Calculated for $H_6N_2PtI_2$: C 0, H 1.25, N 5.80.

% Found: C 0.5, H 1.22, N 5.45.

4,4'-_Bis_-(2-amino-1,4,5,6-tetrahydropyrimidine)benzophenone dihydrochloride (46a)

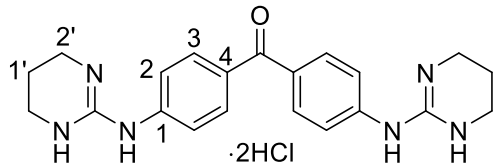

As per *Method A* using Boc-protected derivative **61** (238 mg, 0.31 mmol) and HCl (4M in dioxane, 1.84 mL, 7.35 mmol). After evaporation of the aqueous layer, the product was purified on reverse phase silica, eluting in 100% H_2O as a white solid (94 mg, 69%). **M.p.** 183 °C.

δ_H (400 MHz, D_2O): 2.04 (quin., 4H, J 5.8 Hz, CH_2-1'), 3.44 (t, 8H, J 5.8, CH_2-2'), 7.41 (d, 4H, J 8.6, Ar-2), 7.87 (d, 4H, J 8.6, Ar-3).

δ_C (100 MHz, D_2O): 19.2 (CH_2-1'), 38.4 (CH_2-2'), 122.7 (CH Ar-2), 132.0 (CH Ar-3), 133.8 (q Ar-4), 140.0 (q Ar-1), 151.7 (q C=N), 198.3 (q C=O).

ν_{max} (ATR)/cm^{-1}: 2982 (CH), 2891, 1624 (C=O), 1228, 1147, 1032, 963, 825, 762.

HRMS (*m/z* ESI^+) $[M+H]^+$ calcd for $C_{21}H_{25}N_6O$: 377.2084, found 377.2088.

RP-HPLC (254 nm): t_R= 20.7 min, purity >99%.

4,4'-*Bis*-(2-amino-1,4,5,6-tetrahydropyrimidine)diphenylether dihydrochloride (46b)

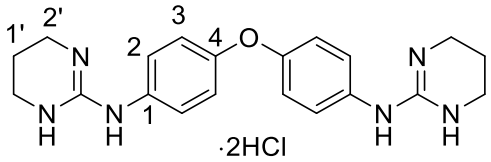

As per *Method B*, employing 4,4'-*bis*-(2-aminopyrimidine)diphenylether **58b** (42.5 mg, 0.119 mmol), yielded a gum (44 mg, 85%) which eluted in reverse phase silica as a yellow solid (44 mg, 85%). **M.p.** 183 °C.

δ_H (400 MHz, D_2O): 1.99 (quin., 4H, J 5.7, CH_2-1'), 3.36-3.39 (m, 8H, CH_2-2'), 7.15 (d, 4H, J 8.7, Ar-3) 7.30 (d, J 8.7, 4H, Ar-2).

δ_C (100 MHz, D_2O): 19.3 (CH_2-1'), 38.2 (CH_2-2'), 120.0 (CH Ar-3), 126.6 (CH Ar-2), 128.0 (q Ar-1), 152.5 (q C=N), 155.6 (q Ar-4).

ν_{max} (ATR)/cm^{-1}: 2982 (CH), 2891, 1711, 1624, 1490, 1317, 1249 (C-O), 1228, 1154, 1032, 824.

HRMS (*m/z* ESI^+) $[M+H]^+$ calcd for $C_{20}H_{25}N_6O$: 365.2084, found 365.2075.

RP-HPLC (254 nm): t_R= 21.3 min, purity >99%.

4,4'-*Bis*-(2-amino-1,4,5,6-tetrahydropyrimidine)diphenylmethane dihydrochloride (46c)

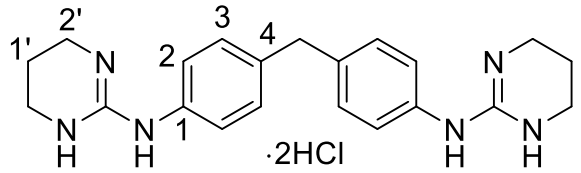

As per *Method B*, employing *bis*-pyrimidine **58a** (50 mg, 0.271 mmol), purifying in reverse phase silica, eluting in 100% H_2O, yielded a grey gum (41 mg, 83%).

δ_H (400 MHz, D_2O): 1.82 (quin., 4H, J 5.8, CH_2-1'), 3.20 (t, 8H, J 5.8, CH_2-2'), 3.89 (s, 2H), 7.06 (d, 4H, J 8.2, Ar-3), 7.22 (d, 4H, J 8.2, Ar-2).

δ_C (100 MHz, D_2O): 19.3 (CH_2-1'), 38.3 (CH_2-2'), 40.1 (CH_2), 126.1 (CH Ar-3), 130.1 (CH Ar-2), 132.2 (q Ar-4), 140.9 (q Ar-1), 152.5 (q C=N).

ν_{max} (ATR)/cm^{-1}: 2983 (CH), 1711 (NH), 1613, 1241, 1165, 1077, 1030.

HRMS (*m/z* ESI^+) $[M+H]^+$ calcd for $C_{21}H_{27}N_6$: 363.2292, found 363.2294.

RP-HPLC (254 nm): t_R= 21.8 min, purity >99%.

4,4'-*Bis*-(2-amino-1,4,5,6-tetrahydropyrimidine)phenylaniline trihydrochloride (46d)

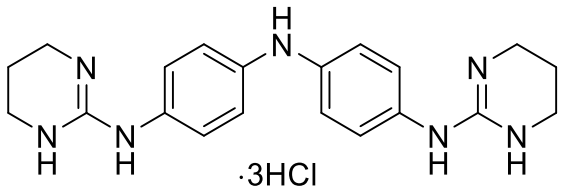

As per *Method B*, using N-Boc protected derivative **58e** (72 mg, 0.16 mmol), following purification on reverse phase silica, eluting in 100% H_2O, afforded a yellow solid (43 mg, 57%). **M.p.** 268 °C.

δ_H (400 MHz, D_2O): 1.75-1.90 (m, 4H, CH_2-1'), 3.17-3.21 (m, 8H, CH_2-2'), 7.05 (s, 8H, Ar).

δ_C (100 MHz, D_2O): 19.3 (CH_2-1'), 38.2 (CH_2-2'), 115.5 (CH Ar), 118.7 (CH Ar), 126.7 (q Ar), 132.2 (q Ar), 142.6 (q C=N).

ν_{max} (ATR)/cm^{-1}: 2981 (CH), 2891, 1710, 1625, 1491, 1318, 1153, 823.

HRMS (*m/z* ESI^+) $[M+H]^+$ calcd for $C_{20}H_{25}N_7$: 364.2244, found: 364.2248.

RP-HPLC (254 nm): t_R= 20.0 min, purity >98%.

***N-tert*-butoxycarbonyl-4,4'-*Bis*-(2-amino-1,4,5,6-tetrahydropyrimidine)diphenylaniline dihydrochloride (46e)**

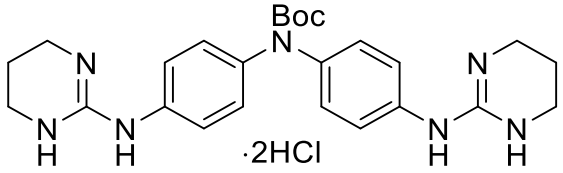

As per *Method B*, using **58e** (72 mg, 0.16 mmol) as the diamine, following purification on reverse phase silica, eluting in 100% H_2O, afforded a purple solid (22.0 mg, 30%). **M.p.** 268 °C.

δ_H (400 MHz, D_2O): 1.48 (s, 9H), 1.95-2.04 (m, 4H), 3.35-3.40 (m, 8H), 7.27-7.31 (m, 4H), 7.37-7.41 (m, 4H).

Upon solvation of the title compound in CH_3OH (0.2 mL), *aq.* HCl (1 mL, 3 M) was added dropwise and the solution was stirred for 17 h. Evaporation under vacuum afforded a red solid that was purified by reverse phase chromatography to afford **46d** (18.1 mg, 81%). Characterisation is identical to that of **46d** synthesised directly using *Method B*.

***Bis*(4-aminophenyl)amine (47d)**

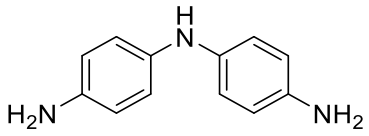

A solution of *bis*(4-nitrophenyl)amine **103** (970 mg, 3.74 mmol) in EtOH (5 ml) was degassed with Ar, followed by the addition of Pd/C (97 mg, 10%). The solution was then purged with H_2 and mixture was stirred at rt for 5 h under a balloon of H_2. Following an argon purge, the solution was filtered and washed with EtOH. The filtrate was collected and the solvent was removed under vacuum, affording a dark purple powder (175 mg, 24%). **M.p.** 70-75 °C.

δ_H (400 MHz, $CDCl_3$): 3.34 (s, 1H, NH), 6.50 (d, 4H, J 7.7, Ar), 6.52 (d, 4H, J 7.7, Ar), 6.70 (s, 4H, NH_2).

δ_C (100 MHz, $CDCl_3$): 115.9 (CH Ar), 119.4 (CH Ar), 125.4 (q Ar), 139.8 (q Ar).

ν_{max} (ATR)/cm^{-1}: 3389 (NH), 3333 (NH), 2974(CH), 1608, 1501, 1428, 1386, 1363, 1309, 1269, 1236, 1189, 1123, 889.

HRMS (*m/z* ESI^+) $[M+H]^+$ calcd for $C_{12}H_{12}N_3$: 198.1031, found 198.1034.

4,4'-Dibromobenzophenone (48a)

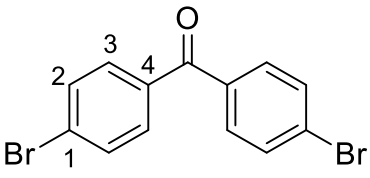

As per *Method C*, using diamine **47a** (700 mg, 3.289 mmol), following recrystallisation from $CHCl_3$, gave the title compound as a red/orange solid (695 mg, 62%). **M.p.** 169-170 °C (lit. 177 °C). [1]

δ_H (400 MHz, $CDCl_3$): 7.64 (s, 8H, Ar).

δ_C (100 MHz, $CDCl_3$): 127.8 (q Ar-1), 131.4 (CH Ar-2), 131.7 (CH Ar-3), 135.8 (q Ar-4), 194.5 (q CO) matches lit.[2]

HRMS (*m/z* EI^+) Found: 337.8941 ($[M]^+$. $C_{18}H_8Br_2O$ Requires 337.8942).

Di-(4-bromophenyl)ether (48b)

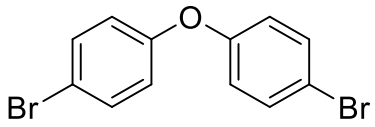

As per *Method C*, using diamine **47b** (659 mg, 3.289 mmol), following purification on silica in 2% EtOAc in hexane, afforded a white solid (640 mg, 59%). **M.p.** 56-57 °C (lit. 60-62 °C).[3]

δ_H (400 MHz, $CDCl_3$): 6.86 (d, 4H, J 8.8, Ar), 7.43 (t, 4H, J 8.8, Ar).

HRMS (*m/z* EI^+) Found: 325.8940 ($[M]^+$. $C_{12}H_8Br_2O$ Requires 325.8942).

4,4'-Dibromo-*N*-(*tert*-butoxycarbonyl)phenylaniline (48e)

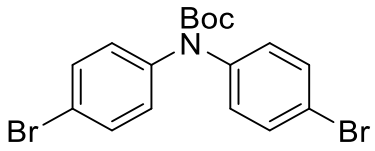

To a vacuum-dried mixture of di(4-bromophenyl)amine **48d** (400 mg, 1.22 mmol), di-*tert*-butyl dicarbonate (293 mg, 1.35 mmol) and DMAP (30 mg, 0.25 mmol) under Ar, was added THF (2 mL) and the solution was heated to reflux for 24 h. After cooling to rt, the mixture was separated between EtOAc (3 x 20 mL) and H_2O (1 x 10 mL). The combined organic layers were washed with brine (10 mL), dried over Na_2SO_4 and purified by flash

chromatography on silica, eluting in 5% EtOAc in hexane to afford the title compound (439 mg, 84%). **M.p.** 121 °C (lit. 113-115 °C).[4]

δ_H (400 MHz, $CDCl_3$): 1.44 (s, 9H), 7.06 (d, 4H, J 8.7, Ar), 7.43 (d, 4H, J 8.7, Ar).

4,4'-*Bis*-(2-aminopyrimidino)benzophenone (58a)

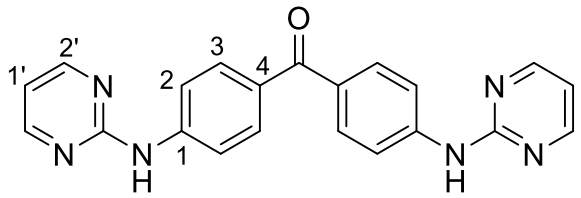

As per *Method D*, using dibromide **48a** (200 mg, 0.592 mmol), after purification in 50% EtOAc in hexane, gave a yellow solid (167 mg, 77%). **M.p.** 250 °C.

δ_H (400 MHz, $CDCl_3$): 6.82 (t, 2H, J 4.6, Ar-1'), 7.42 (br s, 2H, NH), 7.77 (d, 4H, J 8.5, Ar-2), 7.86 (d, 4H, J 8.5, Ar-3), 8.49 (d, 4H, J 4.6, Ar-2').

δ_C (100 MHz, $CDCl_3$): 113.5 (CH Ar-1'), 117.7 (CH Ar-2), 131.6 (CH Ar-3), 131.7 (q Ar-4), 143.2 (q Ar-1), 158.0 (CH Ar-2'), 159.6 (q C=N), 171.1 (q C=O).

ν_{max} (ATR)/cm^{-1}: 1625, 1605, 1510, 1228, 1023.

HRMS (*m/z* ESI^+) $[M+H]^+$ calcd for $C_{21}H_{17}N_6O$: 369.1458, found: 369.1477.

4,4'-*Bis*-(2-aminopyrimidino)diphenylether (58b)

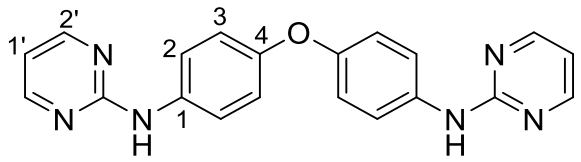

As per *Method D*, using dibromide **48b** (388 mg, 1.184 mmol), after purification in 60% EtOAc in hexane, gave a white solid (133 mg, 31%). **M.p.** 238 °C.

δ_H (400 MHz, $CDCl_3$): 6.73 (t, 2H, J 4.7, Ar-1'), 7.01 (d, 4H, J 8.9, Ar-3), 7.49 (br s, 2H, NH), 7.55 (d, 4H, J 8.9, Ar-2), 8.42 (d, 4H, J 4.7, Ar-2').

δ_C (400 MHz, $CDCl_3$): 112.1 (CH Ar-1'), 118.5 (q Ar-4), 119.2 (CH Ar-3), 121.7 (CH Ar-2), 134.0 (q Ar-1), 152.5 (CH Ar-2'), 157.8 (q C=N).

ν_{max} (ATR)/cm^{-1}: 2982 (CH), 1624, 1510, 1228, 1026, 963.

HRMS (*m/z* ESI^+) calcd for $C_{20}H_{17}N_6O$: 357.1458, found 357.1458.

4,4'-*Bis*-(2-aminopyrimidino)-*N*-(*tert*-butoxycarbonyl)phenylaniline (58e)

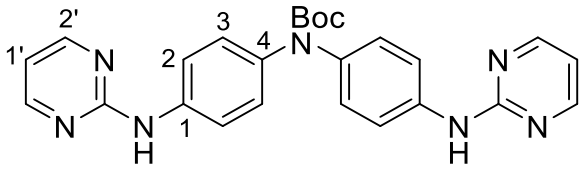

As per *Method D*, using $Pd_2(dba)_3$ (45.9 mg, 0. 050 mmol, 10 mol %), Xantphos (43.5 mg, 0.075 mmol, 15 mol %), NaO^tBu (135 mg, 1.40 mmol), 2-aminopyrimidine (100 mg, 1.05 mmol) and dibromide **48e** (213 mg, 0.5 mmol), in toluene (1.0 mL) at 80 °C after purification in 60% EtOAc in hexane, gave a yellow solid (57 mg, 25%). **M.p.** 220 °C.

δ_H (400 MHz, $CDCl_3$): 1.46 (s, 9H, CH_3), 6.75 (t, 2H, J 4.9, Ar-1'), 7.20 (d, 4H, J 8.8, Ar-2), 7.56 (d, 4H, J 8.4, Ar-3), 7.73 (br s, 2H, NH), 8.42 (d, 4H, J 4.9, Ar-2').

δ_C (100 MHz, $CDCl_3$): 28.3 (CH_3), 80.9 (q $C(CH_3)_3$), 112.5 (CH Ar-1'), 119.4 (CH Ar-2), 127.4 (CH Ar-3), 136.8 (q Ar-1), 137.8 (q Ar-4), 154.0 (q C=O), 157.9 (CH Ar-2'), 159.9 (q C=N).

ν_{max} (ATR)/cm^{-1}: 2982 (CH), 1607, 1392, 1242, 1152, 1025, 963.

HRMS (*m/z* ESI^+) $[M+H]^+$ calcd for $C_{25}H_{26}N_7O_2$: 456.2143, found 456.2142.

***N,N'*-(Di-*tert*-butoxycarbonyl)-3,4,5,6-tetrahydro-1*H*-2-pyrimidinethione (60)**

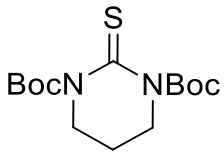

As per *Method E*, using 3,4,5,6-tetrahydro-2-pyrimidinethiol **59** (2.41 g, 20.7 mmol) after removal of solvent, the title compound was recrystallised from hexane: EtOAc (4:1) as yellow crystals (5.45 g, 84%). **M.p.** 91-92 °C (lit. 93-94 °C).[5]

δ_H (400 MHz, $CDCl_3$): 1.53 (s, 18 H, CH_3), 2.14 (quin., 2H, J 6.9, CH_2), 3.67 (t, 4H, J 6.9, CH_2).

HRMS (*m/z* ESI^+) $[M+H]^+$ calcd for $C_{14}H_{25}N_2O_4S$: 317.1530, found: 317.1542.

4,4'-*Bis*-[2-imino-1,3-di-(*tert*-butoxycarbonyl)-1*H*-3,4,5,6-tetrahydropyrimidino]benzophenone (61)

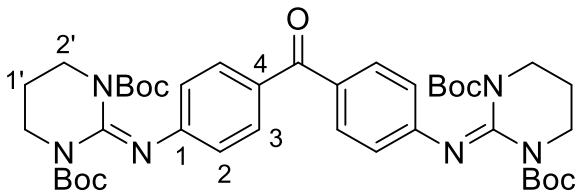

To a solution of 4,4'-diaminobenzophenone (1.060 g, 5.0 mmol), **60** (3.300 g, 10.5 mmol) and Et_3N (4.90 mL, 35.0 mmol) in a mixture of CH_2Cl_2 (2 mL) and DMF (10 mL) at 0 °C under Ar, was added $HgCl_2$ (3.195 g, 11.0 mmol) in one portion. The suspension was stirred at rt for 12 h, diluted with EtOAc (150 mL) and filtered through Celite. The filtrate was washed with H_2O (5 x 50 mL), brine (2 x 40 mL), dried over Na_2SO_4 and evaporated under vacuum to give a yellow liquid. The crude product was purified by flash chromatography on alumina, eluting in 30% EtOAc in hexane to afford the title compound as a clear solid (660 mg, 17%). **M.p.** 159-160 °C.

δ_H (400 MHz, $CDCl_3$): 1.34 (s, 18H, CH_3), 2.11-2.20 (m, 4H, CH_2), 3.77 (br s, 8H, CH_2), 7.08 (br s, 4H, Ar-2), 7.73 (d, 4H, J 8.2, Ar-3).

δ_C (100 MHz, $CDCl_3$): 24.0 (CH_2-1'), 27.9 (CH_3), 41.7 (CH_2-2'), 82.6 (q $C(CH_3)_3$), 121.1 (CH Ar-2), 131.1 (CH Ar-3), 131.7 (q Ar-1 or Ar-4), 132.8 (q Ar-1 or Ar-4), 142.8 (q C=N), 151.3(q C=O Boc), 194.8 (q C=O).

ν_{max} (ATR)/cm^{-1}: 3163 (NH), 2978 (CH), 1715 (C=O), 1539, 1250, 1126, 846, 745.

HRMS (*m/z* ESI^+) $[M+H]^+$ calcd for $C_{41}H_{57}N_6O_9$: 777.4182, found: 777.4220.

1-Amino-2-phenylguanidine hydrochloride (67a)

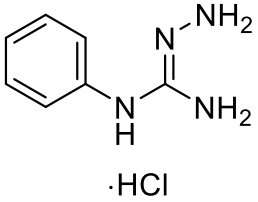

As per *Method A* using compound **94a** (338 mg, 0.97 mmol) and HCl (2.9 mL, 11.58 mmol, 4M in dioxane) compound **67a** was afforded as a pale yellow gum (105 mg, 61%).

δ_H (400 MHz, D_2O): 7.20 (d, 2H, J 7.6, *o*-Ar), 7.29 (t, 1H, J 7.4, *p*-Ar), 7.38 (app. t, 2H, J 7.4, *m*-Ar).

δ_C (100 MHz, D_2O): 126.0 (CH *o*-Ar) 127.95 (CH *p*-Ar), 129.9 (CH *m*-Ar), 133.8 (q Ar), 157.4 (q C=N).

ν_{max} (ATR)/cm^{-1}: 3204 (NH), 3178 (NH), 2240, 1571, 1472, 1365, 954, 418, 237

HRMS (*m/z* ESI^+) $[M+H]^+$ calcd for $C_7H_1N_4$: 151.0982, found 151.0984.

1-Amino-2-(4-methoxyphenyl)guanidine hydrochloride (67b)

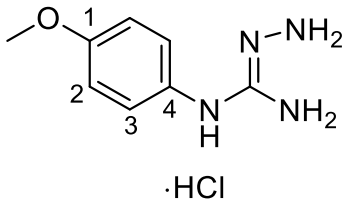

As per *Method A* using aniline **94b** (400 mg, 1.09 mmol) and HCl (3.2 mL, 13.1 mmol, 4M in dioxane), compound **67b** was isolated as a brown coloured gum (176 mg, 76%).

δ_H (400 MHz, D_2O): 3.73 (s, 3H, CH_3), 6.94 (d, 2H, J 8.9, Ar-2), 7.1 (d, 2H, J 8.9, Ar-3).

δ_C (100 MHz, D_2O): 55.6 (CH_3), 115.0 (CH Ar-2) 128.2 (CH Ar-3), 134.3 (q Ar-4), 149.6 (q Ar-1), 152.7 (q C=N).

ν_{max} (ATR)/cm^{-1}: 3341 (NH), 3234 (NH), 2140 (NH), 1572, 1472, 1365, 1156 (C-O), 954.

HRMS (*m/z* ESI^+) $[M+H]^+$ calcd for $C_8H_{13}N_4O$: 181.1089, found 181.1089.

***S*-Methylthiosemicarbazide (84)**

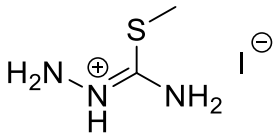

To a solution of thiosemicarbazide **85** (288 mg, 3.0 mmol) in EtOH (3 mL) at rt was added MeI (0.22 mL, 3.6 mmol) dropwise over 5 min. The solution was stirred for 12 h, then the solvent was evaporated under vacuum. The title compound was precipitated out with Et_2O (10 mL), and filtered to give a white solid (595 mg, 91 %). **M.p.** 168-170 °C (lit. 137-139 °C).[250]

δ_H (400 MHz, DMSO-d_6): 2.56 (s, 3H, CH_3), 5.40 (br s, 2H, NH_2), 8.44 (br s, 1H, NH), 8.90 (br s, 2H, NH_2).

***N*-Benzyl-*N*'-phenylthiourea (91)**

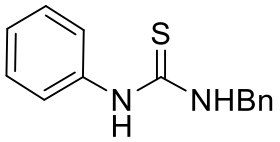

Benzylisothiocyanate (0.80 mL, 1.1 mmol) was dissolved in a solution of aniline (0.65 mL, 1.0 mmol) in EtOH (5 mL) and left to stand for 20 h. Crystallisation was induced by gentle scratching with a pipette. The suspension was then cooled to 0 °C and filtered to give pure cream crystals (1.23 g, 85%). **M.p.** 161-162 °C (lit. 153-154 °C).[163]

δ_H (400 MHz, $CDCl_3$): 4.86 (d, 2H, J 5.4, CH_2), 6.25 (br s, 1H, NH), 7.19 (d, 2H, *o*-Ph), 7.23-7.34 (m, 6H, *p*-Ph, Bn), 7.38 (t, 2H, 7.8, *m*-Ph), 7.95 (bs, 1H, NH).

δ_C (100 MHz, $CDCl_3$): 49.5 (CH_2), 125.3 (CH Ar), 127.4 (CH *p*-Ar), 127.6 (CH Ar), 127.8 (CH *p*-Ar), 128.8 (CH Ar), 130.3 (CH Ar), 135.8 (q Ar), 137.2 (q Ar), 180.9 (q C=S).

ν_{max} (ATR)/cm^{-1}: 3362 (NH), 3140 (NH), 2972 (CH), 1535, 1507, 1297, 1243, 1176, 1068, 1026, 971, 742, 693.

HRMS (*m/z* ESI^-) Found: 241.0797 ($[M+H]^+$. $C_{14}H_{13}N_2S$ Requires 241.0799).

***N*-*tert*-Butoxycarbonyl-*N'*-phenylthiourea (93a)**

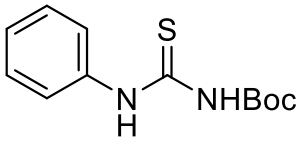

Following *Method F*, using thiourea **96** (1.00 g, 3.62 mmol), and aniline (507 μL, 5.57 mmol) as the amine afforded **93a** as a white crystalline solid (940 mg, 52%). **M.p.** 105 °C.

δ_H (400 MHz, $CDCl_3$): 1.56 (s, 9H, CH_3), 7.29 (1H, t, J 8.0, H-6), 7.42 (2H, t, J 8.0, H-5, H-7), 7.66 (2H, d, J 8.0, H-4, H-8), 8.03 (1H, br s, NH-1') 11.53 (1H, br s, NH-2').

δ_C (100 MHz, $CDCl_3$): 27.6 (CH_3), 83.8 (q $C(CH_3)_3$), 123.8 (CH *m*-Ar) 126.2 (CH *p*-Ar), 128.4 (CH *o*-Ar), 137.2 (q Ar), 151.4 (q C=O), 177.7 (q C=S).

ν_{max} (ATR)/cm^{-1}: 3191 (NH), 3072 (NH), 2954 (CH), 1719 (C=O), 1572, 1530, 1372, 1271, 1214, 1126, 1010, 952, 849, 826, 742, 716.

HRMS (*m/z* ESI^+) $[M+H]^+$ calcd for $C_{12}H_{16}N_2NaOS$: 275.0828, found 275.0825.

***N*-*tert*-Butoxycarbonyl-*N'*-4-methoxyphenylthiourea (93b)**

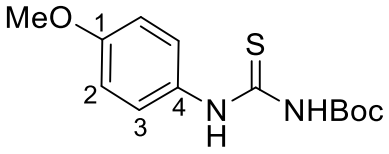

Following *Method F*, using thiourea **96** (1.00 g, 3.62 mmol) and *p*-anisidine (603 mg, 5.57 mmol) as the amine, afforded compound **93b** as a white crystalline solid (780 mg, 78%). **M.p.** 150 °C.

δ_H (400 MHz, $CDCl_3$): 1.54 (s, 9H, CH_3), 3.82 (s, 3H, CH_3), 6.92 (d, 2H, J 8.0, Ar-2), 7.50 (d, 2H, J 8.0, Ar-3), 8.39 (br s, 1H, NHAr), 11.36 (br s, 1H, NHBoc).

δ_C (100 MHz, $CDCl_3$): 28.0 (CH_3), 84.0 (q $C(CH_3)_3$), 113.9 (CH Ar-2) 126.1 (CH Ar-3), 130.7 (q Ar-4), 152.0 (q C=O), 158.1 (q Ar-1), 178.8 (q C=S).

ν_{max} (ATR)/cm^{-1}: 3066 (NH), 2953 (CH), 1690 (C=O), 1538, 1434, 1401, 1316, 1197, 1120, 909, 825, 788, 716, 649.

HRMS (*m/z* ESI^-) $[M-H]^-$ calcd for $C_{13}H_{17}N_2O_3S$: 281.0968, found 281.0960.

***N*-*tert*-Butoxycarbonyl-*N'*-*tert*-butoxycarbonylamino-*N*''-phenylguanidine (94a)**

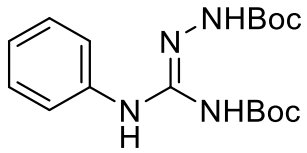

Following *Method G* using compound **93a** as the substituted thiourea (500 mg, 1.98 mmol), Boc-protected hydrazine **98** (262 mg, 1.98 mmol), $HgCl_2$ (591 mg, 2.18 mmol) and Et_3N (6.14 mmol), the title compound was synthesised as a pale yellow amorphous solid (420 mg, 61%).

δ_H (400 MHz, $CDCl_3$): 1.49 (s, 18H, CH_3), 6.07 (br s, 1H, NH), 6.99-7.59 (Signals in this range could not be assigned as they were broad), 7.82 (br s, 1H, NH) 9.22 (br s, 1H, NH).

δ_C (100 MHz, $CDCl_3$): 27.7 (CH_3), 27.8 (CH_3), 80-160 (Signals in this range could not be assigned as they were broad).

υ_{max} (ATR)/cm^{-1}: 3027 (NH), 2953 (NH), 1684 (C=O), 1575, 1525, 1434, 1403, 1381, 1316, 1199, 1119, 1066, 843, 817, 785.

HRMS (*m/z* ESI^+) Found: 351.2032 (M+H, $C_{17}H_{27}N_4O_4$ Requires: 351.2033).

***N*-*tert*-Butoxycarbonyl-*N'*-*tert*-butoxycarbonylamino-*N*''-4-methoxyphenylguanidine (94b)**

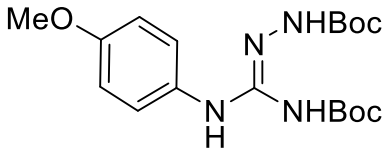

Following *Method G* using compound **93b** as the substituted thiourea (500 mg, 1.77 mmol) Boc-protected hydrazine **98** (262 mg, 1.98 mmol), $HgCl_2$ (592 mg, 2.18 mmol) and Et_3N (856 μL, 6.14 mmol), compound **94b** was synthesized as a pale yellow amorphous solid (450 mg, 57%).

δ_H (400 MHz, $CDCl_3$): 1.47-1.50 (m, 18H, CH_3 Boc), 3.77 (s, 3H, CH_3), 6.20-11.50 (Signals in this range could not be assigned as they were broad).

δ_C (100 MHz, $CDCl_3$): (Signals in this range could not be assigned as they were broad).

υ_{max} (ATR)/cm^{-1}: 3027 (NH), 2977 (NH), 1646 (C=O), 1554, 1511, 1392, 1366, 1381, 1286, 1240, 1147, 1084, 825, 802, 771.

HRMS (*m/z* ESI^+) Found: 381.2138 (M+H, $C_{18}H_{29}N_4O_5$ Requires: 381.2142).

***N,N'*-Di-(*tert*-butoxycarbonyl)thiourea (96)**

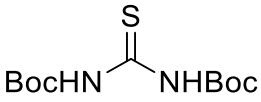

As per *Method E*, using thiourea **95** (2.00 g, 26.3 mmol) NaH (2.84 g, 71 mmol), di-*tert*-butyl dicarbonate (12.6 g, 57.8 mmol) and dry THF (263 mL). The title was purified by recrystallisation from cold hexane to afford white crystals (4.50 g, 62%). **M.p.** 124 °C (lit. 120-122 °C).[125]

δ_H (400 MHz, $CDCl_3$): 1.55 (s, 18H, CH_3), 7.29 (s, 2H, NH).

δ_C (100 MHz, $CDCl_3$): 27.9 (CH_3), 84.2 (q $C(CH_3)_3$), 150.2 (q C=O), 177.7 (q C=S).

ν_{max} (ATR)/cm^{-1}: 3374 (NH), 2977 (CH), 1696, 1628, 1497, 1283, 1164, 1063, 944, 874, 760.

HRMS (*m/z* ESI^-) $[M-H]^-$ calcd for $C_{11}H_{19}N_2O_4S$: 275.1068, found 275.1066.

***N*-*tert*-Butoxycarbonylhydrazine (98)**

Di-*tert*-butyl dicarbonate (5.0 g, 22 mmol) was dissolved in dry THF (3 mL). This solution was then added dropwise to hydrazine (24.2 mL, 24.2 mmol, 1 M in THF) at 0 °C under Ar. After stirring at rt for 2h, the solvent was removed under vacuum and recrystallised from hexane as white crystals (2.00 g, 72%). **M.p.** 40-42 °C (lit. 36-37 °C).[251]

δ_H (400 MHz, $CDCl_3$): 1.47 (s, 9H, CH_3), 1.58 (s, 2H, NH_2), 6.20 (bs, 1H, NH).

HRMS (*m/z* ESI^+) Found: 133.0977 (M+H, $C_5H_{13}N_2O_2$ Requires: 133.0977).

***N*,*N*'-Di-*tert*-butoxycarbonylaminothiocarbonyl(4,4'-oxydianiline) (99a)**

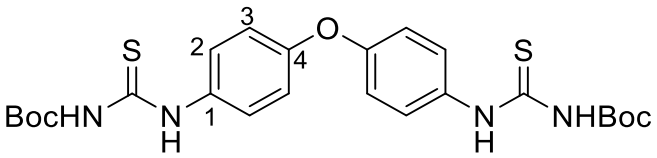

Following *Method H*, using thiourea **96** (1.11 g, 4.0 mmol), NaH (318 mg, 8.0 mmol, 60% in mineral oil), TFAA (0.6 mL, 1.8 mmol), and 4,4' oxydianiline (181 mg, 0.92 mmol) in dry THF (15 mL), compound **99a** was synthesised as a pale yellow powder (88 mg, 67%). **M.p.** 160-163 °C.

δ_H (400 MHz, $CDCl_3$): 1.53 (s, 18H, CH_3), 7.03 (d, 4H, J 8.8, Ar-3), 7.58 (d, 4H, J 8.8, Ar-2), 8.03 (s, 2H, NHAr), 11.44 (s, 2H, NHBoc).

δ_C (100 MHz, $CDCl_3$): 27.9 (CH_3), 84.4 (q $C(CH_3)_3$), 119.1 (CH Ar-3), 126.0 (CH Ar-2), 133.1 (q Ar-1), 151.9 (q Ar-4), 155.3 (q C=O), 178.6 (q C=S).

ν_{max} (ATR)/cm^{-1}: 3188 (NH), 2924 (CH), 2883, 1710, 1619, 1574, 1524, 1497, 1366, 1320, 1252, 1229, 1142, 1047, 1015, 954, 875, 847, 819, 771, 725.

HRMS: (m/z ESI^+): Found: 519.1751 (M+H, $C_{24}H_{31}N_4O_5S_2$ Requires : 519.1736)

***N*',*N*''-Di-*tert*-butoxycarbonylaminothiocarbonyl(4,4'-iminodianiline) (99b)**

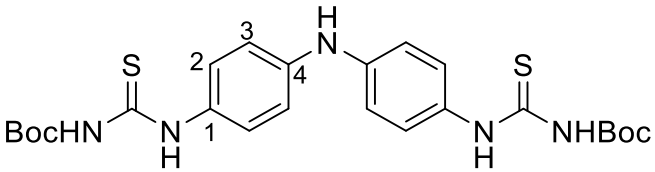

Following *Method H*, using thiourea **96** (1.11 g, 4.0 mmol), NaH (318 mg, 8.0 mmol, 60% in mineral oil), TFAA (0.6 mL, 1.8 mmol), and aniline **5d** (109 mg, 0.55 mmol) in dry THF (15 mL), compound **99b** was synthesized as a brown powder (241 mg, 85%). **M.p.** 70-72 °C.

δ_H (400 MHz, $CDCl_3$): 1.53 (s, 18H, CH_3), 7.07 (d, 4H, J 8.7, Ar-3), 7.48 (d, 4H, J 8.7, Ar-2), 7.98 (br s, 2H, NH), 11.35 (br s, 2H, NH).

δ_C (100 MHz, $CDCl_3$): 28.1 (CH_3), 84.3 (q $C(CH_3)_3$), 117.9 (CH Ar-3), 128.9 (CH Ar-2), 131.1 (q Ar-4), 141.5 (q Ar-1), 152.0 (q C=O), 178.4 (q C=S).

ν_{max} (ATR)/cm^{-1}: 3200 (NH), 2925 (CH), 1709 (C=O), 1606, 1499, 1438, 1334, 1366, 1308, 1252, 1136, 1013, 1044, 817.

HRMS (*m/z* ESI^+) Found: 540.1722 ($[M+Na]^+$. $C_{24}H_{31}N_5O_4S_2Na$ Requires 540.1722).

***N,N'*-Di-*tert*-butoxycarbonylaminothiocarbonyl(4,4'-methylenedianiline) (99c)**

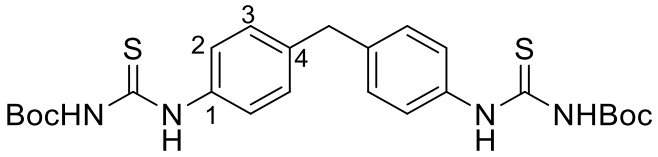

Following *Method H*, using thiourea **96** (1.11 g, 4.0 mmol), NaH (318 mg, 8.0 mmol, 60% in mineral oil), TFAA (0.6 mL, 1.8 mmol), and 4,4'-diaminodiphenylmethane (181 mg, 0.92 mmol) in dry THF (15 mL), compound **99c** was synthesized as a white powder (81 mg, 44%). **M.p.** 85-87 °C.

δ_H (400 MHz, $CDCl_3$): 1.50 (s, 18H, CH_3), 3.95 (s, 2H, CH_2), 7.17 (d, 4H, J 8.4, Ar-3), 7.52 (d, 4H, J 8.4, Ar-2), 8.37 (br s, 2H, NHAr), 11.47 (br s, 2H, NHBoc).

δ_C (100 MHz, $CDCl_3$): 27.9 (CH_3), 40.6 (CH_2), 83.7 (q $C(CH_3)_3$), 124.1 (CH Ar-2), 128.9 (CH Ar-3), 135.5 (q Ar-4), 138.8 (q Ar-1) , 156.2 (q C=O), 178.1 (q C=S).

ν_{max} (ATR)/cm^{-1}: 3179 (NH), 2987 (CH), 1702 (C=O), 1604, 1502, 1365, 1250, 1137, 1016, 1046, 850, 762.

HRMS (m/z ESI^+): Found: 539.1766 (M+Na, $C_{25}H_{32}N_4O_4S_2Na$ Requires : 539.1763).

***N,N'*-Di-*tert*-butoxycarbonylaminothiocarbonyl(4,4'-carbonyldianiline) (99d)**

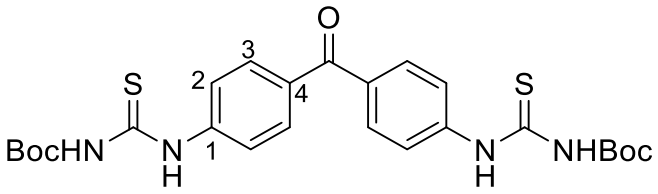

Following *Method H*, using thiourea **96** (1.11 g, 4.0 mmol), NaH (318 mg, 8.0 mmol, 60% in mineral oil), TFAA (0.6 mL, 1.8 mmol), and 4,4'-diaminodiphenylmethane (181 mg, 0.92 mmol) in dry THF (15 mL), the title compound was synthesised as a white powder (76, 16%). **M.p.** 160-163 °C.

δ_H (400 MHz, $CDCl_3$): 1.46 (s, 18H, CH_3), 7.86 (d, 4H, J 8.7, Ar-2), 7.90 (d, 4H, J 8.7, Ar-3), 8.34 (br s, 2H, NHAr) , 11.87 (br s, 2H, NHBoc).

δ_C (100 MHz, $CDCl_3$): 28.0 (CH_3), 84.6 (q $C(CH_3)_3$), 122.9 (CH Ar-2), 130.9 (CH Ar-3), 135.0 (q Ar-1), 141.5 (q Ar-4), 152.1 (q C=O Boc), 178.0 (q C=S), 194.4 (q C=O).

ν_{max} (ATR)/cm^{-1}: 3177 (NH), 2924 (CH), 2851, 1706 (C=O), 1589, 1519, 1368, 1324, 1251, 1134, 1011, 929, 845, 766, 671.

HRMS: (m/z ESI⁻): Found: 529.1581 (M-H, $C_{25}H_{29}N_4O_5S_2$ Requires: 529.1579)

***Bis*-(4-nitrophenyl)amine (103)**

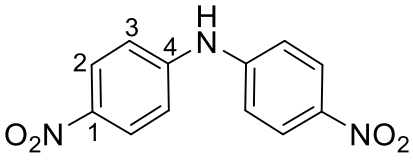

A mixture of 4-nitroaniline **101** (691 mg, 0.5 mmol) and 1-fluoro-4-nitrobenzene **102** (0.53 mL, 0.5 mmol) were dissolved in DMSO (15 mL). Potassium *tert*-butoxide (1.178 g, 1.05 mmol) was then added to the solution. The mixture was stirred under Ar for 3 d at rt, and was then poured onto water (20 mL) which changed the colour from green to yellow. The mixture was then extracted using CH_2Cl_2 (3 x 20 mL) and the combined extracts were washed with brine (3 x 20 mL). The solvent was then removed under vacuum. Product was purified by

recrystallisation from methanol and afforded a yellow/brown powder (880 mg, 67%). **M.p.** (lit. 217-218 °C).[166]

δ_H (400 MHz, $CDCl_3$): 7.21 (d, 4H, J 7.7, Ar-3), 8.23 (d, 4H, J 7.7, Ar-2).

HRMS: (m/z ESI⁻): Found: 258.0516 (M-H, $C_{12}H_8N_3O_4$ Requires: 258.0516).

***N,N'*-Di-*tert*-butoxycarbonylamino(*tert*-butoxycarbonylhyrazino)methine(4,4'-carbonyldianiline) (100)**

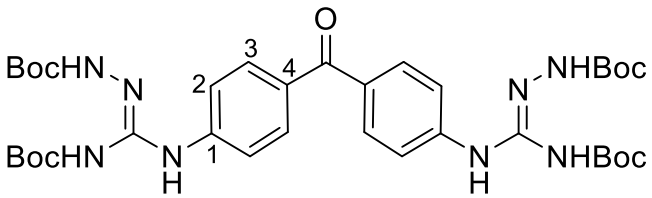

To a solution of thiourea **99d** (65 mg, 0.122 mmol) and NEt_3 (0.12 mL, 0.406 mmol), in CH_2Cl_2 (0.5 mL), Boc-hydrazine **98** (32.2 mg, 0.244 mmol) was added. The reaction mixture was cooled to 0 °C and $CuCl_2$ (16 mg, 0.127 mg) was added. The reaction was stirred at rt for 16 h and then diluted with EtOAc (20 mL). After filtration through Celite® the mixture was washed with H_2O (20 mL) and extracted with EtOAc (3 x 20 mL). The combined organic extracts were washed with brine (15 mL) and dried over $MgSO_4$. The compound was purified by chromatography on silica, eluting in a gradient of EtOAc in hexane as a brown/yellow oil (14 mg, 21%).

δ_H (400 MHz, $CDCl_3$): 1.40 (s, 18H, CH_3), 1.80 (s, 18H, CH_3), 7.63 (d, 4H, J 8.7, Ar-2), 7.79 (d, 4H, J 8.7, Ar-3), 10.16 (br s, 2H, NH), 10.61 (br s, 2H, NH), 11.63 (br s, 2H, NH).

δ_C (100 MHz, $CDCl_3$): 27.8 (CH_3), 29.5 (CH_3), 83.0 (q $C(CH_3)_3$), 83.5 (q $C(CH_3)_3$), 118.6 (CH Ar-2), 120.7 (CH Ar-3), 131.0 (q Ar-1), 132.7 (q Ar-4), 140.8 (q), 148.4 (q), 149.9 (q), 152.8 (q).

ν_{max} (ATR)/cm^{-1}: 3280 (NH), 2926 (CH), 2653, 1799 (N-N), 1717 (C=O), 1607, 1590, 1530, 1479, 1368, 1306, 1234, 1136, 1057, 929, 845, 807, 768, 735, 680.

Diethyl di(4(*N*,*N'*-Di(*tert*-butoxycarbonyl)imidazolidine-2-ylideneamino)phenyl)methylenemalonate (109)

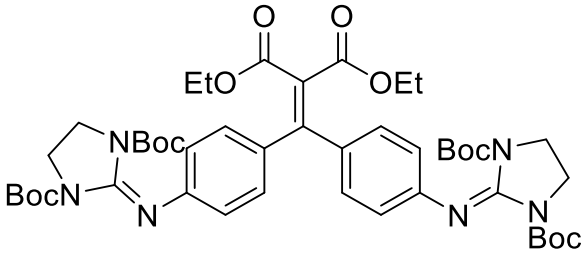

As per *Method* I, using diamine **110** (540 mg, 1.52 mmol), thione **111** (842 mg, 3.05 mmol), Et_3N (1.49 mL, 10.67 mmol), $HgCl_2$ (1.304 g, 3.81 mmol) and DMF (5.6 mL), gave the title compound as a yellow solid (615 mg, 45%). **M.p.** 91 °C.

δ_H (400 MHz, $CDCl_3$): 1.12 (t, 6H, 7.1 Hz, CH_3), 1.36 (s, 36H, CH_3), 3.83 (br s, 8H, CH_2), 4.07 (q, 4H, J 7.1, CH_2), 6.88 (d, 4H, J 8.5, Ar), 7.04 (d, 4H, 8.5 Hz, Ar).

δ_C (100 MHz, $CDCl_3$): 13.8 (CH_3), 27.9 (Boc CH_3), 43.1 (N-CH_2), 60.9 (CH_2), 82.9 ($C(CH_3)$), 120.9 (CH Ar), 123.8 (q C), 130.44 (CH Ar), 134.4 (q C), 139.3 (q C), 149.3 (q C), 150.1 (q C),155.4 (q C), 166.5 (q C).

ν_{max} (ATR)/cm^{-1}: 2978, 1757, 1702, 1596, 1366, 1297, 1230, 1143, 1071, 974, 845, 767.

HRMS (*m/z* APCI$^+$) Found: 891.4466 ($[M+H]^+$. $C_{46}H_{63}N_6O_2$ Requires 891.4498).

Diethyl di(4-aminophenyl)methylenemalonate (110)

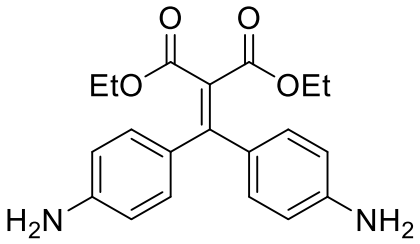

In a Schlenk tube, dibromide **124** (900 mg, 1.9 mmol), CuI (143 mg, 0.75 mmol), *trans*-4-hydroxyproline (197 mg, 1.5 mmol) and K_2CO_3 (1.56 g, 11 mmol) were evacuated and backfilled with Ar. To this, under Ar, were added dry DMSO (3.8 mL) and NH_4OH (1.9 mL, 35% aq. soln.). The Schlenk tube was sealed, covered in aluminium foil and submerged in an oil bath at 50 °C and stirred for 3 d. The reaction mixture was partitioned between EtOAc (50 mL) and H_2O (20 mL), separated and the aqueous layer was re-extracted with EtOAc (7 x 30 mL).The combined organic layers were washed with H_2O (5 x 20 mL) and brine (2 x 20 mL) and dried over Na_2SO_4. The solvent was evaporated and the product was purified by flash chromatography on silica, eluting in 5% EtOAc in petroleum ether followed by recrystallisation from $CHCl_3$ to give a yellow solid (320 mg, 48%). **M.p.** 84-85 °C.

δ_H (400 MHz, $CDCl_3$): 1.09 (t, 6H, 7.1 Hz, CH_3), 3.82 (br s, 4H, N-H), 4.09 (q, 4H, 7.1 Hz, CH_2), 6.56-6.60 (m, 4H, Ar), 6.98-7.01 (m, 4H, Ar).

δ_C (100 MHz, $CDCl_3$): 13.8 (CH_3), 60.8 (CH_2), 114.1 (CH Ar), 121.6, (q C), 130.5 (q C), 131.5 (CH Ar), 147.8 (q Ar), 157.3 (q C), 167.3 (q Ar).

ν_{max} (ATR)/cm^{-1}: 2982, 1728, 1487, 1235, 1161, 1068, 1007, 835.

HRMS (*m/z* APCI$^-$) Found: 353.1542 ([M-H]$^-$. $C_{20}H_{21}N_2O_4$ Requires 353.1507).

***N,N'*-Di(*tert*-butoxycarbonyl)imidazolidine-2-thione (111)**

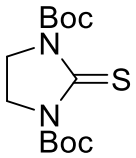

As per *Method E*, using NaH (60% in mineral oil, 3.75 g, 93.7 mmol) imidazolidine-2-thione (2.11 g, 20.7 mmol) and di-*tert*-butyldicarbonate (9.94 g, 45.6 mmol) in dry THF (300 mL), after recrystallisation from hexane:EtOAc (4:1), afforded the title compound as yellow needles (5.23 g, 91% yield). **M.p.** 123 °C (lit. 117-119 °C).[210]

δ_H (400 MHz, $CDCl_3$): 1.54 (s, 18H, CH_3), 3.90 (s, 4H, CH_2).

***4,4'*-Di[*N,N*'-*bis*(*tert*-butoxycarbonyl)imidazolidine-2-imine]benzophenone (114)**

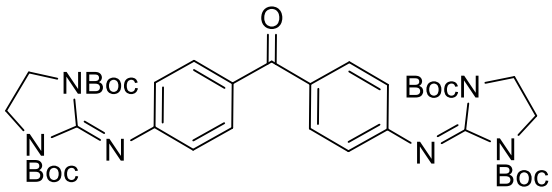

As per *Method* I, using diamine **110** (159 mg, 0.75 mmol), thione **111** (470 mg, 1.56 mmol), Et_3N (0.73 mL, 5.25 mmol), $CuCl_2$ (211 mg, 1.57 mmol) and DMF (4 mL), gave the title compound as a white solid (245 mg, 44%). **M.p.** 86-88 °C (lit. 106-108 °C).[210]

δ_H (400 MHz, $CDCl_3$): 1.38 (s, 36H, CH_3), 3.88 (s, 8H, CH_2), 7.04 (d, 4H, J 8.4, Ar), 7.71 (d, 4H, J 8.4, Ar).

***Bis*(4-fluorophenyl)chloromethane (120)**

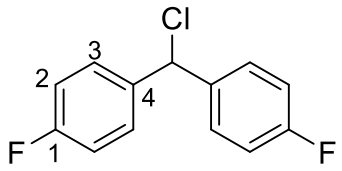

To a mixture of alcohol **121** (83.5 mg, 0.379 mmol) in conc. HCl (1 mL), was added $CaCl_2$ (58 mg, 0.547 mmol) at rt. The reaction was heated to 100 °C for 10 h and then cooled to rt. The solution was extracted with EtOAc (2 × 30 mL), washed with brine (20 mL) and dried over Na_2SO_4 to give the title compound as a clear liquid (89 mg, 98 %) which was used without further purification.[172]

δ_H (400 MHz, $CDCl_3$): 6.10 (s, 1H, CHCl), 6.99-7.08 (m, 4H, Ar-2), 7.33-7.39 (m, 4H, Ar-3).

δ_C (100 MHz, $CDCl_3$): 62.7 (CHCl), 115.5 (CH Ar-2), 129.5 (CH Ar-3), 136.8 (q Ar-4), 162.4 (q Ar-1).

δ_F (376 MHz, $CDCl_3$): -113.69 - -113.60 (m).

***Bis*(4-fluorophenyl)methanol (122)**

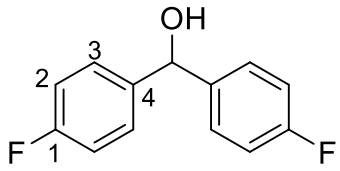

To a stirred solution of 4,4'-difluorobenzophenone **119** (1.0 g, 4.58 mmol), in MeOH (10 mL) was added portionwise $NaBH_4$ (0.26 g, 6.88 mmol) at 0 °C. The suspension was stirred for 2 h at rt and when reaction was complete (as adjudged by TLC) the mixture was quenched with crushed ice (*ca.* 20 mL). MeOH was removed under vacuum and the mixture was extracted with EtOAc (2 × 30 mL), washed with brine (20 mL), dried over Na_2SO_4 and purified by flash chromatography on silica, eluting in a 4:1 EtOAc/ hexane mixture to give the title compound as a clear liquid (946 mg, 94 %).[172]

δ_H (400 MHz, $CDCl_3$): 2.26 (s, 1H, CH), 5.81 (br s, 1H, OH), 6.99-7.06 (m, 4H, Ar-2), 7.29-7.35 (m, 4H, Ar-3).

δ_C (101 MHz, $CDCl_3$): 74.9 (CHOH), 115.4 (CH Ar-2), 128.1 (CH Ar-3), 139.4 (q Ar-4), 162.2 (q Ar-1).

δ_F (376 MHz, $CDCl_3$): -114.79 - -114.69 (m).

Diethyl di(4-bromophenyl)methylenemalonate (124)

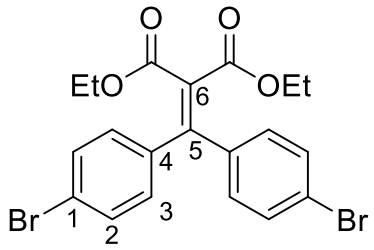

To a solution of freshly distilled diisopropylamine (2.37 mL, 16.82 mmol) in dry THF (30 mL) under Ar at -78 °C, was added n-butyllithium (6.73 mL, 16.82 mmol, 2.5 M in hexanes) and stirred for 10 min. A solution of unsaturated ester **128** (2.30 g, 5.61 mmol) in dry THF (15 mL) was added dropwise and stirred at -78 °C for 10 min. The organolithium intermediate was added over 15 min to a solution of ethyl chloroformate (1.07 mL, 11.22 mmol) in dry Et_2O (30 mL) at 0 °C and warmed to rt over 10 min. The reaction was quenched sequentially with CH_3CH_2OH (1 mL) and H_2O (0.5 mL) and evaporated to dryness. The crude product was purified by silica gel chromatography, in a gradient of 2% EtOAc to 4% EtOAc in hexanes to give an orange liquid (1.732 g, 64 %).

δ_H (400 MHz, $CDCl_3$): 1.09 (t, 6H, 7.1 Hz), 4.11 (q, 4H, 7.1 Hz), 7.04 (d, 4H, J 8.5, Ar), 7.47 (d, 4H, J 8.5, Ar).

δ_C (100 MHz, $CDCl_3$): 13.7 (CH_3), 61.5 (CH_2), 123.9 (q C), 127.0 (q Ar), 130.6 (CH Ar), 131.52 (CH Ar), 138.35 (q C), 153.0 (q C) 165.4 (q CO).

ν_{max} (ATR)/cm^{-1}: 2981 (CH), 1727, 1390, 1364, 1231, 1160, 1067, 1006, 834, 710.

HRMS (*m/z* ESI^+) Found: 502.9465 ($[M+Na]^+$. $C_{20}H_{18}O_4Br_2Na$ Requires 502.9470).

Ethyl 3,3-di(4-bromophenyl)propenoate (128)

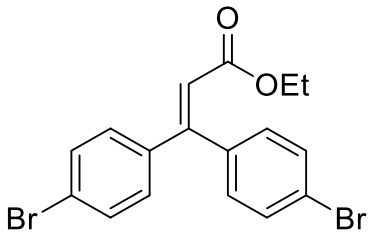

To a suspension of $Pd(OAc)_2$ (60 mg, 0.25 mmol) and Ag_2O (6.75 g, 27.5 mmol) in HOAc (76 mL) at rt was added 1-bromo-4-iodobenzene (22.21 g, 77.5 mmol) and freshly distilled ethyl acrylate (2.66 mL, 25.0 mmol). The mixture was heated to 110 °C and stirred vigorously for 17 hours, then cooled to rt, diluted with Et_2O and filtered through a pad of Celite. The solution evaporated under vacuum and purified on a column of silica, eluting in 2% petroleum ether in EtOAc as a yellow oil (9.97 g, 97%).

δ_H (400 MHz, $CDCl_3$): 1.15 (t, 3H, J 7.1, CH_3), 4.07 (q, 2H, J 7.1, CH_2), 6.34 (s, 1H, CH), 7.07 (d, 2H, J 8.4, Ar), 7.13 (d, 2H, J 8.6, Ar), 7.45 (d, 2H, J 8.6, Ar), 7.51 (d, 2H, J 8.4, Ar).

HRMS (*m/z* $APCI^+$) Found: 410.9372 ($[M+H]^+$. $C_{14}H_{26}Br_2O_2$ Requires 410.9413).

Diethyl di(4-(*N*-*tert*-butoxycarbonyl)aminophenyl)methylenemalonate (138)

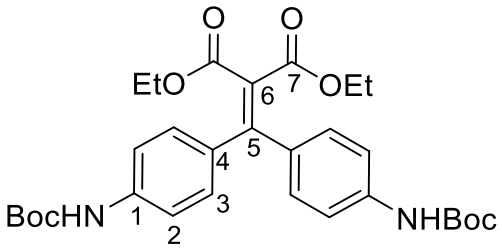

As per *Method J*, using $Pd(OAc)_2$ (13 mg, 0.07 mmol), Xphos (82 mg, 0.17 mmol), Cs_2CO_3 (876 mg, 2.69 mmol), *tert*-butyl carbamate (236 mg, 2.02 mmol) and dibromide **124** (461 mg, 0.96 mmol) in 1,4-dioxane (7.7 mL), after flash chromatography on silica, eluting in 4:1 EtOAc/hexane gave the title compound as a yellow solid (217 mg, 41%). **M.p.** 139 °C.

δ_H (600 MHz, $CDCl_3$): 1.09 (t, 6H, J 7.1, CH_3), 1.51 (s, 18H, CH_3 Boc), 4.09 (q, 4H, J 7.1, CH_2), 6.52 (br s, 2H, NH), 7.10 (d, 4H, J 8.5, Ar-3), 7.31 (d, 4H, J 8.5, Ar-2).

δ_C (150 MHz, $CDCl_3$): 13.8 (CH_3), 28.3 (CH_3 Boc), 61.2 (CH_2), 80.9 (q $C(CH_3)_3$) 117.6 (CH Ar-2), 124.7 (q C-6), 130.6 (CH Ar-3), 134.6 (q Ar-4), 139.6 (q Ar-1), 152.4 (q C=O Boc), 155.1 (q C-5), 166.4 (q C-7).

ν_{max} (ATR)/cm^{-1}: 3363 (NH), 2981 (CH), 1702, 1599, 1508, 1436, 1369, 1328, 1284, 1231, 1155, 1078, 1019, 834, 774.

HRMS (*m/z* APCI$^-$) Found: 553.2693 ($[M-H]^-$. $C_{30}H_{37}N_2O_4$ Requires 553.2555).

Diethyl di(4-(imidazolidine-2-ylideneamino)phenyl)methylenemalonate dihydrochloride (139)

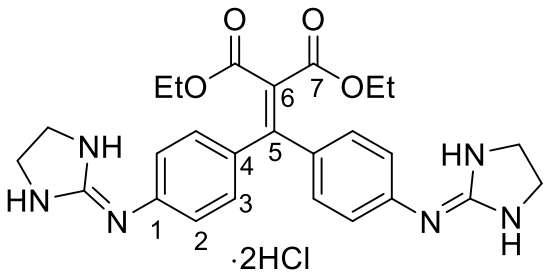

As per *Method A*, using Boc-protected compound **109** (528 mg, 0.593 mmol), dry HCl (3.56 mL, 14.2 mL, 4 M in dioxane) and CH_2Cl_2 (0.5 mL), following purification in reverse phase silica (C-18), eluting in 100% H_2O, gave the title compound as a yellow solid (330 mg, 99%). **M.p.** 68-69 °C.

δ_H (400 MHz, D_2O): 1.12 (t, 6H, J 7.1, CH_3), 3.80 (s, 8H, CH_2), 4.19 (q, 4H, J 7.1, CH_2), 7.25-7.34 (m, 8H, Ar).

δ_C (100 MHz, D_2O): 12.8 (CH_3), 42.7 (N-CH_2), 63.2 (CH_2), 123.4 (CH Ar-2), 125.2 (q C-6), 130.7 (CH Ar-3), 137.0 (q Ar-1), 137.1 (q Ar-4), 156.7 (q C-5), 158.2 (q C=N), 167.5 (q C-7).

ν_{max} (ATR)/cm^{-1}: 3152, 2980, 1709, 1648, 1598, 1510, 1367, 1232, 1162, 1077, 1014, 843.

HRMS (*m/z* ESI^+) Found: 491.2403 ($[M+H]^+$. $C_{26}H_{31}N_6O_4$ Requires 491.2407).

RP-HPLC (254 nm): t_R= 25.0 min, purity >99%.

Diethyl di(4-(imidazolidine-2-ylideneamino)phenyl)methylmalonate dihydrochloride (140)

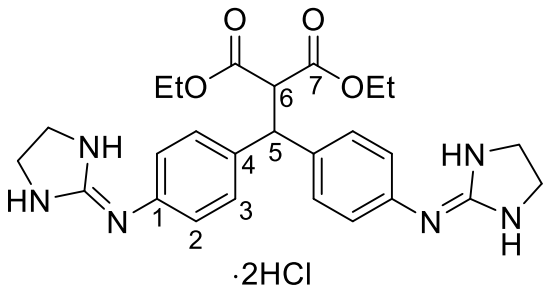

To a solution of **139** (19 mg, 0.0337 mmol) in MeOH (0.5 mL) under Ar, was added 10 % Pd/C (19 mg, 100% w/w). The mixture was put under H_2 (20 atm) and stirred vigorously for 14 h. The mixture was then diluted with MeOH (10 mL), filtered through two layers of filter paper and concentrated. The mixture was purified by passing through a column of reverse phase silica (C-18) to afford the title compound as a colourless gum (13 mg, 67%).

δ_H (400 MHz, D_2O): 1.08 (t, 6H, 7.1 Hz, CH_3), 3.75 (s, 8H, CH_2), 4.09 (q, 4H, 7.1 Hz, CH_2), 4.68 (d, 1H, 12.4 Hz, CH-6), 4.78 (d, 1H, J 12.4, CH-5), 7.27 (d, 4H, J 8.5, Ar-3), 7.52 (d, 4H, J 8.5, Ar-2).

δ_C (100 MHz, D_2O): 12.9 (CH_3), 42.6 (N-CH_2), 50.0 (CH-6), 56.6 (CH-5), 63.1 (CH_2), 124.7 (CH Ar-3), 129.0 (CH Ar-2), 134.3 (q Ar), 139.7 (q Ar), 158.6 (q C=N), 169.5 (q C=O).

HRMS (*m/z* ESI^+) Found: 493.2569 ($[M+H]^+$. $C_{26}H_{33}N_6O_4$ Requires 493.2563).

RP-HPLC (254 nm): t_R= 24.9 min, purity >98%.

Lithium di(4-(imidazolidine-2-ylideneamino)phenyl)methylenemalonate (141)

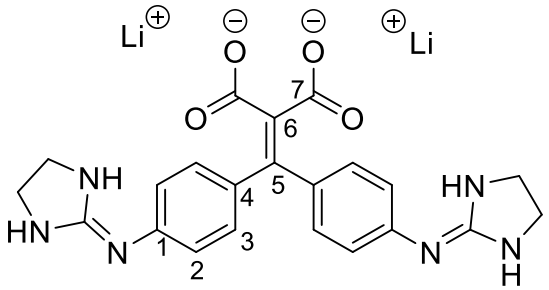

As per *Method K*, using diester **139** (70 mg, 0.124 mmol) and $LiOH \cdot H_2O$ (26 mg, 0.87 mmol) in a 1:1 EtOH/H_2O (1 mL), gave the title compound as a grey gum, which was used without further purification.

δ_H (400 MHz, D_2O): 3.48 (s, 8H, CH_2), 6.92 (d, 4H, 7.6 Hz, Ar-2), 7.16 (d, 4H, 7.6 Hz, Ar-3).

δ_C (150 MHz, D_2O): 42.2 (CH_2), 122.6 (CH Ar-2), 130.3 (CH Ar-3), 136.3 (q Ar-4), 138.1 (q C-6), 139.9 (q Ar-5), 147.9 (q C-1), 161.2 (q C=N), 175.8 (q C-7).

ν_{max} (ATR)/cm^{-1}: 3308 (NH), 2903 (CH), 1650, 1598, 1509, 1443, 1400, 1363, 1241, 1086, 860.

HRMS (*m/z* ESI^+) Found: 435.1797 ($[M+3H]^+$. $C_{22}H_{23}N_6O_4$ Requires 435.1781).

Lithium di(4-(imidazolidine-2-ylideneamino)phenyl)methylmalonate (143)

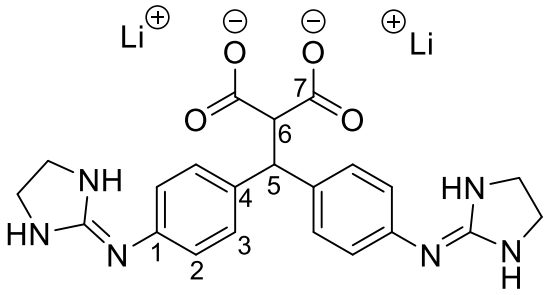

As per *Method K*, using diester **1140** (13 mg, 0.023 mmol) and $LiOH \cdot H_2O$ (7 mg, 0.16 mmol) in a 1:1 $EtOH/H_2O$ (1 mL), gave the title compound, which was used without further purification. **M.p.** 260 °C.

δ_H (400 MHz, D_2O): 3.45 (s, 8H, CH_2), 4.07 (d, 1H, J 12.2, CH), 4.50 (d, 1H, J 12.2, CH), 6.89 (d, 4H, J 8.4, Ar), 7.30 (d, 4H, J 8.4, Ar).

δ_C (150 MHz, D_2O): 42.7 (CH_2), 48.8 (CH), 123.9 (CH Ar-2), 130.4 (CH Ar-3), 135.2 (q C-1), 139.3 (q C-4), 143.2 (q C-7), 158.6 (q C=N).

ν_{max} (ATR)/cm^{-1}: 3307 (NH), 2943 (CH), 1654 (C=O), 1420, 1260, 1086, 1017, 860.

HRMS (*m/z* ESI^+) Found: 437.1941 ($[M+3H]^+$. $C_{22}H_{25}N_6O_4$ Requires 437.1937).

Diethyl 3,6-*bis*(imidazolidine-2-ylideneamino)-9*H*-fluoren-9-ylidenemalonate dihydrochloride (145)

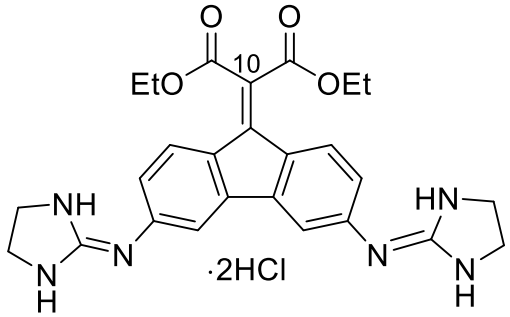

As per *Method A*, using Boc-protected compound **176** (353 mg, 0.397 mmol), dry HCl (2.38 mL, 9.53 mmol, 4 M in dioxane) and CH_2Cl_2 (1 mL), and following purification in reverse phase silica (C-18), eluting in 100% H_2O, gave the title compound as a yellow gum (234 mg, 98%).

δ_H (400 MHz, D_2O): 1.37 (t, 6H, 6.2 Hz, CH_3), 3.82 (s, 8H, CH_2) 4.43 (q, 4H, 6.2 Hz, CH_2), 6.80 (d, 2H, J 8.2, Ar-1 & Ar-8), 7.06 (s, 2H, Ar-4 & Ar-5), 7.34 (d, 2H, J 8.2, Ar-2 & Ar-7).

δ_C (100 MHz, D_2O): 13.1 (CH_3), 42.7 (CH_2 Im), 63.6 (CH_2), 112.4 (CH Ar-4 & Ar-5), 120.5 (CH Ar-1 & Ar-8), 121.1 (q C-10), 126.9 (CH Ar-2 & Ar-7), 131.9 (q Ar-8a & Ar-9a), 137.9 (q Ar-4a & Ar-4b) , 141.6 (q Ar-3 & Ar-4), 142.3 (q C-9), 156.9 (q C=N), 166.1 (q C=O) ppm.

ν_{max} (ATR)/cm^{-1}: 3164 (NH), 2981 (CH), 2900 (CH), 1716 (C=O), 1648, 1578, 1468, 1225, 1173, 1075, 1015, 831.

HRMS (*m/z* ESI^+) Found: 489.2240 ($[M+H]^+$. $C_{26}H_{29}N_6O_4$ Requires 489.2250).

RP-HPLC (254 nm): t_R= 21.1 min, purity >99%.

3,6-*Bis*(imidazolidine-2-ylidineamino)-9*H*-fluorene dihydrochloride (146)

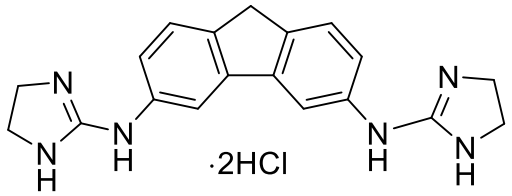

As per *Method A*, using Boc-protected compound **175** (53 mg, 0.072 mmol), dry HCl (0.43 mL, 1.74 mmol, 4 M in dioxane) and CH_2Cl_2 (0.5 mL), and following purification in reverse phase silica (C-18), eluting in 100% H_2O, gave the title compound as a yellow gum (26 mg, 89%).

δ_H (400 MHz, D_2O): 3.75 (s, 8H, CH_2), 3.95 (d, 2H, CH_2-9), 7.25 (d, 2H, 8.0 Hz, Ar-2 & Ar-7), 7.66 (d, 2H, 8.0 Hz, Ar-1 & Ar-8), 7.72 (s, 2H, Ar-4 & Ar-5).

δ_C (150 MHz, D_2O): 36.0 (CH_2-9), 42.8 (CH_2), 116.5 (CH Ar-4 & Ar-5), 123.9 (CH Ar-2 & Ar-7), 126.5 (CH Ar-1 & Ar-8), 134.1 (q Ar-3 & Ar-6), 141.9 (q Ar-8a & Ar-9a), 143.5 (q Ar-4a & Ar-4b), 159.1 (qC=N).

HRMS (*m/z* ESI^+) Found: 333.1823 ($[M+H]^+$. $C_{19}H_{21}N_6$ Requires 333.1828).

RP-HPLC (254 nm): t_R= 26.0 min, purity >95%.

Diethyl 3,6-diamino-9*H*-fluoren-9-ylidenemalonate (150)

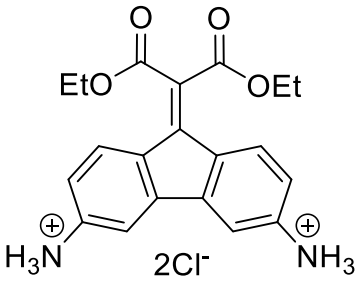

As per *Method A*, using Boc-protected compound **174** (86 mg, 0.156 mmol), dry HCl (0.3 mL, 1.2 mmol, 4 M in dioxane) and CH_2Cl_2 (0.2 mL), without further purification, gave the title compound as a brown solid (50 mg, 89%). **M.p.** 138 °C.

δ_H (400 MHz, D_2O): 1.27 (t, 6H, 7.1 Hz, CH_3), 4.33 (q, 4H, 7.1 Hz, CH_2), 6.70 (d, 2H, 8.4 Hz, Ar-1 & Ar-8), 7.08 (s, 2H, Ar-4 & Ar-5), 7.56 (d, 2H, 8.4 Hz, Ar-2 & Ar-7).

δ_C (150 MHz, D_2O): 14.2 (CH_3), 61.8 (CH_2), 105.4 (q C-10), 107.1 (Ar-4 & Ar-5), 115.7 (CH, Ar-1 & Ar-8), 120.1 (q C-9), 127.8 (Ar-2 & Ar-7), 140.3 (q Ar-4a & Ar-4b), 143.2 (q Ar-8a & Ar-9a), 148.6 (q Ar-3 & Ar-6), 166.3 (q C=O).

ν_{max} (ATR)/cm^{-1}: 3367 (NH), 2814 (CH), 2592, 1734 (C=O), 1719, 1687, 1556, 1525, 1498, 1230, 1068, 878, 833, 780.

HRMS (*m/z* APCI$^-$) Found: 351.1374 ([M-H]$^-$. $C_{20}H_{19}N_2O_4$ Requires 351.1350).

3,6-Diamino-9*H*-fluorene dihydrochloride (153)

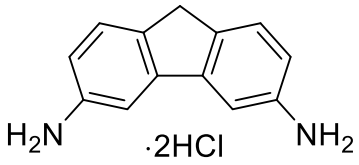

As per *Method A*, using Boc-protected compound **134** (261 mg, 0.658 mmol), dry HCl (0.3 mL, 1.2 mmol, 4 M in dioxane) and CH_2Cl_2 (0.2 mL), without further purification, gave the title compound as a brown gum (170 mg, 96%).

δ_H (400 MHz, DMSO-*d_6*): 4.04 (s, 2H, CH_2-9), 7.41 (dd, 2H, J 1.8, J 8.0, Ar-2 & Ar-7), 7.74 (d, 2H, J 8.0, Ar-1 & Ar-8), 7.92 (d, 2H, J 1.8 & Ar-4, Ar-5), 10.34 (br s, 6H, NH_3).

δ_C (150 MHz, DMSO-*d_6*): 36.4 (CH_2), 115.3 (CH Ar-4 & Ar-5), 122.7 (CH Ar-2 & Ar-7), 127.0 (CH Ar-1 & Ar-8), 131.8 (q Ar-3 & Ar-6), 141.6 (q Ar-4a & 4b), 143.7 (q Ar-8a & Ar-9a).

3,6-Diaminofluoren-9-one
(154)

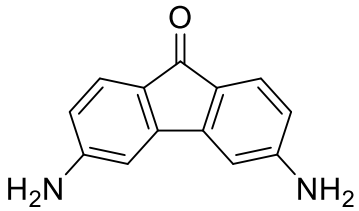

As per *Method A*, using Boc-protected compound **168** (48 mg, 0.11 mmol), dry HCl (0.35 mL, 1.39 mmol, 4M in dioxane) and CH_2Cl_2 (0.2 mL), without further purification, gave the title compound as a dark orange gum (23 mg, 99%).

δ_H (400 MHz, $CDCl_3$): 6.50 (s, 2H, Ar), 6.58 (d, 2H, J 8.0, Ar),6.83 (d, 2H, J 8.0, Ar).

δ_C (100 MHz, $CDCl_3$): 111.2 (CH Ar), 119.0 (CH Ar), 125.3 (CH Ar), 128.7 (q Ar), 143.9 (q Ar), 144.6 (q Ar), 191.7 (q C=O).

2-(3-Aminophenyl)-4-aminobenzonitrile (156)

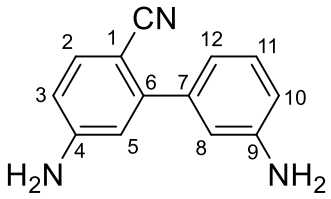

A suspension of compound **157** (200 mg, 0.743 mmol) and $SnCl_2.2H_2O$ (2.01 g, 8.915 mmol) in EtOH (2 mL) was heated to 70 °C under argon for 1 h. The mixture was cooled and poured onto ice. A solution of aq. $NaHCO_3$ (5%, 10 mL) was added and the compound was extracted with EtOAc (3 x 20 mL), washed with brine (20 mL) and dried over Na_2SO_4 to give a yellow gum (188 mg, 90%).

$\boldsymbol{\delta_H}$ (400 MHz, $CDCl_3$): 6.61 (d, 1H, J 8.4, Ar), 6.68 (s, 1H, Ar), 6.72 (d, 1H, J 8.0, Ar), 6.83 (s, 1H, Ar), 6.89 (d, 1H, J 7.6, Ar),7.23 (t, 1H, J 7.8, Ar-11), 7.49 (d, 1H, J 8.4, Ar-2).

$\boldsymbol{\delta_C}$ (150 MHz, $CDCl_3$): 100.0 (q C), 113.6 (CH Ar), 115.5 (CH Ar), 115.6 (2 x CH Ar), 119.2 (CH Ar), 120.3 (q C), 129.9 (CH Ar), 135.7 (CH Ar), 140.0 (q C), 146.8 (q C), 147.7 (q C), 150.4 (q C).

$\boldsymbol{\nu_{max}}$ (ATR)/cm^{-1}: 3446 (NH), 3352 (NH), 3217 (NH), 2923 (CH), 2206 (CN), 1596, 1486, 1251, 863, 819, 788.

HRMS (*m/z* ESI^+) Found: 210.1031 ($[M+H]^+$. $C_{14}H_{26}Br_2O_2$ Requires 210.1026).

2-(3-Nitrophenyl)-4-nitrobenzonitrile (157)

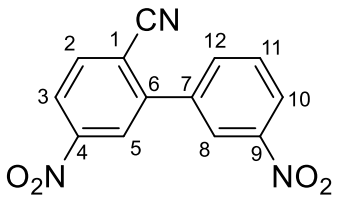

(n a 10 mL microwave vial containing a stirrer bar were added $Pd(OAc)_2$ (9.0 mg, 0.04 mmol), PPh_3 (48 mg, 0.18 mmol), K_2CO_3 (276 mg, 2.0 mmol), KF (90 mg, 1.6 mmol), 3-nitrophenylboronic acid (264 mg, 1.6 mmol)and bromide **161** (300 mg, 1.3 mmol). The vial was sealed, placed under vacuum and backfilled with Ar three times. Dry dioxane (4.5 mL)

was added and the vial was heated to 120 °C in a microwave for 1 h. When the starting material was consumed (as adjudged by TLC), H_2O (10 mL) was added and the mixture was extracted with CH_2Cl_2 (4 x 30 mL), washed with brine (1 x 10 mL) and dried over $MgSO_4$. The solvent was removed and purified by column chromatography on silica, eluting in 20% EtOAc in hexanes as a yellow gum (231 mg, 66 %).

δ_H (400 MHz, $CDCl_3$): 7.79 (t, 1H, 8.0 Hz, Ar-11), 7.97 (d, 1H, 7.7 Hz, Ar-12), 8.06 (d, 1H, 8.4 Hz, Ar-2), 8.39-8.45 (m, 3H, Ar-3, Ar-10, Ar-5), 8.47 (d, 1H, 1.7 Hz, Ar-8) .

δ_C (150 MHz, $CDCl_3$): 116.1 (q CN), 117.2 (q Ar-1), 123.4 (Ar-3), 123.8 (Ar-8), 124.7 (Ar-10), 124.8 (Ar-5), 130.4 (Ar-11), 134.5 (Ar-12), 135.3 (Ar-2), 137.4 (q Ar-7), 144.7 (q Ar-6), 148.7 (q Ar-9), 150.2 (q Ar-4).

2-Bromo-4-nitrobenzonitrile (161)

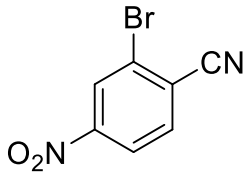

An RBF containing a mixture of 4-nitrobenzonitrile (1.582 g, 10.7 mmol), *N*-bromosuccinimide (1.96 g, 11.1 mmol), $Pd(OAc)_2$ (112 mg, 0.50 mmol) and $pTSA.H_2O$ (960 mg, 5 mmol) in dry 1,2-dichloroethane (40 mL) fitted with a condenser was submerged in an oil bath at 70 °C for 24 h. The solvent was removed under vacuum and the crude solid was purified by column chromatography on silica, eluting the title compound in 5% EtOAc in hexanes as a white solid (788 mg, 32%). **M.p.** 60-61 °C, (lit. 56-57 °C).[189]

δ_H (400 MHz, $CDCl_3$): 7.88 (d, 1H, 8.5 Hz, Ar-6), 8.29 (d, 1H, 8.5 Hz, Ar-5),8.56 (s, 1H, Ar-3).

3,6-Dibromo-9*H*-fluoren-9-one (165)

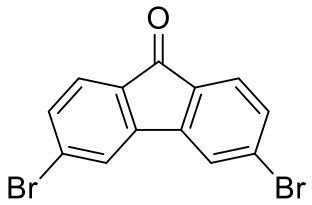

A three-neck RBF containing a solution of phenanthroquinone **167** (6.02 g, 16.4 mmol) and KOH (24.0 g, 426 mmol) in H_2O (30 mL) was fitted with two reflux condensers, heated to 130 °C and stirred for 30 min. Then, $KMnO_4$ (13.73 g, 86.8 mmol) was added in small portions over 1 h. Copious gas evolution was observed *ca.* 1 min after each addition. The mixture was heated for 4 h at 130 °C and then cooled to 0 °C. The mixture was neutralised with conc. H_2SO_4 and then reduced with potassium bisulfate ($KHSO_3$) until the mixture turned light yellow. The product was filtered off, then resuspended in H_2O and re-filtered (× 3), washed with H_2O and EtOH, and dried in vacuo at rt to give a pale cream solid (4.42 g, 80%) which was used without further purification.[196]

δ_H (400 MHz, $CDCl_3$): 7.49 (d, 2H, J 8.2, Ar-2 & Ar-7), 7.55 (d, 2H, J 8.2, Ar-1 & Ar-8), 7.67 (s, 2H, Ar-4 & Ar-5).

HRMS (*m/z* APCI$^+$) Found: 336.8855 ([M+H]$^+$. $C_{13}H_7Br_2O$ Requires 336.8858).

3,6-Dibromo-9,10-phenanthroquinone (167)

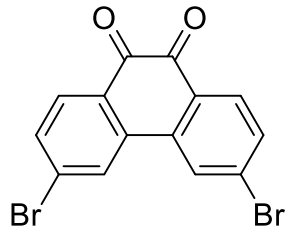

To a solution of 9, 10-phenanthroquinone (3.86 g, 18.5 mmol) and benzoyl peroxide (359 mg, 1.5 mmol) in nitrobenzene (14 mL) at rt, bromine (1.91 mL, 27 mmol) was added slowly. The reaction mixture was heated to 120 °C for 21 h. After cooling to rt, the product was precipitated by addition of EtOH (100 mL) and filtered off, washing with further portions of

EtOH (300 mL). The brown-yellow solid was dried *in vacuo* and used without further purification (5.44 g, 80%).[196]

δ_H (400 MHz, $CDCl_3$): 7.67 (dd, 2H, J 8.3, J 1.6, Ar-2 & Ar-7), 8.07 (d, 2H, J 8.3, Ar-1 & Ar-8), 8.12 (d, 2H, J 1.6, Ar-4 & Ar-5).

HRMS (*m/z* APCI$^+$) Found: 364.8801 ([M+H]$^+$. $C_{14}H_7Br_2O_2$ Requires 364.8807).

3,6-*Bis*(*tert*-butoxycarbonylamino)fluoren-9-one (168)

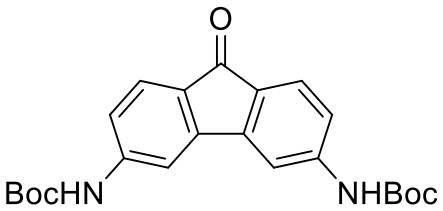

As per *Method J*, using $Pd(OAc)_2$ (12 mg, 0.05 mmol), Xphos (78 mg, 0.16 mmol), Cs_2CO_3 (822 mg, 2.49 mmol), *tert*-butyl carbamate (252 mg, 2.13 mmol) and dibromide **165** (300 mg, 0.89 mmol) in 1,4-dioxane (7.5 mL), after flash chromatography on silica, eluting in 3:1 EtOAc/hexane gave the title compound as a yellow solid (273 mg, 75%). **M.p.** 220 °C.

δ_H (400 MHz, $CDCl_3$): 1.55 (s, 18H, CH_3), 6.68 (br s, 2H, CH_2), 7.10 (dd, 2H, J 1.8, J 8.1, Ar-2 & Ar-7), 7.56 (d, 2H, 8.1, Ar-1 & Ar-8), 7.75 (d, 2H, J 1.8, Ar-4 & Ar-5).

δ_C (150 MHz, $CDCl_3$): 28.2 (CH_3), 81.4 ($C(CH_3)_3$ Boc), 110.1 (CH Ar-4 & Ar-5), 117.6 (CH Ar-2 & Ar-7), 125.1 (CH Ar-1 & Ar-8), 129.6 (q Ar-3 & Ar-6), 144.2 (q Ar), 145.5(q Ar), 152.0 (q C=O Boc), 191.5 (q C=O).

ν_{max} (ATR)/cm^{-1}: 3475, 3308 (N-H), 2980 (C-H), 1686, 1599, 1347, 1225, 1150, 1115, 1049, 1021, 782.

HRMS (*m/z* APCI$^+$) Found: 411.1907 ([M+H]$^+$. $C_{23}H_{27}N_2O_5$ Requires 411.1914).

3,6-*Bis*(*tert*-butoxycarbonylamino)-9*H*-fluorene (170)

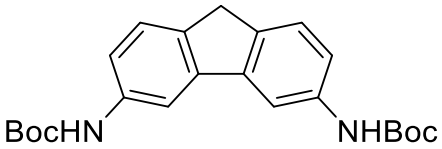

To a solution of ketone **168** (270mg, 0.66 mmol) dissolved in a mixture of MeOH (2.5 mL) and aq. HCl (0.6 mL, 1 M) under Ar, was added Pd/C (200 mg, 10% w/w). The solution was stirred under an atmosphere of H_2 for 4 h at rt, diluted with MeOH (20 mL) and filtered through two fluted filter papers to give the title compound as a white solid (149 mg, 57%). **M.p.** 210-211 °C

δ_H (600 MHz, $CDCl_3$): 1.55 (s, 18H, CH_3),3.78 (s, 2H, CH_2),6.52 (bs, 2H, NH), 7.24 (d, 2H, J 7.9, Ar-4 & Ar-5), 7.41 (d, 2H, J 8.1, Ar-1 & Ar-8), 7.82 (s, 2H, CH Ar-2 & Ar-7).

δ_C (150 MHz, $CDCl_3$): 28.4 (CH_3), 35.9 (CH_2), 80.4 (q C), 110.5 (CH Ar-4 & Ar-5), 117.7 (CH Ar-2 & Ar-7), 125.2 (CH Ar-1 & Ar-8), 137.3 (q Ar 3 & Ar 6), 138.6 (q Ar 8a & 9a), 142.4 (q Ar 4a & 4b), 152.9 (q C=O).

ν_{max} (ATR)/cm^{-1}: 3317, 3129, 2975, 1691, 1530, 1404, 1299, 1246, 1151, 1054, 1025, 874, 816, 738.

HRMS (*m/z* $APCI^+$) Found: 396.2039 ($[M+H]^+$. $C_{23}H_{28}N_2O_4$ Requires 396.2044).

(Ethoxycarbonylmethyl)triphenylphosphonium bromide (171)

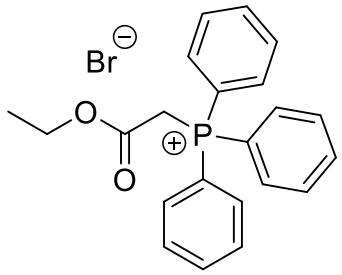

To a solution of PPh_3 (2.62 g, 10.6 mmol) in EtOAc (20 mL) was added ethyl bromoacetate (1.17 mL, 11.2 mmol) and the mixture was stirred at reflux for 5 h. Once the mixture cooled to rt, the resulting white precipitate was filtered off and washed with EtOAc (30 mL) to give the title compound in sufficient purity (3.74 g, 82 %). **M.p.** 168-170 °C (lit. 145-150 °C).[252]

δ_H (400 MHz, $CDCl_3$): 1.07 (t, 3H, 7.2 Hz, CH_3), 4.04 (q, 2H, 7.2 Hz, CH_2), 5.60 (d, 2H, 13.8 Hz, PCH_2), 7.64-7.70 (m, 6H, *m*-Ar), 7.75-7.82 (m, 3H, *p*-Ar), 7.86-7.95 (m, 6H, *o*-Ar).

Ethyl 3,6-dibromo-9*H*-fluoren-9-ylideneacetate (172)

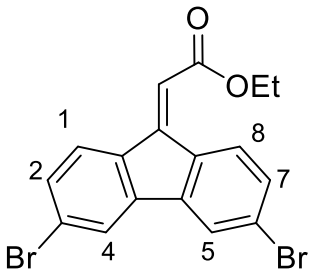

Phosphonium salt **171** (2.538 g, 5.92 mmol) was dissolved in CH_2Cl_2 (50 mL), extracted from aq. NaOH (1M, 100 mL) and the aqueous layer was extracted with a further portion of CH_2Cl_2 (50 mL). The combined organic layers were washed with brine (30 mL), dried over $MgSO_4$, and evaporated to dryness, to give the ylide as a pale yellow oil. To this, was added ketone **165** (2.000 g, 5.92 mmol), and dry 1,4-dioxane (9 mL). The mixture was heated at reflux for 42 h, then cooled and diluted with EtOAc (20 mL). H_2O (20 mL) was added and the mixture was separated. The aqueous layer was further extracted with EtOAc (20 mL). The combined organic layers were washed with brine and dried over Na_2SO_4. After evaporation of solvent, the product was purified by column chromatography on silica, eluting in 5% EtOAc in hexanes to give a yellow solid (986 mg, 41%). **M.p.** 154-155 °C.

$\boldsymbol{\delta_H}$ (400 MHz, $CDCl_3$): 1.39 (t, 3H, 7.1 Hz, CH_3), 4.33 (q, 2H, 7.2 Hz, CH_2), 6.71 (s, 1H, CH), 7.40 (dd, 1H, 1.7 Hz, 8.2 Hz, Ar-2), 7.44 (dd, 1H, 1.9 Hz, 8.4 Hz, Ar-2), 7.49 (d, 1H, 8.2 Hz, Ar-7), 7.68-7.71 (m, 2H, Ar-4 & Ar-5), 8.81 (d, 1H, 8.4 Hz, Ar-8).

$\boldsymbol{\delta_C}$ (100 MHz, $CDCl_3$): 14.3 (CH_3), 61.0 (CH_2), 115.2 (CH), 122.6 (CH Ar-1), 123.1 (CH Ar-5), 123.4 (CH Ar-4), 124.9 (q C-3), 125.6 (q C-6), 130.7 (CH Ar-8), 130.9 (CH Ar-2), 131.5 (CH Ar-7), 133.9 (q C-8a), 137.8 (q C-9a), 141.1 (q C-4a), 142.9 (q C-4b), 146.2 (q C-9), 166.0 (q C=O).

$\boldsymbol{\nu_{max}}$ (ATR)/cm^{-1}: 2977, 1712 (C=O), 1591, 1286, 1209, 1174, 1064, 824, 747.

HRMS (*m/z* ESI^-) Found: 814.8278 ($[2M-H]^-$. $C_{34}H_{23}O_4{}^{79}Br_2{}^{81}Br_2$ Requires 814.8294).

Diethyl 3,6-dibromo-9*H*-fluoren-9-ylidenemalonate (173)

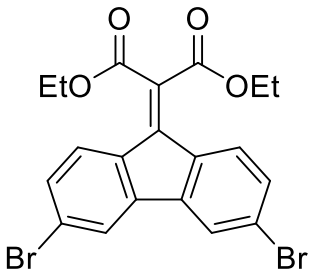

To a mixture of ketone **165** (104 mg, 0.22 mmol) and diethyl malonate (45.5 μL, 0.22 mmol) in dry CCl_4 (10 mL) in an RBF fitted with a rubber septum, was added slowly $TiCl_4$ (0.6 mL, 0.60 mmol, 1M in CH_2Cl_2). The flask was cooled to 0 °C and dry pyridine (97 μL, 0.88 mmol) was added dropwise over 2 min. The solution was stirred for 2 h at 0 °C and stirred at rt for 4 d. Once ketone **165** had been consumed (as visualised by TLC), the mixture was extracted from H_2O (20 mL) with CH_2Cl_2 (3 x 20 mL). The combined organic layers were washed with brine (15 mL) and dried over Na_2SO_4. The solvent was removed under vacuum and the residue was purified by silica chromatography, eluting in 1.5% EtOAc in hexanes to give a yellow solid (61 mg, 59%). **M.p.** 236-237 °C.

δ_H (400 MHz, $CDCl_3$): 1.38 (t, 6H, 7.1 Hz, CH_3), 4.42 (q, 4H, 7.1 Hz, CH_2), 7.37(dd, 2H, 2.0 Hz, 8.4 Hz, Ar-2 & Ar-7), 7.69-7.74 (m, 4H, Ar-1, Ar-4, Ar-5, Ar-8).

δ_C (100 MHz, $CDCl_3$): 14.0 (CH_3), 62.3 (CH_2), 123.3 (CH Ar-4 & Ar-5), 124.1(q C-10), 125.7(q Ar-3 & Ar-6), 127.6 (CH Ar-1 & Ar-8), 131.2 (CH Ar-2 & Ar-7), 134.6(q Ar-8a & Ar-8b), 142.2 (q Ar-4a & Ar-4b), 142.3 (q C=C9), 165.0 (q C=O).

ν_{max} (ATR)/cm^{-1}: 2983 (C-H), 1712 (C=O), 1591 , 1239, 1217, 1163, 1065, 865, 833, 782.

HRMS (*m/z* ESI^+) Found: 500.9317 ($[M+Na]^+$. $C_{20}H_{18}O_4Br_2Na$ Requires 500.9313).

Diethyl 3,6-*bis*(*N*-*tert*-butoxycarbonyl)amino-9*H*-fluoren-9-ylidenemalonate (174)

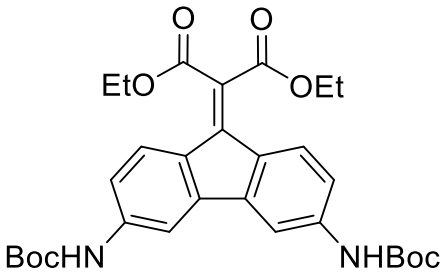

As per *Method J*, using $Pd(OAc)_2$ (15 mg, 0.067 mmol), XPhos (96 mg, 0.20 mmol), Cs_2CO_3 (1.025 g, 3.14 mmol), *tert*-butyl carbamate (276 mg, 2.60 mmol) and bromide **173** (539 mg, 1.12 mmol) in dry 1,4-dioxane (9 mL), followed by flash purification on silica, eluting in 15% EtOAc in hexanes gave the title compound as a yellow solid (515 mg, 83%). **M.p**. 103-104 °C.

δ_H (400 MHz, $CDCl_3$): 1.34 (t, 6H, 7.1 Hz, CH_3), 1.52 (s, 18H, CH_3), 4.37 (q, 4H, 7.1 Hz, CH_2), 6.89 (br s, 2H, NH), 7.06 (dd, 2H, 2.1 Hz, 8.6 Hz, Ar-2 & Ar-7), 7.69 (d, 2H, 1.7 Hz, Ar-4 & Ar-5), 7.72 (d, 2H, 8.6 Hz, Ar-1 & Ar-8).

δ_C (150 MHz, $CDCl_3$): 14.0 (CH_3), 28.3 (Boc CH_3), 61.8 (CH_2), 81.0 (q $\underline{C}(CH_3)$), 109.3 (CH, Ar-4 & Ar-5), 117.0 (CH, Ar-2 & Ar-7), 120.0 (q O=C-$\underline{C}$), 127.2 (CH, Ar-1 & Ar-8), 130.9 (q Ar-3 & Ar-6), 141.1 (q Ar-8a & Ar-9a), 142.9 (q Ar-4a & Ar-4b), 144.3 (q O=C-C=$\underline{C}$), 152.3 (q C=O Boc), 165.8 (q C=O).

ν_{max} (ATR)/cm^{-1}: 3337 (NH), 2981 (CH), 1701, 1588, 1523, 1219, 1150, 1109, 1051, 865, 829, 768.

HRMS (*m/z* ESI^-) Found: 551.2386 ($[M-H]^+$. $C_{30}H_{35}N_2O_8$ Requires 551.2393).

3,6-*Bis*(*N,N'*-di-*tert*-butoxycarbonylimidazolidine-2-ylidineamino)-9*H*-fluorene (175)

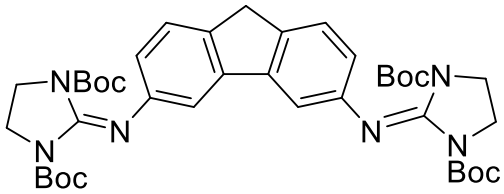

As per *Method* I, using diamine **153** (50 mg, 0.186 mmol), thione **111** (103 mg, 0.372 mmol), Et_3N (223 μL, 1.674 mmol), $HgCl_2$ (126 mg, 0.465 mmol) and DMF (1 mL), gave the title compound as a red foam (53 mg, 39%).

δ_H (400 MHz, $CDCl_3$): 1.25 (s, 36H, CH_3), 3.73 (s, 2H, CH_2), 3.83 (s, 8H, CH_2), 6.90 (dd, 2H, Ar-2 & Ar-7), 7.30-7.33 (m, 4H, Ar-1, Ar-4, Ar-5, Ar-8).

δ_C (150 MHz, $CDCl_3$): 27.9 (CH_3 Boc) 35.7 (CH_2-9), 43.2 (NCH_2), 82.7 (q $\underline{C}(CH_3)$), 113.6 (CH Ar-1 & Ar-8), 119.6 (CH Ar-2 & Ar-7), 124.7 (CH Ar-4 & Ar-5), 138.2 (q Ar-8a & Ar-9a), 142.5 (q Ar-4a & Ar-4b), 147.2 (q Ar-3 & Ar-6), 150.4 (q C=N).

ν_{max} (ATR)/cm^{-1}: 2981 (CH), 1808 (C=O), 1709, 1367, 1248, 1143, 966, 849, 775.

HRMS (*m/z* ESI^+) Found: 733.3930 ($[M+H]^+$. $C_{39}H_{53}N_6O_8$ Requires 733.3925).

Diethyl 3,6-*bis*(*N*,*N*'-di(*tert*-butoxycarbonyl)imidazolidine-2-ylideneamino)-9*H*-fluoren-9-ylidenemalonate (176)

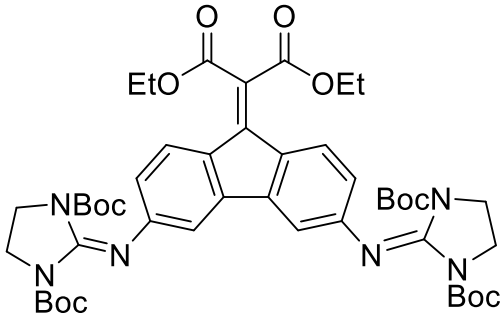

As per *Method* I, using diamine **150** (50 mg, 0.118 mmol), thione **111** (65 mg, 0.236 mmol), Et_3N (148 μL, 1.062 mmol), $HgCl_2$ (80 mg, 0.295 mmol) and DMF (0.5 mL), following purification on neutral alumina, eluting in 33% EtOAc in hexane, gave the title compound as a red solid (53 mg, 39%). **M.p.** 124 °C.

δ_H (600 MHz, DMSO-d_6): 1.25-1.29 (m, 42H, CH_3), 3.79 (s, 8H, CH_2), 4.33 (q, 4H, 7.1 Hz, CH_2), 6.67 (dd, 2H, 1.8 Hz, 8.4 Hz, Ar-2 & Ar-7), 7.16 (d, 2H, 1.8 Hz, Ar-4 & Ar-5), 7.54 (d, 2H, 8.4 Hz, Ar-1 & Ar-8).

δ_C (150 MHz, DMSO-d_6): 14.2 (CH_3 Ester), 28.0 (CH_3 Boc), 43.5 (CH_2 Im), 62.0 (CH_2 Ester), 82.2 (qC Boc), 113.2 (CH Ar-4 & Ar-5), 118.5 (q C=C10), 120.0 (CH Ar-2 & Ar-7), 126.6 (CH Ar-1 & Ar-8), 129.3 (q Ar-3 & Ar-6), 140.6 (q C=N), 142.8 (q Ar-4a & Ar-4b), 150.0 (q C=O Boc), 150.2 (q C-9), 152.6 (q Ar-8a & Ar-9a), 165.8 (q C=O ester) (Tentatively assigned since the compound decomposes over the time course of the experiment).

ν_{max} (ATR)/cm^{-1}: 2979 (NH), 1758 (C=O), 1706, 1598, 1578, 1366, 1295, 1145, 975, 847, 766.

HRMS (*m/z* ESI^+) Found: 889.4330 ($[M+H]^+$. $C_{46}H_{61}N_6O_{12}$ Requires 889.4347).

Sodium 3,6-*bis*(imidazolidine-2-ylideneamino)-9*H*-fluoren-9-ylidenemalonate (281)

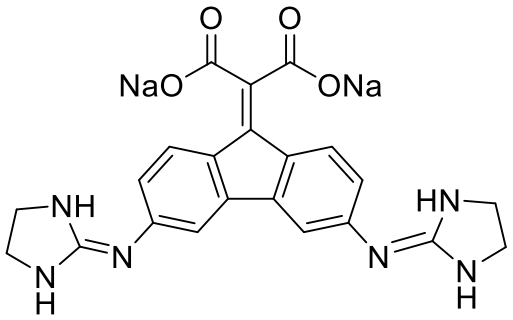

As per *Method K*, using diester **145** (189 mg, 0.337 mmol) and NaOH (68 mg, 1.685 mmol) in 4:1 MeOH/H_2O (5 mL), after heating at 80 °C for 17 h, gave the title compound as a grey gum, which was used without further purification.

δ_H (400 MHz, D_2O): 3.51 (s, 8H, CH_2), 6.72 (d, 2H, 7.5 Hz, Ar-2 & Ar-7), 7.37 (s, 2H, Ar-4 & Ar-5),7.77 (d, 2H, Ar-1 & Ar-8).

δ_C (100 MHz, D_2O): 42.3 (CH_2), 113.9 (CH Ar-4 & Ar-5), 122.3 (CH Ar-2 & Ar-7), 124.4 (Ar-1 & Ar-8), 125.4 (O=C-C), 131.9 (CH Ar-8a & Ar-9a), 135.8 (q O=C-C=C), 140.5 (CH Ar-4a & Ar-4b), 148.6 (CH Ar-3 & Ar-6), 161.2 (q C=N), 174.2 (q C=O).

ν_{max} (ATR)/cm^{-1}: 3172 (NH), 2918 (CH), 1655, 1578, 1345, 1282, 1085.

3,6-*Bis*(imidazolidine-2-ylideneamino)-9*H*-fluoren-9-ylmalonic acid dihydrochloride (282)

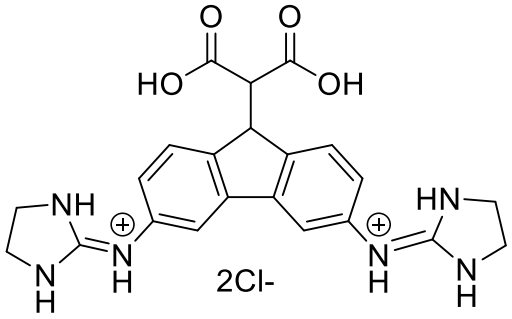

To a solution of dicarboxylate salt **281** (20 mg, 0.042 mmol) in 4:1 MeOH/H_2O (1 mL) under Ar, was added 10 % Pd/C (10 mg, 50% w/w) and the flask was put under a balloon of H_2 and stirred for 2 h. The flask was purged with Ar and 1M HCl (1 mL) was added. The compound was filtered through a syringe filter to remove Pd. Then, the solvent was evaporated in vacuo to give the title compound, which was used without further purification.

δ_H (400 MHz, D_2O): 3.81 (br s, 8H, CH_2), 4.37 (s, 1H, CH), 4.60 (s, 1H, CH), 7.27 (d, 2H, J 5.8, Ar-2 & Ar-7), 7.50-7.85 (m, 4H, Ar-1, Ar-4, Ar-5, Ar-8).

***N*,*N*'-Di-*tert*-butoxycarbonyl-*N*''-phenylguanidine (203a)**

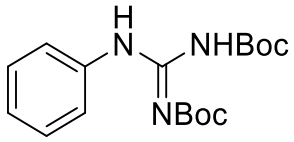

As per *Method L*, using aniline (0.59 mL, 6.44 mmol), *N*,*N*'-*bis*(*tert*-butoxycarbonyl)-*S*-methylthiopseudourea (1.963 g, 6.76 mmol), Et_3N (2.78 mL, 20.0 mmol), $HgCl_2$ (1.844 g, 6.78 mmol) and CH_2Cl_2 (15 mL), following purification on silica, eluting in 4% EtOAc in hexane, gave the title compound as a white solid (1.641 g, 76%). **M.p.** 126 °C (lit. 118-120 °C).[167]

δ_H (400 MHz, $CDCl_3$): 1.52 (s, 18H, CH_3), 7.12 (t, 1H, J 7.2, *p*-Ar), 7.30-7.35 (m, 2H, *m*-Ar), 7.57 (d, 2H, J 7.8, *o*-Ar), 10.41 (br s, 1H, NHAr), 11.71 (br s, 1H, NHBoc).

***N*,*N*'-Di-*tert*-butoxycarbonyl-*N*''-4-methoxyphenylguanidine (203b)**

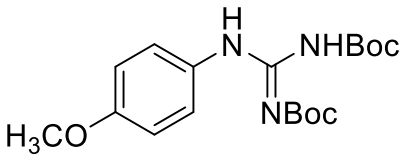

As per *Method L*, using *p*-anisidine (200 mg, 1.62 mmol), *N*,*N*'-*bis*(*tert*-butoxycarbonyl)-*S*-methylthiopseudourea (470 mg, 1.62 mmol), Et_3N (0.80 mL, 5.68 mmol), $HgCl_2$ (529 mg, 1.95 mmol) and CH_2Cl_2 (6 mL), following purification on silica, eluting in 5% EtOAc in hexane, gave the title compound as a cream solid (500 mg, 84%). **M.p.** 135-136 °C (lit. 138-140 °C).

δ_H (400 MHz, $CDCl_3$): 1.49 (s, 9H, CH_3 Boc), 1.53 (s, 9H, CH_3 Boc), 3.79 (s, 3H, OCH_3), 6.86 (d, 2H, J 8.9, Ar), 7.48 (d, 2H, J 8.9, Ar), 10.19 (br s, 1H, NHAr), 11.64 (br s, 1H, NHBoc).

***N*-(Pyridin-2-yl)-*N',N''*-*bis*(*tert*-butoxycarbonyl)guanidine (203c)**

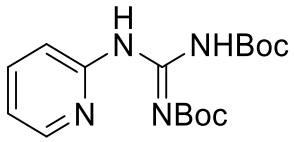

As per *Method L*, using 2-aminopyridine (200 mg, 2.12 mmol), *N*,*N*'-*bis*(*tert*-butoxycarbonyl)-*S*-methylthiopseudourea (648 mg, 2.23 mmol), Et_3N (1.36 mL, 9.75 mmol), $HgCl_2$ (606 mg, 2.23 mmol) and CH_2Cl_2 (10 mL), following purification on silica, eluting in 4% EtOAc in hexane, gave the title compound as a cream solid (601 mg, 84%). **M.p.** 125 °C (lit. 120-122 °C).[253]

δ_H (400 MHz, $CDCl_3$): 1.51 (br s, 18H, CH_3), 6.97-7.02 (m, 1H, Ar), 7.69 (t, 1H, J 7.9, Ar), 8.28 (d, 1H, J 4.9, Ar), 8.29 (br s, 1H, Ar), 10.91 (br s, 1H, NHAr), 11.48 (br s, 1H, NHBoc).

***N*-(Pyridin-3-yl)-*N'*,*N''*-*bis*(*tert*-butoxycarbonyl)guanidine (203d)**

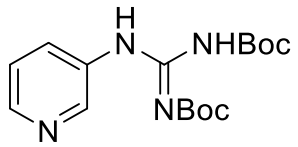

As per *Method L*, using 3-aminopyridine (200 mg, 2.12 mmol), *N*,*N*'-*bis*(*tert*-butoxycarbonyl)-*S*-methylthiopseudourea (648 mg, 2.23 mmol), Et_3N (1.36 mL, 9.75 mmol), $HgCl_2$ (606 mg, 2.23 mmol) and CH_2Cl_2 (10 mL), following purification on silica, eluting in 4% EtOAc in hexane, gave the title compound as a white solid (607 mg, 85%). **M.p.** 95-96 °C (lit. 99-101 °C).[253]

δ_H (400 MHz, $CDCl_3$): 1.50 (s, 9H, CH_3), 1.54 (s, 9H, CH_3), 7.30 (dd, 1H, J 8.3, J 4.7, Ar), 8.22 (d, 1H, 8.3 Hz, Ar), 8.35 (br s, 1H, Ar), 8.70 (br s, 1H, Ar), 10.42 (br s, 1H, NHAr), 11.60 (br s, 1H, NHBoc).

***N*-(2-Aminophenyl)-*N*',*N*''-*bis*(*tert*-butoxycarbonyl)guanidine (203e)**

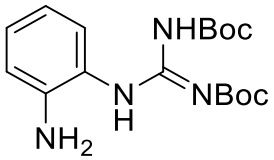

As per *Method L*, using *o*-phenylenediamine (400 mg, 3.70 mmol), *N*,*N*'-*bis*(*tert*-butoxycarbonyl)-*S*-methylthiopseudourea (537 mg, 1.85 mmol), Et_3N (0.90 mL, 6.47 mmol), $HgCl_2$ (502 mg, 1.85 mmol) and CH_2Cl_2 (14 mL), following purification on silica, eluting in 10% EtOAc in hexane, gave the title compound as an orange solid (660 mg, 99%). **M.p.** 115 °C.

δ_H (400 MHz, DMSO-d_6): 1.35 (s, 9H, CH_3), 1.51 (s, 9H, CH_3), 5.05 (br s, 2H, NH_2), 6.55 (t, 1H, J 7.6, Ar-5), 6.73 (d, 1H, J 7.1, Ar-3), 6.96 (t, 1H, J 7.0, Ar-4), 7.11 (d, 1H, J 7.6, Ar-6), 9.37 (br s, 1H, NHAr), 11.57 (br s, 1H, NHBoc).

δ_C (100 MHz, DMSO-d_6): 22.7 (CH_3), 22.9 (CH_3), 78.4 (q $C(CH_3)_3$), 83.0 (q $C(CH_3)_3$), 115.6 (CH Ar-3), 116.0 (CH Ar-5), 121.4 (q Ar-2). 127.2 (CH Ar-4), 127.6 (CH Ar-6), 143.5 (q Ar-1), 152.2 (q C=O), 154.9 (q C=O), 163.0 (q C=N).

ν_{max} (ATR)/cm^{-1}: 3407, 3321, 3262, 2980, 1717, 1607, 1406, 1347, 1308, 1147, 1116, 1057, 857, 811, 752.

HRMS (*m/z* ESI^+) Found: 373.1854 ($[M+Na]^+$. $C_{17}H_{26}N_4O_4Na$ Requires 373.1852).

***N,N'-Bis*(*tert*-butoxy)iminoimidazolidinobenzene (206)**

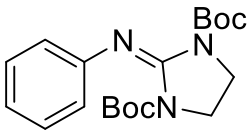

As per *Method L*, using aniline (182 μL, 2.0 mmol), thione **111** (605 mg, 2.0 mmol), Et_3N (976 μL, 7.0 mmol), $HgCl_2$ (639 mg, 2.2 mmol) and CH_2Cl_2 (7.5 mL), following recrystallisation from 6:1 hexane/Et_2O, gave the title compound as a white solid (475 mg, 66%). **M.p.** 142-144 °C (lit. 142-144 °C).[138]

δ_H (400 MHz, $CDCl_3$): 1.32 (s, 18H, CH_3), 3.87 (s, 4H, CH_2), 6.97 (t, 1H, J 7.2, *p*-Ar), 7.04 (d, 2H, J 7.2, *o*-Ar), 7.23 (t, 2H, J 7.8, *m*-Ar).

***N*-benzyl-*N'*,*N''*-*bis*(*tert*-butoxycarbonyl)guanidine (208)**

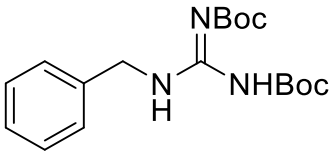

As per *Method L*, using benzylamine (232 μL, 2.12 mmol), *N,N'-bis*(*tert*-butoxycarbonyl)-*S*-methylthiopseudourea (648 mg, 2.23 mmol), Et_3N (1.36 mL, 9.75 mmol), $HgCl_2$ (606 mg, 2.23 mmol) and CH_2Cl_2 (10 mL), following purification on silica, eluting in 15% EtOAc in

hexane, gave the title compound as a white solid (595 mg, 80%). **M.p.** 123-125 °C. (lit. 124-125 °C).[253]

δ_H (400 MHz, $CDCl_3$): 1.46 (s, 9H, CH_3), 1.50 (s, 9H, CH_3), 4.61 (d, 2H, J 5.1, CH_2), 7.30 (m, 5H, Ar), 8.57 (br s, 1H, NHBn), 11.52 (br s, 1H, NHBoc).

δ_C (100 MHz, $CDCl_3$): 28.0 (CH_3), 28.1 (CH_3), 45.0 (CH_2), 83.2 (q $C(CH_3)$), 127.6 (CH *p*-Ar), 127.8 (CH *o*-Ar), 128.7 (CH *m*-Ar), 137.2 (q Ar), 153.1 (q C=N) 156.1 (q C=O).

Benzylguanidine hydrochloride (210)

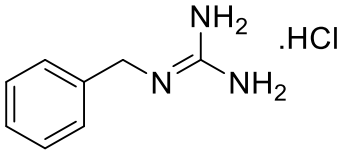

As per *Method A* using compound **198** (581 mg, 1.66 mmol) and HCl (4.99 mL, 19.9 mmol, 4M in dioxane) compound **200** was obtained as a yellow gum (121 mg, 79%).[167]

δ_H (400 MHz, D_2O): 4.23 (s, 2H, CH_2), 7.15-7.21 (m, 3H, *o*-Ar and *p*-Ar), 7.22-7.29 (m, 2H, *m*-Ar).

HRMS (*m/z* ESI^+) Found: 150.1028 ($[M+H]^+$. $C_8H_{12}N_3$ Requires 150.1031).

Phenylguanidine hydrochloride (211a)

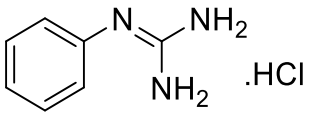

As per *Method A*, using compound **203a** (1.053 g, 3.14 mmol) and HCl (9.42 mL, 37.7 mmol, 4M in dioxane) in CH_2Cl_2 (6.3 mL), the title compound was obtained as a pale yellow gum (534 mg, 99%).[212]

δ_H (400 MHz, D_2O): 7.28-7.32 (app. d, 2H, *o*-Ar), 7.37-7.42 (app. t, 1H, *p*-Ar), 7.44-7.50 (app. t, 2H, *m*-Ar).

HRMS (*m/z* ESI^+) Found: 136.0866 ($[M+H]^+$. $C_7H_{10}N_3$ Requires 136.0869).

4-Methoxyphenylguanidine hydrochloride (211b)

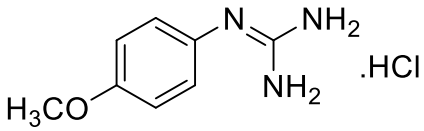

As per *Method A* using compound **203b** (200 mg, 0.547 mmol) and HCl (1.64 mL, 6.586 mmol, 4M in dioxane) in CH_2Cl_2 (1.1 mL), the title compound was obtained as a white solid (98 mg, 89%). **M.p.** 144-146 °C (lit. 139-141 °C).[212]

δ_H (400 MHz, D_2O): 3.87 (s, 3H, CH_3), 7.09 (d, 2H, J 8.9, Ar), 7.30 (d, 2H, J 8.9, Ar).

HRMS (*m/z* ESI^+) Found: 166.0977 ($[M+H]^+$. $C_8H_{12}N_3O$ Requires 166.0975).

Pyridine-2-guanidine hydrochloride (211c)

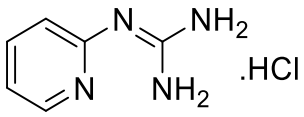

As per *Method A* using compound **203c** (404 mg, 1.2 mmol) and HCl (3.6 mL, 14.4 mmol, 4M in dioxane) in CH_2Cl_2 (2.4 mL), the title compound was obtained as a white gum (155 mg, 89%).[253]

δ_H (400 MHz, D_2O): 6.99-7.02 (app. d, 1H, Ar), 7.17-7.21 (app. dd, 1H, Ar), 7.80-7.87 (app. t, 1H, Ar), 8.25-8.28 (app. d, 1H, Ar).

HRMS (*m/z* ESI^+) Found: 137.0826 ($[M+H]^+$. $C_6H_9N_4$ Requires 137.0827).

Pyridine-3-guanidine hydrochloride (211d)

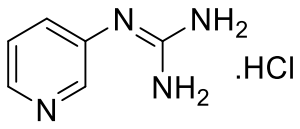

As per *Method A* using compound **203d** (607 mg, 1.8 mmol) and HCl (5.4 mL, 21.7 mmol, 4M in dioxane) in CH_2Cl_2 (3.6 mL), the title compound was obtained as an orange gum (293 mg, 94%).[253]

δ_H (400 MHz, D_2O): 8.07-8.15 (app. dd, 1H, Ar), 8.51-8.55 (m, 1H, Ar), 8.72-8.74 (app. d, 1H, Ar), 8.85-8.88 (app. d, 1H, Ar).

HRMS (*m/z* ESI^+) Found: 151.0975 ($[M+H]^+$. $C_7H_{11}N_4$ Requires 151.0978).

2-Aminophenylguanidine (211e)

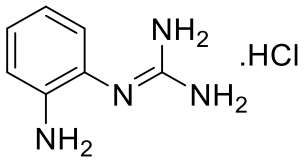

To a solution of **203e** (300 mg, 0.86 mmol) in EtOAc (5 mL) at rt was added anhydrous $SnCl_4$ (0.4 mL, 3.42 mmol). The reaction was stirred for 35 min at rt and when starting material was consumed (as adjudged by TLC) the solvent was evaporated *in vacuo* and then any remaining $SnCl_4$ was quenched with MeOH (1 mL). Upon rotary evaporation of MeOH, the crude oil was dissolved in hexane to give a bilayer from which the hexane layer was decanted. This procedure was repeated until the title compound was precipitated as a dark purple solid (150 mg, 93%). **M.p.** 244 °C.

δ_H (400 MHz, DMSO-*d_6*): 5.19 (br s, 2H, NH_2),6.59 (t, 1H, J 7.4, Ar-5), 6.79 (d, 1H, J 7.9, Ar-3),6.96 (d, 1H, J 7.4, Ar-6), 7.03 (br s, 4H, NH_2), 7.04-7.09 (m, 1H, Ar-4), 8.81 (br s, 1H, NH).

δ_C (100 MHz, DMSO-*d_6*): 115.9 (CH Ar-3), 116.5 (CH Ar-5), 118.6 (q Ar-2), 128.2 (CH Ar-6), 128.9 (CH Ar-4), 145.1 (q Ar-1), 156.5 (q C=N).

ν_{max} (ATR)/cm^{-1}: 3411 (NH), 3311 (NH), 3159 (NH), 1674, 1654, 1590, 1493, 1269, 1123, 759.

HRMS (*m/z* ESI^+) Found: 151.0976 ($[M+H]^+$. $C_7H_{11}N_4$ Requires 151.0978).

2-(Phenylamino)imidazoline hydrochloride (212)

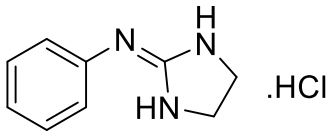

As per *Method A* using compound **206** (475 mg, 1.31 mmol) and HCl (3.9 mL, 15.8 mmol, 4M in dioxane) in CH_2Cl_2 (2.6 mL), the title compound was obtained as a white solid (254 mg, 98%). **M.p.** 214-216 °C (lit. 211-213 °C).[138]

δ_H (400 MHz, D_2O): 3.79 (s, 4H, CH_2), 7.32 (d, 2H, J 7.5), 7.40 (t, 1H, J 7.5, Ar), 7.51 (app. t, 2H, J 7.8, Ar).

HRMS (*m/z* ESI^+) Found: 162.1022 ($[M+H]^+$. $C_9H_{12}N_3$ Requires 162.1026).

Phenylguanidine free base (213a)

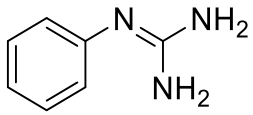

As per *Method N*, using guanidinium chloride salt **211a** (562 mg, 3.27 mmol) and Na metal (83 mg, 3.6 mmol) in EtOH (6.4 mL), afforded the title compound as a yellow solid (439 mg, 99%). **M.p.** 139 °C

δ_H (400 MHz, DMSO-*d_6*): 6.84 (d, 2H, J 7.5, *o*-Ar), 6.88 (t, 1H, 7.8, *p*-Ar), 7.18-7.24 (app. t, 2H, *m*-Ar).

δ_C (100 MHz, DMSO-*d_6*): 123.1 (CH p-Ar), 123.9 (CH *o*-Ar), 129.6 (CH *m*-Ar), 144.7 (q Ar), 154.3 (q C=N).

ν_{max} (ATR)/cm^{-1}: 3434 (NH), 3377 (NH), 3316 (NH), 3118, 2984, 2758, 1678, 1624, 1577, 1477, 1343, 1269, 876, 754, 688.

HRMS (*m/z* ESI^+) Found: 136.0876 ($[M+H]^+$. $C_7H_{10}N_3$ Requires 136.0875).

4-Methoxyphenylguanidine free base (213b)

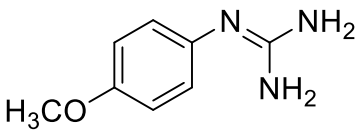

As per *Method N*, using guanidinium chloride salt **211b** (800 mg, 3.97 mmol) and Na metal (100 mg, 4.36 mmol) in EtOH (22 mL), afforded the title compound as a yellow solid (684 mg, 104% including NaOEt). **M.p.** 205 °C.

δ_H (400 MHz, DMSO-*d_6*): 3.67 (s, 3H, CH_3), 4.30 (br s, 4H, NH_2), 6.70 (d, 2H, J ,Ar-2), 6.77 (d, 2H, J , Ar-3).

δ_C (100 MHz, DMSO-d_6): 55.1 (CH_3), 114.3 (CH Ar-3), 123.7 (CH Ar-2), 142.8 (q Ar-4), 152.7 (q C=N), 153.7 (q Ar-1).

ν_{max} (ATR)/cm^{-1}: 3473 (NH), 3314 (NH), 3171, 1648, 1554, 1491, 1438, 1232, 1232, 1101, 853 811.

HRMS (*m/z* ESI^+) Found: 166.0971 ($[M+H]^+$. $C_8H_{12}N_3O$ Requires 166.0975).

Pyridine-2-guanidine free base (213c)

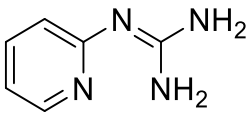

As per *Method N*, using guanidinium chloride salt **211c** (155 mg, 0.90 mmol) and Na metal (25 mg, 1.08 mmol) in EtOH (4 mL), afforded the title compound as an orange solid (133 mg, 108% including NaOEt). **M.p.** 134-136 °C.

δ_H (600 MHz, DMSO-d_6): 6.59-6.62 (m, 2H, H-4 and H-5), 6.74 (br s, 4H, NH), 7.43 (br s, 1H, H-3), 8.04 (br s, 1H, H-6).

δ_C (150 MHz, DMSO-d_6): 113.5 (CH Ar-5), 118.8 (CH Ar-4), 136.3 (CH Ar-3), 145.8 (CH Ar-6), 157.5 (q C=N), 163.7 (q Ar-2).

ν_{max} (ATR)/cm^{-1}: 3202 (NH), 3129 (NH), 2953 (CH), 2765, 1702, 1638, 1603, 1554, 1472, 1419, 1383, 1324, 1284, 1144, 875, 769, 672.

HRMS (*m/z* ESI^+) Found: 137.0822 ($[M+H]^+$. $C_6H_9N_4$ Requires 137.0827).

Pyridine-3-guanidine free base (213d)

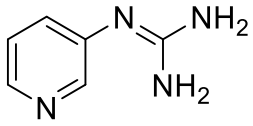

As per *Method N*, using guanidinium chloride salt **211d** (250 mg, 1.45 mmol) and Na metal (37 mg, 1.59 mmol) in EtOH (8 mL) and H_2O (0.5 mL), afforded the title compound as a white solid (220 mg, 110% including NaOEt). **M.p.** 148-149 °C.

δ_H (600 MHz, DMSO-*d_6*): 7.43 (dd, 1H, J 8.1, J 4.8, H-4), 7.62 (ddd, 1H, J 8.1, J 2.5, J 1.6, H-5), 7.73 (br s, 4H, NH_2), 8.41-8.43 (m, 2H, H-2 and H-6).

δ_C (150 MHz, DMSO-*d_6*): 124.2 (CH Ar-5), 131.9 (CH Ar-4), 134.0 (q Ar-3), 145.7 (CH Ar-2), 146.5 (CH Ar-6), 156.1 (q C=N).

ν_{max} (ATR)/cm^{-1}: 3362 (NH), 3297 (NH), 3209, 2980 (CH), 2938, 1678, 1635, 1592, 1483, 1399, 1326, 1269, 1192, 1162, 1030, 856, 806.

HRMS (*m/z* ESI^+) Found: 137.0819 ($[M+H]^+$. $C_6H_9N_4$ Requires 137.0822).

2-Aminophenylguanidine (213e)

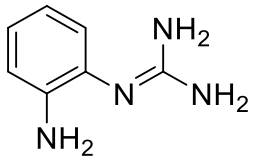

As per *Method N*, using guanidinium chloride salt **211e** (100 mg, 0.54 mmol) and Na metal (13.5 mg, 0.59 mmol) in EtOH (5 mL), afforded the title compound as a yellow solid (85 mg, 105% including NaOEt). **M.p.** 260 °C.

δ_H (400 MHz, DMSO-*d_6*): 4.78 (br s, 2H, NH_2),6.19 (br s, 4H, NH_2), 6.51 (t, 1H, J 7.5, Ar-C5), 6.67 (d, 1H, J 8.0, Ar-C3),6.77 (d, 1H, J 7.7, Ar-C6), 6.82, (d, 1H, J 7.1, Ar-C4).

δ_C (100 MHz, DMSO-*d_6*): 115.9 (CH Ar-3), 116.5 (CH Ar-5), 118.6 (q Ar-1), 128.2 (CH Ar-6), 128.9 (CH Ar-4), 145.1 (q Ar-2), 156.5 (q C=N).

ν_{max} (ATR)/cm^{-1}: 3320 (NH), 3145 (NH), 1674, 1637, 1584, 1499, 1269, 836, 757.

HRMS (*m/z* ESI^+) Found: 151.0977 ($[M+H]^+$. $C_7H_{11}N_4$ Requires 151.0978).

Imidazolidine-2-phenylimine free base (214)

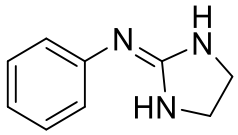

As per *Method N*, using 2-aminoimidazolinium chloride salt **212** (100 mg, 0.51 mmol) and Na metal (15 mg, 0.61 mmol) in EtOH (1 mL), afforded the title compound as a white solid (76 mg, 93%). **M.p.** 144-145 °C.

δ_H (400 MHz, DMSO-*d_6*): 3.52 (s, 4H, CH_2), 6.10 (br s, 2H, NH), 7.08 (t, 1H, *p*-Ar), 7.18 (d, 2H, *o*-Ar), 7.32 (t, 2H, *m*-Ar).

δ_C (100 MHz, DMSO-*d_6*): 43.9 (CH_2), 121.3 (CH *p*- Ar), 122.0 (CH *o*-Ar), 129.5 (CH *m*-Ar), 146.7 (q Ar), 158.2 (q C=N).

ν_{max} (ATR)/cm^{-1}: 3358, 3312 (NH), 3053 (NH), 2860 (CH), 1654, 1587, 1482, 1416, 1266, 1245, 1086, 835, 775, 691.

HRMS (*m/z* ESI^+) Found: 162.1027 ($[M+H]^+$. $C_9H_{12}N_3$ Requires 162.1022).

Benzylguanidine free base (215)

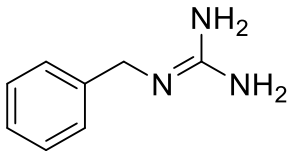

As per *Method N*, using guanidinium chloride salt **210** (94 mg, 0.50 mmol) and Na metal (13 mg, 0.55 mmol) in EtOH (5 mL), afforded the title compound as an orange solid (78 mg, 104% including NaOEt). **M.p.** <300 °C.

δ_H (400 MHz, DMSO-d_6): 4.09 (s, 2H, CH_2), 7.23-7.28 (m, 3H, *o*-Ar & *p*-Ar), 7.36-39 (m, 2H, *m*-Ar).

δ_C (150 MHz, DMSO-d_6): 44.3 (CH_2), 127.2 (CH *o*-Ar & *p*-Ar), 128.4 (CH *m*-Ar), 138.2 (q Ar), 157.1 (C=N).

ν_{max} (ATR)/cm^{-1}: 3240 (NH), 3137 (NH), 2984 (CH), 1637, 1453, 1349, 752.

HRMS (*m/z* ESI^+) Found: 150.1033 ($[M+H]^+$. $C_8H_{12}N_3$ Requires 150.1031).

4,4'-*Bis*(*N*,*N*'-*bis*[*tert*-butoxycarbonyl]guanidino)benzophenone (216a)

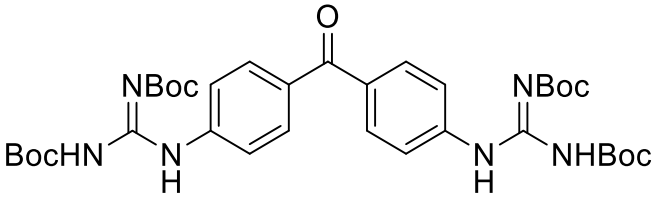

As per *Method L*, using 4,4'-diaminobenzophenone (1.59 g, 7.5 mmol), *N*,*N*'-*bis*(*tert*-butoxycarbonyl)-*S*-methylthiopseudourea (4.35 g, 15.0 mmol), Et_3N (5 mL, 36.0 mmol), $HgCl_2$ (4.50 g, 16.0 mmol) and DMF (40 mL), following purification on silica, eluting in 6% EtOAc in petroleum ether, gave the title compound as a white solid (504 mg, 10%).[212]

δ_H (400 MHz, $CDCl_3$): 1.52 (s, 18H, Boc CH_3), 1.55 (s, 18H, Boc CH_3), 7.72- 7.87 (m, 8H, Ar), 10.59 (br s, 2H, NHAr), 11.63 (br s, 2H, NHBoc).

HRMS (*m/z* ESI^+) Found: 697.3572 ($[M+H]^+$. $C_{35}H_{49}N_6O_9$ Requires 697.3561).

4,4'-*Bis*(*N*,*N*'-*bis*-(*tert*-butylcarbonyl)guanidino)diphenylether (216b)

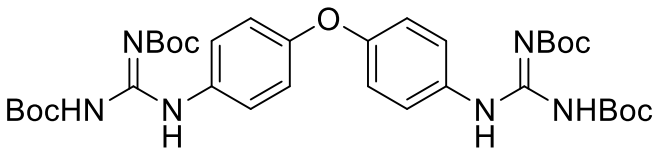

As per *Method L*, using 4,4'-oxydianiline (1.502 g, 7.5 mmol), *N*,*N*'-*bis*(*tert*-butoxycarbonyl)-*S*-methylthiopseudourea (4.356 g, 15.0 mmol), Et_3N (7.3 mL, 52.5 mmol), $HgCl_2$ (4.480 g, 16.5 mmol) and DMF (12.5 mL), following recrystallisation from 30% EtOAc in hexane, gave the title compound as a white solid (1.641 g, 76%). **M.p.** <300°C (lit. <300).[212]

δ_H (400 MHz, $CDCl_3$): 1.50 (s, 18H, Boc), 1.54 (s, 18H, Boc), 6.97 (d, 4H, J 9.0, Ar-3), 7.54 (d, 4H, J 9.0, Ar-2), 10.28 (br s, 2H, NHAr), 11.64 (br s, 2H, NHBoc).

4,4'-*Bis*-guanidinobenzophenone dihydrochloride (217a)

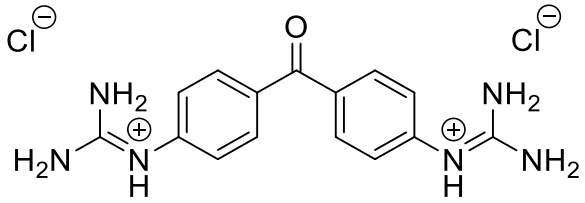

As per *Method A* using compound **216a** (504 mg, 0.724 mmol) and HCl (4.34 mL, 17.4 mmol, 4M in dioxane), the title compound was obtained as a yellow gum (235 mg, 88%).[212]

δ_H (400 MHz, D_2O): 7.49 (d, 4H, 8.7 Hz, Ar), 7.90 (d, 4H, 8.7 Hz, Ar).

HRMS (*m/z* ESI^+) Found: 297.1461 ($[M+H]^+$. $C_{15}H_{17}N_6O$ Requires 297.1464).

Di-(4-guanidinophenyl)ether dihydrochloride (217b)

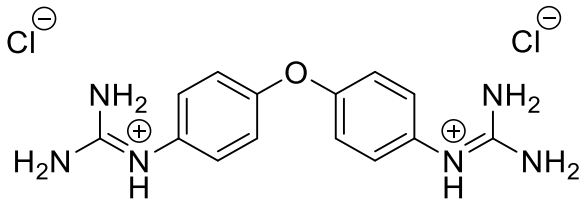

As per *Method A* using compound **216b** (685 mg, 1.00 mmol) and HCl (6.0 mL, 24. mmol, 4M in dioxane), the title compound was obtained as a yellow gum (355 mg, 99%). **M.p.** 225 °C (lit. 230 °C).[212]

δ_H (400 MHz, D_2O): 7.11-7.23 (m, 4H, Ar), 7.30-7.42 (m, 4H, Ar).

4-4'-*Bis*-guanidinobenzophenone free base (218a)

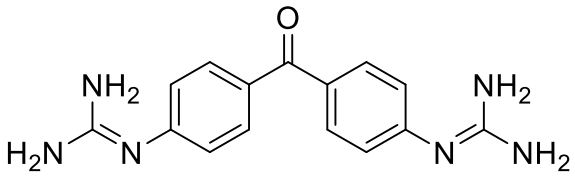

As per *Method N*, using *bis*-guanidinium salt **217a** (219 mg, 0.59 mmol) and Na metal (30 mg, 1.31 mmol) in EtOH (2.5 mL), afforded the title compound as a white gum (178 mg, 102% with NaOEt).

δ_H (400 MHz, DMSO-d_6): 5.61 (br s, 8H, NH_2), 6.91 (d, 4H, J 8.5, Ar-2), 7.59 (d, 4H, J 8.5, Ar-3).

δ_C (100 MHz, DMSO-d_6): 127.3 (Ar CH-2), 134.4 (q Ar-1), 136.1 (Ar CH-3), 158.5 (q Ar-4), 159.7 (q C=N), 198.3 (q C=O).

ν_{max} (ATR)/cm^{-1}: 3362 (NH), 3312 (NH), 3066, 1630 (C=N), 1560, 1532, 1441, 1406, 1309, 1170, 930, 864, 771.

HRMS (*m/z* ESI^+) Found: 297.1460 ($[M+H]^+$. $C_{15}H_{17}N_6O$ Requires 297.1464).

Di-(4-guanidinophenyl)ether free base (218b)

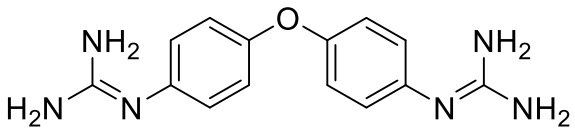

As per *Method N*, using *bis*-guanidinium salt **217b** (420 mg, 1.18 mmol) and Na metal (51 mg, 2.60 mmol) in EtOH (6.0 mL), afforded the title compound as a white solid (356 mg, 99%). **M.p.** 205-207 °C.

δ_H (400 MHz, DMSO-d_6): 5.18 (br s, 8H, NH), 6.72 (d, 4H, 8.8 Hz, Ar), 6.80 (d, 4H, 8.8 Hz, Ar).

δ_C (100 MHz, DMSO-d_6): 119.3 (CH Ar-3), 124.3 (CH Ar-2), 146.3 (q Ar-1), 151.5 (q C=N), 153.0 (q Ar-4).

ν_{max} (ATR)/cm^{-1}: 3457 (NH), 3332 (NH), 3179, 3031, 2930 (CH), 1635, 1583, 1489, 1436, 1219, 855, 810.

HRMS (*m/z* ESI^+) Found: 285.1461 ($[M+H]^+$. $C_{14}H_{17}N_6O$ Requires 285.1464).

Phenylguanidinium tetrachloroplatinate salt (219a)

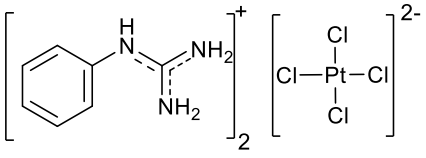

As per *Method M*, a solution of arylguanidinium chloride **211a**, (93 mg, 0.54 mmol) in H_2O (1 mL) was added to potassium tetrachloroplatinate (45 mg, 0.11 mmol) in H_2O (1 mL) and stirred for 15 min. The pink precipitate was dried *in vacuo*, filtered and washed to afford pink crystals (55 mg, 82%). **M.p.** 160-162 °C.

δ_H (400 MHz, DMSO-d_6): 7.23 (d, 2H, J 7.8, *o*-Ar), 7.30 (t, 1H, J 7.4, *p*-Ar), 7.43–7.49 (m, 6H, NH and *m*-Ar), 9.94 (br s, 1H, NH).

δ_C (100 MHz, DMSO-d_6): 124.9 (CH *o*-Ar), 127.0 (CH *p*-Ar), 130.2 (CH *m*-Ar), 135.7 (q Ar), 156.4 (q C=N).

δ_{Pt} (86 MHz, DMSO-d_6): -2954, -3444.

ν_{max} (ATR)/cm^{-1}: 3380, 3303, 3174 (N-H), 1727, 1635, 1594 (C=N), 1494, 1493, 1240, 756, 692.

HRMS (*m/z* ESI^+) Found: 136.0874 (M^+. $C_7H_{10}N_3$ Requires: 136.0875).

(4-Methoxyphenyl)guanidinium tetrachloroplatinate salt (219b)

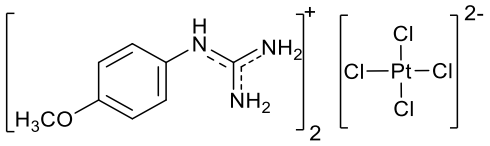

As per *Method M*, a solution of arylguanidinium chloride **211b**, (90 mg, 0.45 mmol) in H_2O (1 mL) was added to potassium tetrachloroplatinate (37 mg, 0.09 mmol) in H_2O (1 mL) and stirred for 15 min. The pink precipitate was dried *in vacuo*, filtered and washed to afford pink crystals (45 mg, 75%). **M.p.** 205 °C, decomposition.

δ_H (400 MHz, DMSO-d_6): 3.75 (s, 3H, CH_3), 6.99 (d, 2H, J 8.8, Ar), 7.16 (d, 2H, J 8.8, Ar), 7.22 (br s, 2H, NH), 9.46 (br s, 1H, NH).

δ_C (150 MHz, DMSO-d_6): 56.0 (CH_3), 115.6 (CH Ar), 127.5 (q Ar), 127.9 (CH Ar), 156.7 (q Ar), 158.9 (q C=N).

δ_N (60 MHz, DMSO-d_6): 76.1, 96.4.

δ_{Pt} (86 MHz, DMSO-d_6): -2960, -3447.

ν_{max} (ATR)/cm^{-1}: 3453, 3288, 3184 (NH), 2982 (CH), 2839, 1661(C=N), 1510, 1419, 1240, 1148, 849, 763.

% Calculated for $C_{16}H_{24}Cl_4N_6O_2Pt$: C 28.71, H 3.61, N 12.56.

% Found: C 28.48, H 3.65, N 11.97.

HRMS (*m/z* ESI^+) Found: 166.0685 (M^+. $C_8H_{12}N_3O$ Requires: 166.0980).

***a*-Chlorido-*b*-(dmso-*S*)-*cd*-(2-phenylyl-κC^2-guanidine-κN)platinum(II) (220a)**

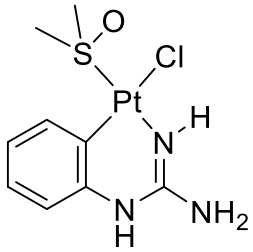

As per *Method O*, free base **213a** (119 mg, 0.888 mmol) and *cis*-[$PtCl_2(dmso)_2$] (360 mg, 0.888 mmol) were added to a freshly prepared NaOMe solution produced from Na metal (24 mg, 1.00 mmol) and MeOH (24 mL), affording after precipitation the title compound as a yellow solid (94 mg, 24%). Crystals suitable for XRD were grown over three months by slow evaporation of H_2O into a concentrated solution of the title compound in DMSO.

δ_H (400 MHz, DMSO-d_6): 3.35 (s, 6H, CH_3), 6.19 (br s, 1H, PtNH), 6.31 (br s, 2H, NH_2), 6.59-6.72 (m, 2H, Ar-3 & Ar-4), 6.96 (t, 1H, J 7.4, Ar-5), 7.97 (d+dd, 1H, J 7.7 + J 62.6, Ar-6), 9.13 (br s, 1H, ArNH).

δ_C (100 MHz, DMSO-d_6): 46.2 (CH_3), 113.1 (q Ar-1), 115.0 (CH Ar-3), 121.2 (CH Ar-4), 124.1 (CH Ar-5), 137.0 (q Ar-2), 138.3 (CH Ar-6), 150.4 (q C=N).

δ_{Pt} (86 MHz, DMSO-d_6): -3582.

ν_{max} (ATR)/cm^{-1}: 3407 (NH), 3310 (N), 3193 (NH), 2352, 1645 (C=N), 1602, 1551, 1479, 1399, 1300, 1091 (S-O), 1022, 758, 721.

% Calculated for $C_9H_{14}N_3OPtClS\cdot 0.5NaCl\cdot 1.5H_2O\cdot 0.5DMSO$: C 22.32, H 3.28, N 7.81.

% Found: C 22.12, H 3.01, N 8.01.

LRMS (*m/z* ESI^+) Found: 444.2 ($[M+H]^+$. $C_9H_{15}N_3OSCl_2Pt$ Requires 444.03).

***a*-Chlorido-*b*-(dmso-*S*)-*cd*-([2-aminophenylyl]-κC^2-imidazoline-κN)platinum(II) (221)**

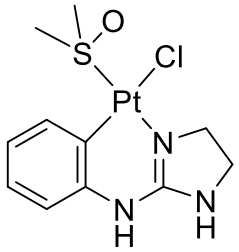

As per *Method O*, free base **214** (200 mg, 1.15 mmol) and *cis*-[$PtCl_2(dmso)_2$] (462 mg, 1.15 mmol) were added to a freshly prepared NaOMe solution produced from Na metal (29 mg, 1.18 mmol) and MeOH (25 mL), affording after precipitation the title compound as a dark blue solid (90 mg, 18%). **M.p.** 223-224 °C. Crystals suitable for XRD were grown over three months by slow evaporation of H_2O into a concentrated solution of the title compound in DMSO.

δ_H (400 MHz, DMSO-d_6): 3.14-3.57 (m, 8H, 2 x CH_3 & CH_2), 3.99 (br s, 2H, CH_2), 6.37-6.77 (m, 2H, Ar-3 & Ar-4), 6.77-7.11 (m, 1H, Ar-5), 7.11-7.57 (m, 1H, NH), 7.57-8.01 (m, 1H, Ar-6), 9.53 (br s, 1H, NH).

δ_C (100 MHz, DMSO-d_6): 44.0 (CH_2), 46.1 (CH_3), 51.5 (CH_2), 114.9 (q Ar-1), 115.0 (CH Ar-4), 121.8 (CH Ar-3), 124.6 (CH Ar-5), 137.8 (q Ar-2), 139.6 (CH Ar-6), 156.0 (q C=N).

δ_{Pt} (86 MHz, DMSO-d_6) -3633.

ν_{max} (ATR)/cm^{-1}: 3339, 3282 (NH), 3185 (NH), 2994 (CH), 1606, 1578, 1465, 1413, 1288, 1094, 1017, 743.

% Calculated for $C_{11}H_{17}N_3OPtClS \cdot H_2O \cdot 0.5DMSO$: C 27.35, H 3.73, N 7.97.

% Found: C 27.16, H 3.45, N 8.16.

***Bis*-Pt Complex of 2-aminophenylguanidine (222)**

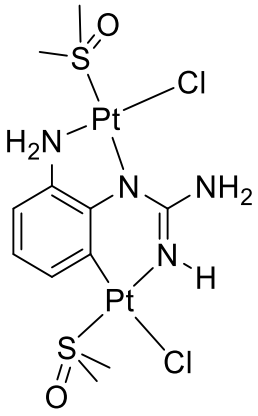

As per *Method O*, free base **213e** (15 mg, 0.1 mmol) and *cis*-[$PtCl_2(dmso)_2$] (20 mg, 0.05 mmol) were dissolved in DMSO-d_6 (1 mL), affording after precipitation the title compound as a dark purple solid (6 mg, 24%). Crystals suitable for XRD were grown over three months by slow evaporation of H_2O into a concentrated solution of the title compound in DMSO.

Triiodo-*tris*(4-methoxyguanidine)*bis*-platinum (III) complex (223)

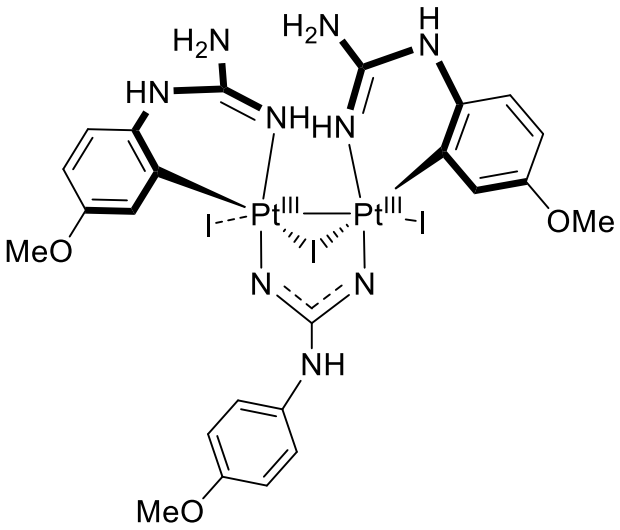

To K_2PtCl_4 (41 mg, 0.1 mmol) in H_2O (1 mL) at 60 °C, was added KI (100 mg, 0.6 mmol). The mixture was stirred in the dark for 20 min, after which free base **213b** (37 mg, 0.2 mmol) was added. The yellow mixture was stirred at rt for 15 min and the brown precipitate was filtered and washed with H_2O. The compound was dissolved in EtOAc and crystallised out by slow evaporation of hexane to give crystals suitable for XRD.

***trans*-[Dichloro(dmso)(2-[phenylamino]imidazoline-*κN*)platinum] (232)**

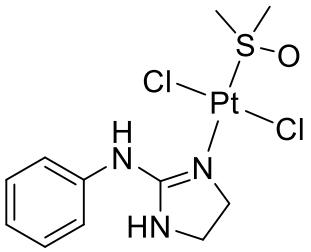

To a solution of K_2PtCl_4 (139 mg, 0.335 mmol) in H_2O (0.5 mL) was added dropwise a solution of DMSO (24 μL, 0.335 mmol) in H_2O (0.5 mL) and the reaction was stirred at rt for 4 h until the colour changed from red to yellow. The solid free base **214** (54 mg, 0.335 mmol) and CH_2Cl_2 (0.5 mL) were then added and the reaction was stirred at rt for 16 h. The organic layer was separated and evaporated at rt by blowing with Ar to give a crude oil which was purified on silica, eluting in 0.5% acetone in CH_2Cl_2 to give the title compound as a yellow solid (33 mg, 19%). Crystals suitable for XRD were grown over 4 h by slow evaporation of Et_2O into a concentrated solution of the title compound in CH_2Cl_2.

δ_H (400 MHz, DMF-d_7): 3.37 (s, 6H, CH_3), 3.59 (t, 2H, J 9.1, CH_2), 3.85 (t, 2H, J 9.1, CH_2), 7.15 (br s, 1H, NH), 7.20 (t, 1H, J 7.4, *p*-Ar), 7.30 (d, 2H, J 7.5, *o*-Ar), 7.38-7.43 (m, 2H, *m*-Ar), 8.88 (br s, 1H, NH).

δ_C (100 MHz, DMF-d_7): 42.5 (CH_3), 43.5 (CH_2), 51.4 (CH_2), 123.1 (CH *o*-Ar), 124.8 (CH *p*-Ar), 129.4 (CH *m*-Ar), 138.6 (q Ar), 160.7 (q C=N).

δ_{Pt} (86 MHz, DMF-d_7): -3033.

ν_{max} (ATR)/cm^{-1}: 3289 (NH), 3090 (NH), 1617 (C=N), 1093 (S-O), 3018, 1588, 1571, 1478, 1432, 1267, 1022, 730 .

HRMS (*m/z* ESI^-) Found: 503.0063 ($[M-H]^-$. $C_{11}H_{16}N_3OSCl_2Pt$ Requires 503.0039).

***cis*-[Dichloro(phenyliminoguanidine (*N*,*N*'))platinum] (233)**

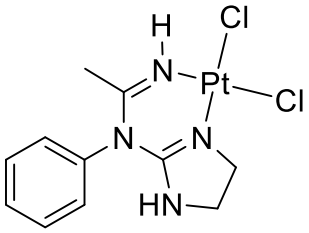

To a crude mixture of **232** prior to column chromatography was added CH_3CN (1 mL). Crystals suitable for XRD were grown over a period of months from this standing solution.

δ_H (400 MHz, DMF-d_7): 3.52-3.58 (m, 2H, CH_2), 4.25-4.33 (m, 2H, CH_2), 6.55 (br s 1H, NH), 7.75-7.81 (m, 3H, Ar), 7.86-7.90 (m, 2H, Ar), 10.04 (br s, 1H, NH). NOTE: CH_3 obscured by H_2O peak.

δ_C (100 MHz, DMF-d_7): decomposed over time of experiment (v dilute).

ν_{max} (ATR)/cm^{-1}: 3390, 3254 (NH), 2350, 2164 (CN), 1622(C=N), 1576, 1436, 1271, 1098, 1030, 730.

***trans*-[Dichloro-*bis*-((amino-*κN*)guanidinium)platinum] dichloride (238)**

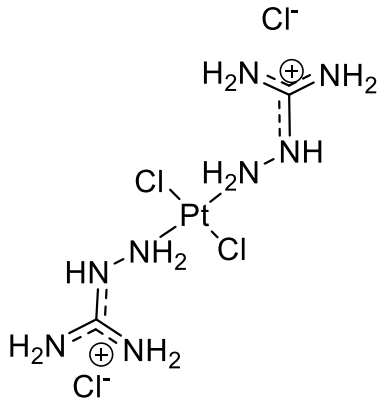

As per *Method M*, a solution of aminoguanidinium chloride (220 mg, 2.0 mmol) in H_2O (0.5 mL) was added to K_2PtCl_4 (166 mg, 0.40 mmol) in H_2O (0.5 mL) and stirred for 15 min. The pink precipitate was dried *in vacuo*, filtered and washed to afford a yellow powder (131 mg, 67%).

δ_H (400 MHz, DMSO-d_6): 7.20 (br s, 2H), 8.84 (br s, 8H).

δ_C (100 MHz, DMSO-d_6): 159.5.

δ_{Pt} (86 MHz, DMSO-d_6): -2957.

HRMS (*m/z* ESI^+) Found 413.0219 (M^+. $C_2H_{12}N_8Cl_2Pt$ Requires 413.0210).

***trans*-[Dichlorido-*bis*[N^1-amino-N^2-(4-methoxy)phenylguanidinium-κ*N*]platinum] dichloride (242)**

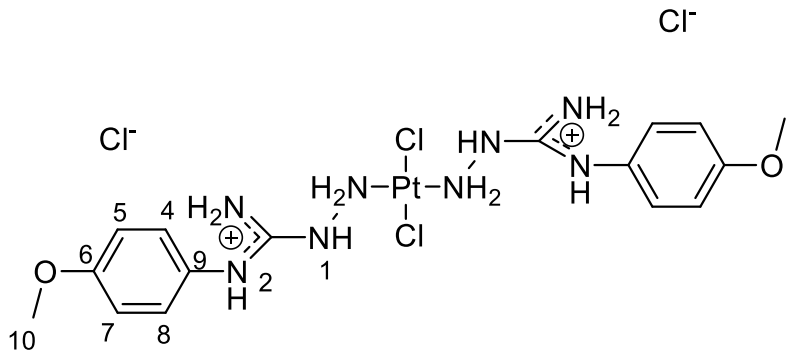

Following *Method M*, using compound **67b** (0.231 mmol) and K_2PtCl_4 (0.05 mmol) in H_2O (1 mL) compound **242** was afforded as a brown amorphous solid (32 mg, 22%).

δ_H (400 MHz, DMF-d_7): 3.85 (3H, s, CH_3), 7.03 (2H, d, J 8.2, H-4, H-8), 7.27 (2H, d, J 8.2, H-5, H-7), 7.79 (br s, 1H, NH), 7.93 (br s, 1H, NH), 8.06 (br s, 2H, NH).

δ_C (100 MHz, DMF-d_7): 55.3 (CH_3), 114.7 (CH 4,8) 127.2 (CH 5,7), 151.3 (q C), 155.3 (q C), 155.7 (q C).

ν_{max} (ATR)/cm^{-1}: 3323 (NH), 3184 (NH), 2145, 1467, 1454, 1398, 1148, 825, 765, 740.

HRMS (*m/z* ESI^-) Found: 624.0969 (M-H, $C_{16}H_{23}N_8O_2Cl_2Pt$ Requires: 624.0938).

Chlorido[N^1-amino-N^2-(4-methoxy)phenylguanidine-κ$^2N,N^2$][dmso]platinum(II) chloride (244)

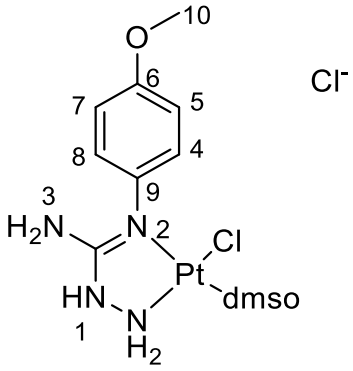

To a solution of Na metal (0.188 mmol) in EtOH (1 mL) was added aryl aminoguanidinium salt **37b** (0.188 mmol). After stirring for 1 h, the solution was left to stand at 0 °C for 15 min, filtered to remove NaCl solvent evaporated by rotary evaporation. To this was added $[PtCl_2(dmso)_2]$ (0.188 mmol) and MeOH (15 mL) and the mixture was heated to 65 °C for 2 h. Upon removal of solvent, the title compound was afforded as a brown amorphous solid (24 mg, 26%).

δ_H (400 MHz, DMF-d_7): 3.88 (3H, s, CH_3), 7.08 (2H, d, J 8.4, H-4, H-8), 7.37 (2H, d, J 8.4, H-5, H-7), 10.12 (1H, s, NH), 10.90 (1H, s, NH), 11.18 (1H, s, NH).

δ_C (100 MHz, DMF-d_7): 55.4 (CH_3-10), 114.9 (CH 5,7), 128.2 (CH 4,8).

δ_{Pt} (86 MHz, DMF-*d7*): -2957.

ν_{max} (ATR)/cm^{-1}: 3327 (NH), 3098 (NH), 2765, 1765, 1536, 1495, 1448, 965, 939, 872, 849.

HRMS (*m/z* ESI$^-$) Found: 488.0487 (M-H, $C_{16}H_{18}N_4O_2SClPt$ Requires: 488.0494)

***4,4'-Bis*-[*a*-Chlorido-*b*-(dmso-*S*)-*cd*-(2-phenylyl-κC^2-guanidine-κN)platinum(II)]ketone (246a)**

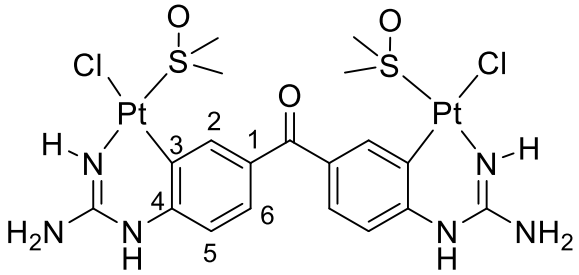

As per *Method O*, free base **218a** (15 mg, 0.05 mmol) and *cis*-[$PtCl_2(dmso)_2$] (40.5 mg, 0.1 mmol) dissolved in DMSO-d_6 (1 mL) at 80 °C for 48 h, afforded after precipitation the title compound as a yellow solid (16 mg, 32%). **M.p.** 250 °C. Crystals suitable for XRD were grown over three months by slow evaporation of H_2O into a concentrated solution of the title compound in DMSO.

δ_H (400 MHz, DMSO-d_6): 3.36 (s, 12H, CH_3), 6.40 (d, 2H, J 2.5, PtNH), 6.43 (s, 4H, NH_2), 6.75 (d, 2H, J 8.2, Ar-5), 7.38 (dd, 2H, J 1.9, J 8.2, Ar-6), 8.48 (d, 2H, J 1.9, Ar-2), 9.48 (d, 2H, J 2.5, NH).

δ_C (150 MHz, DMSO-d_6): 46.0 (CH_3), 112.2 (q Ar C-3), 114.4 (Ar C-5), 126.4 (Ar C-6), 131.0 (Ar C-1), 140.3 (q Ar C-4), 140.8 (Ar C-2), 150.1 (q C=N), 194.4 (q C=O).

δ_{Pt} (86 MHz, DMSO-d_6): -3556, -3559.

ν_{max} (ATR)/cm^{-1}: 3356 (NH), 3206 (NH), 3000, 2917 (CH), 1649, 1619, 1535, 1477, 1304, 1288, 1249, 1093, 1017, 1002, 947, 823, 748, 677.

% Calculated for $C_{19}H_{26}N_6O_3Pt_2Cl_2S_2 \cdot 6NaCl \cdot 6H_2O \cdot 4DMSO$: C 19.27, H 2.55, N 4.99.

% Found: C 19.32, H 2.90, N 5.21.

Diethyl diphenylmethylenemalonate (276)

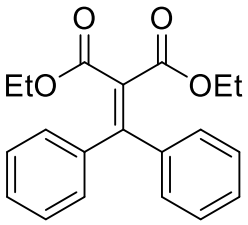

To a mixture of benzophenone (270 mg, 1.48 mmol) and diethyl malonate (227.5 μL, 1.48 mmol) in dry CCl_4 (10 mL) in an RBF fitted with a rubber septum, was added slowly $TiCl_4$ (3.0 mL, 2.96 mmol, 1M in CH_2Cl_2). The flask was cooled to 0 °C and dry pyridine (485.3 μL, 5.92 mmol) was added dropwise over 2 min. The solution was stirred for 2 h at 0 °C and stirred at rt for 4 d. Once benzophenone had been consumed (as visualised by TLC), the mixture was extracted from H_2O (20 mL) with CH_2Cl_2 (3 x 20 mL). The combined organic layers were washed with brine (15 mL) and dried over Na_2SO_4. The solvent was removed under vacuum and the residue was purified by silica chromatography, eluting in 1.5% EtOAc in hexanes to give a white gum (60 mg, 13%).

δ_H (400 MHz, $CDCl_3$): 1.02 (t, 6H, 7.1 Hz, CH_3), 4.07 (q, 4H, 7.1 Hz, CH_2), 7.17-7.21 (m, 4H, *m*-Ar), 7.28-7.39 (m, 6H, *o*-Ar & *p*-Ar).

δ_C (150 MHz, $CDCl_3$): 13.6 (CH_3), 61.2 (CH_2), 126.4 (q O=C-C), 128.1 (CH *o*-Ar), 129.0 (CH *m*-Ar) 129.1 (CH *p*-Ar), 140.1 (q O=C-C=C), 155.7 (q Ar), 166.0 (q C=O).

ν_{max} (ATR)/cm^{-1}: 2981 (CH), 1719 (C=O), 1697, 1443, 1367, 1328, 1302, 1255, 1067, 866, 769, 698.

HRMS (*m/z* ESI^+) Found: 347.1264 ($[M+Na]^+$. $C_{20}H_{20}O_4Na$ Requires 347.1259).

Sodium diphenylmethylenemalonate (277)

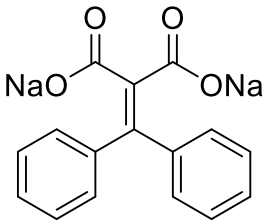

To a suspension of ester **276** (60 mg, 0.185 mmol) in 5:1 MeOH/H_2O (3 mL) was added NaOH (74 mg, 1.84 mmol) and the mixture was heated at reflux for 48 h until the reaction was complete (as adjudged by TLC). The mixture was concentrated under vacuum to give a crude grey solid (50 mg, 94 %) which was used without further purification.

δ_H (600 MHz, D_2O): 7.25-7.29 (m, 4H, *m*-Ar), 7.36-7.40 (m, 6H, *o*-Ar & *p*-Ar).

δ_C (150 MHz, D_2O): 127.8 (CH *p*-Ar), 128.1 (CH *o*-Ar), 129.3 (CH *m*-Ar), 139.5 (q C=C), 139.6 (q C=C), 141.8 (q Ar), 175.4 (q C=O).

1,2-(*R*,*R*)Diaminocyclohexane-[3,6-*bis*(imidazolidine-2-ylideneamino)-9*H*-fluoren-9-ylidinemalonato-*O,O'*]platinum (285)

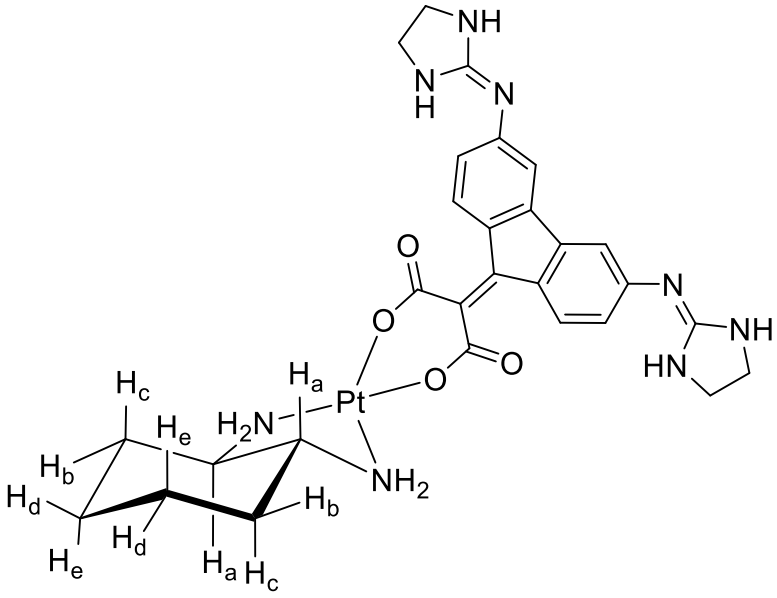

To a solution (A) of carboxylate salt **145** (40 mg, 0.084 mmol) in H_2O (1 mL), was added $Ba(OH)_2{\cdot}8H_2O$ (26.5 mg, 0.084 mmol). The solution was stirred for 24 h. During this time, in a separate flask (B), a suspension of $AgSO_4$ (26 mg, 0.084 mmol) and Pt complex **289** (47 mg, 0.084 mmol) were mixed in H_2O (1 mL) for 4 h at rt. The solution from B was filtered through a syringe filter into solution A and stirred for a further 24-72 h. The solvent was evaporated and NMR samples were taken in D_2O. An orange gum (65 mg) was isolated.

δ_H (600 MHz, D_2O): 1.12-1.22 (m, 3H, 7.2 Hz, CH_2, H_e),1.24- 1.36 (m, 2H, 7.2 Hz, CH_2, H_c), 1.60 (d, 2H, 7.8 Hz, CH_2 H_d), 2.04 (d, 2H, 11.7, CH_2, H_b), 2.31-2.40 (m, 2H, H_a), 3.48 (br s, 4H, CH_2), 3.55 (br s, 4H, CH_2), 6.88 (br s, 2H, Ar), 7.15 (br s, 2H, Ar-4 & Ar-5), 7.73 (br s, 2H, Ar).

δ_C (150 MHz, D_2O): 24.0 (CH_2, C-3), 32.2 (CH_2, C-2), 40.6 (CH_2, C-1), 62.3 (NCH_2), 114.0 (q C), 122.1 (CH Ar), 124.3 (CH Ar), 125.0 (q C), 132.9 (CH Ar-4 & Ar-5), 136.8 (q C), 140.1 (q C), 160.7 (q C), 167.5 (q C), 173.9 (q C).

ν_{max} (ATR)/cm^{-1}: 3307 (NH), 2932 (CH), 2857 (CH), 1722 (CO), 1694, 1591, 1519, 1464, 1407, 1368, 1316, 1235, 1155, 1055, 843, 769.

***cis*-[(1,2-Diaminocyclohexane)diiodoplatinum] (289)**

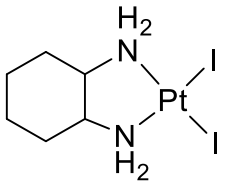

To a solution of K_2PtCl_4 (250 mg, 0.6 mmol) and KI (1.0 g, 6 mmol) in deoxygenated distilled H_2O (5 mL) at was added dropwise a solution of 1,2-diaminocyclohexane (690 mg) in H_2O (0.25 mL) and the solution was stirred in the dark for 1 h to give a yellow precipitate. The precipitate was filtered and washed with H_2O, cold acetone and Et_2O and then vacuum dried at rt to give a yellow powder (212 mg, 68%).[229]

ν_{max} (ATR)/cm^{-1}: 3254, 3182, 3104, 2936, 1557, 1449, 1147, 1117, 1060, 1027, 736.

% Calculated for $C_6H_{14}N_2PtI_2 \cdot MeOH$: C14.13, H 3.05, N 4.71.

% Found: C 14.26, H 2.78, N 5.26.

5.2 Computational Methods

Structure optimisation

All compounds proposed were optimised using the Gaussian09 package[145] at the B3LYP[141,140] computational level with the 6-31G* basis set.[143] Frequency calculations have been performed at the same computational level to confirm that the resulting optimized structures are energetic minima.

Docking

Receptor preparation: The pdb file for DNA-ligand crystal 3FSI was downloaded from the PDB. The solvent, protein and metal ions were removed using AutoDockTools 1.5.4.[128] The coordinates of the binding site around the *bis*-aminoimidazoline ligand was found using the AutoGrid function and the ligand was removed. The Gasteiger charge for the DNA octamer was computed as -12 and polar hydrogens were added. The macromolecule was saved as a .pdbqt file.

Ligand preparation: The optimised structure of **4a** was opened in GaussView 5.0 and its dihedral angles were changed to match the crystal structure of the *bis*-aminoimidazoline ligand from 3FSI. The linker atom in this skeleton was modified to create structures of ligands. In AutoDock 1.5.4, Gasteiger charges and polar hydrogens were added as before and the rotation of all bonds in each molecule was made rigid.

Docking: The ligands were docked into binding site of the DNA octamer using AutoDockVina 1.1.2.[128]

5.3 Biophysical Methods

DNA thermal denaturation

Thermal melting experiments were conducted with a Varian Cary 300 Bio spectrophotometer equipped with a 6×6 multicell temperature-controlled block. Temperatures were monitored with a thermistor inserted into a 1 cm quartz cuvette containing the same volume of water as in the sample cells. Absorbance changes at 260 nm were monitored from a range of 30 °C to 90 °C with a heating rate of 1 °C min^{-1} and a data collection rate of five points per °C. The salmon sperm DNA and poly(dA-dT)$_2$ were purchased from Sigma Aldrich (extinction coefficient ε_{260}=6600 M^{-1} cm^{-1} for both oligomers). A quartz cell with a 1 cm path length was filled with a 1 mL solution of DNA polymer or DNA-compound complex. For thermal denaturation, the DNA polymer (150 µM base) and the compound solution (15 µM) were prepared in a phosphate buffer [0.01 M Na_2HPO_4/NaH_2PO_4], adjusted to pH 7) so that a compound to DNA base ratio of 0.1 was obtained. The thermal melting temperatures of the duplex or duplex-compound complex obtained from the first derivative of the melting curves are reported.

Circular Dichroism

CD spectra were collected with a JASCO J–800 spectrometer at different ratios of compound to DNA polymer [ssDNA or poly(dA-dT)$_2$] at 25 °C in phosphate buffer at pH 7.0. Titrations were carried out by adding the compound (1.5 µM to 15 µM over 10 additions) in a DNA polymer solution (ssDNA: 150 µM or poly(dA-dT)$_2$: 37.5 µM) in a 1 cm quartz cuvette and scanned over a desired wavelength range. Data points for ssDNA were taken at an interval of 0.5 nm, scanning at 50 nm min^{-1}. Data points for poly(dA-dT)$_2$ were taken at an interval of 1 nm, scanning at 200 nm min^{-1}. Data are an average of 3 accumulations. The ICD spectra were obtained by subtracting the CD spectrum of the compound with DNA from the spectrum of DNA in buffer alone. The data were smoothed using an FFT filter with a cut-off frequency of 0.25.

5.4 Growth and Maintenance of the Cell Lines

HL-60 Cell Line

The HL-60 (human caucasian promyelocytic leukemia) cell line was maintained between 200,000 – 2,000,000 cells/mL in Roswell Park Memorial Institute (RPMI) 1640 medium with stable glutamate (GlutaMax I) supplemented with 10% (v/v) foetal bovine serum (FBS) and 50 μg/mL penicillin/streptomycin (pen-strep). The growth medium was stored in the fridge at 4 °C and heated to 37 °C prior to culture work. Cells were grown at 37 °C in a humidified environment maintained at 95% O_2 and 5% CO_2 and passaged at least three times weekly depending on their levels of confluency. When required for sub-culturing, cells were transferred to a sterile tube and centrifuged at 1296 rpm for 5 min. The supernatant was discarded and the cell pellet was resuspended in fresh medium. Cells were then counted using a haemocytometer slide and seeded at the required density.

Cell Viability Assays

HL-60 cells in the log phase of growth were seeded in 96-well plates at a density of 50,000 cells/mL (200 μL/well or 10,000 cells/well) in complete RPMI medium the same day of the experiment. Compounds **46a**, **46b**, **139**, **140**, **145** and **146** were dissolved in ddH_2O to obtain a starting 10 mM stock solution. Compounds **220a**, **221**, **222** and **246a** were dissolved in DMSO to obtain a starting 100 mM stock solution. The cells were then treated with either 2 μL of a 1:100 dilution of stock concentrations of drugs or ddH_2O as vehicle control, or 0.2 μL of a 1:1000 dilution of stock concentrations of drugs or DMSO as vehicle control. All experiment were repeated in triplicate for at least three times. Three wells containing 200 μL RPMI with no cells were also set up as blanks.

After 72 h incubation, 20 μL AlamarBlue® was added to each well. The plates were incubated in darkness at 37 $^{\circ}$C for 5 hours. Using a Molecular Devices microplate reader, the fluorescence (F) was then read at an excitation wavelength of 544 nm and an emission wavelength of 590 nm. Cell viability was then determined by subtracting the mean blank fluorescence (Fb) from the treated sample fluorescence (Fs) and expressing this as a percentage of the fluorescence of the blanked vehicle control (Fc). This is demonstrated in

the equation below. The results were then plotted as nonlinear regression, sigmoidal dose-response curves on Prism GraphPad 5 software, from which the IC_{50} value for each drug was determined.

$$\frac{(\mathrm{Fs}-\mathrm{Fb})}{(\mathrm{Fc}-\mathrm{Fb})}\times\frac{100}{1}=\%\ \text{Cell Viability}$$

6.0 References

1. A. Jemal, F. Bray and J. Ferlay, *CA. Cancer J. Clin.*, 2011, **61**, 69–90.

2. *The global burden of disease 2004*, World Health Organisation, 2008.

3. L. Pecorino, *Molecular Biology of Cancer*, Oxford University Press, 2008.

4. http://www.ncri.ie/

5. D. E. Thurston, *Chemistry and Pharmacology of Anticancer Drugs*, CRC Press, 2007.

6. S. Pelengaris and M. Khan, *The Molecular Biology of Cancer*, Blackwell Publishing, 2006.

7. D. Hanahan and R. A. Weinberg, *Cell*, 2011, **144**, 646–74.

8. M. F. Berger, M. S. Lawrence, F. Demichelis, Y. Drier, K. Cibulskis, A. Y. Sivachenko, A. Sboner, R. Esgueva, D. Pflueger, C. Sougnez, R. Onofrio, S. L. Carter, K. Park, L. Habegger, L. Ambrogio, T. Fennell, M. Parkin, G. Saksena, D. Voet, A. H. Ramos, T. J. Pugh, J. Wilkinson, S. Fisher, W. Winckler, S. Mahan, K. Ardlie, J. Baldwin, J. W. Simons, N. Kitabayashi, T. Y. MacDonald, P. W. Kantoff, L. Chin, S. B. Gabriel, M. B. Gerstein, T. R. Golub, M. Meyerson, A. Tewari, E. S. Lander, G. Getz, M. A. Rubin and L. A Garraway, *Nature*, 2011, **470**, 214–220.

9. C. Greenman, P. Stephens, R. Smith, G. L. Dalgliesh, C. Hunter, G. Bignell, H. Davies, J. Teague, A. Butler, C. Stevens, S. Edkins, S. O'Meara, I. Vastrik, E. E. Schmidt, T. Avis, S. Barthorpe, G. Bhamra, G. Buck, B. Choudhury, J. Clements, J. Cole, E. Dicks, S. Forbes, K. Gray, K. Halliday, R. Harrison, K. Hills, J. Hinton, A. Jenkinson, D. Jones, A. Menzies, T. Mironenko, J. Perry, K. Raine, D. Richardson, R. Shepherd, A. Small, C. Tofts, J. Varian, T. Webb, S. West, S. Widaa, A. Yates, D. P. Cahill, D. N. Louis, P. Goldstraw, A. G. Nicholson, F. Brasseur, L. Looijenga, B. L. Weber, Y.-E. Chiew, A. DeFazio, M. F. Greaves, A. R. Green, P. Campbell, E. Birney, D. F. Easton, G. Chenevix-Trench, M.-H. Tan, S. K. Khoo, B. T. Teh, S. T. Yuen, S. Y. Leung, R. Wooster, P. A. Futreal and M. R. Stratton, *Nature*, 2007, **446**, 153–158.

10. C. Sonnenschein and A. M. Soto, *Cancer Res.*, 2011, **71**, 4334–4337.

11. S. G. Baker, *J. Natl. Cancer Inst.*, 2014, **107**, dju405–dju405.

12. F. J. Kaye, *J. Natl. Cancer Inst.*, 2015, **107**, djv060–djv060.

13. Y. Lazebnik, *Nat. Rev. Cancer*, 2010, **10**, 232–233.

14. R. J. Epstein, *Futur. Oncol*, 2015, **11**, 785–800.

15. J. Kaiser, C. Bledowski and J. Dietrich, *Cortex*, 2014, **54**, 33–50.

16. http://www.cancerresearchuk.org/content/cancer-statistics-for-the-uk

17. M. Vanneman and G. Dranoff, *Nat. Rev. Cancer*, 2012, **12**, 237–251.

18. W. O. Foye, *Cancer Chemotherapeutic Agents*, American Chemical Society, 1995.

19. S. Gross, R. Rahal, N. Stransky, C. Lengauer, and K. P. Hoeflich, *J. Clin. Invest.*, 2015, **125**, 1780–1789.

20. K. Politi, D. Ayeni, and T. Lynch, *Cancer Cell*, 2015, **27**, 751–753.

21. H. Ü. Kaniskan and J. Jin, *Chem. Biol.*, 2015, **10**, 40–50.

22. L. Strekowski and B. Wilson, *Mutat. Res. Mol. Mech. Mutagen.*, 2007, **623**, 3–13.

23. D. Sriram, P. Yogeeswari, R. Thirumurugan, and T. Ratan Bal, *Nat. Prod. Res.*, 2005, **19**, 393–412.

24. X. Cai, P. J. Gray and D. D. Von Hoff, *Cancer Treat. Rev.*, 2009, **35**, 437–50.

25. G. Kroemer, L. Galluzzi, P. Vandenabeele, J. Abrams, E. S. Alnemri, E. H. Baehrecke, M. V Blagosklonny, W. S. El-Deiry, P. Golstein, D. R. Green, M. Hengartner, R. A Knight, S. Kumar, S. a Lipton, W. Malorni, G. Nuñez, M. E. Peter, J. Tschopp, J. Yuan, M. Piacentini, B. Zhivotovsky, and G. Melino, *Cell Death Differ.*, 2009, **16**, 3–11.

26. S. Orrenius, B. Zhivotovsky, and P. Nicotera, *Nat. Rev. Mol. Cell Biol.*, 2003, **4**, 552–565.

27. A. Degterev, Z. Huang, M. Boyce, Y. Li, P. Jagtap, N. Mizushima, G. D. Cuny, T. J. Mitchison, M. A. Moskowitz and J. Yuan, *Nat. Chem. Biol.*, 2005, **1**, 112–119.

28. H. Kono and K. L. Rock, *Nat. Rev. Immunol.*, 2008, **8**, 279–289.

29. H. Inoue and K. Tani, *Cell Death Differ.*, 2014, **21**, 39–49.

30. D. C. Wallace, *Nat. Rev. Cancer*, 2012, **12**, 685–98.

31. T. N. Seyfried, R. E. Flores, A. M. Poff and D. P. D'Agostino, *Carcinogenesis*, 2014, **35**, 515–527.

32. V. Panda, P. Khambat and S. Patil, *Int. J. Clin. Med.*, 2011, **2**, 515–529.

33. J. Montero, K. A. Sarosiek, J. D. DeAngelo, O. Maertens, J. Ryan, D. Ercan, H. Piao, N. S. Horowitz, R. S. Berkowitz, U. Matulonis, P. A. Jänne, P. C. Amrein, K. Cichowski, R. Drapkin and A. Letai, *Cell*, 2015, **160**, 977–989.

34. S. D. Bell, M. Méchali, and M. L. DePamphilis, *DNA Replication*, Cold Springs Harbor Laboratory Press, 1st edn., 2013.

35. D. W. Ussery, *Encycl. Life Sci.*, 2002, 1–11.

36. S. Neidle, *Principles of Nucleic Acid Structure*, Elsevier, 1st edn., 2008.

37. G. Biffi, D. Tannahill, J. McCafferty and S. Balasubramanian, *Nat. Chem.*, 2013, **5**, 182–6.

38. T. Mitchell, A. Ramos-montoya, M. Di Antonio, P. Murat, S. Ohnmacht, M. Micco, S. Jurmeister, L. Fryer, S. Balasubramanian, S. Neidle and D. E. Neal, *Biochemistry*, 2013, **52**, 1429–1436.

39. S. Balasubramanian, L. H. Hurley and S. Neidle, *Nat. Rev. Drug Discov.*, 2011, **10**, 261–75.

40. J. E. Rosenberg, R. Bambury, H. A. Drabkin, P. N. J. Lara, A. L. Harzstark, R. A. Figlin, G. W. Smith, T. Choueiri and F. Erlandsson, *Invest New Drugs*, 2014, **32**, 178–187.

41. C. A. Davey, D. F. Sargent, K. Luger, A. W. Maeder and T. J. Richmond, *J. Mol. Biol.*, 2002, **319**, 1097–1113.

42. C. C. Wu, T. K. Li, L. Farh, L. Y. Lin, T. S. Lin, Y. J. Yu, T. J. Yen, C. W. Chiang and N. L. Chan, *Science*, 2011, **333**, 459–462.

43. J. Chen and J. Stubbe, *Nat. Rev. Cancer*, 2005, **5**, 102–112.

44. S. Marchal, A. François, D. Dumas, F. Guillemin and L. Bezdetnaya, *Br. J. Cancer*, 2007, **96**, 944–51.

45. A.R. Azzouzi, E. Barret, C. M. Moore, A. Villers, C. Allen, A. Scherz, G. Muir, M. de Wildt, N. J. Barber, S. Lebdai and M. Emberton, *BJU Int.*, 2013, **112**, 766–774.

46. N. Ashley and J. Poulton, *Biochem. Biophys. Res. Commun.*, 2009, **378**, 450–455.

47. D. L. Boger and D. S. Johnson, *Proc. Natl. Acad. Sci. U. S. A.*, 1995, **92**, 3642–3649.

48. D. H. Nguyen-Hackley, E. Ramm, C. M. Taylor, J. K. Joung, P. B. Dervan, and C. O. Pabo, *Biochemistry*, 2004, **43**, 3880–3890.

49. S. Neidle, *Nat. Prod. Rep.*, 2001, **18**, 291–309.

50. N. V. Hud and M. Polak, *Curr. Opin. Struct. Biol.*, 2001, **11**, 293–301.

51. M. P. Barrett, C. G. Gemmell and C. J. Suckling, *Pharmacol. Ther.*, 2013, **139**, 12–23.

52. M. P. Barrett, I. M. Vincent, R. J. Burchmore, A. J. Kazibwe and E. Matovu, *Future Microbiol.*, 2011, **6**, 1037–1047.

53. J. K. Thuita, K. K. Wolf, G. a. Murilla, Q. Liu, J. N. Mutuku, Y. Chen, A. S. Bridges, R. E. Mdachi, M. a. Ismail, S. Ching, D. W. Boykin, J. E. Hall, R. R. Tidwell, M. F. Paine, R. Brun and M. Z. Wang, *PLoS Negl. Trop. Dis.*, 2013, **7**, e2230.

54. M. N. C. Soeiro, K. Werbovetz, D. W. Boykin, W. D. Wilson, M. Z. Wang and A. Hemphill, *Parasitology*, 2013, **140**, 929–951.

55. S. Yang, T. Wenzler, P. N. Miller, H. Wu, D. W. Boykin, R. Brun and M. Z. Wang, *Antimicrob. Agents Chemother.*, 2014, **58**, 4064–4074.

56. S. Kuriakose and J. E. Uzonna, *Int. Immunopharmacol.*, 2014, **21**, 342–345.

57. F. Zsila, *Phys. Chem. Chem. Phys.*, 2015, **17**, 24560–24565.

58. C. a. Rice, B. L. Colon, M. Alp, H. Göker, D. W. Boykin and D. E. Kyle, *Antimicrob. Agents Chemother.*, 2015, **59**, 2037–2044.

59. P. Athri and W. D. Wilson, *J. Am. Chem. Soc.*, 2009, **131**, 7618-7625.

60. R. K. Arafa, R. Brun, T. Wenzler, F. A. Tanious, W. D. Wilson, C. E. Stephens and D. W. Boykin, *J. Med. Chem.*, 2005, **48**, 5480–5488.

61. L. Janovec, M. Kožurková, D. Sabolová, J. Ungvarský, H. Paulíková, J. Plšíková, Z. Vantová and J. Imrich, *Bioorg. Med. Chem.*, 2011, **19**, 1790–1801.

62. A. Paul, R. Nanjunda, A. Kumar, S. Laughlin, R. Nhili, S. Depauw, S. S. Deuser, Y. Chai, A. S. Chaudhary, M.H. David-Cordonnier, D. W. Boykin and W. D. Wilson, *Bioorg. Med. Chem. Lett.*, 2015, **25**, 4927-4932.

63. J. B. Chaires and X. Shi, in *Sequence-Specific DNA Binding Agents*, Royal Society of Chemistry, 2006, pp. 130–151.

64. R. Karlsson, *J. Mol. Recognit.*, 2004, **17**, 151–161.

65. S. Di Micco, C. Bassarello, G. Bifulco, R. Riccio, and L. Gomez-Paloma, *Angew. Chemie*, 2006, **118**, 230–234.

66. R. F. Dickerson and H. R. Drew, *J. Mol. Biol.*, 1981, **149**, 761–786.

67. S. Komeda, T. Moulaei, K. K. Woods, M. Chikuma, N. P. Farrell and L. D. Williams, *J. Am. Chem. Soc.*, 2006, **128**, 16092–103.

68. B. Nordén and T. Kurucsev, *J. Mol. Recognit.*, 1994, **7**, 141–55.

69. J. Kypr, I. Kejnovska, D. Renciuk and M. Vorlickova, *Nucleic Acids Res.*, 2009, **37**, 1713–1725.

70. B. Rosenberg, L. VanCamp, J. E. Trosko and V. H. Mansour, *Nature*, 1969, **222**, 385–386.

71. B. Lippert, *Cisplatin- Chemistry and Biochemistry of a Leading Anticancer Drug*, Verlag Helvetica Chimica Acta, Zürich, 1999.

72. N. Hadjiliadis and E. Sletten, *Metal Complex-DNA Interactions*, Blackwell Publishing, 2009.

73. D. Wang and S. J. Lippard, *Nat. Rev. Drug Discov.*, 2005, **4**, 307–20.

74. Z. Yang, L. M. Schumaker, M. J. Egorin, E. G. Zuhowski, Z. Guo and K. J. Cullen, *Clin. Cancer Res.*, 2006, **12**, 5817–25.

75. H. Alborzinia, S. Can, P. Holenya, C. Scholl, E. Lederer, I. Kitanovic and S. Wölfl, *PLoS One*, 2011, **6**, e19714.

76. M. S. Davies, M. D. Hall, S. J. Berners-Price and T. W. Hambley, *Inorg. Chem.*, 2008, **47**, 7673–80.

77. J. Hartwig, *Organotransition Metal Chemistry: From Bonding to Catalysis*, University Science Books, 1st edn., 2010.

78. M. W. Saif and J. Reardon, *Ther. Clin. Risk Manag.*, 2005, **1**, 249–58.

79. L. M. Pasetto, M. R. D'Andrea, E. Rossi and S. Monfardini, *Crit. Rev. Oncol. Hematol.*, 2006, **59**, 159–68.

80. F. D. Rochon and L. M. Gruia, *Inorganica Chim. Acta*, 2000, **306**, 193–204.

81. G. Ciarimboli, *Scientifica*, 2012, **2012**, 473829.

82. S. B. Howell, R. Safaei, C. A. Larson and M. J. Sailor, 2010, **77**, 887–894.

83. L. Kelland, *Nat. Rev. Cancer*, 2007, **7**, 573–84.

84. T. Boulikas, A. Pantos, E. Bellis and P. Christofis, *Designing platinum compounds in cancer : structures and mechanisms Review Article*, 2007, vol. 5.

85. N. J. Wheate, *Nanomedicine*, 2012, **7**, 1285–1287.

86. X. Wang and Z. Guo, *Chem. Soc. Rev.*, 2013.

87. D. P. Nowotnik and E. Cvitkovic, *Adv. Drug Deliv. Rev.*, 2009, **61**, 1214–1219.

88. I. Romero-Canelón and P. J. Sadler, *Inorg. Chem.*, 2013, **52**, 12276–91.

89. F. a Serrano, A. L. Matsuo, P. T. Monteforte, A. Bechara, S. S. Smaili, D. P. Santana, T. Rodrigues, F. V Pereira, L. S. Silva, J. Machado, E. L. Santos, J. B. Pesquero, R. M. Martins, L. R. Travassos, A. C. F. Caires and E. G. Rodrigues, *BMC Cancer*, 2011, **11**, 296.

90. D. Palanimuthu, S. V. Shinde, K. Somasundaram, and A. G. Samuelson, *J. Med. Chem.*, 2013, **56**, 722–34.

91. E. Alessio, *Bioinorganic Medicinal Chemistry*, John Wiley & Sons, Ltd, 2011.

92. a Bergamo, C. Gaiddon, J. H. M. Schellens, J. H. Beijnen and G. Sava, *J. Inorg. Biochem.*, 2012, **106**, 90–9.

93. Z. Liu, I. Romero-Canelón, B. Qamar, J. M. Hearn, A. Habtemariam, N. P. E. Barry, A. M. Pizarro, G. J. Clarkson and P. J. Sadler, *Angew. Chem. Int. Ed. Engl.*, 2014, 1–7.

94. J. J. Wilson and S. J. Lippard, *Chem. Rev.*, 2014, **114**, 4470-4495.

95. M. Coluccia, J. A. Nassi, F. Loseto, A. Boccarelli, M. A. Mariggio, D. Giordano, F. P. Intini, P. Caputo and G. Natile, *J. Med. Chem.* , 1993, **36**, 510–512.

96. M. Coluccia, A. Nassi, A. Boccarelli, D. Giordano, N. Cardellicchio, F. Intini, G. Natile, A. Barletta and A. Paradiso, *Int. J. Oncol.*, 1999, **15**, 1039–1083.

97. E. I. Montero, J. M. Pérez, A. Schwartz, M. a Fuertes, J. M. Malinge, C. Alonso, M. Leng and C. Navarro-Ranninger, *Chembiochem*, 2002, **3**, 61–7.

98. S. M. Aris and N. P. Farrell, *Eur. J. Inorg. Chem.*, 2009, **2009**, 1293.

99. D. Wang, G. Zhu, X. Huang and S. J. Lippard, *Proc. Natl. Acad. Sci. U. S. A.*, 2010, **107**, 9584–9.

100. G. Y. Park, J. J. Wilson, Y. Song and S. J. Lippard, *Proc. Natl. Acad. Sci. U. S. A.*, 2012, **2**, 1–6.

101. K. B. Garbutcheon-Singh, P. Leverett, S. Myers and J. R. Aldrich-Wright, *Dalt. Trans.*, 2013, 918–926.

102. A. A. Legin, M. A. Jakupec, N. A. Bokach, M. R. Tyan, V. Y. Kukushkin and B. K. Keppler, *J. Inorg. Biochem.*, 2014, **133**, 33–39.

103. A. Medrano, S. M. Dennis, A. Alvarez-Valdés, J. Perles, T. McGregor Mason and A. G. Quiroga, *Dalt. Trans.*, 2015, **44**, 3557–3562.

104. M. Skander, P. Retailleau, B. Bourrié, L. Schio, P. Mailliet and A. Marinetti, *J. Med. Chem.*, 2010, **53**, 2146–54.

105. M. Uemura, M. Hoshiyama, A. Furukawa, T. Sato, Y. Higuchi and S. Komeda, *Metallomics*, 2015.

106. J. Malina, N. P. Farrell and V. Brabec, *Inorg. Chem.*, 2014, **53**, 1662–71.

107. Y. Shi, S.-A. Liu, D. J. Kerwood, J. Goodisman and J. C. Dabrowiak, *J. Inorg. Biochem.*, 2012, **107**, 6–14.

108. B. W. Harper, A. M. Krause-Heuer, M. P. Grant, M. Manohar, K. B. Garbutcheon-Singh and J. R. Aldrich-Wright, *Chemistry*, 2010, **16**, 7064–77.

109. H. Li, X. Gao, R. Liu, Y. Wang, M. Zhang, Z. Fu, Y. Mi, Y. Wang, Z. Yao and Q. Gao, *Eur. J. Med. Chem.*, 2015, **101**, 400–408.

110. D. Griffith, M. P. Morgan and C. J. Marmion, *Chem. Commun.*, 2009, 6735–7.

111. J. P. Parker, H. Nimir, D. M. Griffith, B. Duff, A. J. Chubb, M. P. Brennan, M. P. Morgan, D. A. Egan and C. J. Marmion, *J. Inorg. Biochem.*, 2013, **124**, 70–77.

112. V. Brabec, D. M. Griffith, A. Kisova, H. Kostrhunova, L. Zerzankova, C. J. Marmion and J. Kasparkova, *Mol. Pharm.*, 2012, 1990–1999.

113. T. Sun, X. Guan, M. Zheng, X. Jing and Z. Xie, *ACS Med. Chem. Lett.*, 2015, **6**, 430–433.

114. B. J. Pages, D. L. Ang, E. P. Wright and J. R. Aldrich-Wright, *Dalt. Trans.*, 2015, **44**, 3505–3526.

115. S. Banerjee, E. B. Veale, C. M. Phelan, S. A. Murphy, G. M. Tocci, L. J. Gillespie, D. O. Frimannsson, J. M. Kelly and T. Gunnlaugsson, *Chem. Soc. Rev.*, 2013, **42**, 1601–18.

116. R. I. Taleb, D. Jaramillo, N. J. Wheate and J. R. Aldrich-Wright, *Chemistry*, 2007, **13**, 3177–86.

117. C. McKeever, PhD Thesis, University of Dublin, 2012.

118. A. Kahvedžić, PhD Thesis, University of Dublin, 2011.

119. A. Kahvedžić, S. M. Nathwani, D. M. Zisterer and I. Rozas, *J. Med. Chem.*, 2013, **56**, 451–459.

120. F. Rodríguez, I. Rozas, M. Kaiser, R. Brun, B. Nguyen, W. D. Wilson, R. N. García and C. Dardonville, *J. Med. Chem.*, 2008, **51**, 909–23.

121. P. S. Nagle, F. Rodriguez, A. Kahvedzić, S. J. Quinn and I. Rozas, *J. Med. Chem.*, 2009, **52**, 7113–21.

122. C. McKeever, M. Kaiser and I. Rozas, *J. Med. Chem.*, 2013, **56**, 700-711.

123. P. S. Nagle, S. J. Quinn, J. M. Kelly, D. H. O'Donovan, A. R. Khan, F. Rodriguez, B. Nguyen, W. D. Wilson and I. Rozas, *Org. Biomol. Chem.*, 2010, **8**, 5558–67.

124. P. S. Nagle, C. Mckeever, F. Rodriguez, B. Nguyen, W. D. Wilson and I. Rozas, *J. Med. Chem.* 2014,**57**, 7663-72.

125. E. Diez-Cecilia, B. Kelly, C. Perez, D. M. Zisterer, D. K. Nevin, D. G. Lloyd and I. Rozas, *Eur. J. Med. Chem.*, 2014, **81**, 427–441.

126. P. O'Sullivan and I. Rozas, *ChemMedChem*, 2014, **9**, 2065–2073.

127. ChemAxon (http://www.chemaxon.com).

128. O. Trott and A. J. Olson, *J. Comp. Chem.*, 2009, **31**, 455–461.

129. L. S. Glass, B. Nguyen, K. D. Goodwin, C. Dardonville, W. D. Wilson, E. C. Long, and M. M. Georgiadis, *Biochemistry*, 2009, **48**, 5943–52.

130. J. W. Shaw, D. H. Grayson and I. Rozas, Arkivoc, 2014, **2014**, 161–174.

131. B. R. B. Moodie, K. Schofield and J. B. Weston, *J. Chem. Soc. Perkin Trans. II*, 1976, 1089-1100.

132. A. I. Vogel, A. R. Tatchell, B. S. Furnis, A. J. Hannaford and P. W. G. Smith, *Vogel's Textbook of Practical Organic Chemistry*, 1996.

133. L. Kurti and B. Czakó, *Strategic Applications of Named Reactions in Organic Synthesis*, Elsevier, 1st edn., 2005.

134. J. K. Kochi, *J. Chem. Soc.*, 1956, **79**, 2942–2948.

135. E. Diez-Cecilia, B. Kelly and I. Rozas, *Tetrahedron Lett.*, 2011, **52**, 6702–6704.

136. D. S. Surry and S. L. Buchwald, *Chem. Sci.*, 2011, **2**, 27.

137. T. Kurita, F. Aoki, T. Mizumoto, T. Maejima, H. Esaki, T. Maegawa, Y. Monguchi and H. Sajiki, *Chemistry*, 2008, **14**, 3371–9.

138. F. Rodriguez, I. Rozas, J. E. Ortega, A. M. Erdozain, J. J. Meana and L. F. Callado, *J. Med. Chem.*, 2008, **51**, 3304–12.

139. N. Matsumura, A. Noguchi, A. Kitayoshi and H. Inoue, *J. Chem. Soc. Perkin Trans. I*, 1995, 2953–2954.

140. C. . Lee, W. Yang and R. G. Parr, *Phys. Rev. B*, 1988, **37**, 785–789.

141. A. D. Becke, *J. Chem. Phys.*, 1993, **98**, 1372–1377.

142. H. K. Srivastava, M. Chourasia, D. Kumar and G. N. Sastry, *J. Chem. Inf. Model.*, 2011, **51**, 558–71.

143. W. J. Hehre, R. Ditchfield and J. A. Pople, *J Chem. Phys.*, 1972, **56**, 2257–2262.

144. J. Tomasi, B. Mennucci and R. Cammi, *Chem. Rev.*, 2005, **105**, 2999–3093.

145. Gaussian 09, Revision A.1, M. J. Frisch, G. W. Trucks, H. B. Schlegel, G. E. Scuseria, M. A. Robb, J. R. Cheeseman, G. Scalmani, V. Barone, B. Mennucci, G. A. Petersson, H. Nakatsuji, M. Caricato, X. Li, H. P. Hratchian, A. F. Izmaylov, J. Bloino and G. Zhen, *Gaussian 09*, 2009.

146. D. Aitken, A. Albinati, A. Gautier, H. Husson, G. Morgant, J. Kozelka, P. Lemoine, S. Ongeri, S. Rizzato and B. Voissat, *Eur. J. Inorg. Chem.*, 2007, 3327–3334.

147. L. S. Glass, B. Nguyen, K. D. Goodwin, C. Dardonville, W. D. Wilson, E. C. Long and M. M. Georgiadis, *Biochemistry*, 2009, **48**, 5943–5952.

148. C. C. Group and Montreal, *www.chemcomp.com*, 2011.

149. W. L. Jorgensen, J. Chandrasekhar, J. D. Madura, R. W. Impey and M. L. Klein, *J Chem. Phys.*, 1983, **79**, 926–935.

150. P. Labute, *J. Chem. Inf. Model.*, 2010, **50**, 792–800.

151. J. Wang, R. M. Wolf, J. W. Caldwell, P. A. Kollman and D. A. Case, *J. Comput. Chem.*, 2004, **25**, 1157–1174.

152. D. A. Case, T. E. Cheatham III, T. Darden, H. Gohlke, R. Luo, K. M. Merz Jr., A. Onufriev, C. Simmerling, B. Wang and R. J. Woods, *J. Comput. Chem.*, 2005, **26**, 1668–1688.

153. P. A. Kollman, I. Massova, C. Reyes, B. Kuhn, S. Huo, L. Chong, M. Lee, T. Lee, Y. Duan, W. Wang, O. Donini, P. Cieplak, J. Srinivasan, D. A. Case and T. E. Cheatham, *Acc. Chem. Res.*, 2000, **33**, 889–897.

154. T. Hou, J. Wang, Y. Li and W. Wang, *J. Chem. Inf. Model.*, 2011, **51**, 69–82.

155. E. Lieber and G. B. L. Smith, *Chem. Rev.*, 1939, **25**, 213–271.

156. N. H. Lundstrom, 2000, US6045638.

157. B. Y. F. L. Scott, D. G. O. Donovan and J. Reilly, *J. Am. Chem. Soc.* 1953, **75**, 1294-1297.

158. C. F. Purchase Jr and A. D. White, 1994, US5362744.

159. M. Dobosz and M. Wujec, *Heterocycles*, 2002, **57**, 1135–1141.

160. G. L. Sommen, A. Linden and H. Heimgartner, *Helv. Chim. Acta*, 2007, **90**, 641–651.

161. N. I. Martin, W. T. Beeson, J. J. Woodward and M. A. Marletta, *J. Med. Chem.*, 2008, **51**, 924–31.

162. A. Kahvedzic, PhD Thesis, University of Dublin, 2011.

163. A. E. Dixon, *J. Chem. Soc. Trans.*, 1889, **55**, 300–305.

164. D. H. O'Donovan and I. Rozas, *Tetrahedron Lett.*, 2011, **52**, 4117–4119.

165. D. H. O'Donovan, B. Kelly, E. Diez-Cecilia, M. Kitson and I. Rozas, *New J. Chem.*, 2013, **37**, 2408.

166. J. H. Gorvin, *J. Chem. Soc. Perkin Trans I*, 1988, 1331–1335.

167. B. Kelly and I. Rozas, *Tetrahedron Lett.*, 2013, **54**, 3982–3984.

168. D. Griffith, M. P. Morgan and C. J. Marmion, *Chem. Commun.*, 2009, **65**, 6735–7.

169. J. Clayden, N. Greeves and S. Warren, *Organic Chemistry*, Oxford University Press, 2nd edn., 2012.

170. H. Chen, J.P. Luzy and C. Garbay, *Tetrahedron Lett.*, 2005, **46**, 3319–3322.

171. P. S. Nagle, PhD Thesis, University of Dublin, 2010.

172. A. Narsaiah and J. Kumar, *Synthesis*, 2010, **2010**, 1989–1991.

173. H. Mayr, T. Bug, M. F. Gotta, N. Hering, B. Irrgang, B. Janker, B. Kempf, R. Loos, A. R. Ofial, G. Remennikov and H. Schimmel, *J. Am. Chem. Soc.*, 2001, **123**, 9500–12.

174. D. Xu, C. Lu and W. Chen, *Tetrahedron*, 2012, **68**, 1466–1474.

175. C. Almansa, A. Gómez, Luis, L. Cavalcanti, F, F. de Arriba, A, R. Rodríguez, E. Carcellar, J. García-Rafanell and J. Forn, *J. Med. Chem.*, 1996, **39**, 2197–2206.

176. Y. Aubin, C. Fischmeister, C. M. Thomas and J.L. Renaud, *Chem. Soc. Rev.*, 2010, **39**, 4130–4145.

177. L. Qin, H. Cui, D. Zou, J. Li, Y. Wu, Z. Zhu and Y. Wu, *Tetrahedron Lett.*, 2010, **51**, 4445–4448.

178. I. P. Beletskaya and A. V. Cheprakov, *Organometallics*, 2012, **31**, 7753–7808.

179. C. Tao, W. Liu, A. Lv, M. Sun, Y. Tian, Q. Wang and J. Zhao, *Synlett*, 2010, 1355–1358.

180. A. Tlili, F. Monnier and M. Taillefer, *Chem. Eur. J*, 2010, **16**, 12299–302.

181. L. Jiang, X. Lu, H. Zhang, Y. Jiang, and D. Ma, *J. Org. Chem.*, 2009, **74**, 4542–4546.

182. J. A. Nicasio, S. Steinberg, B. Inés and M. Alcarazo, *Chem. Eur. J.*, 2013, **19**, 11016–11020.

183. N. C. Garbett, P. A.Ragazzon and J. B. Chaires, *Nat. Protoc.*, 2007, **2**, 3166–72.

184. L. H. Fornander, L. Wu, M. Billeter, P. Lincoln and B. Nordén, *J. Phys. Chem. B*, 2013, **117**, 5820–5830.

185. F. A. Tanious, D. Ding, D. A. Patrick, R. R. Tidwell and W. D. Wilson, *Biochemistry*, 1997, **36**, 15315–25.

186. F. A. Tanious, D. Ding, D. A. Patrick, C. Bailly, R. R. Tidwell and W. D. Wilson, *Biochemistry*, 2000, **39**, 12091–12101.

187. C. C. Barker, *J. Chem. Soc.*,1953, 870–873.

188. Z. Yu and D. Velasco, *Tetrahedron Lett.*, 1999, **40**, 3229–3232.

189. B. Du, X. Jiang, and P. Sun, *J. Org. Chem.*, 2013, **78**, 2786–2791.

190. J. F. Callahan, T. Li, Z. Wan and H. Yan, 2009, WO2009100169A1 Cpd 53.

191. A. B. Gamble, J. Garner, C. P. Gordon, S. M. J. O'Conner and P. A. Keller, *Synth. Commun.*, 2007, **37**, 2777–2786.

192. F. D. Bellamy and K. Ou, *Tetrahedron Lett.*, 1984, **25**, 839–842.

193. S. Reim, M. Lau and P. Langer, *Tetrahedron Lett.*, 2006, **47**, 6903–6905.

194. J. H. Forsberg, V. T. Spaziano, T. M. Balasubramanian, G. K. Liu, S. A. Kinsley, C. A. Duckworth, J. J. Poteruca, P. S. Brown and J. L. Miller, *J. Org. Chem.*, 1987, **52**, 1017–1021.

195. K. Brunner, A. van Dijken, H. Borner, J. J. A. M. Bastiaansen, N. M. M. Kiggen and B. M. W. Langeveld, *J. Am. Chem. Soc.*, 2004, **126**, 6035–6042.

196. B. Kobin, L. Grubert, S. Blumstengel, F. Henneberger and S. Hecht, *J. Mater. Chem.*, 2012, **22**, 4383.

197. S. B. Ferreira, C. R. Kaiser and V. F. Ferreira, *Synlett*, 2008, 2625–2628.

198. Y. Song, W. X. and D. Zhu, *Tetrahedron Lett.*, 2010, **51**, 4894–4897.

199. S. Lee, M. Jørgensen and J. F. Hartwig, *Org. Lett.*, 2001, **3**, 2729–2732.

200. K. Vandyck, G. Y. P. Haché, G. Rombouts, W. G. Verschueren and P. J.M. B. Raboisson, WO2013102655A1, Cpd 32.

201. T. Li, W. Cui, J. Liu, J. Zhao and Z. Wang, *Chem. Commun.*, 2000, 139–140.

202. P. J. Bailey and S. Pace, *Coord. Chem. Rev.*, 2001, **214**, 91–141.

203. P. V Gushchin, N. A. Bokach, K. V Luzyanin, A. A. Nazarov, M. Haukka, V. Y. Kukushkin and A. R. Pais, *Inorg. Chem.*, 2007, **46**, 1684–1693.

204. U. Wild, P. Roquette, E. Kaifer, J. Mautz, O. Hübner, H. Wadepohl and H.J. Himmel, *Eur. J. Inorg. Chem.*, 2008, **8**, 1248–1257.

205. P. Elumalai, N. Thirupathi and M. Nethaji, *Inorg. Chem.*, 2013, **4**, 1883-1894.

206. M. B. Dinger, W. Henderson and B. K. Nicholson, *J. Organomet. Chem.*, 1998, **556**, 75–88.

207. M. B. Dinger and W. Henderson, *Chem. Commun.*, 1996, **1**, 211–212.

208. D. Nieto, S. Bruña, A. M. González-Vadillo, J. Perles, F. Carrillo-Hermosilla, A. Antiñolo, J. M. Padrón, G. B. Plata and I. Cuadrado, *Organometallics*, 2015, **34**, 5407-5417.

209. N. Aoyagi, Y. Furusho and T. Endo, *Synlett*, 2014, **25**, 983–986.

210. C. Dardonville, P. Goya, I. Rozas, A. Alsasua, M. I. Martín and M. J. Borrego, *Bioorg. Med. Chem.*, 2000, **8**, 1567–77.

211. T. Yamada, X. Liu, U. Englert, H. Yamane and R. Dronskowski, *Chemistry*, 2009, **15**, 5651–5.

212. F. Rodriguez, I. Rozas, J. E. Ortega, J. J. Meana and L. F. Callado, *J. Med. Chem.*, 2007, **50**, 4516–27.

213. J. H. Price, A. N. Williamson, R. F. Schramm and B. B. Wayland, *Inorg. Chem.*, 1972, **11**, 1280–1284.

214. V. Sicilia, M. Baya, P. Borja and A. Martín, *Inorg. Chem.*, 2015, **54**, 7316–7324.

215. E. Anger, M. Rudolph, C. Shen, N. Vanthuyne, L. Toupet, C. Roussel, J. Autschbach, J. Crassous and R. Réau, *J. Am. Chem. Soc.*, 2011, **133**, 3800–3803.

216. K. Matsumoto and M. Ochiai, *Coord. Chem. Rev.*, 2002, **231**, 229–238.

217. J. J. Wilson and S. J. Lippard, *Inorg. Chem.*, 2012, **51**, 9852–9864.

218. S. U. Pandya, K. C. Moss, M. R. Bryce, A. S. Batsanov, M. A. Fox, V. Jankus, H. A. Al Attar and A. P. Monkman, *Eur. J. Inorg. Chem.*, 2010, 1963–1972.

219. Y. Y. Scaffidi-Domianello, A. a. Nazarov, M. Haukka, M. Galanski, B. K. Keppler, J. Schneider, P. Du, R. Eisenberg and V. Y. Kukushkin, *Inorg. Chem.*, 2007, **46**, 4469–4482.

220. V. Y. Kukushkin and A. J. L. Pombeiro, *Chem. Rev.*, 2002, **102**, 1771–1802.

221. D. Ashen-Garry and M. Selke, *Photochem. Photobiol.*, 2014, **90**, 257–274.

222. W. Spiller, H. Kliesch, D. Wöhrle, S. Hackbarth, B. Röder and G. Schnurpfeil, *J. Porphyrins Phthalocyanines*, 1998, **02**, 145–158.

223. P. R. Ogilby, *Chem. Soc. Rev.*, 2010, **39**, 3181.

224. J. Brooks, Y. Babayan, S. Lamansky, P. I. Djurovich, I. Tsyba, R. Bau and M. E. Thompson, *Inorg. Chem.*, 2002, **41**, 3055–3066.

225. W. J. Choi, S. Choi, K. Ohkubo, S. Fukuzumi, E. J. Cho and Y. You, *Chem. Sci.*, 2015, **6**, 1454–1464.

226. F. D. Rochon and G. Massarweh, *Inorganica Chim. Acta*, 2006, **359**, 4095–4104.

227. Y. S. Sohn and K. M. Kim, 1992, US5142075.

228. J. F. Arambula, J. L. Sessler, M. E. Fountain, W. Wei, D. Magda and Z. H. Siddik, *Dalt. Trans.*, 2009, 10834–10840.

229. J. F. Arambula, J. L. Sessler and Z. H. Siddik, *Med. Chem. Commum.*, 2012, **3**, 1275–1281.

230. X. Chen, Y. Yan, X. Meng, F. Zhao, Z. Gao and S. Wen, 2014, US 2014/0142079 A1.

231. R. G. Johnson and R. K. Ingham, *Chem. Rev.*, 1956, **56**, 219–269.

232. N. G. Connelly and W. E. Geiger, *Chem. Rev.*, 1996, **96**, 877–910.

233. E. Lee, L. Piao and J. Kim, *Bull. Korean Chem. Soc.*, 2012, **33**, 60–64.

234. Y.-A. Lee, O.S. Jung, Y. S. Sohn and K. B. Lee, *Polyhedron*, 1995, **14**, 2099–2106.

235. Y.-A. Lee, Y. K. Chung, K. M. Kim and Y. S. Sohn, *Inorg. Chim. Acta.*, 1998, **279**, 116–120.

236. M. L. Tobe and J. Burgess, *Inorganic Reaction Mechanisms*, Longman, 1999.

237. R. H. Crabtree, *The Organometallic Chemistry of the Transition Metals*, Wiley, 6th Editio., 2014.

238. L. Cai, K. Lim, S. Ren, R. S. Cadena and W. T. Beck, *J. Med. Chem.*, 2001, **44**, 2959–2965.

239. B. Lippert, C. J. L. Lock and R. A. Speranzini, *Inorg. Chem.*, 1981, **20**, 808–813.

240. Y. Kasherman, S. Sturup and D. Gibson, *J. Biol. Inorg. Chem.*, 2009, **14**, 387–399.

241. Y. Lee, O. Jung, S. Kang, K. Lee and Y. S. Sohn, *Inorg. Chem.*, 1996, **35**, 1641–1646.

242. W. Zhao, T. Zhang, B. Qu, X. Wu, X. Zhu, F. Meng, Y. Gu, Y. Shu, Y. Shen, Y. Sun and Q. Xu, *Anticancer. Drugs*, 2011, **22**, 79–88.

243. www.thermofisher.com/order/catalog/product/88951

244. www.chem.canterbury.ac.nz/researchgroup/antony_fai

245. S. N. Rampersad, *Sensors*, 2012, **12**, 12347–12360.

246. G. K. Kinsella, F. Rodriguez, G. W. Watson and I. Rozas, *Bioorg. Med. Chem.*, 2007, **15**, 2850–5.

247. E. D. Cecilia, P. D. Zisterer and P. I. Rozas, 2011, **7**, 6702.

248. L. A. Graham, J. Suryadi, T. K. West, G. L. Kucera and U. Bierbach, *J. Med. Chem.*, 2012, **55**, 7817–27.

249. S. M. O. Quintal, Y. Qu, A. G. Quiroga, J. Moniodis, H. I. S. Nogueira and N. Farrell, *Inorg. Chem.*, 2005, **44**, 5247–5253.

250. N. Aoyagi, Y. Furusho and T. Endo, *Synlett*, 2014, **25**, 983–986.

251. A. Bredihhin and U. Mäeorg, *Tetrahedron*, 2008, **64**, 6788–6793.

252. B. Goldfuss, T. Löschmann, T. Kop-Weiershausen, J. Neudörfl and F. Rominger, *Beilstein J. Org. Chem.*, 2006, **2**, 7.

253. B. Kelly, M. McMullan, C. Muguruza, J. E. Ortega, J. J. Meana, L. F. Callado and I. Rozas, *J. Med. Chem.*, 2015, **58**, 963–977.

Appendix

X-ray Crystallography Data

Crystal data for 220

A specimen of $C_9H_{14}ClN_3OPtS$, approximate dimensions 0.100 mm x 0.100 mm x 0.180 mm, was used for the X-ray crystallographic analysis. The X-ray intensity data were measured. The X-ray intensity data were measured at 100(2)K using an Oxford Cryosystems Cobra low temperature device using a MiTeGen micromount. See Table 1 for collection parameters and exposure time. Bruker APEX software was used to correct for Lorentz and polarization effects.

A total of 733 frames were collected. The total exposure time was 4.89 hours. The integration of the data using an orthorhombic unit cell yielded a total of 21346 reflections to a maximum θ angle of 30.09° (0.71 Å resolution), of which 3528 were independent (average redundancy 6.050, completeness = 100.0%, R_{int} = 1.47%, R_{sig} = 1.95%) and 3401 (96.40%) were greater than $2\sigma(F^2)$. The final cell constants of a = 11.6799(6) Å, b = 8.0262(4) Å, c = 13.2131(7) Å, volume = 1238.66(11) $Å^3$, are based upon the refinement of the XYZ-centroids of reflections above 20 σ(I). The calculated minimum and maximum transmission coefficients (based on crystal size) are 0.2469 and0.4128.

The structure was solved and refined using the Bruker SHELXTL Software Package, using the space group $Pna2_1$, with Z = 4 for the formula unit, $C_9H_{14}ClN_3OPtS$. The final anisotropic full-matrix least-squares refinement on F^2 with 145 variables converged at R1 = 0.87%, for the observed data and wR2 = 2.01% for all data. The goodness-of-fit was 1.075. The largest peak in the final difference electron density synthesis was 0.304 $e^-/Å^3$ and the largest hole was -0.445 $e^-/Å^3$ with an RMS deviation of 0.062 $e^-/Å^3$. On the basis of the final model, the calculated density was 2.375 g/cm^3 and F(000), 832 e^-.

Table 1. Crystal data and structure refinement for 220.

Identification code	tcd152	
Empirical formula	C9H14ClN3OPtS	
Formula weight	442.83	
Temperature	100(2) K	
Wavelength	0.71073 Å	
Crystal system	Orthorhombic	
Space group	Pna21	
Unit cell dimensions	a = 11.6799(6) Å	α= 90°.
	b = 8.0262(4) Å	β= 90°.
	c = 13.2131(7) Å	γ = 90°.
Volume	1238.66(11) Å3	
Z	4	
Density (calculated)	2.375 Mg/m3	
Absorption coefficient	11.694 mm-1	
F(000)	832	
Crystal size	0.180 x 0.100 x 0.100 mm3	
Theta range for data collection	2.969 to 30.090°.	
Index ranges	-16≤h≤16, -11≤k≤11, -18≤l≤18	
Reflections collected	21346	
Independent reflections	3528 [R(int) = 0.0147]	
Completeness to theta = 25.242°	100.0 %	
Absorption correction	Numerical	
Max. and min. transmission	0.4128 and 0.2469	
Refinement method	Full-matrix least-squares on F2	
Data / restraints / parameters	3528 / 1 / 145	
Goodness-of-fit on F2	1.075	
Final R indices [I>2σ(I)]	R1 = 0.0087, wR2 = 0.0200	
R indices (all data)	R1 = 0.0096, wR2 = 0.0201	
Absolute structure parameter	-0.002(2)	
Largest diff. peak and hole	0.304 and -0.445 e.Å-3	

Crystal data for 221

A clear bronze needle-like specimen of $C_{11}H_{16}ClN_3OPtS$, approximate dimensions 0.040 mm x 0.090 mm x 0.100 mm, was used for the X-ray crystallographic analysis. The X-ray intensity data were measured at 100(2)K using an Oxford Cryosystems Cobra low temperature device using a MiTeGen micromount. See Table 1 for collection parameters and exposure time. Bruker APEX software was used to correct for Lorentz and polarization effects.

A total of 1433 frames were collected. The total exposure time was 3.98 hours. The frames were integrated with the Bruker SAINT software package using a narrow-frame algorithm. The integration of the data using an orthorhombic unit cell yielded a total of 42495 reflections to a maximum θ angle of 30.14° (0.71 Å resolution), of which 4105 were independent (average redundancy 10.352, completeness = 100.0%, R_{int} = 2.59%, R_{sig} = 1.23%) and 3622 (88.23%) were greater than $2\sigma(F^2)$. The final cell constants of a = 11.8110(5) Å, b = 12.8065(5) Å, c = 18.3660(7) Å, volume = 2778.00(19) $Å^3$, are based upon the refinement of the XYZ-centroids of 9988 reflections above 20 σ(I) with 5.189° < 2θ < 60.28°. Data were corrected for absorption effects using the multi-scan method (SADABS). The ratio of minimum to maximum apparent transmission was 0.800. The calculated minimum and maximum transmission coefficients (based on crystal size) are 0.5968 and 0.7460.

The structure was solved and refined using the Bruker SHELXTL Software Package, using the space group Pbca, with Z = 8 for the formula unit, $C_{11}H_{16}ClN_3OPtS$. The final anisotropic full-matrix least-squares refinement on F^2 with 173 variables converged at R1 = 1.19%, for the observed data and wR2 = 2.35% for all data. The goodness-of-fit was 1.023. The largest peak in the final difference electron density synthesis was 0.435 $e^-/Å^3$ and the largest hole was -0.475 $e^-/Å^3$ with an RMS deviation of 0.085 $e^-/Å^3$. On the basis of the final model, the calculated density was 2.242 g/cm^3 and F(000), 1776 e^-.

Table 2. Crystal data and structure refinement for 221

Identification code	tcd177	
Empirical formula	C11H16ClN3OPtS	
Formula weight	468.87	
Temperature	100(2) K	
Wavelength	0.71073 Å	
Crystal system	Orthorhombic	
Space group	Pbca	
Unit cell dimensions	a = 11.8110(5) Å	α= 90°.
	b = 12.8065(5) Å	β= 90°.
	c = 18.3660(7) Å	γ = 90°.
Volume	2778.00(19) Å3	
Z	8	
Density (calculated)	2.242 Mg/m3	
Absorption coefficient	10.436 mm-1	
F(000)	1776	
Crystal size	0.100 x 0.090 x 0.040 mm3	
Theta range for data collection	2.218 to 30.142°.	
Index ranges	-16≤h≤16, -18≤k≤17, -25≤l≤25	
Reflections collected	42495	
Independent reflections	4105 [R(int) = 0.0259]	
Completeness to theta = 25.242°	100.0 %	
Absorption correction	Semi-empirical from equivalents	
Max. and min. transmission	0.7460 and 0.5968	
Refinement method	Full-matrix least-squares on F2	
Data / restraints / parameters	4105 / 0 / 173	
Goodness-of-fit on F2	1.023	
Final R indices [I>2σ(I)]	R1 = 0.0119, wR2 = 0.0226	
R indices (all data)	R1 = 0.0168, wR2 = 0.0235	
Largest diff. peak and hole	0.435 and -0.475 e.Å-3	

Crystal data for 222

A specimen of $C_{11}H_{20}Cl_2N_4O_{2.25}Pt_2S_2$, approximate dimensions 0.050 mm x 0.090 mm x 0.120 mm, was used for the X-ray crystallographic analysis. The X-ray intensity data were measured at 100(2)K using an Oxford Cryosystems Cobra low temperature device using a MiTeGen micromount. See Table 1 for collection parameters and exposure time. Bruker APEX software was used to correct for Lorentz and polarization effects.

A total of 2479 frames were collected. The total exposure time was 16.53 hours. The frames were integrated with the Bruker SAINT software package using a narrow-frame algorithm. The integration of the data using a monoclinic unit cell yielded a total of 40546 reflections to a maximum θ angle of 26.08° (0.81 Å resolution), of which 7486 were independent (average redundancy 5.416, completeness = 99.8%, R_{int} = 3.55%, R_{sig} = 2.87%) and 6846 (91.45%) were greater than $2\sigma(F^2)$.The final cell constants of a = 9.6070(8) Å, b = 9.4042(8) Å, c = 21.1395(17) Å, β = 96.965(2)°, volume = 1895.8(3) $Å^3$, are based upon the refinement of the XYZ-centroids of 9269 reflections above 20 σ(I) with 4.723° < 2θ < 54.81°.Data were corrected for absorption effects using the multi-scan method (SADABS). The ratio of minimum to maximum apparent transmission was 0.708. The calculated minimum and maximum transmission coefficients (based on crystal size) are 0.5277 and 0.7456.

The structure was solved and refined using the Bruker SHELXTL Software Package, using the space group $P2_1$, with Z = 4 for the formula unit, $C_{11}H_{20}Cl_2N_4O_{2.25}Pt_2S_2$.The final anisotropic full-matrix least-squares refinement on F^2 with 409 variables converged at R1 = 3.23%, for the observed data and wR2 = 7.58% for all data. The goodness-of-fit was 1.053. The largest peak in the final difference electron density synthesis was 1.450 $e^-/Å^3$ and the largest hole was -1.773 $e^-/Å^3$ with an RMS deviation of 0.213 $e^-/Å^3$. On the basis of the final model, the calculated density was 2.696 g/cm^3 and F(000), 1416 e^-.

Refinement Note: The compound was refined as an inversion twin with a ratio of 0.50(2) in P2(1). The refinement in the centrosymmetric space group P2(1)/n led to a worse solution with R = 4.68% and large residuals of ca. 4.4e^-/Å. There are 171 lattice exception > 3s for the n glide. Restraints and constraints are needed for both solutions. No hydrogen atoms were

located. All hydrogen atoms were placed in calculated positions riding on the carrier atom according to the synthetic model.

Table 3. Crystal data and structure refinement for 222

Identification code	tcd259	
Empirical formula	C11H20Cl2N4O2.25Pt2S2	
Formula weight	769.51	
Temperature	100(2) K	
Wavelength	0.71073 Å	
Crystal system	Monoclinic	
Space group	P21	
Unit cell dimensions	a = 9.6070(8) Å	α= 90°.
	b = 9.4042(8) Å	β= 96.965(2)°.
	c = 21.1395(17) Å	γ = 90°.
Volume	1895.8(3) Å3	
Z	4	
Density (calculated)	2.696 Mg/m3	
Absorption coefficient	15.257 mm-1	
F(000)	1416	
Crystal size	0.120 x 0.090 x 0.050 mm3	
Theta range for data collection	0.970 to 26.084°.	
Index ranges	-11≤h≤11, -11≤k≤11, -26≤l≤25	
Reflections collected	40546	
Independent reflections	7486 [R(int) = 0.0355]	
Completeness to theta = 25.242°	100.0 %	
Absorption correction	Semi-empirical from equivalents	
Max. and min. transmission	0.7456 and 0.5277	
Refinement method	Full-matrix least-squares on F2	
Data / restraints / parameters	7486 / 199 / 409	
Goodness-of-fit on F2	1.053	
Final R indices [I>2σ(I)]	R1 = 0.0323, wR2 = 0.0738	
R indices (all data)	R1 = 0.0371, wR2 = 0.0758	
Absolute structure parameter	0.50(2)	
Largest diff. peak and hole	1.450 and -1.773 e.Å-3	

Crystal data for 223

A specimen of $C_{28}H_{44}I_3N_9O_6Pt_2$, approximate dimensions 0.013 mm x 0.020 mm x 0.150 mm, was used for the X-ray crystallographic analysis. The X-ray intensity data were measured at 100(2)K using an Oxford Cryosystems Cobra low temperature device using a MiTeGen micromount. See Table 1 for collection parameters and exposure time.

A total of 633 frames were collected. The total exposure time was 3.34 hours. The frames were integrated with the Bruker SAINT software package using a narrow-frame algorithm. The integration of the data using a monoclinic unit cell yielded a total of 71636 reflections to a maximum θ angle of 27.14° (0.78 Å resolution), of which 8483 were independent (average redundancy 8.445, completeness = 99.9%, R_{int} = 6.76%, R_{sig} = 3.90%) and 6996 (82.47%) were greater than $2\sigma(F^2)$. The final cell constants of a = 15.3526(11) Å, b = 15.6010(11) Å, c = 16.0353(12) Å, β = 94.2679(10)°, volume = 3830.1(5) $Å^3$, are based upon the refinement of the XYZ-centroids of 9967 reflections above 20 σ(I) with 4.625° < 2θ < 54.18°. Data were corrected for absorption effects using the multi-scan method (SADABS). The ratio of minimum to maximum apparent transmission was 0.665. The calculated minimum and maximum transmission coefficients (based on crystal size) are 0.4960 and 0.7455.

The structure was solved and refined using the Bruker SHELXTL Software Package, using the space group $P2_1/c$, with Z = 4 for the formula unit, $C_{28}H_{44}I_3N_9O_6Pt_2$. The final anisotropic full-matrix least-squares refinement on F^2 with 438 variables converged at R1 = 2.62%, for the observed data and wR2 = 6.88% for all data. The goodness-of-fit was 1.020. The largest peak in the final difference electron density synthesis was 1.942 $e^-/Å^3$ and the largest hole was -2.071 $e^-/Å^3$ with an RMS deviation of 0.201 $e^-/Å^3$. On the basis of the final model, the calculated density was 2.382 g/cm^3 and F(000), 2552 e^-.

Refinement Note: Two atoms (C24, C41) were modelled with restraints (ISOR). Donor hydrogen atoms located on the difference map but then refined with a riding model (AFIX).

Table 4. Crystal data and structure refinement for 223

Identification code	tcd230	
Empirical formula	$C_{28}H_{44}I_3N_9O_6Pt_2$	
Formula weight	1373.60	
Temperature	100(2) K	
Wavelength	0.71073 Å	
Crystal system	Monoclinic	
Space group	$P2_1/c$	
Unit cell dimensions	a = 15.3526(11) Å	α= 90°.
	b = 15.6010(11) Å	β= 94.2679(10)°.
	c = 16.0353(12) Å	γ = 90°.
Volume	3830.1(5) $Å^3$	
Z	4	
Density (calculated)	2.382 Mg/m^3	
Absorption coefficient	9.766 mm^{-1}	
F(000)	2552	
Crystal size	0.150 x 0.020 x 0.013 mm^3	
Theta range for data collection	1.824 to 27.142°.	
Index ranges	-19≤h≤19, -19≤k≤20, -20≤l≤19	
Reflections collected	71636	
Independent reflections	8483 [R(int) = 0.0676]	
Completeness to theta = 25.242°	100.0 %	
Absorption correction	Semi-empirical from equivalents	
Max. and min. transmission	0.7455 and 0.4960	
Refinement method	Full-matrix least-squares on F^2	
Data / restraints / parameters	8483 / 12 / 438	
Goodness-of-fit on F^2	1.020	
Final R indices [I>2σ(I)]	R1 = 0.0262, wR2 = 0.0613	
R indices (all data)	R1 = 0.0413, wR2 = 0.0688	
Largest diff. peak and hole	1.942 and -2.071 $e.Å^{-3}$	

Crystal data for 232

A specimen of $C_{11}H_{17}Cl_2N_3OPtS$, approximate dimensions 0.080 mm x 0.080 mm x 0.150 mm, was used for the X-ray crystallographic analysis. The X-ray intensity data were measured at 100(2)K using an Oxford Cryosystems Cobra low temperature device using a MiTeGen micromount. See Table 1 for collection parameters and exposure time. Bruker APEX software was used to correct for Lorentz and polarization effects.

A total of 784 frames were collected. The total exposure time was 2.18 hours. The integration of the data using an orthorhombic unit cell yielded a total of 50835 reflections to a maximum θ angle of 30.07° (0.71 Å resolution), of which 4405 were independent (average redundancy 11.540, completeness = 100.0%, R_{int} = 4.33%, R_{sig} = 2.44%) and 4177 (94.82%) were greater than $2\sigma(F^2)$. The final cell constants of $\underline{a}$ = 7.1928(4) Å, $\underline{b}$ = 13.8777(8) Å, $\underline{c}$ = 15.0416(9) Å, volume = 1501.45(15) $Å^3$, are based upon the refinement of the XYZ-centroids of reflections above 20 σ(I). Data were corrected for absorption effects using the multi-scan method (SADABS). The calculated minimum and maximum transmission coefficients (based on crystal size) are 0.4700 and 0.7460.

The structure was solved and refined using the Bruker SHELXTL Software Package, using the space group $P2_12_12_1$, with Z = 4 for the formula unit, $C_{11}H_{17}Cl_2N_3OPtS$. The final anisotropic full-matrix least-squares refinement on F^2 with 178 variables converged at R1 = 1.52%, for the observed data and wR2 = 3.14% for all data. The goodness-of-fit was 1.020. The largest peak in the final difference electron density synthesis was 1.123 $e^-/Å^3$ and the largest hole was -0.734 $e^-/Å^3$ with an RMS deviation of 0.097 $e^-/Å^3$. On the basis of the final model, the calculated density was 2.235 g/cm^3 and F(000), 960 e^-.

Table 5. Crystal data and structure refinement for 232

Identification code	tcd181	
Empirical formula	C11H17Cl2N3OPtS	
Formula weight	505.32	
Temperature	100(2) K	
Wavelength	0.71073 Å	
Crystal system	Orthorhombic	
Space group	P212121	
Unit cell dimensions	a = 7.1928(4) Å	α= 90°.
	b = 13.8777(8) Å	β= 90°.
	c = 15.0416(9) Å	γ = 90°.
Volume	1501.45(15) Å3	
Z	4	
Density (calculated)	2.235 Mg/m3	
Absorption coefficient	9.835 mm-1	
F(000)	960	
Crystal size	0.150 x 0.080 x 0.080 mm3	
Theta range for data collection	1.997 to 30.072°.	
Index ranges	-10≤h≤10, -18≤k≤19, -21≤l≤21	
Reflections collected	50835	
Independent reflections	4405 [R(int) = 0.0433]	
Completeness to theta = 25.242°	100.0 %	
Absorption correction	Semi-empirical from equivalents	
Max. and min. transmission	0.7460 and 0.4700	
Refinement method	Full-matrix least-squares on F2	
Data / restraints / parameters	4405 / 2 / 178	
Goodness-of-fit on F2	1.020	
Final R indices [I>2σ(I)]	R1 = 0.0152, wR2 = 0.0309	
R indices (all data)	R1 = 0.0176, wR2 = 0.0314	
Absolute structure parameter	-0.001(3)	
Largest diff. peak and hole	1.123 and -0.734 e.Å-3	

Crystal data for 233

A specimen of $C_{13}H_{17}Cl_2N_5Pt$, approximate dimensions 0.060 mm x 0.070 mm x 0.180 mm, was used for the X-ray crystallographic analysis. The X-ray intensity data were measured at 100(2)K using an Oxford Cryosystems Cobra low temperature device using a MiTeGen micromount. See Table 1 for collection parameters and exposure time. Bruker APEX software was used to correct for Lorentz and polarization effects.

A total of 2013 frames were collected. The total exposure time was 3.36 hours. The integration of the data using a monoclinic unit cell yielded a total of 78514 reflections to a maximum θ angle of 32.72° (0.66 Å resolution), of which 5862 were independent (average redundancy 13.394, completeness = 100.0%, R_{int} = 3.36%, R_{sig} = 1.69%) and 5093 (86.88%) were greater than $2\sigma(F^2)$.The final cell constants of a = 7.2417(2) Å, b = 11.2409(3) Å, c = 19.6167(6) Å, β = 91.9052(11)°, volume = 1595.98(8) $Å^3$, are based upon the refinement of the XYZ-centroids of reflections above 20 σ(I).The calculated minimum and maximum transmission coefficients (based on crystal size) are 0.5523 and 0.7464.

The structure was solved and refined using the Bruker SHELXTL Software Package, using the space group $P2_1/c$, with Z = 4 for the formula unit, $C_{13}H_{17}Cl_2N_5Pt$.The final anisotropic full-matrix least-squares refinement on F^2 with 196 variables converged at R1 = 1.76%, for the observed data and wR2 = 3.67% for all data. The goodness-of-fit was 1.033. The largest peak in the final difference electron density synthesis was 1.494 $e^-/Å^3$ and the largest hole was -0.825 $e^-/Å^3$ with an RMS deviation of 0.116 $e^-/Å^3$. On the basis of the final model, the calculated density was 2.120 g/cm^3 and F(000), 968 e^-.

Refinement Note: Amido hydrogen atoms were located and refined using a DFIX restraint.

Table 6. Crystal data and structure refinement for 233

Identification code	tcd193	
Empirical formula	C13H17Cl2N5Pt	
Formula weight	509.30	
Temperature	100(2) K	
Wavelength	0.71073 Å	
Crystal system	Monoclinic	
Space group	P21/c	
Unit cell dimensions	a = 7.2417(2) Å	α= 90°.
	b = 11.2409(3) Å	β= 91.9052(11)°.
	c = 19.6167(6) Å	γ = 90°.
Volume	1595.98(8) Å3	
Z	4	
Density (calculated)	2.120 Mg/m3	
Absorption coefficient	9.126 mm-1	
F(000)	968	
Crystal size	0.180 x 0.070 x 0.060 mm3	
Theta range for data collection	2.077 to 32.715°.	
Index ranges	-10≤h≤11, -17≤k≤17, -29≤l≤29	
Reflections collected	78514	
Independent reflections	5862 [R(int) = 0.0336]	
Completeness to theta = 25.242°	100.0 %	
Absorption correction	Semi-empirical from equivalents	
Max. and min. transmission	0.7464 and 0.5523	
Refinement method	Full-matrix least-squares on F2	
Data / restraints / parameters	5862 / 2 / 196	
Goodness-of-fit on F2	1.033	
Final R indices [I>2σ(I)]	R1 = 0.0176, wR2 = 0.0348	
R indices (all data)	R1 = 0.0247, wR2 = 0.0367	
Largest diff. peak and hole	1.494 and -0.825 e.Å-3	

Crystal data (i) for 246a

A specimen of $C_{38}H_{66}Cl_4N_{12}O_{13}Pt_4S_4$, approximate dimensions 0.010 mm x 0.110 mm x 0.170 mm, was used for the X-ray crystallographic analysis. The X-ray intensity data were measured at 100(2)K using an Oxford Cryosystems Cobra low temperature device using a MiTeGen micromount. See Table 1 for collection parameters and exposure time. Bruker APEX software was used to correct for Lorentz and polarization effects.

A total of 3366 frames were collected. The total exposure time was 14.03 hours. The frames were integrated with the Bruker SAINT software package using a narrow-frame algorithm. The integration of the data using an orthorhombic unit cell yielded a total of 85945 reflections to a maximum θ angle of 26.46° (0.80 Å resolution), of which 6036 were independent (average redundancy 14.239, completeness = 99.7%, R_{int} = 8.02%, R_{sig} = 3.76%) and 5118 (84.79%) were greater than $2\sigma(F^2)$.The final cell constants of a = 21.4574(13) Å, b = 12.2646(8) Å, c = 11.1760(6) Å, volume = 2941.1(3) $Å^3$, are based upon the refinement of the XYZ-centroids of 9965 reflections above 20 σ(I) with 4.931° < 2θ < 50.81°.Data were corrected for absorption effects using the multi-scan method (SADABS). The ratio of minimum to maximum apparent transmission was 0.656. The calculated minimum and maximum transmission coefficients (based on crystal size) are 0.4890 and 0.7454.

The structure was solved and refined using the Bruker SHELXTL Software Package, using the space group $Pna2_1$, with Z = 2 for the formula unit, $C_{38}H_{66}Cl_4N_{12}O_{13}Pt_4S_4$.The final anisotropic full-matrix least-squares refinement on F^2 with 361 variables converged at R1 = 4.53%, for the observed data and wR2 = 11.09% for all data. The goodness-of-fit was 1.073. The largest peak in the final difference electron density synthesis was 2.919 $e^-/Å^3$ and the largest hole was -3.232 $e^-/Å^3$ with an RMS deviation of 0.234 $e^-/Å^3$. On the basis of the final model, the calculated density was 2.201 g/cm^3 and F(000), 1852 e^-.

Refinement Note: Refined as a 2-component twin. BASF = 0.489. Restraints (SADI, ISOR, SIMU) and constraints (EADP) used to model the disorder in the Cl position (72/18% occupancy) and also several atoms (O, C, N, Cl). No hydrogen atoms could be located for the solvent water atoms in this heavy atom structure. All hydrogen atoms have been included in the sum formula.

Table 7. Crystal data and structure refinement for 246a.

Identification code	tcd257	
Empirical formula	$C_{38}H_{66}Cl_4N_{12}O_{13}Pt_4S_4$	
Formula weight	1949.42	
Temperature	100(2) K	
Wavelength	0.71073 Å	
Crystal system	Orthorhombic	
Space group	$Pna2_1$	
Unit cell dimensions	a = 21.4574(13) Å	α= 90°.
	b = 12.2646(8) Å	β= 90°.
	c = 11.1760(6) Å	γ = 90°.
Volume	2941.1(3) $Å^3$	
Z	2	
Density (calculated)	2.201 Mg/m^3	
Absorption coefficient	9.872 mm^{-1}	
F(000)	1852	
Crystal size	0.170 x 0.110 x 0.010 mm^3	
Theta range for data collection	0.949 to 26.457°.	
Index ranges	$-26\leq h\leq 26$, $-15\leq k\leq 15$, $-13\leq l\leq 13$	
Reflections collected	85945	
Independent reflections	6036 [R(int) = 0.0802]	
Completeness to theta = 25.242°	100.0 %	
Absorption correction	Semi-empirical from equivalents	
Max. and min. transmission	0.7454 and 0.4890	
Refinement method	Full-matrix least-squares on F^2	
Data / restraints / parameters	6036 / 68 / 361	
Goodness-of-fit on F^2	1.073	
Final R indices [$I>2\sigma(I)$]	R1 = 0.0453, wR2 = 0.1020	
R indices (all data)	R1 = 0.0601, wR2 = 0.1109	
Absolute structure parameter	0.002(6)	
Largest diff. peak and hole	2.919 and -3.232 $e.Å^{-3}$	

Crystal data(ii) for 246a

A specimen of $C_{19}H_{30}Cl_2N_6O_5Pt_2S_2$, approximate dimensions 0.030 mm x 0.120 mm x 0.310 mm, was used for the X-ray crystallographic analysis. The X-ray intensity data were measured at 100(2)K using an Oxford Cryosystems Cobra low temperature device using a MiTeGen micromount. See Table 1 for collection parameters and exposure time. Bruker APEX software was used to correct for Lorentz and polarization effects.

A total of 1070 frames were collected. The total exposure time was 2.97 hours. The frames were integrated with the Bruker SAINT software package using a wide-frame algorithm. The integration of the data using a triclinic unit cell yielded a total of 49640 reflections to a maximum θ angle of 27.12° (0.78 Å resolution), of which 6173 were independent (average redundancy 8.041, completeness = 100.0%, R_{int} = 5.66%, R_{sig} = 3.29%) and 5107 (82.73%) were greater than $2\sigma(F^2)$.The final cell constants of a = 11.0607(7) Å, b = 11.0707(7) Å, c = 12.6727(8) Å, α = 114.8432(18)°, β = 93.5680(19)°, γ = 94.7534(19)°, volume = 1395.22(15) $Å^3$, are based upon the refinement of the XYZ-centroids of 9130 reflections above 20 σ(I) with 4.864° < 2θ < 54.16°.Data were corrected for absorption effects using the multi-scan method (SADABS). The ratio of minimum to maximum apparent transmission was 0.532. The calculated minimum and maximum transmission coefficients (based on crystal size) are 0.3964 and 0.7455.

The structure was solved and refined using the Bruker SHELXTL Software Package, using the space group Pī, with Z = 2 for the formula unit, $C_{19}H_{30}Cl_2N_6O_5Pt_2S_2$.The final anisotropic full-matrix least-squares refinement on F^2 with 331 variables converged at R1 = 2.38%, for the observed data and wR2 = 5.50% for all data. The goodness-of-fit was 1.006. The largest peak in the final difference electron density synthesis was 1.679 $e^-/Å^3$ and the largest hole was -1.845 $e^-/Å^3$ with an RMS deviation of 0.156 $e^-/Å^3$. On the basis of the final model, the calculated density was 2.256 g/cm^3 and F(000), 896 e^-.

Table 8. Crystal data and structure refinement for 246a

Identification code	tcd309	
Empirical formula	$C_{19}H_{30}Cl_2N_6O_5Pt_2S_2$	
Formula weight	947.69	
Temperature	100(2) K	
Wavelength	0.71073 Å	
Crystal system	Triclinic	
Space group	$P\bar{1}$	
Unit cell dimensions	a = 11.0607(7) Å	α= 114.8432(18)°.
	b = 11.0707(7) Å	β= 93.5680(19)°.
	c = 12.6727(8) Å	γ = 94.7534(19)°.
Volume	1395.22(15) $Å^3$	
Z	2	
Density (calculated)	2.256 Mg/m^3	
Absorption coefficient	10.398 mm^{-1}	
F(000)	896	
Crystal size	0.310 x 0.120 x 0.030 mm^3	
Theta range for data collection	1.858 to 27.124°.	
Index ranges	-14≤h≤14, -14≤k≤14, -16≤l≤16	
Reflections collected	49640	
Independent reflections	6173 [R(int) = 0.0566]	
Completeness to theta = 25.242°	100.0 %	
Absorption correction	Semi-empirical from equivalents	
Max. and min. transmission	0.7455 and 0.3964	
Refinement method	Full-matrix least-squares on F^2	
Data / restraints / parameters	6173 / 4 / 331	
Goodness-of-fit on F^2	1.006	
Final R indices [I>2σ(I)]	R1 = 0.0238, wR2 = 0.0509	
R indices (all data)	R1 = 0.0353, wR2 = 0.0550	
Largest diff. peak and hole	1.679 and -1.845 $e.Å^{-3}$	